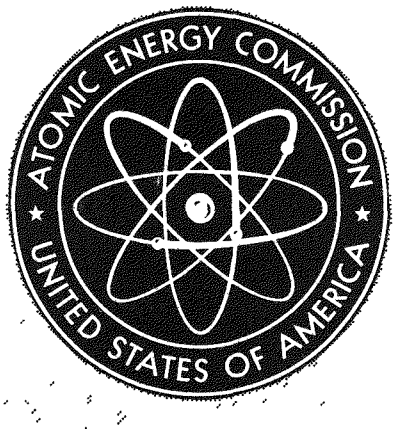

NYO-9064

FUEL ELEMENT DEVELOPMENT PROGRAM FOR THE PEBBLE BED REACTOR

Final Report

April 30, 1961

Sanderson and Porter
New York, New York

UNITED STATES ATOMIC ENERGY COMMISSION • DIVISION OF TECHNICAL INFORMATION

LEGAL NOTICE

Printed in USA. Price $3.00. Available from the Office of Technical Services, Department of Commerce, Washington 25, D. C.

USAEC Division of Technical Information Extension, Oak Ridge, Tennessee

DISCLAIMER

NYO-9064

METALS, CERAMICS, AND MATERIALS

FUEL ELEMENT DEVELOPMENT PROGRAM
for the
PEBBLE BED REACTOR

FINAL REPORT

April 30, 1961

Work Performed Under AEC Contract AT(30-1)-2378

SANDERSON & PORTER

NEW YORK, N. Y.

TABLE OF CONTENTS

Table of Contents (Continued) Page

NYO 9064

FINAL REPORT ON THE DEVELOPMENT OF FUEL ELEMENTS FOR THE PEBBLE BED REACTOR

April 30, 1961

Abstract

This report describes the development and evaluation of fuel element materials for the Pebble Bed Reactor which is a high-temperature, all-ceramic, helium-cooled reactor. The basic fuel element consists of a uniform dispersion of fuel in a 1-1/2 inch diameter graphite sphere. Major emphasis was on ceramic coatings for the retention of fission products. Of a wide variety of materials, it was found that "molecularly deposited" ceramics such as alumina, siliconized silicon-carbide, and pyrolytic carbon were excellent barriers to fission product leakage. The most advantageous location for ceramic coatings was found to be on the individual fuel particles where the coating is subject to less forces and a larger thickness-to-diameter ratio can be used than if the coating were on the surface of the graphite sphere. Twenty full scale fuel elements were irradiated in a number of capsules to burnups ranging up to about 6 a/o U235. In all specimens containing a uniform dispersion of fuel, the graphite spheres were found to retain their excellent structural properties after irradiation. In one irradiation at 1400°F of a graphite sphere fueled with Al_2O_3 coated UO_2, gaseous fission products were found to leak from this specimen at only 10^{-6} of their rate of production up to about 1.5 a/o U235 burnup. This report contains data on fuel particle coatings of Al_2O_3, pyrolytic carbon, and metals; surface coatings of siliconized silicon carbide, pyrolytic carbon, and metal carbides; properties of and the effects of irradiation on graphite spheres; the use of natural graphite in preparing a high-density matrix material; graphite fueling by thorium nitrate infiltration; subsurface metal and metal carbide coatings for graphite; and an In-Pile Loop program on the behavior of fission products in a recycle helium stream.

Summary & Conclusions

The original concept of a fuel element for the Pebble Bed Reactor was an uncoated sphere of graphite fueled with fissile and/or fertile material. This concept was based on the use of an exceedingly cheap fuel element to offset the increased costs associated with the resulting higher activity levels in the primary coolant stream. However, in view of the experimental programs which would be required to properly assess the increased primary loop costs (i.e. shielding, maintenance, and hazards), the use of ceramic coatings to retain fission products within the fuel element at high temperature was selected as the major undertaking of the PBR Fuel Element Development Program under Contract AT(30-1)-2378. Two methods of retaining fission products were extensively investigated. These were coatings on the fuel element surface, and coatings on individual fuel particles.

Surface Coated Fuel Elements. A total of ten PBR fuel element specimens with surface coatings were subjected to varying amounts of high level irradiation in the Capsule Irradiation program. Of this number, cracks or pinholes have been found in eight of the coatings. The exact causes of the failures are not known precisely, but evidence indicates that changes in the graphite matrix contributed to most of the failures.

It is unfortunate that the failure statistics were so oppressive because at least one of the surface coating materials - siliconized silicon carbide - was found to be an excellent barrier to fission product leakage, a property heretofore thought to be solely in the realm of metallic claddings. In neutron activation tests on Si-SiC coated specimens, less than 2.2×10^{-7} of the contained Xe 133 was released during a four hour period at 2000°F. In a low level Furnace Capsule Test, leakage factors (i.e. rate of release/rate of production) for gaseous fission products of the order of 10^{-7} to 10^{-6} were found at temperatures of 200°F to 1900°F. In high level Sweep Capsule tests, leakage factors of the order of 10^{-9} were found during a one month irradiation period prior to coating failure. Subsequent examination of this specimen indicated that the coating failure was caused by cracking in the unfueled graphite shell on this specimen. All specimens having an unfueled graphite shell surrounding the fueled graphite core were found to develop cracks in their unfueled shells during capsule irradiation. This type of cracking was not detected in any of the specimens where the fuel was dispersed throughout the graphite sphere. The mode of failure in shelled specimens suggested that failures were associated with changes in the the internal temperature gradients in the specimen and incipient flaws in the shell.

Pre-irradiation examination of Si-SiC coated specimens showed that this type of coating is well bonded to the graphite matrix but that coating fracture under impact load is very sensitive to the type of graphite. Several specimens were found to meet the 2.0 ft-lb. impact requirement and all specimens met the 500 lb. compressive load requirement. An internal gas pressure test at 300 psi, simulating fission gas pressure buildup in a PBR fuel element, showed no damage to the coating on the test specimen. Self-welding tests showed that Si-SiC coated specimens will have a surface temperature limitation slightly in excess of 2000°F due to migration of the free-phase silicon in the coating which would cause adjacent spheres to stick together. It was found necessary to incorporate an unfueled graphite shell between the Si-SiC coating and the fueled graphite sphere to prevent serious uranium contamination of the coating from a uranium silicon reaction. However, in view of the difficulties with graphite shells noted above, another reaction barrier, such as pyrolytic carbon coatings on the fuel particles, would be desirable if an Si-SiC coating were to be used.

Other types of metal carbide coatings, such as TiC, ZrC, and SiC which did not have an excess metal phase, were found to be too porous to act as a fission product barrier. In some cases, poor bonding of the metal carbide coating to the graphite sphere was noted.

The pyrolytic carbon surface coating has shown some promise as a fission product barrier in several neutron activation tests. Best results were obtained with pyrolytic carbon deposited above 3000°F in a 9.5 mil thickness. One such specimen released less than 9.3×10^{-7} of its Xe 133 in a neutron activation test at 1900°F for three hours. A measurable fission product release rate was found from a specimen having a thinner coating deposited at 3000°F. In this Furnace Capsule Test, fission product leakage factors were found to range from about 10^{-4} to 10^{-2} at temperatures of 150°F to 1900°F. A corrosive attack was also noted in this specimen, believed to have been caused by moisture in the sweep helium stream. Impact and abrasion resistance were found to be marginal for this type of coating with interlayer chipping being the typical mode of failure. This coating can be deposited directly on fueled graphite without any significant uranium contamination of the coating.

Future work with the Si-SiC or the pyrolytic carbon surface coatings would have to include a detailed understanding of the properties of the underlying graphite body as they affect coating integrity and a rather large quantity of specimens would have to be fabricated and tested in order to insure statistical confidence in this type of coating.

Alumina Coated UO_2 Particles. Fifteen batches of UO_2 particles have been coated with Al_2O_3 by the vapor deposition process. UO_2 particle sizes ranged from 100 to 400 microns and coating thicknesses ranged from 20 to 150 microns. At the 1800°F deposition temperature used for most of the runs, the UO_2 particles were uniformly coated with a dense impermeable layer of Al_2O_3. Greater than 99% of the particles were found to be adequately coated as shown by a subsequent oxidation test in 1200°F air. Uranium contamination on the coating can be kept below 10^{-6} of the contained uranium by rinsing the particles and the equipment after the first thin layer has been deposited. Successive layers can then be well bonded to each other.

Spherically shaped UO_2 particles were used in most of the batches to avoid possibility of coating failure at sharp corners. However, it was noted that irregular fuel particles could still be uniformly coated and there may be an economic incentive to use other than spherical fuel particles. Two batches were made with ThO_2-UO_2 particles and no problem was encountered with the use of thoria. One batch was successfully coated containing a porous inner layer of Al_2O_3 deposited at 1400°F which would be useful as a reservoir for fission product gases. However, some difficulty was encountered when this type of coating was applied to irregularly shaped UO_2 particles.

Several graphite spheres were successfully fueled with Al_2O_3 coated UO_2, although some slight uranium contamination of the graphite matrix was found. Sources of contamination can arise from uranium on the particle surfaces, from particles broken during the admixture process, and possibly from contaminated process equipment. The operating temperatures of graphite bodies fueled with Al_2O_3 coated UO_2 will be limited to less than 2500°F in order to avoid reaction between Al_2O_3 and graphite. Short time processing temperatures of 2500°F will be satisfactory but this means that the graphite body cannot be completely graphitized. Thermal expansion tests have shown that the Al_2O_3 coating thickness should exceed about 30% of the UO_2 particle diameter so that the slightly higher expansion coefficient of the UO_2 will not rupture the coating at 2500°F. Fuel particles occupy about 1.7 v/o of the graphite matrix in the reference PBR fuel element and the use of coated fuel particles increases this volume to about 10 v/o depending upon the ratio of coating thickness to fuel particle diameter. No loss in strength has been found in both impact and compression testing of graphite spheres fueled with coated particles. However, there is some evidence that thin particle coatings (40 microns or less) can be damaged in these tests. Massive coatings (~250 microns thick) were not found to be damaged.

Fission product retention tests at low burnup levels have shown vapor deposited Al_2O_3 to be an excellent barrier to fission product release. Typical neutron activation test results show that only 10^{-6} of the contained Xe 133 is released from a graphite sphere fueled with Al_2O_3 coated UO_2 when the specimen is heated at 2000°F for four hours. In Furnace Capule Tests a similar specimen was found to have leakage factors for the long-lived fission product gases of 10^{-6} to 10^{-7} at 300°F which increased to 10^{-4} to 10^{-5} at 1800°F. From both of these tests, it is concluded that the "leakage" was primarily due to uranium contamination in the specimen rather than diffusion through the Al_2O_3 coatings.

The most significant test of this type specimen was a high level irradiation in Sweep Capsule SP-5. The specimen operated at average conditions of 1.5 KW, 1350°F surface temperature and 1550°F central temperature. A burnup of 6 a/o U 235 was achieved in this experiment. Up to about 1.5 a/o, the leakage factors for ten isotopes ranging in half-life from 20.8d I 131 to 1.7s Xe 141 were found to be in the range of 10^{-6} to 10^{-9}. Between 1.5 a/o and 3 a/o the leakage factors for the longer-lived isotopes began to increase indicating that measurable diffusion may have started to occur through the Al_2O_3 as a result of radiation damage. At 6 a/o, the leakage factors ranged from 10^{-2} for Xe 133 to 10^{-6} for the very short-lived fission gases. Hot cell examination revealed that the increased fission product leakage was caused by cracks in about 10% of the particle coatings. The cracked particle coatings were located predominantly in the outer half of the graphite sphere. The cause of these cracks has not been established. However, the thermal neutron flux depression towards the center of the specimen during capsule irradiation suggested that cracks were caused by an irradiation effect. One possibility is that fission gas pressure buildup ruptured the coatings which had been weakened by a radiation-induced embrittlement since it was estimated that the maximum pressure-induced stress in the Al_2O_3 was well below the rupture stress of about 30,000 psi for unirradiated Al_2O_3.

Further work with Al_2O_3 coated UO_2 should emphasize extending the low leakage factors obtained at the 1.5 a/o level to at least 6 a/o burnup. The use of porous inner layers in the particle coating and porous UO_2 particles to minimize rupture due to fission gas pressure buildup should be explored. A fundamental study of neutron and fission fragment damage to the molecularly deposited Al_2O_3 material should be made to determine whether other process conditions or the use of coating additives will minimize radiation-induced porosity and embrittlement. A better understanding of factors which influence the reaction between Al_2O_3 and graphite should be obtained. These factors may include the type of filler and binder used in the graphite matrix, the

final bakeout cycle, and the impurity levels in the matrix. An optimum particle size should be established since it appears that large particles, of about 400 micron UO_2 with a 200 micron Al_2O_3 coating, would be desirable to minimize both physical damage to the coating and fission product leakage.

Pyrolytic Carbon Coated UC_2 Particles. The interest in this type of coated particle stems from the absence of a temperature limitation due to reaction between the particle coating and the graphite matrix. Also, this type of coating does not effectively displace moderator atoms. Eight batches of coated particles were prepared at deposition temperatures ranging from 1900°F to 3600°F. Four of these batches were obtained from commercial sources and had already been subjected to a 3600°F thermal cycle test and an acid rinse before evaluation under the PBR Program.

Evaluation of as-fabricated batches showed that better than 99.99% of the particles were adequately coated. Uranium contamination by alpha assay was of the order of 10^{-6} of the contained uranium. Thermal cycle tests showed a definite tendency for the coatings to rupture when heated above their deposition temperature due to the higher expansion coefficient of the UC_2.

Evaluation of the as-received commerical batches showed uranium contaminations by alpha assay of the order of 10^{-5} to 10^{-4} of the contained uranium. There was no metallographic evidence of the thermal cycle treatment having ruptured coatings in these batches. The higher uranium contamination was due to either uranium carbide dust included in the coating during the fabrication process or the redistribution of uranium from a few poorly coated particles during the initial acid rinsing.

Neutron activation tests on several of the as-fabricated batches showed Xe 133 release fractions of less than 10^{-6} in several hours of heating at temperatures at or below the coating fabrication temperature, while greater Xe 133 release occurred above this temperature. Several of the batches were neutron activation tested after incorporation in graphite spheres. In two cases, severe damage to the particle coatings was indicated by high Xe 133 release. This damage was caused by either the use of irregularly shaped fuel particles or an excessively vigorous mixing step prior to molding into the graphite sphere. The Xe 133 release fraction for three other fueled spheres ranged from 10^{-5} to 10^{-4} in several hours at temperatures to 2500°F. Metallographic examination of the fueled graphite bodies of these latter specimen types showed no evidence of damage to the particle coatings.

Further work on pyrolytic carbon coated UC_2 should include minimizing uranium contamination in the coatings, the determination of the optimum coating deposition temperature based on strength, permeability, and thermal cycle rupture, and the effects of radiation damage on coating permeability.

In other materials developments, it was found that metal coated UO_2 particles could not be used in a graphite matrix due to the severe metal-graphite reaction which was noted. A study of the preparation of graphite blanket elements loaded with ThO_2 by the thorium nitrate infiltration process was conducted. It was found that graphite densities below 1.45 g/cc and more than 5 infiltration steps were required to achieve the desired ThO_2 loading. A variety of subsurface coating materials for graphite spheres were studied. It was found that the best results would be obtained if a hot-pressing technique were used so that the coating material located beneath an unfueled graphite shell was in a molten phase during fabrication. High density spheres were made with natural graphite filler materials. Densities of 2.0 g/cc were achieved but the spheres did not have adequate strength at the low binder contents needed to achieve the high density.

In-Pile Loop Operating difficulties and fund limitations prevented the full utilization of the in-pile loop in a study of the behavior of fission products in a recycled helium stream. Irradiation of a graphite sphere fueled with Al_2O_3/UO_2 showed excellent fission product retention as had been previously indicated by capsule irradiations. Irradiation of a graphite sphere fueled with uncoated UO_2 shot showed fission product leakage factors of 10^{-3} to 10^{-4}. A large portion of the resulting system activity was due to short-lived fission products. This was shown by the sharp drop in system activity when helium circulation was stopped and a decrease in deposited activity with increasing flow distance from the fuel element. A negligible gas phase radioactivity was noted when the discharge of helium from the system had no effect on the rate of decay of system activity. Numerous coupons and system components from this loop were provided to ORNL for fission product deposition and decontamination studies.

Reference Fuel Element. The basic design of the PBR Fuel Element which was evolved from this work consists of a molded graphite sphere containing a dispersion of coated fuel particles. No significant deterioration of the structural properties of the graphite matrix was found after irradiation to about 6000 KWH which is the present design objective of the 125 eMW Pebble Bed Reactor. A number of high temperature ceramic coatings have been found which can offer essentially complete retention of fission products. However, if radiation induced permeability in these

coatings cannot be avoided, it appears that the coatings could still afford sufficient delay time for the short-lived volatile fission products, which are precursors of the troublesome non-volatile fission products, to decay before escaping from the fuel element.

The final choice of fuel particle coating cannot be made as yet. Pyrolytic carbon coated UC_2 particles are favored because they offer an all carbon system with temperature limits above 3000°F. However, there is no information on radiation damage effects on this material. Al_2O_3 coated UO_2 has shown good fission product retention up to at least 1.5 a/o burnup. If future work shows that metal oxide coatings such as Al_2O_3 can be developed to maintain coating integrity to higher burnups, it will be possible to utilize these coatings in Pebble Bed Reactors by limiting top fuel temperatures to about 2500°F.

Some method will be needed to prevent damage or loss of coated fuel particles at the surface of the fuel element, such as a pyrolytic carbon or siliconized silicon carbide surface coating. Since oxidation protection may be required on PBR fuel elements, the surface coating could serve a dual function. Two types of possible attack are of concern: the mass transfer of carbon by reaction with trace impurities of CO_2 or H_2O in the helium coolant and the sudden oxidation by the admission of air in the event of a rupture in the primary loop. Si-SiC coatings can prevent these types of attack, however the effects of pinholes and cracks in the coatings should be assessed. Al_2O_3 coated UO_2 could not be used in this type of fuel element because relatively high fabrication temperatures are needed to apply the Si-SiC coating. The resistance of pyrolytic carbon, known to be less reactive than graphite, to this type of attack should be determined.

All of the materials studied in the present program have been made only in laboratory quantities at high unit costs. Manufacturing cost studies were not included in the scope of the present program. However, now that a basic design has evolved, sufficient work should be done to permit realistic fuel element cost estimates to be made.

1.0 Introduction

This Final Report covers a two-year program which had as its basic objective the development and/or evaluation of fuel elements which would be suitable for the economic operation of a large-scale Pebble Bed Reactor. The characteristics of a reference design fuel element have been based on design studies of a 125 eMW Pebble Bed Reactor Steam Power Plant (1, 2). This reactor is a high-temperature, all-ceramic, helium-cooled reactor, consisting of a randomly packed static bed of fueled graphite spheres. Its fuel element characteristics are summarized below.

1. The fuel element is a 1-1/2 inch diameter sphere of fueled graphite.

2. Fuel loading is 4.75 gms of uranium in the form of either the oxide or the carbide.

3. The maximum power density is 3 KW per sphere. Maximum surface and center temperatures are 1800°F and 2100°F respectively. The design burnup is 5500 KWH per sphere which is equivalent to a 6 a/o of total uranium or 48,000 MWD/metric ton of uranium.

4. Fission product retention should be such that the external fission product radioactivity level is $<10^{-6}$ of the activity which would result from the complete release of all isotope chains containing volatile fission products.

5. The spheres shall withstand a 2.0 ft-lb. impact load and a 500 lb. compressive load.

6. Other pertinent features are that adjacent fuel elements should not self weld, fuel element coatings should withstand internal pressure buildup of gaseous fission products and fuel element surfaces should not dust, abrade or erode.

The PBR Fuel Element Development Program was arranged to evaluate these various characteristics. Figure 1-1 is a schematic outline of the evaluation program. In general, fuel element specimens were subjected to pre-irradiation testing, followed by irradiation tests to measure fission

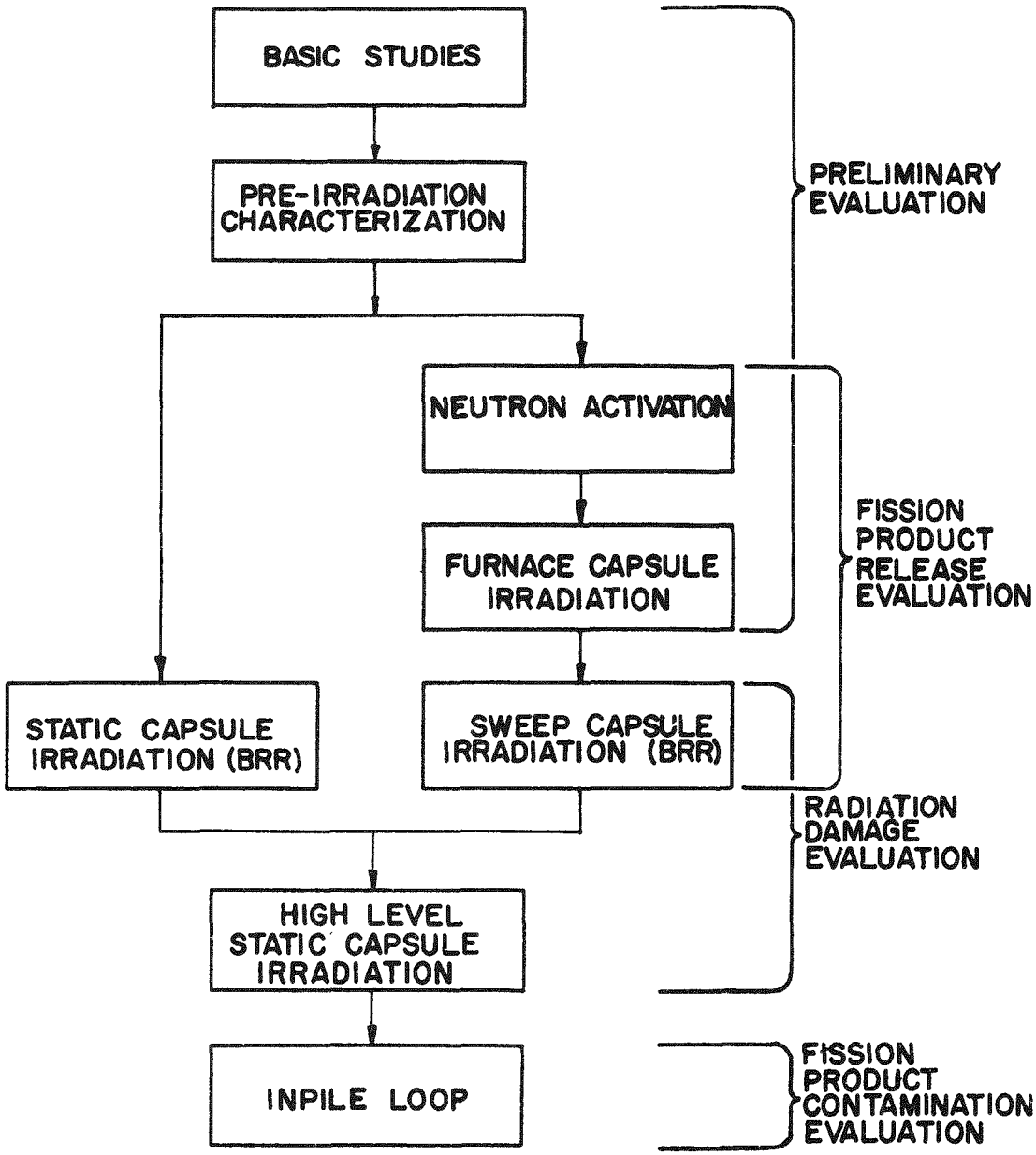

FIG. 1-1 PBR FUEL ELEMENT DEVELOPMENT PROCEDURE

product retention characteristics and/or the effects of irradiation on physical properties. An in-pile loop was operated to simulate problems in the primary loop of a Pebble Bed Reactor. The test apparatus used in this program has been described in ref. (4). All phases of the evaluation program up to and including the capsule irradiations were conducted at the Battelle Memorial Institute. The in-pile program was conducted by the Nuclear Science and Engineering Corp.

During the course of the PBR Fuel Element Development Program, numerous Quarterly Reports, Phase Reports and Topical Reports have been issued. All of these reports have been included in the "List of References" appearing at the end of this report. This Final Report has been prepared as a summary of the entire PBR Fuel Element Development Program.

2.0 Fuel Element Materials

The earliest fuel element concept for the Pebble Bed Reactor was a simple uncoated graphite sphere fueled with uranium. This concept was based on the desire to produce an exceedingly cheap fuel element where precision of manufacture was not critical and where large quantities could be produced by economical mass production methods. The use of the spherical fuel element would also mean that a Pebble Bed Reactor could be refueled on a semi-continuous basis using relatively simple handling techniques.

Graphite was selected as the fuel element structural material because of its low cost and its excellent high temperature strength properties. Three methods of fueling the graphite were considered——infiltration, admixture, and lumping. The infiltration and admixture methods result in a uniform dispersion of the fuel throughout the graphite in contrast to the lumping method where the fuel is concentrated in a portion of the graphite. In the infiltration procedure, a preformed and graphitized sphere is infiltrated with a uranyl nitrate solution, dried and denitrated by heating so that UO_2 particles are deposited in the pores of the graphite body. The primary advantage of this type lies in its potential economy of manufacture, particularly if hot refabrication is considered. However, due to the small fuel particle size, approximately 1 micron, nearly all of the fission fragments will recoil into the graphite matrix, thus maximizing radiation effects in the graphite. In the admixture type fuel element, preformed fuel particles of a larger selected size are admixed with graphite flour and a binder, molded into a spherical shape, and baked. If a bake temperature below 2500°F is chosen, the matrix will be only partially graphitized but the integrity of uranium oxide fuel particles would be preserved. If a bake temperature over 4000°F is chosen, the final form of the fuel particles will be uranium carbide and a high degree of graphitization of the matrix will be achieved. The primary advantage of the admixture type lies in the trapping of most of the recoil fission fragments within the fuel particles thus minimizing damage to the graphite and enhancing fission product retention. In the third method of manufacture, a pellet of fissile material is incorporated in the center of a unfueled shell of graphite, either by a molding technique or by placing the pellet in a drilled hole and sealing with a graphite plug. The advantage of this type is that the graphite shell, which is subjected to essentially no fission fragment damage, takes all of the fuel element loads irrespective of damage to the fuel pellet and maximum use is made of the graphite in retaining

fission products. This type is somewhat limited in power density due to the high temperature gradients through the relatively thick graphite shell. A modification to these three basic types is the use of either an admixed or infiltrated core surrounded by an unfueled graphite shell. The diameter of the core piece can be selected to lower the temperature gradient through the graphite shell while still providing a fuel free surface.

The initial concern with uranium graphite fuel elements was whether they would have sufficient strength, not only after irradiation, but in the as-fabricated condition as well. Concern over this latter point stemmed from the classification of graphite as a ceramic, and the supposition, therefore, that it would be too brittle or fragile for our purposes. The well known test of bouncing a graphite sphere off of any convenient surface readily illustrated that graphite was indeed a rugged material of construction.

In order to study the properties of fueled graphite spheres after irradiation, an evaluation program was started at the Battelle Memorial Institute under a previous contract, AT(30-1)-2207. This work was initially concerned with the evaluation of uncoated specimens of the types discussed above. Pre-irradiation and post irradiation physical property tests were conducted and fission product release characteristics were obtained. Capsule irradiations were one of the tools used to evaluate the specimens. High level irradiation effects on the physical properties of the three basic types of fuel elements were determined in Static Capsule SP-1. Fission product release from an admixtured UO_2 fueled specimen was determined with Sweep Capsule SP-2. Results of these earlier tests have been described in detail in ref. (2). Briefly, it was shown that there was no significant deterioration in the impact strength, compressive strength and abrasion resistance of infiltrated and admixtured fuel elements. A fission product release rate of about two orders of magnitude lower than the production rate could be expected for an admixtured fuel element.

This fission product release rate from an uncoated admixtured specimen would produce an activity level in the primary loop of a Pebble Bed Reactor of the order of 10,000 curies per MW of reactor power. In spite of the economic attractiveness of the simple uncoated fuel element, the economic feasibility of a system with these high activity levels remained a question pending further evaluation of such areas as fission product deposition, gas stream purification, and equipment decontamination and maintenance. Consequently, as work was starting under the present Contract AT(30-1)-2378, the emphasis in the PBR Fuel Element Development Program shifted to methods of further retention of fission products within the fuel elements.

Three locations for coatings to retain fission products were visualized:

1. A coating can be applied to the outside surface of the fueled graphite sphere. A surface coating can be applied to any of the three types of fueled graphite spheres and it is relatively easy to apply. However, the coating is subject to stresses arising from both external loads (i.e. impact, compression) and possible differential expansion with the graphite sphere due to temperature cycling or radiation damage effects.

2. A coating can be located beneath the surface of the graphite sphere, with the fueled region being inside the coating. The coating is not subjected directly to external loads applied to the fuel element but the manufacturing process is somewhat more complex.

3. Coatings can be applied to the individual fuel particles in an admixtured type fuel element. Ceramic coatings on small fuel particles can be used in large thickness-to-diameter ratios which are more stable and individual coating failures would expose only a very small portion of the fuel. However, the fuel particle coatings are subjected to fission fragment recoil damage and rupture due to fission gas pressure buildup which could limit the useful life of the coating.

A wide variety of coatings were evaluated in the course of the Program. The most promising coatings were found to be siliconized silicon carbide, pyrolytic carbon, and vapor deposited alumina. These ceramic coatings were found to have low permeabilities, of the order of that found for metals. Indeed, the permeability of these special ceramics remains low at temperatures which are beyond the safe limits for many metals. Section 3.0 summarizes all the work on siliconized silicon carbide and pyrolytic carbon surface coatings. Coated fuel particles are discussed in Section 4.0 (Alumina) and Section 5.0 (Pyrolytic Carbon).

Other types of coatings which were developed and/or evaluated under this Program are described in Section 6.0. These include metal carbide surface coatings (SiC, TiC, and ZrC), subsurface coatings (both metal and ceramic) and metal coated UO_2 particles.

Work relating to uncoated fuel elements is discussed in Section 7.0. This includes irradiation effects on fueled graphite spheres, a study of the thorium oxide loadings which can be achieved in graphite by infiltration with

thorium nitrate, the use of natural graphite in preparing a high density matrix material, the strength characteristics of graphite spheres and fission product release from uncoated specimens.

The In-Pile Loop for studying the behaviour of fission products in a recycled helium stream is described in Section 9.0.

The most probable application of the Pebble Bed Reactor will be as a high temperature breeder reactor employing a uranium-thorium loading in the core and a thorium loading in the blanket. For purposes of the experimental program, the thorium is replaced with an equivalent weight of uranium. Normal enrichment uranium is used in specimens for pre-irradiation tests and certain low level fission product diffusion tests. The use of fully enriched uranium in capsule irradiations greatly accelerates irradiation damage tests such that anticipated burnups in Pebble Bed Reactors can be readily achieved in lower flux research reactors. The design and operation of the various capsules are given in Section 8.0. Table 8-1 in that section lists all of the fuel element types which were subjected to capsule irradiations and/or fission product retention tests.

Table 2-1 has been prepared to summarize the various types of fuel element specimens evaluated during the program. The manufacturer and pertinent characteristics of the fuel elements are listed. Each type of specimen has been assigned a type number. The letters FA and FI refer to the method of fueling the graphite (i.e. admixture and infiltration). In the case of unfueled specimens, the designation FX is used. Numbers are assigned serially within each group, and have no special significance. Occasionally, when it is desired to identify a particular sphere within a group, an additional identification number in parentheses will be added to the type number. Throughout this report, specimens are referred to only by type number. Consequently, the specimens have been listed numerically in Table 2-1 to permit rapid identification.

TABLE 2-1

SUMMARY OF FUEL ELEMENT TYPES

	INFILTRATED			LUMPED			UNFUELED			
Number	FI-1	FI-5	FI-6	FL-1	FL-2	FL-3	FX-1	FX-2	FX-3	FX-5
Mfgr.	Syl.	AMP	AMP	AMP	AMP	AMP	Plas	Plas	Ray	AMP
FUEL										
Loaded As	UNH	UNH	UNH	UC_2	UC_2	UC_2	—	—	—	—
Final Form	UO_2	UC_2	UC_2	UC_2	UC_2	UC_2	—	—	—	—
Particle Size, μ	1	1	1	3/8"	3/8"	3/8"	—	—	—	—
MATRIX										
Reimpreg.	no	yes	yes	yes	yes	yes	—	—	—	—
Net Density	1.65	1.85	1.85	1.85	1.85	1.85	—	—	—	—
Shell Thick.	0	0	0	0.35"	0.35"	0.35"	—	—	—	—
Bake Temp, °F	1470	3500	3500	3500	3500	3500	—	—	—	—
COATING										
Location	—	Surf.	Surf.	—	Surf	Surf.	Surf.	Surf.	Surf.	Surf.
Material	—	SiC	ZrC	—	ZrC	SiC	TiC	ZrC	PyC	PyC
Thickness, mils	—	1	1	—	1	1	10	10	60	0.5

COATED PARTICLES

Type	Batch No	Mfgr
Al_2O_3/UO_2	1 to 11	BMI
"	12	NUMEC
PyC/UC_2	1 to 6	BMI
"	7	3M
"	8	HTM
"	9	NC
"	10	AMP

Manufacturers

AMP	-	American Metal Products
BMI	-	Battelle Memorial Institute
Carbo	-	Carborundum
GLC	-	Great Lakes Carbon
HTM	-	High Temperature Materials
3M	-	Minnesota Mining and Manufacturing
NC	-	National Carbon
NUMEC	-	Nuclear Materials and Equipment Corp.
Plas	-	Plasmakote
Ray	-	Raytheon
Speer	-	Speer Carbon
Syl	-	Sylvania-Corning Nuclear

	ADMIXTURED																				
Number	FA-1	FA-2	FA-5	FA-6	FA-7	FA-8	FA-9	FA-10	FA-11	FA-14	FA-16	FA-17	FA-19	FA-20	FA-21	FA-22	FA-23	FA-24	FA-25	FA-26	FA-27
Mfgr.	NC	BMI	3M	3M	Carbo	Carbo	NC	GLC	NC	NC	3M	NC	NC	NC	Ray	NC[a]	3M	Carbo[a]	3M	Speer[a]	NC
FUEL																					
Loaded As	UO_2	UO_2	UO_2	UO_2	UC_2	UC_2	UO_2	UO_2	UO_2	ThO_2/UO_2	UO_2	UO_2	UO_2	UO_2	UO_2	UO_2	UO_2	UC_2	UC_2	UC_2	UC_2
Final Form	UO_2	UO_2	UC	UC	UC_2	UC_2	UO_2	UO_2	UO_2	ThO_2/UO_2	UC	UO_2	UC_2	UC_2	UC_2	UO_2	UC	UC_2	UC_2	UC_2	UC_2
Particle Size, μ	100/150	67	100/200	100/200	100/200	100/200	100/150	350/420	100/150	100/150	100/200	100/150	100/150	100/150	100/150	100/150	100/200	177/250	177/250	150/250	177/250
MATRIX																					
Reimpreg.	no	no	yes	yes	no	no	yes	yes	yes	no	yes	no	no	no	no	no	yes	no	yes	no	no
Net Density	1.62	1.63	1.80	1.80	1.63	1.63	1.68	1.80	1.68	1.62	1.75	1.62	1.65	1.65	1.65	1.57	1.75	1.55	1.75	1.61	1.65
Shell Thick	0	0	0.15"	0.15"	0	0	0	0	0	0	.060"	0	0	0	0	0	.125"	0	0	.125"	0
Bake Temp, °F	2560	2000	3600	3600	3600	3600	2560	2000	2560	2560	3600	2560	4400	4400	4400	2300	3600	2000	3000	2500	4000
COATING																					
Location	—	—	—	Surf.	—	Surf.	—	—	Surf.	—	Surf.	Surf.	—	Surf.	Surf.	Part.	Surf.	Part.	Part.	Part.	Part.
Material	—	—	—	Si-SiC	—	Si-SiC	—	—	PyC	—	Si-SiC	PyC	—	PyC	PyC	Al_2O_3	Si-SiC	PyC	PyC	PyC	PyC
Thickness, mils	—	—	—	3	—	30	—	—	5	—	4	2	—	2-10	50	2	4-10	2	3	3	3

(a) Coated Particles Manufactured by BMI

3.0 Surface Coated Fuel Elements

One of the earliest approaches to fission product retention was the application of a ceramic coating to the outside surface of the spherical PBR fuel element. Two of the most promising types - siliconized silicon carbide (Si-SiC) and pyrolytically deposited carbon - are described in this section. Other types of surface coatings are described in Section 6.2. The use of surface coatings presents certain problem areas. The allowable impact load on the fuel element is significantly reduced due to the thin, hard and less resilient nature of the coating compared with the graphite matrix. However, by proper choice of graphite composition and coating thickness, fuel elements meeting the 2.0 ft-lb. requirement can be made. Coatings must have adequate adherence to the graphite body and sufficient abrasion resistance to withstand the fuel flow pattern through PBR cores. Coating materials which will self weld and cause the packed bed to freeze up must be avoided. Also, if the coating material reacts with uranium, an unfueled graphite shell must be placed between the fueled graphite core and the coating. These factors, together with the ability of the coating to retain fission products, have formed the basis for the evaluation program.

3.1 Silicon Carbide Surface Coatings

The interest in silicon carbide coatings for Pebble Bed Reactor fuel elements stems from their excellent potential as a barrier to fission product leakage at high temperatures. Actually, this property is due to the presence of a continuous phase of silicon throughout the silicon carbide grains in the coating. This material is referred to as siliconized silicon carbide (Si-SiC).

Two types of Si-SiC coatings were evaluated. Photomicrographs of these two types are shown in Figures 3-1 and 3-2. The coating shown in Figure 3-1 is similar to the coatings on specimen types FA-6, FA-16, and FA-23 which represent a sequence of specimens from one manufacturer, all containing an unfueled graphite shell between the fueled core and the Si-SiC coating. The coating on an FA-8 specimen is seen in Figure 3-2. A description of these four types of specimens is given in Table 2-1. In both coatings, the continuous free silicon phase and the excellent bonding to the graphite matrix can be seen. The lower free Si content of the FA-8 coating can also be noted.

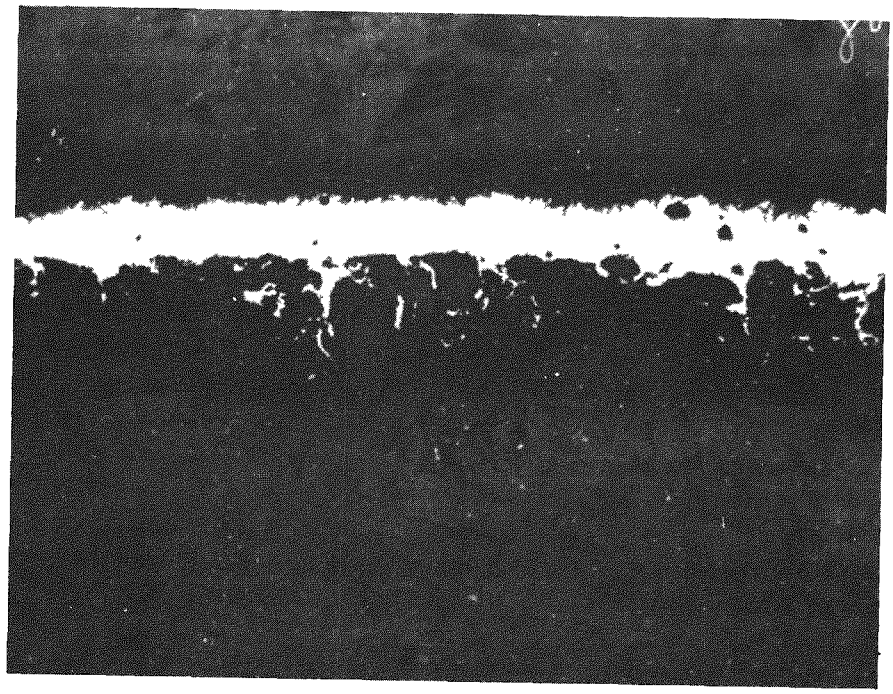

FIG. 3-1 Si-SiC Coating Similar to Coatings on Specimens FA-6, FA-16, and FA-23. (100X)

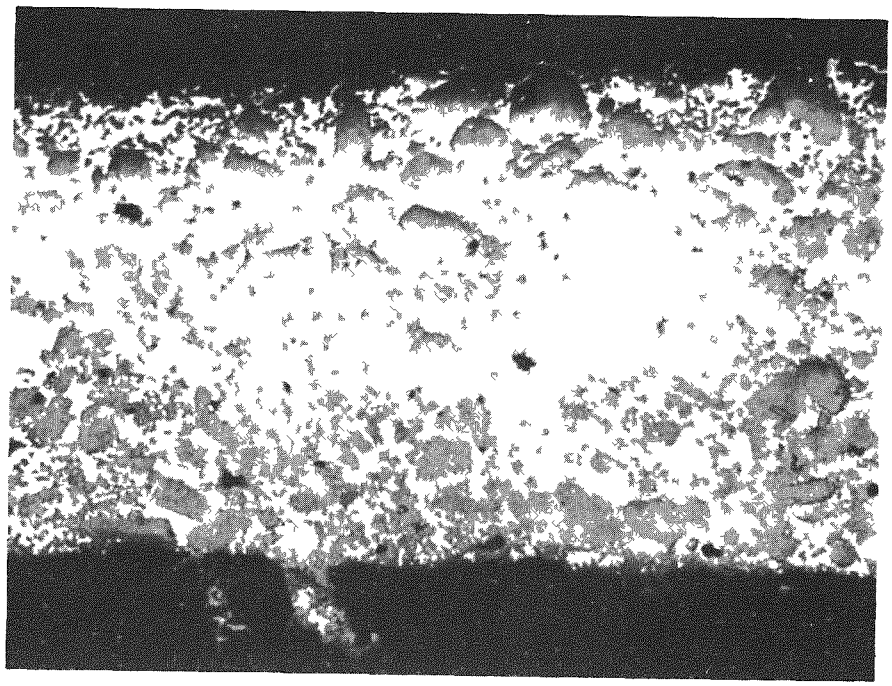

FIG. 3-2 Si-SiC Coating on an FA-8 Specimen. (100X)

3.1.1 Pre-irradiation Evaluation

All of the pre-irradiation tests on Si-SiC coated specimens are described in this section.

Coating Permeability. The standard screening test for determining the presence of pinholes or cracks in a sphere coating is to immerse the specimen in a 375°F silicon oil bath and observe whether bubble streams issue from the specimen. No leaks were found in 11 of the 23 FA-6 specimens, 7 of the 17 FA-8 specimens, 6 of the 7 FA-16 specimens, and 9 of the 10 FA-23 specimens. All of the specimens which failed this test had random pinhole leaks in their coatings. Many of the specimens had only a single pinhole. Several of the specimens which had leaks were returned to the manufacturer. In all cases it was possible to repair the leaks in these specimens.

A few anisotropic graphite spheres were coated with Si-SiC. Hot oil tests showed that all of these spheres had circumferential cracks in the coating. This indicates that a very low degree of anisotropy is desirable in graphite spheres which are to be coated with Si-SiC.

Uranium Contamination. One of the problems with the use of an Si-SiC coating is the potential reaction between uranium in the fueled graphite body and the silicon in the coating which can result in uranium contamination throughout the coating. This factor can be noted in Table 3-1 which is a summary of all of the alpha assays made on Si-SiC coated specimens. The area at each position corresponded to 1/7 of the total sphere surface area, but the value shown has been normalized to the whole sphere surface. Rather large amounts of surface contamination can be noted on the FA-8 specimens in which the Si-SiC coating is placed directly on the fueled graphite sphere. Much lower contamination is noted in the other specimens which have an unfueled shell between the fueled core and the coating.

Impact and Compression Tests. Data from these tests are summarized in Table 3-2. All of the impact failures were evidenced by noting the load after which the coating was found to leak in the hot oil test. All of these failures are well below the 7 to 12 ft-lb range found for uncoated specimens. In several cases, repeated impacts on the same spot caused an early failure of the coating. The effect of first subjecting the specimen to an abrasion tumbling test was to lower its impact resistance. Typical impact failures for FA-6 and FA-8 specimens can be seen in Fig. 3-3. Several attempts were made to see whether the coating failed before the sphere broke by running the compressive test with the specimen submersed

TABLE 3-1

Surface Uranium Contamination of Si-SiC Coated Specimens[a]

Sphere No.	Position 1	Position 2	Position 3
FA-8 (E2)	1.1×10^{-3}	-	-
" (E3)	1.8×10^{-3}	-	-
" (E6)	1.8×10^{-3}	-	-
" (E7)	5.4×10^{-3}	-	-
" (E8)	2.6×10^{-3}	-	-
" (E9)	1.4×10^{-3}	-	-
" (E10)	2.7×10^{-3}	-	-
" (E11)	2.6×10^{-3}	-	-
" (E12)	6.3×10^{-3}	-	-
FA-6 (17E)	6.3×10^{-6}	-	-
" (19E)	5.6×10^{-6}	1.1×10^{-5}	nil
FA-16 (N15)	3.8×10^{-6}	-	-
FA-16 (N13)	3.4×10^{-5}	2.9×10^{-5}	3.4×10^{-5}
FA-16 (N16)	1.2×10^{-5}	1.7×10^{-5}	1.6×10^{-5}
FA-16 (E16-4)	8.4×10^{-6}	4.4×10^{-6}	7.0×10^{-6}
FA-23 (E8-1)	1.6×10^{-7}	nil	2.3×10^{-7}
" (E8-7)	nil	4.0×10^{-7}	2.3×10^{-7}
" (E8-12)	2.3×10^{-7}	2.3×10^{-7}	3.1×10^{-7}

(a) Expressed as fraction of total uranium in sphere and normalized to whole sphere surface.

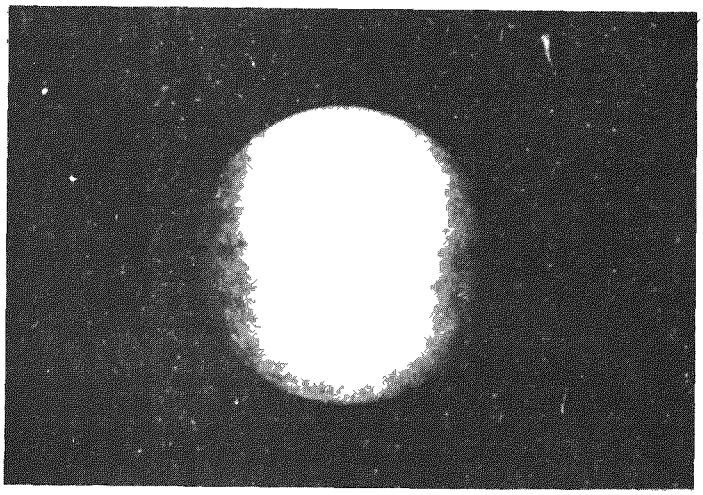

(a) Type FA-6

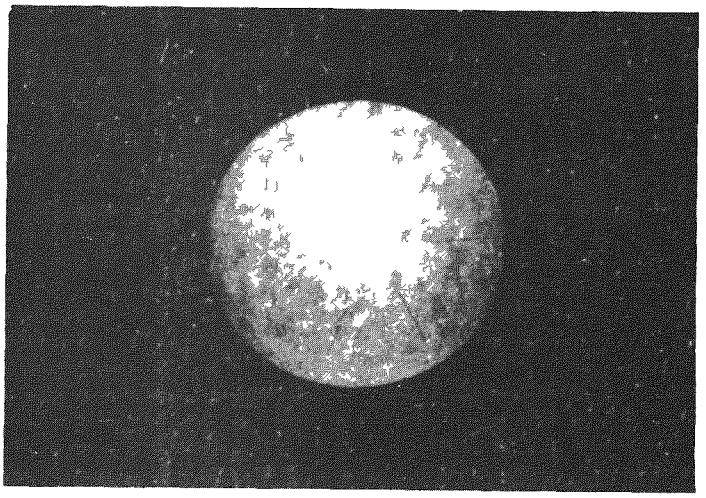

(b) Type FA-8

FIG. 3-3 Typical Impact Fractures for Type FA-6 and FA-8 Specimens

in hot oil. No evidence of bubbling was found prior to sphere failure.

1500 1-1/2" diameter unfueled graphite spheres coated with Si-SiC were purchased and used under Contract AT(30-1)-2207 to study the pressure drop and thermal expansion characteristics of packed ball beds (19). The acceptance tests for the procurement of the 1500 spheres included a 2 ft-lb impact load and a 500 lb. compressive load applied to each sphere with no evidence of coating failure as indicated by the hot oil leakage test. All of the 1500 spheres passed these tests. However, when the spheres were subsequently used in an oxidizing atmosphere at 1500°F, corrosive attack to the underlying graphite was noted in many of the spheres. From the nature of the damage, it was concluded that the Si-SiC coating had been bruised during the impact tests such that the graphite could be attacked by the highly oxidizing atmosphere through the weakened spots in the coating.

TABLE 3-2

Impact and Compression Tests on Si-SiC Coated Specimens

Type	Impact Failure,[a] Ft-lbs.	Compressive Failure[b] Load, lbs.	Compressive Failure[b] Deflection, in.
FA-6	1.33[c]	2070	0.040
	1.25[c]	1595	0.062
	3.0	1162	0.05
	1.9	1925	0.03
FA-16	0.6[d]	825[d]	0.068
FA-23	0.5[d]	1445	0.060
FA-8	0.5[c]	530	0.011
	0.42[c]	837	0.036
	1.0		
	0.6		
	0.5		

(a) Load to cause defect in coating as indicated by hot oil test.
(b) Load to fracture sphere.
(c) Impacts made at one location. In all other tests, specimens were rotated between impacts.
(d) Test conducted after specimen had been subjected to abrasion test.

Abrasion Tests. Abrasion tests were run on 5 specimens. This test consists of tumbling the spheres for a 20 min period inside a rotating drum which also contains some dummy graphite spheres to enhance the tumbling action. The abrasion test results are summarized in Table 3-3. The specimens with the thickest coatings suffered no noticeable damage except for some weight loss. The thinner coatings developed pinhole leaks. These were most likely due to thin spots in the coating which were damaged by the tumbling action.

TABLE 3-3

Abrasion Tests on Si-SiC Coated Spheres

Specimen No.	Coating Thickness, in.	Hot Oil Test	Time in Hot Oil, Min.
FA-16(N12)	.004	Several small leaks	10
FA-16(N14)	.004	" "	10
FA-23(E8-1)	.010	No leaks	5
FA-23(E8-2)	.010	" "	5
FA-23(E8-6)	.0075	" "	5

Self Welding. In view of the presence of free phase silicon (i.e. having a 2600°F melting point) in the Si-SiC coating, there is some concern about adjacent fuel elements being fused together which would hinder the unloading of a reactor core. Tests were run on unfueled spherical specimens having coatings similar to the FA-16 and FA-23 types. In one test, two spheres were subjected to a 50 lb. compressive load for 66 hours while at 2500°F. A whitish film which appeared on the surface of the specimen due to a reaction with contaminants in the furnace may have accentuated the welding that was observed at the point of contact. The test was repeated with similar specimens at 2300°F and no evidence of self welding was found. Thus, it appears that the permissible surface temperature for this type of specimen will be below 2500°F.

Internal Pressure. As fission product gases accumulate inside a coated graphite sphere under irradiation, there is a possibility that gas pressure could cause the coating to rupture. It has been calculated that a pressure of about 300 psi could exist inside such a coated sphere in a typical Pebble Bed Reactor. A special test apparatus was constructed to

explore this point. The apparatus consisted of a tube fitting gasketed to a coated sphere which had a 1/16" diameter hole in its coating. This assembly was mounted in a beaker of 375°F silicone oil. An FA-8 specimen was tested with 300 psi argon. The coating did not crack off, indicating that it was securely bonded to the graphite, and no pinhole leaks appeared in the coating.

3.1.2 Irradiation Effects

Seven Si-SiC coated specimens were subjected to high level irradiation in three capsules. The design and operation of each capsule is described in Section 8.0. Fission product release from several of the specimens was measured and these results are described in Section 3.1.3. Since the Hot Cell examination for Capsule SP-5 was conducted under Contract W-7405-eng-92, results for the FA-23 specimens were taken from ref. (21).

A summary of the operating conditions and the results of the post-irradiation examination for the seven Si-SiC specimens are given in Table 3-4. The Hot Cell examination included visual examination, hot oil testing, weight change, dimensional change, impact testing, and metallography.

Visual Examination. Major cracks were observed in all four of the admixtured/shelled specimens (Types FA-6 and -23). Figure 3-4 is a view of the inner capsule from SP-3, which contained the two FA-6 specimens, just after it was opened in the Hot Cell. A portion of the graphite support and a thermocouple lead can be seen. Specimen 18E is seen to have an equatorial crack which was the most prominent crack in this specimen. The prominent crack in 20E was about 30° above the equatorial plane. There was visible evidence that the prominent cracks penetrated into the graphite sphere. In addition, there were numerous hairline cracks intersecting the major cracks in FA-6(18E). Small shiny areas along the major crack can be noted which appear to be interlayer chipping of the Si-SiC coating. The two FA-23 specimens in SP-5 both had a prominent crack on a great circle with a second prominent crack intersecting it. These cracks had the same appearance as the one shown in Figure 3-5.

All three FA-8 specimens appeared in good condition with no visible evidence of cracks or any other flaws. The typical surface condition of an irradiated FA-8 specimen is shown in Figure 3-6 which is a 4X photograph of specimen FA-8(E5) and shows the cracks produced by the impact test described below.

Hot Oil Tests. The three FA-8 specimens and two of FA-6 specimens, in spite of their visible cracks, were immersed in 375°F silicone oil. As expected, the two FA-6 specimens bubbled vigorously from their cracks. After oil testing, the specimens 18E and 20E showed weight gains of 2.4% and 0.6% respectively due to oil pickup.

TABLE 3-4

Capsule Irradiation Results for Si-SiC Coated Specimens

Specimen	Specimen Power KW/ball	Temp., °F Surface	Temp., °F Center	Burnup KWH	Weight Change %	Diameter Change %	Passed Hot Oil Test	Impact or Compression Test	Visual Appearance
Capsule SP-3									
FA-6(18E)	1.7	1300	1450	2400	-0.1	-0.3	No	-	Several large cracks
FA-6(20E)	1.7	1300	1450	1950	0.0	0.0	No	-	Several large cracks
FA-8(E4)	2.2	1600	1700	2400	-0.3	+0.01	No	1697 lbs (C)	No cracks
FA-8(E5)	2.2	1600	1700	2600	-0.1	+0.08	Yes	0.75 ft.-lb (I)	No cracks
Capsule SP-4									
FA-8(E6)	2.2	1750	1850	7400	+0.14	+0.3	No	-	No cracks
Capsule SP-5									
FA-23(E8-7)	1.6	1300	1450	5900	-0.11	+0.1	No	-	Several large cracks
FA-23(E8-12)	1.0	1300	1400	3600	-0.08	+0.2	No	-	Several large cracks

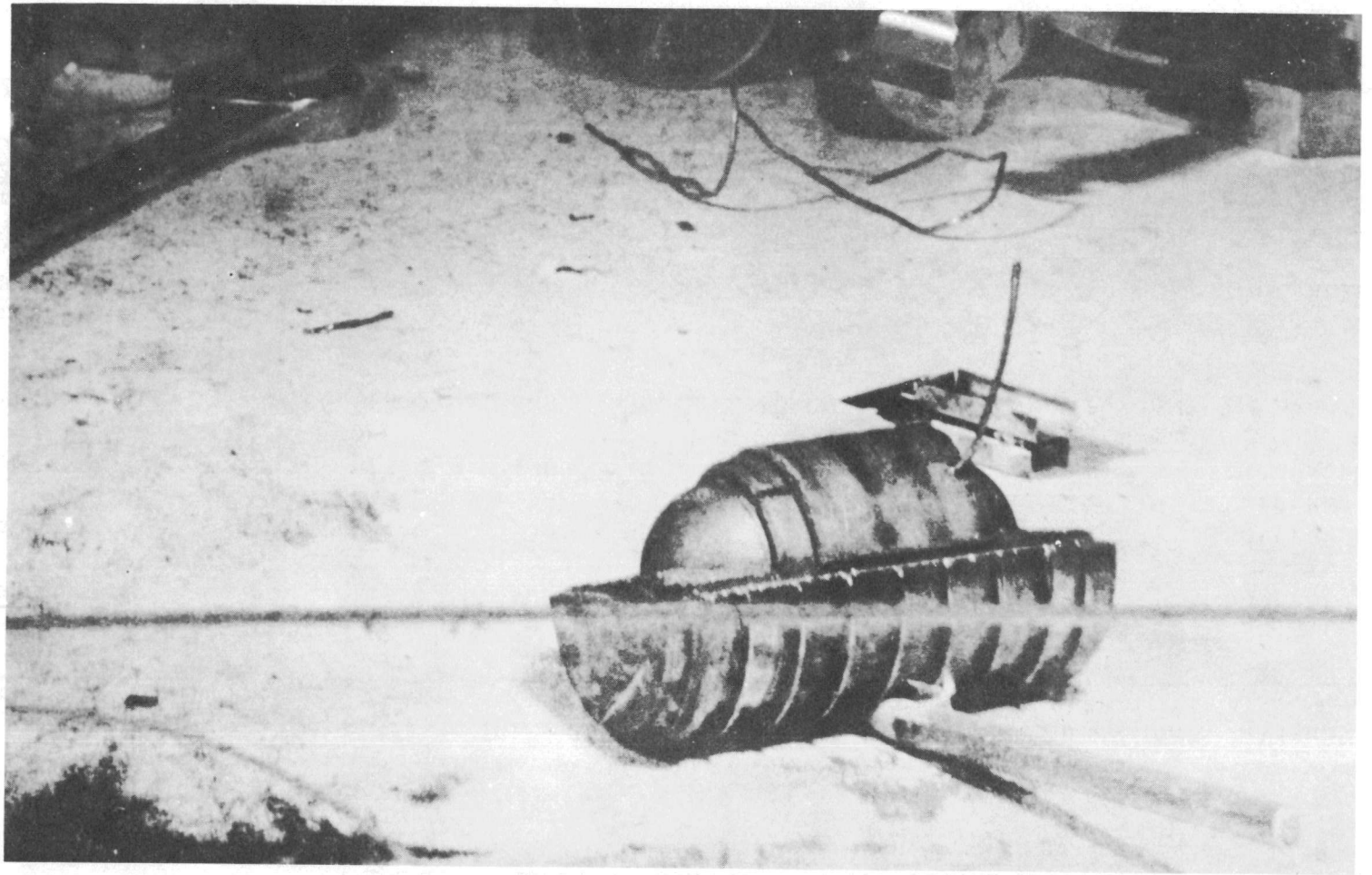

FIG. 3-4 View of FA-6 Specimens After Opening Capsule SP-3 In Hot Cell.

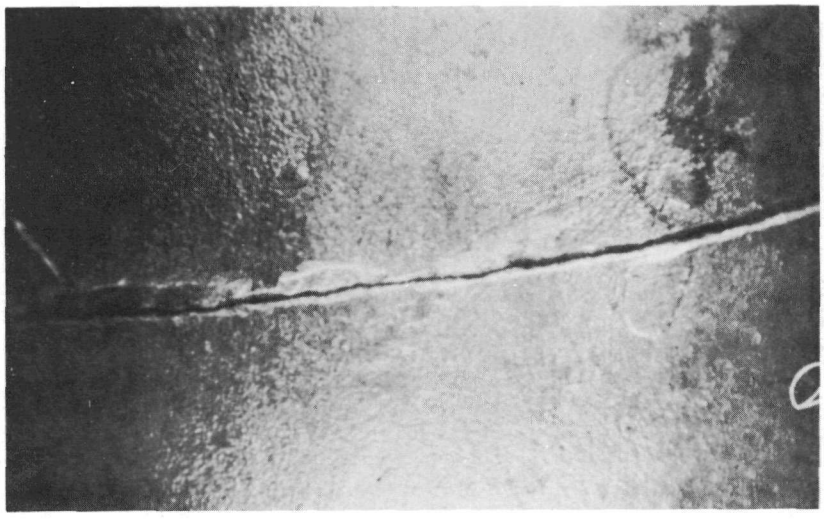

FIG. 3-5 Typical View (at 4X) of Major Crack in FA-6(18E) Specimen After Irradiation in Capsule SP-3.

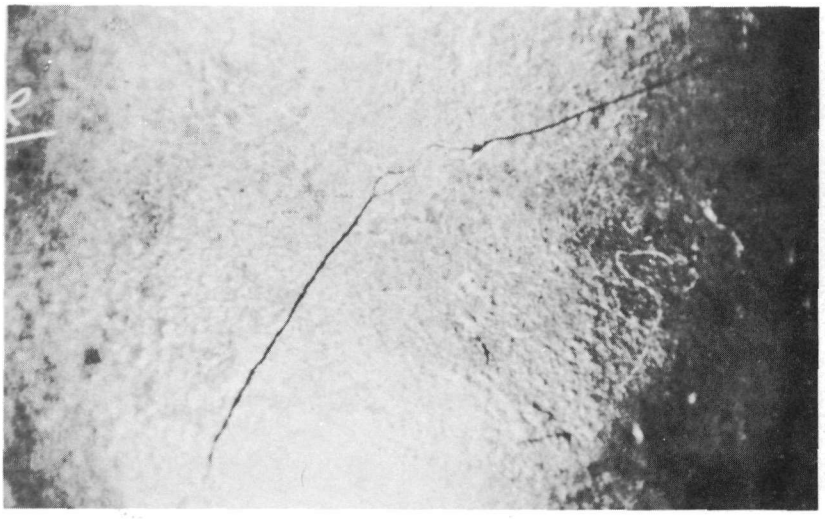

FIG. 3-6 Irradiated Specimen FA-8(E5) After 15 in-lb Impact.

Only one of the FA-8 specimens (No. E5) exhibited no leakage during the 17 minute immersion in the hot oil. Specimen E4 was nearly perfect in that no bubble streams appeared for 52 seconds at which time a single bubble stream appeared. The test on this specimen was interrupted after three minutes and in two subsequent tests no bubble streams appeared.

When specimen FA-8(E6), which had no visible defects, was tested in hot oil a line of bubble streams clearly showed a single surface crack about 1/4" long to be present. No other defects were noted. Further description of this crack is given below under Metallographic Inspection.

Weight and Dimension Measurements. The weight and dimension changes for these specimens were given in Table 3-4. Since it was not desirable to machine flats on the coated spheres, measurements were made at various crayon-marked spots on the spheres. Repeated measurements at the same spot showed that the dimensional changes were very sensitive to micrometer position. Although the values listed in Table 3-4 are averages of numerous readings, little significance can be placed on these measurements.

Specimen FA-23 (E8-7) fell apart in handling before weighing so that the weight loss includes any physical loss which might have occurred. The weight changes for specimens FA-8(E4) and (E5) were based on measurements after hot oil testing while all others were weighed before hot oil testing.

Factors which would affect the weight change in a coated specimen are losses by flaking of the coating, and, possibly, some sort of radiation induced devolatilization of binder constituents. Weight gains could be caused by re-adsorption of atmospheric gases on the graphic matrix through a fault in the coating. The relative effects of these factors are not clear from the data shown in Table 3-4.

Impact Tests. Since the FA-6(20E) specimen was visibly cracked, it was subjected to a 1 ft. free fall impact test rather than the normal impact test. On impact, the specimen fractured into four approximately equal segments and a few chips. This load was equivalent to a 1.5 in.-lb. impact, well below the pre-irradiation values of 24 to 36 in.-lb., indicating that the presence of the cracks seriously weakened the specimen.

The FA-8(E5) specimen was first subjected to a 1 ft. free fall test. A subsequent hot oil test showed no damage to the coating. This specimen was then transferred to the standard impact test machine for further testing.

The test was started by dropping a 1 lb. weight from a 1 inch height onto the specimen and increasing the height of the fall in 1 inch increments. After each impact, the specimen was given a 3 min. hot oil test to detect the point of coating failure. A different point on the sphere was impacted each time. At 9 in.-lb., a bubble stream appeared. At 12 in.-lb., the first visible crack appeared. Figure 3.6 shows the crack developed by the 15 in.-lb. impact. Testing was continued up to 24 in.-lb., the limit of the apparatus, where the specimen was badly cracked, but still in one piece. The 9 in.-lb. load at which the coating was first damaged is slightly above the average of 7 in.-lb. pre-irradiation load noted in Table 3-2. The slight increase is probably due to hardening of the graphite causing better support for the Si-SiC coating.

Compression Tests Specimen FA-8(E4) was compression-tested while immersed in hot oil in an attempt to determine whether there was any coating failure prior to matrix failure. The specimen failed at a compressive load of 1697 lbs. where the deflection was 0.0172 in. The slope of the straight line portion of the load-deflection curve was 146,000 lbs./in. Comparable values for unirradiated specimens were 500 to 800 lbs. load at failure and 50,000 to 80,000 lbs./in. load modulus. The effect of irradiation hardening is to increase the compressive strength of fueled graphite spheres.

The FA-6(18E) and FA-8(E6) specimens were not subjected to either the compression or impact test so that they could be selected in an attempt to learn more about the mature of the cracks in these specimens. No destructive testing was scheduled for the Capsule SP-5 specimens.

Metallographic Examinations. Specimens FA-6(18E) and FA-8(E6) were metallographically examined in order to study their Si-SiC coatings. The specimens were mounted in plastic so that they could be gripped while being sectioned. In the case of the FA-6(18E) specimen, an unanticipated radiation hardening of the plastic occurred causing the specimen and mount to drop from the jig as the plastic was being cut. This drop fractured the specimen. From visual examination of the pieces it appeared that the major cracks penetrated through the shell into the core of the specimen. One of the pieces was remounted, polished and etched for metallographic examination. Figure 3-7 shows the Si-SiC coating on specimen FA-6(18E) and can be compared with a pre-irradiation view of the coating on another specimen in Figure 3-1. There is no evidence of radiation damage to either the SiC grains or Si matrix. Also, there is no evidence of any separation of the coating from the graphite. Figure 3-8 is a 4X photograph of one of the pieces of FA-6(20E) which also shows no coating-graphite separation and, in addition no separation between the unfueled graphite shell and the fueled core.

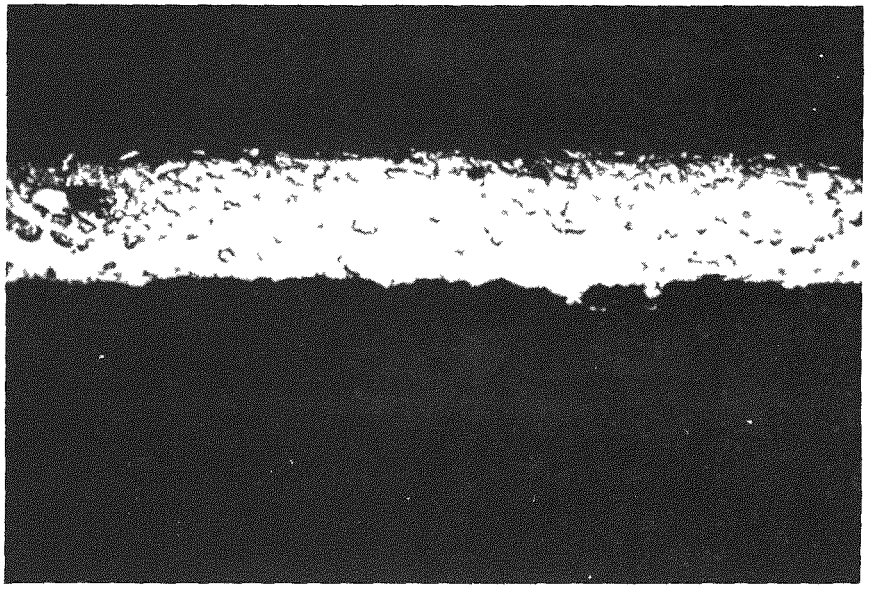

FIG. 3-7 Si-SiC Coating on Specimen FA-6(18E) After Irradiation in Capsule SP-3. (100X)

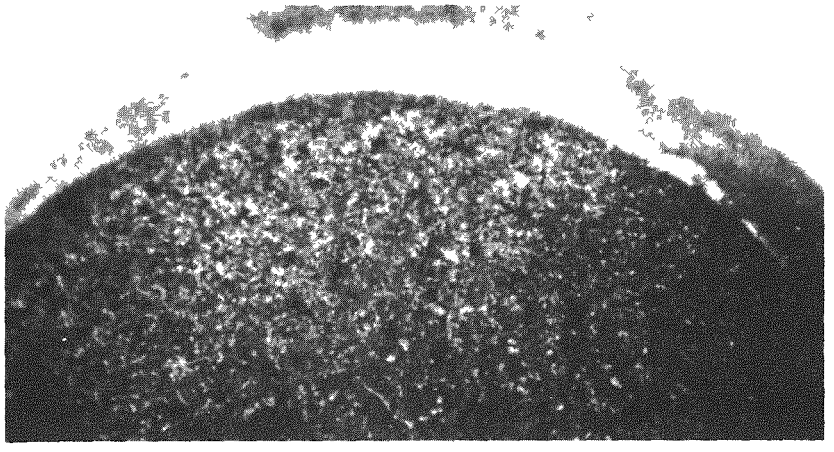

FIG. 3-8 Piece of Irradiated Specimen FA-6(20E) at 4X Showing Adherence of Si-SiC Coating and Graphite Shell to Fueled Graphite Core.

Figure 3-9 is a 34X photograph of the crack which was detected in specimen FA-8(E6) by the hot oil test. This specimen was mounted in plastic so that it could be sectioned and polished to further study the crack. Examination of the polished section actually revealed three cracks through the coating. Two of the cracks were quite large and obviously would have been revealed in the hot oil test. It was likely that the cutting and polishing operation caused these cracks. The third crack is shown in Figure 3-10. There is not conclusive evidence that this is actually the crack previously observed in the hot oil test since in mounting the sphere in plastic, the orientation of the crack may have been lost. However, it does not have the large, jagged appearance of the other two cracks and is therefore believed to be the crack of interest. As can be noted in Figure 3-10, the crack appears to be along the SiC grain boundaries. The crack was probably caused by a stress in the coating which either resulted from the internal temperature gradient in the specimen or from an initial coating flaw in fabrication which did not leak in the pre-irradiation hot oil test but which propogated under the operating conditions. No evidence of coating separation from the graphite matrix can be noted in Figure 3-10. These lack of separations are significant because it was thought that radiation-induced shrinkage of the graphite matrix might have produced some coating separation. Except for the crack, there is no other visible evidence of a radiation-induced change to the Si-SiC material.

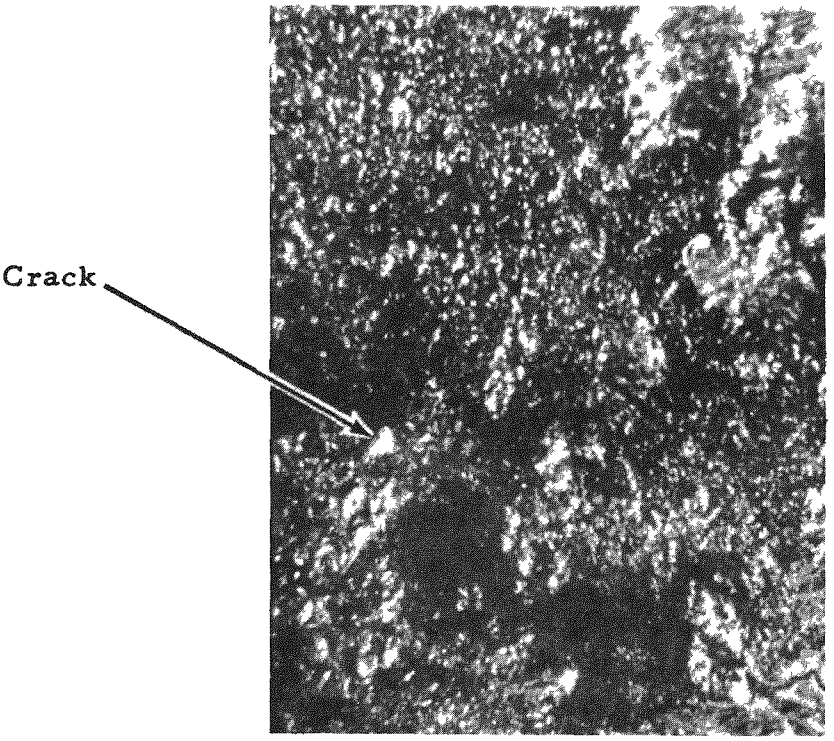

FIG. 3-9 External view (34x) of crack in Si-SiC coating of specimen FA-8 (E6) after irradiation in Capsule SP-4.

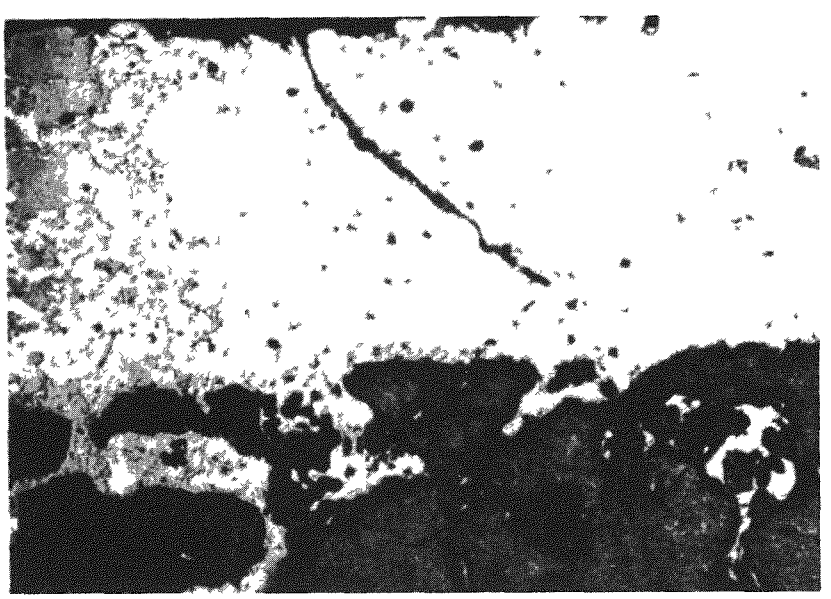

FIG. 3-10 Crack in Si-SiC coating of specimen FA-8 (E6) after irradiation in Capsule SP-4. View at 100x.

3.1.3 Fission Product Retention

Si-SiC coated specimens were subjected to all three types of fission product retention tests (i.e. neutron activation, furnace capsule, and sweep capsule) as described below.

Neutron Activation. A summary of all neutron activation tests on Si-SiC coated specimens is given in Table 3-5. The excellent fission product retention characteristic of an Si-SiC coating was first noted in the tests on specimens FA-6(N1) and FA-8(N4). To determine the effect of coating faults, a 0.030" diameter hole was ultrasonically drilled through the coating on FA-8(N4) and a circumferential crack was produced in the coating on FA-8(N7) by an impact load. The Xe 133 release from these defected specimens was comparable to the release of 3×10^{-3} in 20 minutes from a similar uncoated specimen (Type FA-7) indicating that once a fault develops in a coating, very little fission product retention can be expected by that fuel element.

TABLE 3-5

Neutron Activation Tests on Si-SiC Coated Specimens

Specimen No.	Temp, °F	Time at Temp, min	Fraction of Xe 133 Released
FA-6(N1)	1500	240	$< 2 \times 10^{-6}$
FA-8(N4)	1500	240	$< 4 \times 10^{-5}$
FA-8(N4)(a)	1500	22	4×10^{-3}
FA-8(N7)(b)	1200	2	5×10^{-3}
FA-16(N16)(c)	1700	90	1×10^{-4}
	2100	120	5×10^{-4}
	1600	50	2×10^{-3}
FA-16(N15)	1650	100	$< 1 \times 10^{-5}$
	1650	70	$< 5 \times 10^{-5}$
FA-16(N13)	1650	100	5×10^{-6}
	2100	80	1.5×10^{-5}
FA-23(E8-7)	2000	240	$< 2.2 \times 10^{-7}$

(a) A .030" diameter hole was drilled through the coating prior to this test.
(b) Specimen was subjected to an impact load, causing a circumferential crack in the coating, prior to this test.
(c) After testing, a pinhole was detected in the coating by the hot oil method.

Specimen FA-16(N16), which had successfully passed a hot oil test prior to the neutron activation test, released a greater amount of Xe 133 than anticipated. Subsequent hot oil and visual examination revealed a tiny chip in the coating. It could not be established whether this fault was the result of an inadvertent mechanical load applied to the coating or temperature cycling during the neutron activation test. The relatively higher release at the final 1600°F run tends to support the latter possibility.

The limit of Xe 133 detection of 2.2×10^{-7} for the test of specimen FA-23(E8-7) was about equal to the surface uranium contamination predicted by the alpha assay in Table 3-1.

Furnace Capsule. Furnace Capsule SPF-2 contained specimen FA-16(N15), fueled with normal enrichment uranium. Capsule design is described in Section 8.2. A total of 13 off-gas samples from this experiment were analyzed for long-lived noble fission product gases covering an operating temperature range of 200°F to 1900°F. Initial operation of this capsule was in a thermal flux of 1.7×10^{10}. The fission product retention was so good for this specimen that the capsule was ultimately moved into a flux of 3×10^{12} to achieve maximum sensitivity. A summary of the data obtained is given in Table 3-6.

TABLE 3-6

Summary of Fission Product Release Data
For Si-SiC Coated FA-16(N15) Specimen in Furnace Capsule SPF-2

Sample No.	Temp. °F	Flux n/cm²-sec.	R/B, (Rate of Release/Rate of Production) Xe 133	Xe 135	Kr 85m	Kr 87	Kr 88
1	200	1.7×10^{10}	← (No detectable release) →				
2	1000	"			"		
3	1000	3×10^{11}			"		
4	1000	"			"		
5	1000	"			"		
6	1500	3×10^{12}	6.1×10^{-6}	6.1×10^{-7}	5.1×10^{-7}	$< 1.3 \times 10^{-7}$	3.0×10^{-7}
7	1500	"	2.8×10^{-6}	2.0×10^{-7}	8.1×10^{-7}	"	2.7×10^{-7}
8	1500	"	2.1×10^{-6}	1.6×10^{-7}	3.1×10^{-7}	"	1.7×10^{-7}
9	1500	"	1.7×10^{-6}	1.1×10^{-7}	3.1×10^{-7}	"	1.7×10^{-7}
10	1900	"	2.6×10^{-6}	3.8×10^{-7}	6.7×10^{-7}	"	1.5×10^{-7}
11	1900	"	4.5×10^{-6}	4.2×10^{-7}	4.1×10^{-7}	"	1.2×10^{-7}
12	1900	"	8.2×10^{-6}	2.0×10^{-7}	7.0×10^{-7}	"	3.0×10^{-7}
13	1900	"	4.3×10^{-6}	2.5×10^{-7}	4.7×10^{-7}	"	1.0×10^{-7}

As can be noted in Table 3-6, the release rates for these long-lived fission product gases are extremely low. No significant effect of temperature on leakage rate can be noted. An alpha assay of FA-16(N15) indicated a surface uranium contamination of about 4×10^{-6}. These factors, together with the neutron activation results in Table 3-5, indicate that the observed "leakage" rates are principally due to fissioning of the slight uranium contamination on the surface of the specimen.

Sweep Capsules. Two FA-6 and two FA-8 specimens were irradiated in Sweep Capsule SP-3 and one FA-23 specimen was irradiated in the sweep compartment of Capsule SP-5. The design and operating features of these capsules are described in Section 8.3 and 8.5. The post-irradiation examination of these specimens has been described in Section 3.1.2.

Full power irradiation of Capsule SP-3 was initiated in the BRR on May 6, 1959. On May 8, the first attempts were made to sample the off-gas from both compartments. The level of activity in the line leading from the FA-8 specimens was too high to permit safe sampling of the gas from this compartment. A sample was obtained from the FA-6 specimens, however. The gas lines for both compartments were then shut off over the week-end. On May 11, when the gas lines were opened to permit further sampling, the activity levels were too high to permit safe sampling and the lines were again shut off. On May 18, a special low power run at 100 KW (BRR power) was made. At this condition, specimen power was down by a factor of 20, the specimen temperature was only 170°F, and it was possible to successfully sample the off-gas from the FA-6 specimens. The results of these two samples are given in Table 3-7.

TABLE 3-7

Fission Product Release From Si-SiC Coated FA-6 Specimens in Capsule SP-3

	Sample No. 1	Sample No. 2
Date	5/8/59	5/18/59
Reactor Power	2 MW	100 KW
Specimen Power	2 KW	100 watts
Specimen Temp.	1300°F	170°F
Release Fraction[(a)]		
Kr 85m	2×10^{-7}	8×10^{-5}
Xe 135	3×10^{-8}	3×10^{-6}
Xe 133	2×10^{-6}	(b)

(a) R/B = rate of release/rate of production

(b) Activity level in trap too high to count.

Further difficulties and revisions to the gas train prevented the obtaining of more data from Capsule SP-3 prior to its removal from the BRR on Aug. 3, 1959. The subsequent hót cell examination revealed that cracks had developed in the FA-6 specimens. It is most probable that the cracks occurred after May 8 since sample No. 2 definitely confirmed an increase in fission product leakage rate. The high activity levels in the line from the FA-8 specimen appears to be due to the high surface uranium contamination which was subsequently detected in alpha assays of similar specimens.

The FA-23 specimens irradiated in Capsule SP-5 represented improved specimens to overcome incipient cracks in the as-fabricated graphite matrix which were thought to be responsible for the cracks noted in the FA-6 specimens in Capsule SP-3. Radiography and visual examination of sectioned FA-23 specimens indicated a high probability that no incipient cracks were present in the FA-23 specimens. Irradiation of FA-23(E8-7) in the sweep compartment of Capsule SP-5 was started on April 6, 1960. As described in Section 8.5, this specimen operated at 1.6 KW and 1300°F surface temperature. The release data for long lived krypton and xenon isotopes are given in Table 3-8. The data for samples 8 to 11 are taken from ref. (20).

Extremely low fission product release was noted during the first 17 days of irradiation. Sample No. 4 was taken just after Capsule SP-5 was brought up to power for its third cycle. Just prior to startup, gas flow through the compartment containing the FA-23(E8-7) specimen showed no evidence of high fission product leakage. It is therefore assumed that the coating cracks observed in the post-irradiation examination (Section 3.1.2) were associated with the increase in internal temperature gradient as the specimen came up to power. Several additional long lived gaseous fission product samples were taken during the remainder of the irradiation. As noted in Table 3-8, the leakage factors rose from about 10^{-4} after the crack first started to about 10^{-2} at the end of the irradiation.

In addition the long-lived gas samples, two non-volatile trap samples were taken of the off-gas from specimen FA-23(E8-7). The procedures used were similar to those used for the non-volatiles trap experiments with the FA-22 specimen in Capsule SP-5 described in Section 4.4.3. The first sample was taken on the day when the large increase in long lived gaseous fission product release rate was first noted. The second sample was taken at the end of the irradiation. The results from both samples are given in Table 3-9.

TABLE 3-8

Long-Lived Xe and Kr Release From Si-SiC Coated Specimen FA-23(E8-7) in Capsule SP-5

Sample No.	Days of Irradiation	R/B, (Rate of Release/Rate of Production) Kr 85m	Kr 87	Kr 88	Xe 133	Xe 135
1	11	Nil	Nil	Nil	Nil	Nil
2	12	Nil	Nil	Nil	Nil	Nil
3	16-17(a)	1.9×10^{-9}	Nil	1.5×10^{-9}	5.7×10^{-9}	1.5×10^{-9}
4	21	(b)	(b)	(b)	7.9×10^{-3}	(b)
5	21	4.9×10^{-4}	2.0×10^{-4}	1.7×10^{-4}	3.0×10^{-3}	1.1×10^{-4}
6	21	2.8×10^{-3}	1.2×10^{-3}	6.6×10^{-4}	6.3×10^{-3}	9.3×10^{-4}
7	32	2.8×10^{-4}	1.3×10^{-4}	2.0×10^{-4}	5.2×10^{-4}	1.0×10^{-4}
8(c)	155	1.3×10^{-2}	3.1×10^{-3}	5.5×10^{-3}	4.5×10^{-2}	8.0×10^{-3}
9	160	9.2×10^{-3}	1.9×10^{-3}	—	2.3×10^{-2}	4.2×10^{-3}
10	168	1.2×10^{-2}	2.5×10^{-3}	3.8×10^{-3}	5.9×10^{-2}	5.2×10^{-3}
11	170	1.3×10^{-2}	3.5×10^{-3}	4.6×10^{-3}	2.6×10^{-2}	6.7×10^{-3}

(a) Sample collected over 22 hr. period (rather than 2 hr. period) because of low release rate.
(b) These species decayed out during long cooling period necessitated by high activity in this sample.
(c) Specimen surface temperature down to 1100°F for samples 8 to 11. Temperature for previous samples was 1300°F.

TABLE 3-9

Summary of Short-Lived Gaseous Fission Product Release Data From Specimen FA-23(E8-7) in Capsule SP-5

Trapped Species	Precursor Species	Half-Life	R/B(a) of Precursor Sample #1 (b)	Sample #2 (c)
Cs 137	Xe 137	3.9 min	4.0×10^{-4}	—
Sr 89	Kr 89	3.2 min	7.2×10^{-4}	2.5×10^{-3}
Ba 140	Xe 140	16 sec	3.4×10^{-5}	7.3×10^{-4}
Y 91	Kr 91	9.8 sec	—	9.8×10^{-4}
Ce 141	Xe 141	1.7 sec	4.6×10^{-6}	6.8×10^{-4}

(a) R/B = rate of release/rate of production
(b) On 21st day of irradiation
(c) On 170th day of irradiation; data taken from ref. (21).

For all isotopes in Sample No. 1 and Y 91, Ba 140, and Ce 141 in Sample No. 2, the plots of these isotope concentrations as a function of travel time through the trap showed excellent agreement with the theoretical prediction based on half-lives of the volatile precursors. The Sr 89 curve from Sample No. 2 appeared to consist of two straight line components, one of which was characteristic of Kr 89 decay and the other of Br 89 decay assuming no further mobility after its decay. The resultant R/B for Br 89 was 3.3×10^{-4}. No R/B value could be reported for Xe 137 from Sample No. 2 since the Cs 137 curve was too complex. This complexity might have been due to a contribution from the diffusion of Cs 137 itself from the fuel element.

Comparison of the data in Table 3-9 with the corresponding data for the longer-lived gases in Table 3-8 shows only a slight dependancy of leakage factor on half life. This indicates very little gaseous fission product retention time in the fuel element and is further verified by the nature of the cracks observed in hot cell examination.

3.2 Pyrolytic Carbon Surface Coatings

This type of coating contains no metal or metal carbide phase and consists solely of carbon deposited on the fuel element surface by the pyrolysis of a hydrocarbon gas. The type of carbon structure which is formed has an extremely low permeability. The bulk density of the coating can be made to closely approach theoretical carbon density, depending upon the temperature of deposition. The main advantage of this type of coating is that the coating itself will not dictate the temperature limit of the whole fuel element but instead the limit will be set by the properties of the fissile material and the graphite matrix.

Five types of pyrolytic carbon coatings were evaluated during the Program. These types varied primarily in thickness and, to some extent, in deposition temperature. The thickest coating was on the FA-21 (fueled) and FX-3 (unfueled) types which had similar coatings deposited in the range of 3300 to 3400°F. The FA-21 specimens were made by depositing the coating on UC_2 fueled FA-19 specimens. Specimens of the second type (FA-20) included some having 2 to 5 mil thick coatings deposited at 3000°F and others with thicker coatings, ranging up to 12 mils, deposited at 3200°F. The FA-20 specimens were also made by coating FA-19 specimens. Specimens of the third type are represented by the designation FX-5. This type has a thin 0.5 mil coating deposited at about 3000°F. The last two types (FA-11 and FA-17) were deposited on UO_2 fueled specimens at 2500°F. FA-17 specimens consist of a pyrolytic carbon coating on an FA-1 specimen. Before coating the FA-11 specimens, the UO_2 fueled graphite sphere was carbonaceously reimpregnated (Type FA-9) in order to raise its density. In general, better adherence of the pyrolytic carbon coating was found on the non-reimpregnated spheres (Type FA-17). A further description of these pyrolytic carbon surface coated specimens can be found in Table 2-1.

Photomicrographs of three types of pyrolytic carbon surface coatings are shown in Figures 3-11, 3-12 and 3-13. The FA-20 coating shown in Figure 3-11 is 5 mils thick. The typical conical growth patterns of pyrolytically deposited carbon can be seen in this picture which was taken under polarized light. Good bonding of the coating to the graphite body was achieved. However, a crack running parallel to the graphite surface can be noted. This type of cracking has been noted in a number of other samples of pyrolytic carbon coating and is due to stresses during fabrication arising from a difference in thermal expansion coefficient of the pyrolytic carbon coating and the graphite sphere. The FA-21 coating shown in Figure 3-12 is 50 mils thick and has purposely been prepared to be somewhat thicker than the FA-20 coating. Again, the conical growth patterns and the presence

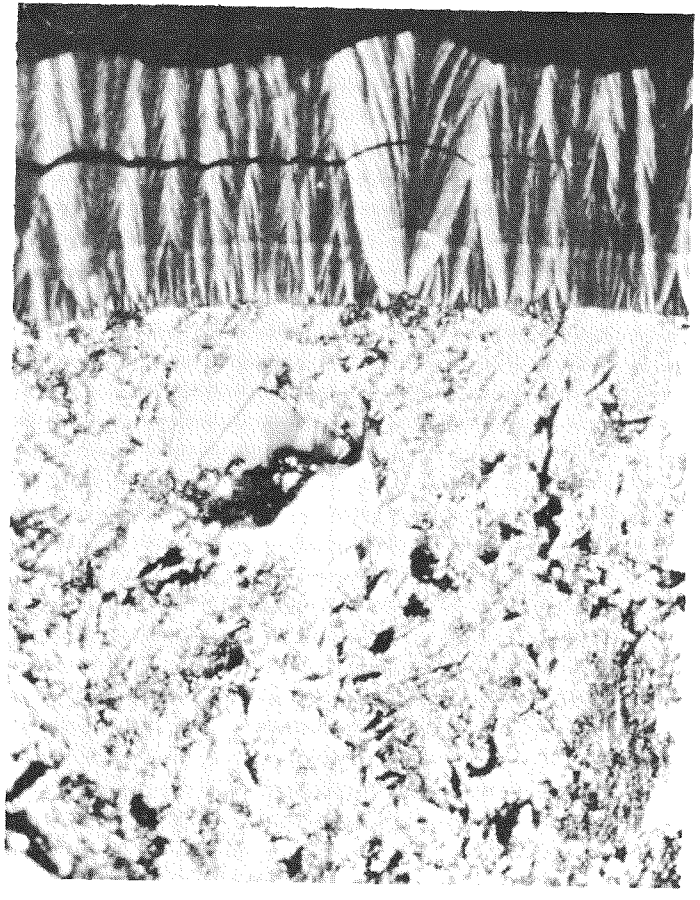

FIG. 3-11 Pyrolytic carbon coating on specimen type FA-20. View at 250x.

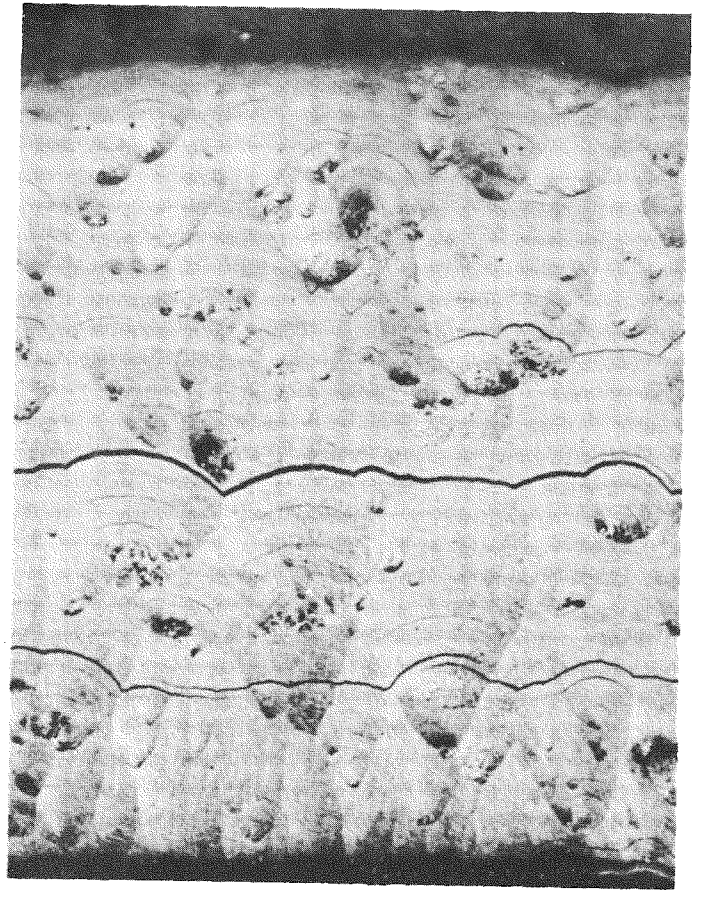

FIG. 3-12 Pyrolytic carbon coating on specimen type FA-21. View at 100x.

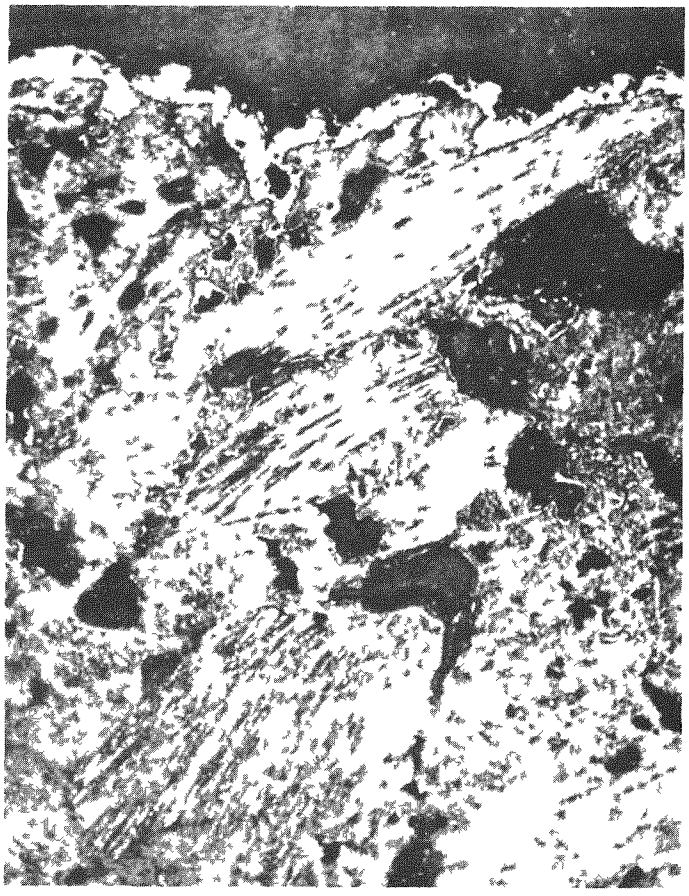

FIG. 3-13 Pyrolytic carbon coating on specimen type FX-5. View at 250x.

of cracks parallel to the base plane can be noted. The FX-5 coating shown in Figure 3-13 averages only 1/2 mil thick. As noted below, this coating was quite porous but more resistant to impact loads than the FA-20 and FA-21 types

3.2.1 Pre-irradiation Evaluation

All of the pre-irradiation tests on pyrolytic carbon surface coated specimens are given in this section.

Coating Permeability. Both of the FA-17 specimens and all twenty-one of the FA-20 specimens received for evaluation were found to pass the hot oil leakage test while only one of three FA-11 specimens were found to pass this test which illustrates the difficulty in achieving a tight pyrolytic carbon coating on a reimpregnated graphite base. Three of the four thicker-coated FA-21 specimens successfully passed the hot oil test with one specimen showing a single pinhole leak. One of the FA-21 specimens which passed the hot oil test had a number of carbon growths about 1/8 inch long protruding from its surface. When these carbon growths were removed by polishing, pinhole leaks were observed where most of the growths had been. The thin coatings on the FX-5 specimens were all found to be porous by the hot oil leakage test.

Uranium Contamination. Since the pyrolytic carbon is deposited directly on the fueled graphite surface, it was of interest to know whether uranium would migrate through the coating or otherwise contaminate the coating surface. A number of FA-11, FA-20 and FA-21 specimens were assayed for surface uranium contamination by alpha counting. The results are tabulated in Table 3-10. Occasionally, several spots on the sphere have been found to have a somewhat higher uranium contamination but on the whole, it can be seen that there is no serious uranium contamination of this type coating.

Abrasion Tests. Abrasion tests were run on four FA-20 specimens and two FX-5 specimens. The spheres were tumbled for 60 minutes inside a rotating drum which also contained some dummy graphite spheres. The abrasion test results are summarized in Table 3-11. As can be noted, there was more tendency for coating to flake off the spheres with the thicker coatings. Even though parts of the coatings flaked off specimen 342E, which had the thickest coating, it still did not leak. Some leaks appeared in the thinner coatings. These observations imply that the method of failure in these types of coatings is by chipping off of successive layers and that the innermost layer is most securely bonded to the graphite matrix.

TABLE 3-10

Surface Uranium Contamination of PyC Coated Specimens

Sphere No.	Equivalent Fraction of Total U in Sphere		
	Position 1	Position 2	Position 3
FA-11 (336N)	4.4×10^{-5}	-	-
FA-20 (330N)	7.0×10^{-5}	-	-
FA-20 (314N)	2.1×10^{-5}	-	-
FA-20 (399N)	2.1×10^{-6}	-	-
FA-20 (427N)	1.7×10^{-6}	-	-
FA-20 (431N)	5.9×10^{-7}	-	-
FA-20 (433N)	7.8×10^{-7}	-	-
FA-20 (435N)	1.4×10^{-6}	-	-
FA-20 (429N)	5.9×10^{-7}	7.8×10^{-7}	1.7×10^{-6}
FA-20 (338E)	7.1×10^{-7}	5.7×10^{-7}	7.1×10^{-7}
FA-20 (345E)	5.7×10^{-7}	6.3×10^{-7}	2.3×10^{-6}
FA-20 (325E)	4.8×10^{-7}	2.1×10^{-6}	3.2×10^{-7}
FA-20 (329E)	1.6×10^{-7}	8.8×10^{-6}	3.2×10^{-6}
FA-20 (344E)	1.6×10^{-7}	4.4×10^{-7}	nil
FA-21 (N1)	5.9×10^{-7}	7.8×10^{-7}	1.9×10^{-7}
FA-21 (N2)	1.9×10^{-7}	5.9×10^{-7}	nil

TABLE 3-11

Abrasion Tests on Pyrolytic Carbon Coated Spheres

Specimen No.	Coating Thickness, mils	Time in Hot Oil, Min	Hot Oil Test	Visual Inspection
FA-20(342E)	8.5	8	No leaks	Coating flaked and cracked
FA-20(427N)	2.7	10	Profuse leaks	Coating flaked
FA-20(431N)	2.3	10	Profuse leaks	Coating flaked
FA-20(435N)	4.1	10	Several small leaks.	No damage
FX-5(X3)	0.5	5	Several leaks[a]	No damage
FX-5(U1)	0.5	5	Several leaks[a]	No damage

(a) These specimens showed general porosity prior to the abrasion test.

Impact Tests. A summary of impact tests on pyrolytic carbon coated spheres is given in Table 3-12. With the FA-20 specimens, visual damage to the coating (i.e. chipping) and the appearance of a leak usually occurred at the same impact load. In one case (399N), the leak appeared at a higher impact load than required to flake off a portion of the coating. The point of impact failure on FA-21(N1) was "spongy" after the test which indicated that this coating consisted of numerous poorly bonded layers. The thin coatings on the FX-5 type specimens did not break away from the graphite matrix up to the point where the sphere broke. In most cases it was not possible to detect whether pinholes developed before the sphere broke due to the porous nature of this coating. All of these results generally confirm the observations noted in the abrasion tests.

TABLE 3-12

Impact Tests on Pyrolytic Carbon Coated Spheres

Specimen No.	Thickness, mils	Impact Load, Ft-lbs. Coating Failure		Graphite Failure
		Hot Oil Test	Visual	
FA-11 (50N)	5.0	1.1	1.1	-
FA-20 (353N)	2.0	3.6	3.6	-
FA-20 (433N)	3.4	1.7	1.7	-
FA-20 (399N)	4.2	2.2	2.0	-
FA-20 (326E)	9.3	1.1	1.1	-
FX-3 (44)	50	2.5	2.5	-
FA-21 (N1)	50	1.0	1.0	-
FX-5 (U1)	0.5	0.4	none	8.0
FX-5 (U2)	0.5	(a)	none	7.0
FX-5 (X3)	0.5	(a)	8.5	-
FX-5 (S)	0.5	(a)	7.5	-

(a) Leakage was too great to define coating failure.

Compression Tests. Three FA-20 specimens were subjected to a compression test. Specimen FA-20 (302N) failed at 2577 lbs. and 0.097" deflection. Specimen FA- 20 (435N) failed at 2830 lbs. and 0.182" deflection. Specimen FA-20 (342E) failed at 3275 lbs. and 0.200" deflection. Although these values are well above the desired compressive strength of 500 lbs., it was not possible to determine with certainty that there was no coating failure prior to sphere failure.

3.2.2 Irradiation Effects

Three pyrolytic carbon surface coated specimens were subjected to high level irradiation —— one in Capsule SP-4 and two in the static section of Capsule SP-5. The design and operating features of these Capsules are given in Section 8.0. The hot cell results for the specimens in Capsule SP-5 were taken from ref. (21).

A summary of the operating conditions and the results of the post-irradiation examinations are given in Table 3-13. In general, the hot cell examinations included visual examination, hot oil testing, weight change, dimensional change, and metallography.

TABLE 3-13

Capsule Irradiation Results for Pyrolytic Carbon Surface Coated Specimens

Capsule No.	SP-4	SP-5	SP-5
Specimen No.	FA-20(336E)	FA-20(338E)	FA-20(345E)
Coating Thickness, inches	.002	.0095	.0125
Coating Deposition Temp, °F	3000	3200	3200
Specimen Power, KW/Ball	2.0	1.3	0.8
Temperature, °F			
Surface	1550	1360	1360
Center	1750	1460	1420
Burnup, KWH/Ball	6700	4500	2700
Weight Change, %	+0.19	+0.02	0.0
Diameter Change, %	-0.4	-1.2	-0.7
Passed Hot Oil Test	No	No	Yes
Visual Appearance	Several fine cracks	Several fine cracks	No Visible defects

Visual Examination. The post-irradiation appearance of the pyrolytic carbon was clean and shiny as was the pre-irradiation appearance. Fig. 3-14 and 3-15 are views of the same location on the surface of specimen FA-20 (338E) taken before and after irradiation. No change in the appearance of the pyrolytic carbon can be noted. Similar cracks were noted in specimens 336E and 338E. They consisted of several parallel hairline cracks running almost entirely around the specimen. A typical view of these cracks is seen in Figs. 3-15 and 3-16. There was no evidence of any defect in specimen FA-20(345E).

FIG. 3-14 View of Pyrolytic Carbon Coating on FA-20(338E) Before Irradiation.

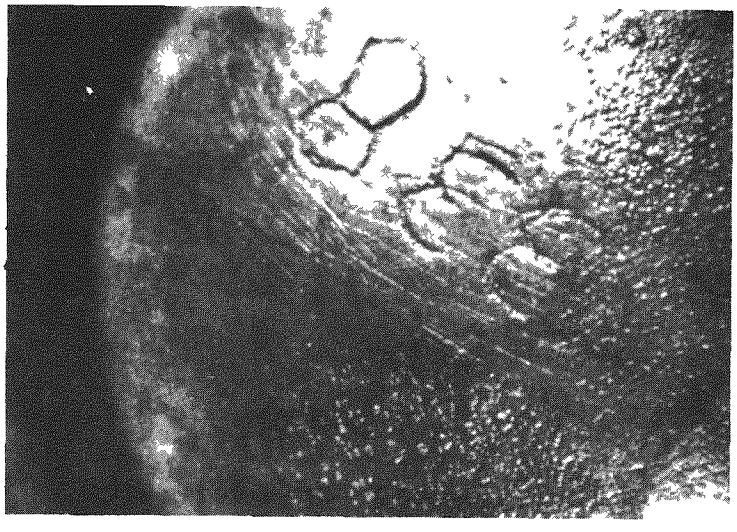

FIG. 3-15 View of Pyrolytic Carbon Coating on FA-20(338E) After Irradiation.

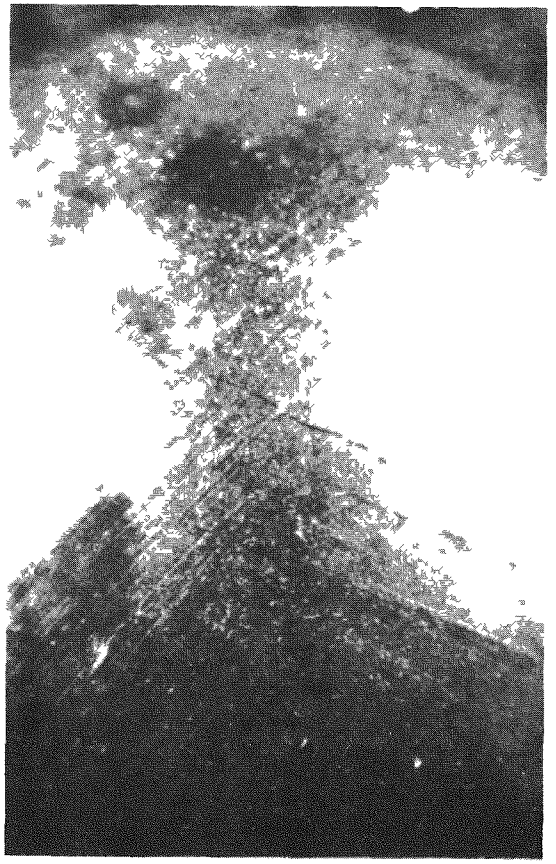

FIG. 3-16 Cracks in surface of pyrolytic carbon coated specimen FA-20 (336E) after irradiation in Capsule SP-4. View at 4x.

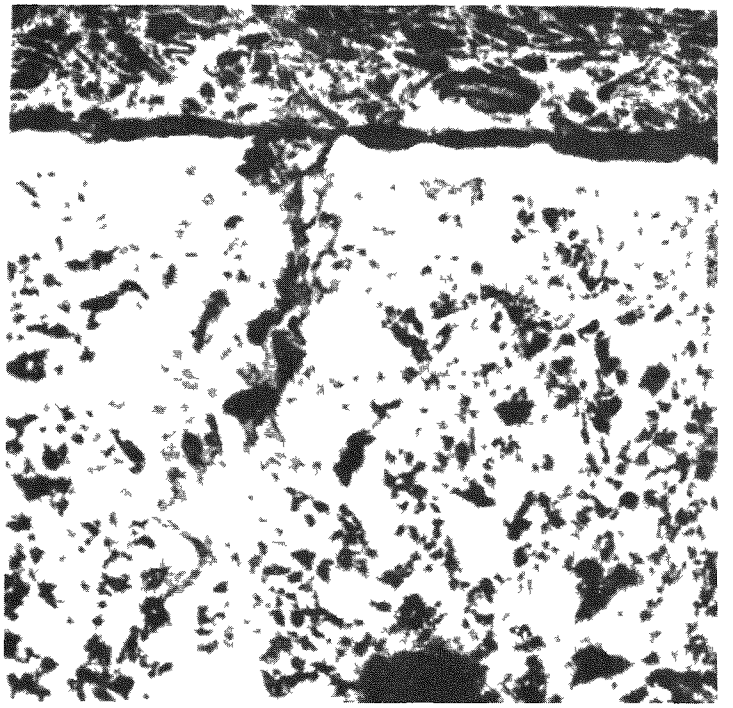

FIG. 3-17 One of the cracks in the surface of pyrolytic carbon coated specimen FA-20 (336E) after irradiation in Capsule SP-4. View at 100x.

Hot Oil Tests. The cracked specimens 336E and 338E were found to bubble profusely from their cracks when immersed in hot silicone oil. There appeared to be some slight leakage in areas removed from the crack region. However, this could not be definitely confirmed due to the profuse bubbling from the cracks. Specimen 345E showed occasional indications of very fine bubble streams which may have actually been eddy currents in the oil.

Weight and Dimension Measurements. The weight and dimension changes for these specimens were given in Table 3-13. The slight weight gains noted for the cracked specimens could be primarily due to readsorption of atmospheric gases. The dimensional changes on all the FA-20 specimens were larger than the changes noted for the Si-SiC coated specimens in Table 3-4 and all the FA-20 dimensional changes were negative. These factors support the view that an irradiation induced shrinkage occurred in the graphite matrix and possibly in the pyrolytic carbon coating.

Metallographic Examination. Specimen FA-20(336E) was mounted in plastic and sectioned in order to learn more about the hairline cracks which occurred in its coating. Fig. 3-17 is a photomicrograph of a section through the coating. One of the cracks can be seen in this view. The coating appears to have separated. A surface crack in the graphite beneath the coating can also be seen. Cracks of this type have not been previously noted in the surface of uncoated graphite and it is possible that strains in the coating actually caused this crack in the graphite. Due to the orderly nature of the cracks, the most likely cause is an anisotropic radiation induced dimensional changes in the graphite sphere.

3.2.3 Fission Product Retention

Pyrolytic carbon surface coated specimens were subjected to neutron activation tests and one furnace capsule irradiation as described below.

Neutron Activation. A summary of all neutron activation tests on pyrolytic carbon surface coated specimens is given in Table 3-14. The coating thicknesses and coating deposition temperatures are also shown. The Xe 133 release from specimens FA-11(298N) and FA-20(310N) steadily increased with time as seen in Fig. 3-18 which is a plot of fraction of Xe 133 release as a function of time for FA-20(310N). However, essentially no Xe 133 was released from the subsequent pyrolytic carbon coated specimens. This indicates a much lower permeability for pyrolytic carbon coatings deposited above 3000°F.

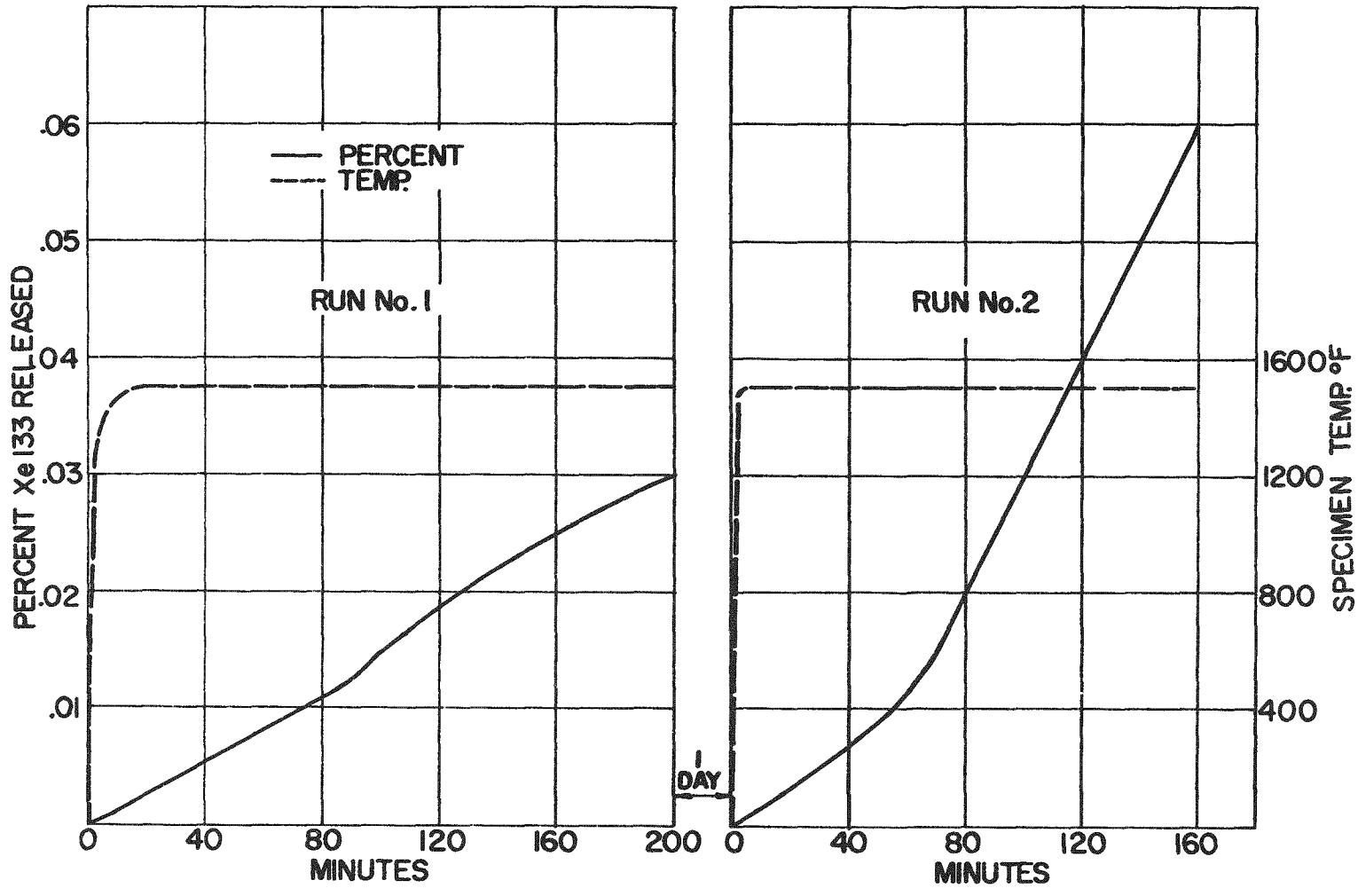

FIG. 3-18 Neutron Activation Data for Specimen FA-20(310N)

TABLE 3-14

Neutron Activation Tests on Pyrolytic Carbon Surface Coated Specimens

Specimen No.	Coating Th[a]	Coating DT[b]	Test Temp, °F	Time at Temp, min.	Fraction of Xe 133 Released
FA-11(298N)	5	2500	1500	220	7×10^{-4}
			1500	110	8×10^{-4}
FA-20(310N)	2	3000	1500	200	3×10^{-4}
			1500	158	6×10^{-4}
FA-20(429N)	4.9	3200	1700	70	$<4 \times 10^{-5}$
			2200	100	$<4 \times 10^{-5}$
FA-20(338E)	9.5	3200	1900	180	$<9.3 \times 10^{-7}$
FA-21(N2)	50	3400	1650	75	$<4 \times 10^{-5}$
			2300	80	4×10^{-5}

(a) Th = Coating thickness, mils
(b) DT = Pyrolytic carbon deposition temperature, °F.

Furnace Capsule. An experiment on the continuous release of fission products from specimen FA-20(310N) was conducted in Furnace Capsule SPF-1. The design of this type of capsule is described in Section 8.2. The specimen was operated at temperatures ranging from 150°F to 1900°F. The leakage factors for five long-lived gaseous fission products are summarized in Table 3-15.

TABLE 3-15

Summary of Fission Product Release From Specimen FA-20(310N) in Furnace Capsule SPF-1

Specimen Temp.	R/B, (Release Rate/Production Rate) Kr 85m	Kr 87	Kr 88	Xe 133	Xe 135
150°F	.00038	.00016	(a)	.0046	.0015
1000°F	.0043	.0023	.0038	.0057	.0039
1500°F	.016	.013	.016	.041	.009
1900°F	.026	.0107	.0224	.067	.019

(a) Not measured.

The results with specimen FA-20(310N) in both the neutron activation and the furnace capsule tests indicate that there was a measurable diffusion of fission products through the pyrolytic carbon coating. It is of interest to attempt mathematical correlations for this type of experiment since only a single controlling mode of diffusion (i.e. through the surface coating) is present rather than the multiple paths for leakage from an uncoated specimen. Equations for the diffusion of fission products through coatings on spherical fuel elements were developed by Battelle Memorial Institute and an outline of this development was given in ref. (4).

For post-irradiation release of fission products, the following equation was derived:

$$\frac{R}{M} = \frac{3\,Df}{ah}\phi$$

For continuous release of fission products during irradiation, the following equation was derived:

$$\frac{R}{B} = \frac{3f}{a\sqrt{\lambda/D}\,\sinh\,(h\sqrt{\lambda/D}) + 3\cosh\,(h\sqrt{\lambda/D})}$$

where R = Rate of release from coating, atoms/sec
M = Concentration in sphere, atoms.
B = Rate of production in sphere, atoms/sec.
f = Recoil fraction from fuel particle to graphite matrix.
D = Diffusion coefficient, cm^2/sec.
a = Sphere radius, cm.
h = Coating thickness, cm.
λ = Isotope decay constant, sec^{-1}.
ϕ = Function of D, h, and time of post-irradiation heating.

These equations were used to solve for D, the diffusion coefficient for the coating, employing both the neutron activation and furnace capsule data. Based on neutron activation data, values of D were found to be 1.1×10^{-8} for the FA-11 specimen and 2.4×10^{-9} for the FA-20 specimen. The results from the furnace capsule data are shown in Fig. 3-19 where D is plotted against the reciprocal of the absolute temperature.

The higher diffusion coefficient for the FA-11 specimen compared with the FA-20 specimen in neutron activation tests could indicate that the lower deposition temperature for the FA-11 specimen resulted in a

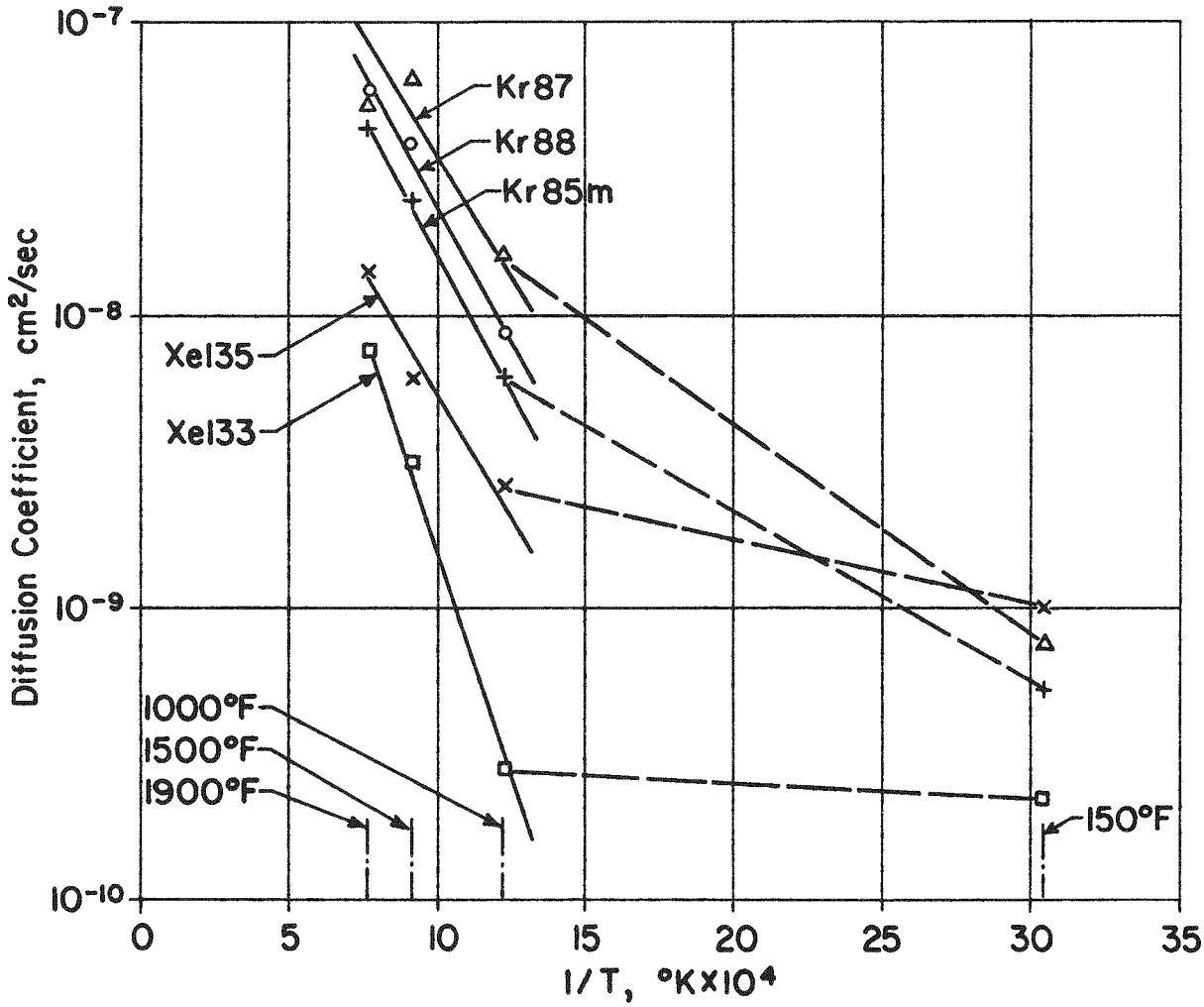

FIG. 3-19 Fission Product Diffusion Coefficients for Pyrolytic Carbon Coating on Specimen FA-20 (310N) in Capsule SPF-1.

higher permeability. Rather good agreement can be noted between the diffusion coefficient for specimen FA-20(310N) calculated from neutron activation data and the corresponding value for Xe 133 at 1500°F of 3.1×10^{-9} calculated from furnace capsule data. Fig. 3-19 shows a rather good correlation for the 1000°F, 1500°F, and 1900°F data but not for the 150°F data.

Furnace Capsule SPF-1 was first operated at 1500°F. The capsule was then shut down for 6 weeks for modifications to the off-gas train which would permit unattended capsule operation. After recommencing operation, the order of the temperature runs was 1000°F, 1900°F, and 150°F. Suspiciously high leakage rates had been noted during the 150°F run. Consequently it was decided to open Capsule SPF-1 in the Hot Cell in order to examine the specimen.

Upon removal of the specimen from the capsule, a large number of pits were readily visible in the surface of the specimen as shown in Fig. 3-20. The pits are seen to be largely concentrated in one region of the specimen. They had the appearance of corrosion pits in metal. Many of the pits appeared to be undercut, that is, the underlying graphite had been removed to a greater extent than the pyrolytic carbon surface coating. From these observations, it was concluded that the sweep helium stream for transporting fission products from the specimen to the trapping system must have become contaminated with oxygen or moisture. Although the gas stream was not analyzed for contaminants, some difficulty had been experienced in shakedown testing during the 6 week shutdown following the 1500°F run. The cold traps tended to plug due to excessive moisture believed to come from the particular helium tank in use at the time. It is probable that the rate of attack did not become excessive until the 1900°F run, causing the significant release rates during the subsequent 150°F run.

This experience with Capsule SPF-1 had indicated that excessive rates of attack could occur to pyrolytic carbon coatings if the primary coolant stream of the reactor should become contaminated with moisture from a boiler tube rupture. The fission product release data from Capsule SPF-1 prior to the 150°F run is thought to be valid, however, for a 3000°F pyrolytic carbon coating such as on FA-20(310N). From the neutron activation data, it appears that even greater fission product retention can be achieved with pyrolytic carbon coatings deposited above 3000°F.

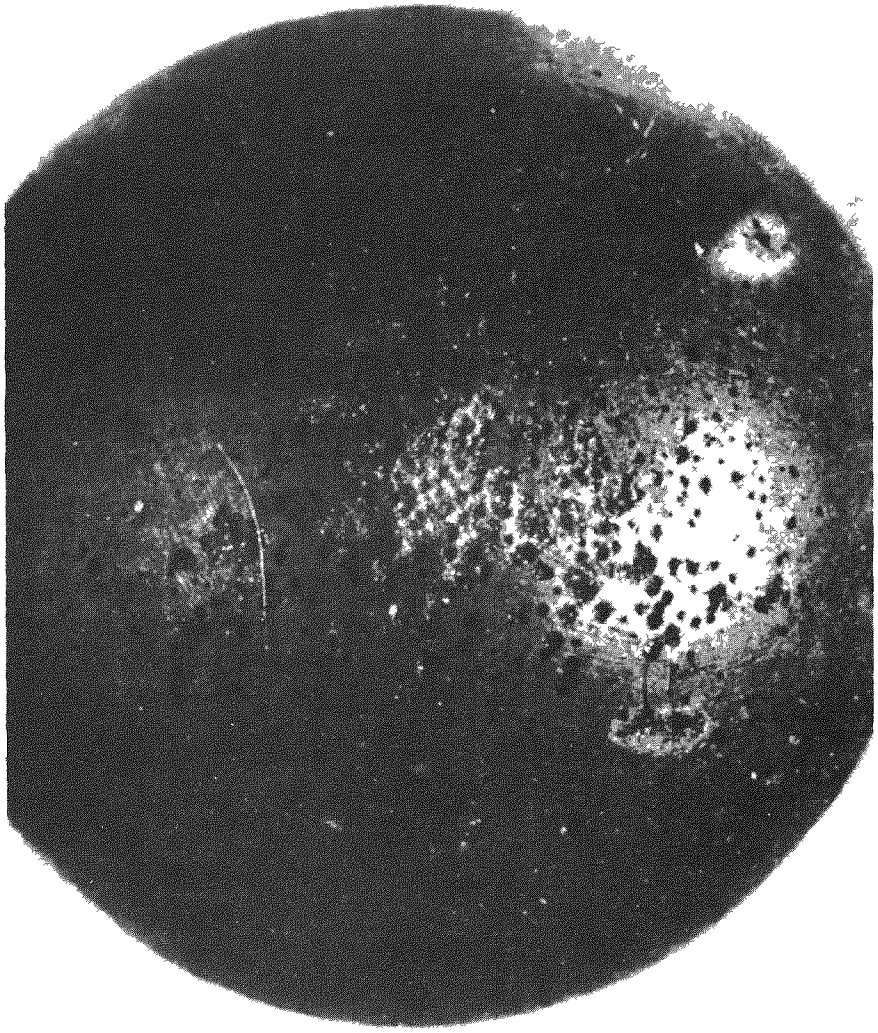

FIG. 3-20 Corrosion pits in surface of pyrolytic carbon coated specimen FA-20 (310N) after exposure in Furnace Capsule SPF-1.

4.0 Alumina Coated Fuel Particles

Another method of retaining fission products in a uranium-graphite fuel element is to place a coating on each individual fuel particle of an admixture type element. There are several advantages of coatings on fuel particles. Fission products are retained at their source. The coating material is not subjected to such external loads as impact, compression, or abrasion, nor such internal loads as thermal stress which are normally applied to a PBR fuel element. The fracture of a PBR fuel element will not expose uncoated fuel particles, thus fission product retention will be maintained. There should be a minor beneficial effect on manufacturing costs since the graphite fabricator will not have to handle exposed fuel. There may well be an advantage in reprocessing in that the graphite matrix can be removed and disposed of with little regard for the contained uranium and fission products inside the particle coatings.

The first development work on coated fuel particles, involving a sintered alumina coating for UO_2 particles, was proposed by the Battelle Memorial Institute (4). This process consisted of preparing fuel particles from a sintered grade urania powder, dusting the fuel particles with a sinterable grade alumina powder while in a pelletizing drum, isostatically pressing the coated particles and then sintering them. A typical coated particle produced by this process can be seen in Fig. 4-13. The main problems with this type of coated particle were the lower sintering shrinkage of UO_2 compared with the alumina coating, and reproducibility, particularly when thinner coatings (i.e. in the range of coating thickness equal to the fuel particle radius) are employed. A number of variations in the fuel particle were tried. These included the use of UO_3, mixtures of UO_3 and UO_2, and the addition of alumina monohydrate to the starting UO_2 powder. The best solution to the differential shrinkage problem was found to be the addition of 65 w/o UO_3 to the UO_2. However, it was found that reproducibly good coatings could only be made with excessive coating thicknesses (i.e. coating thickness equal to the fuel particle diameter). Consequently, this work on sintered alumina was abandoned in favor of another process proposed by Battelle.

This new process, known as vapor deposited alumina, was first attractive because extremely thin coatings (i.e. 10 microns and less) could be produced and the material appeared dense and impermeable. Subsequent development work and irradiation test results obtained showed that this was indeed a most promising type of coating. The work on alumina coated UO_2 described in the following sections all relates to vapor deposited alumina, except where specifically noted.

4.1 Coated Particle Fabrication

The process for applying vapor deposited alumina coatings on UO_2 particles was performed at Battelle in a fluidized bed. The apparatus used for all work reported herein was a 1" diameter externally heated quartz tube having a conical bottom to support the bed of UO_2 particles. The particles were fluidized by a hydrogen stream containing aluminum chloride vapor. An additional stream of hydrogen is introduced into the lower part of the bed through a water vaporizer. About 50% of the alumina formed by hydrolysis at approximately 1800°F is deposited on the surfaces of the UO_2 particles. The remainder of the alumina passes out of the reaction vessel as fines along with the by-product HCl. Measurement of HCl production is used to follow the alumina production rate. The convenient batch size for the experimental apparatus is 100 gms of UO_2. High-fired UO_2 spherical shot was used for practically all of the runs.

Uranium contamination of the coating by UO_2 dusting during the initial stages of fabrication is minimized by stopping the process after several microns of alumina have been deposited, rinsing both the particles and the reaction vessel, and restarting the process. When large coating thicknesses are desired, volumetric expansion of the coated particle bed limits the run, making it necessary to split the batch in half and continue coating each half in separate runs.

The large number of particle collisions during the fluidized coating process, each tending to form a new growth site, is believed to be a major factor in forming the dense coating. No sintering step is required after the fluidization process. The deposition temperature is perhaps the most important process variable. In the 1800°F to 2000°F range, a dense impermeable alpha-phase alumina is formed while at a lower temperature a porous coating is formed. A further description of the manufacturing process used at Battelle is given in reference (10).

A summary of all alumina coated UO_2 particles made to date is given in Table 4-1. Batches which have been used to fuel graphite spheres are also indicated. Batches 1B through 11C were made at Battelle. Batch 12H was obtained from the Nuclear Materials & Equipment Corp.

TABLE 4-1

List of Alumina Coated Particles and Fueled Graphite Spheres

Batch No.	UO_2 Size, μ	Uranium Enrich.	Coating Thick, μ	Deposit. Temp., °F	No. of Spheres
1B	105/149	Nat.	20	1830	3
2A	105/149	Nat.	38	1830	2
3C	105/149	Nat.	50	2010	0
4E	105/149	Enr.	55	1830	3
5D	250/420	Dep.	40	2010	0
6F	105/149	Enr.	42	1830	0
6H	105/149	Enr.	48	1830	5
6J	105/149	Enr.	66	1830	0
7H	105/149	(a)	40	1830	0
7J	105/149	(a)	44	1830	0
8G	297/350	Nat.	150	1380(b), 1830	0
9	105/149	Nat.	14	1830	0
9A	105/149	Nat.	26	1830	0
11C	105/149	Enr.	59	1380(b), 1830	0
12H(c)	105/149	Nat.	40	1830	0

(a) Particle composition was ThO_2 and UO_2 in 11:1 ratio.
(b) 20 microns of porous Al_2O_3 was deposited at this temperature.
(c) Made by NUMEC, all other types made by BMI.

Batches 1B and 2A. These were the first batches of alumina coated UO_2 made for the PBR Fuel Element Development Program. Batch 1B was prepared in 3 stages and was subjected to a nitric acid leach after the first stage (9 microns) to remove uranium contamination. Batch 2A was prepared by making two additional runs on batch 1B. Particles from Batch 1B are seen in Fig. 4-1 and particles from batch 2A are seen in Fig. 4-2. All runs were done at 1830°F. No evidence of laminations between the successive runs can be noted. The dense continuous appearance of the particles on all coatings was most encouraging.

Batch 3C and 5D. Two variables were studied in these batches. A higher deposition temperature (2010°F) was used for batch 3C and both the 2010°F deposition temperature and larger particles were used in batch

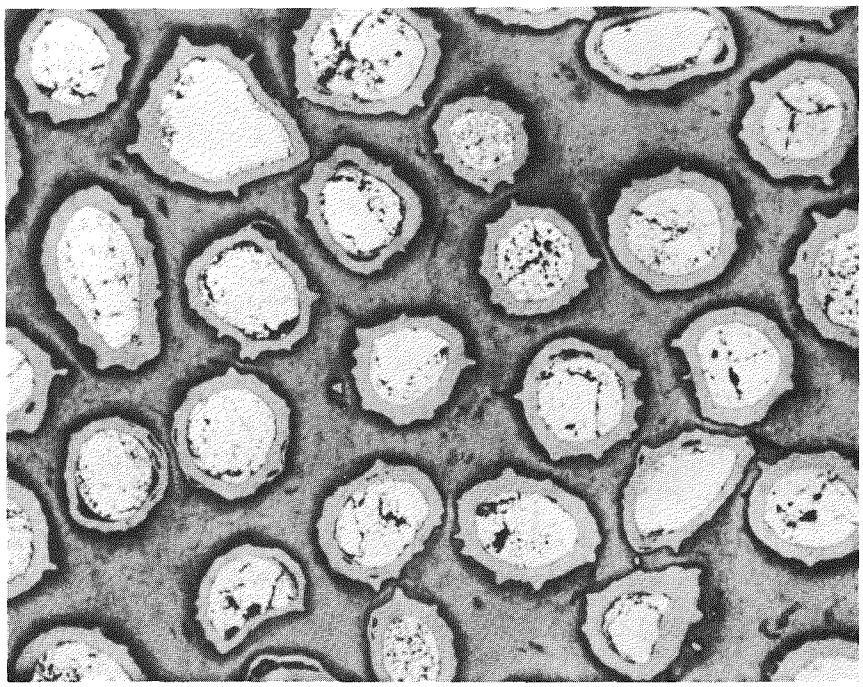

FIG. 4-1 Al_2O_3 coating on UO_2, from batch No. 1B 100x

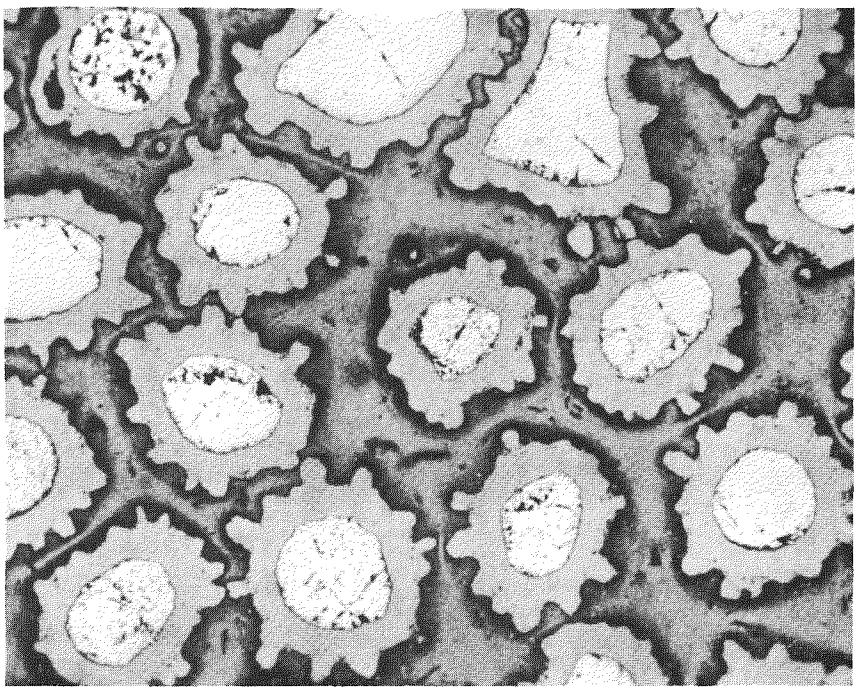

FIG. 4-2 Al_2O_3 coating on UO_2, from batch No. 2A 100x

5D. A greater amount of included porosity was noted in batch 3C as seen in Fig. 4-3. The porosity does not appear to be interconnected in the radial direction but does appear to be oriented parallel to the coating surfaces. The UO_2 used in batch 5D was somewhat irregular in shape as seen in Fig. 4-4. More evidence of included porosity can be noted. In spite of the angular nature of the UO_2, all surfaces are uniformly coated.

Batch 4E. This batch of enriched UO_2 shot was coated for high level irradiation testing. Particles from this batch were eventually incorporated into the FA-22 specimens which were irradiated in Capsule SP-5. Figure 4-5 shows a 500X view of a particle from this batch together with a 5000X picture which was taken in order to study the structure of the coating in more detail. The dark band in the coating is now believed to be a porous alumina region which was inadvertently deposited during the fabrication of this batch. In the 5000X view, the dense and continuous band of impermeable alumina can be noted between the UO_2 and the porous alumina. Grain boundaries can be clearly noted in the UO_2. The absence of such boundaries in the alumina phase is the major reason why this type of coating has shown such good fission product retention.

Batch 6F, 6H, and 6J. These batches containing enriched uranium were made in order that additional fueled graphite spheres could be prepared for irradiation in the in-pile loop (see Section 9.0). A single batch of enriched UO_2 particles was first coated with 23 microns of alumina in 3 steps. The batch was then split with batch 6F being produced in 3 more runs on one half and batch 6H being produced in 2 more runs on the other half. Batch 6J, which approaches the maximum thickness to diameter ratio considered for use in the PBR, was prepared by making two additional runs on a portion of batch 6F. Fig. 4-6 is a photomicrograph of particles from batch 6F where the good bonding between successive coating runs is apparent by the lack of any visible interfaces within the coating.

Batch 7H and 7J. Thoria-urania particles were used in batches 7H and 7J to determine whether there would be any unanticipated effects due to the presence of thoria. The nominal 11:1 Th/U atom ratio used in these particles resulted from a design study of a 125 eMW Pebble Bed Reactor Steam Power Plant (1). A single batch of ThO_2/UO_2 particles was first coated with 24 microns of alumina in 5 steps. After splitting this batch, 3 more runs were made on each half to produce batches 7H and 7J. A photomicrograph of a typical batch of coated particles from batch 7H is seen in Fig. 4-7. Although the ThO_2/UO_2 particles are somewhat irregular, all particles are seen to be adequately coated with no evidence of gaps between successive coating layers.

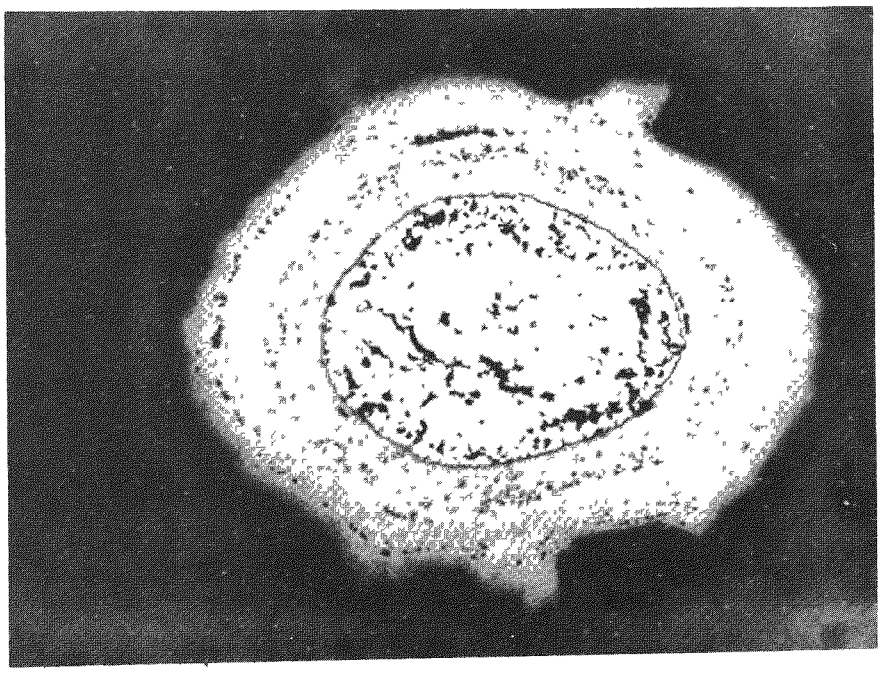

FIG. 4-3 Al_2O_3 Coating on UO_2 from Batch No. 3C. (250X)

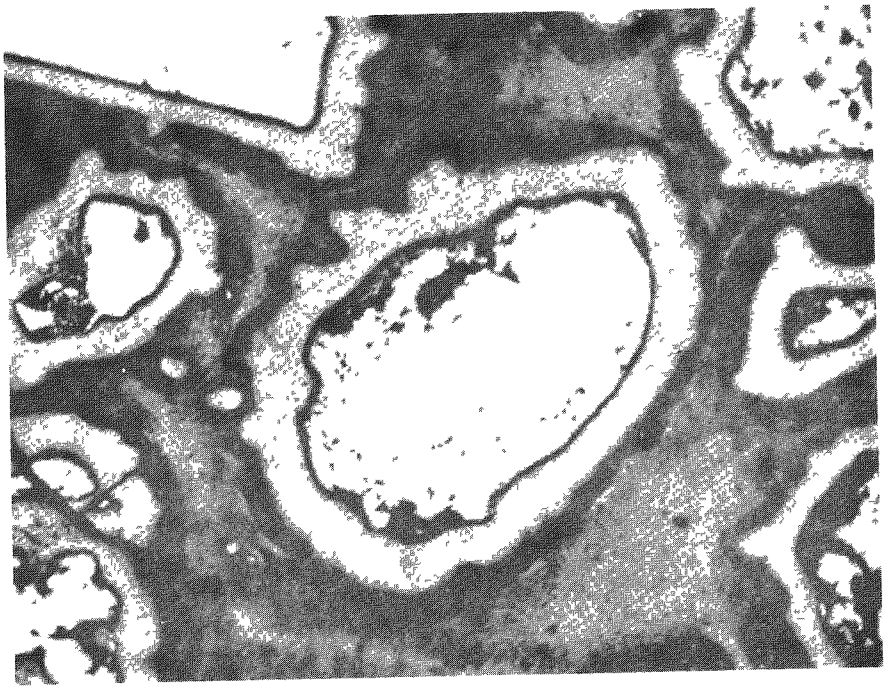

FIG. 4-4 Al_2O_3 Coating on UO_2 from Batch No. 5D. (100X)

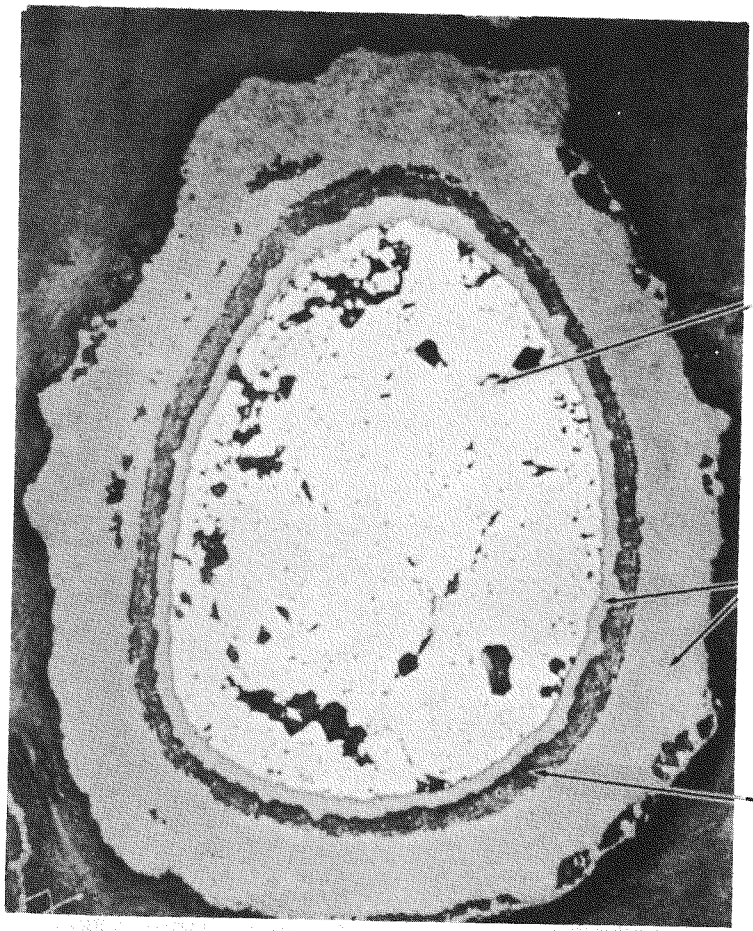

Al_2O_3 coated UO_2 particle from Batch 4E (500X).

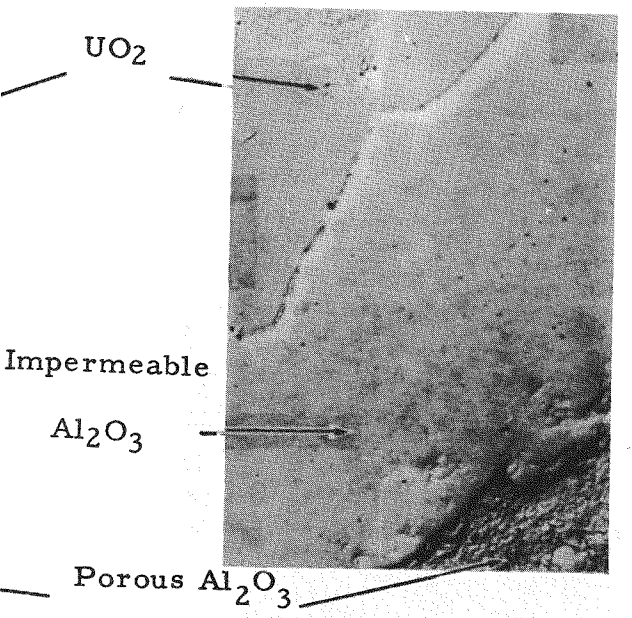

5000X magnification at Al_2O_3-UO_2 interface. Unetched.

FIG. 4-5

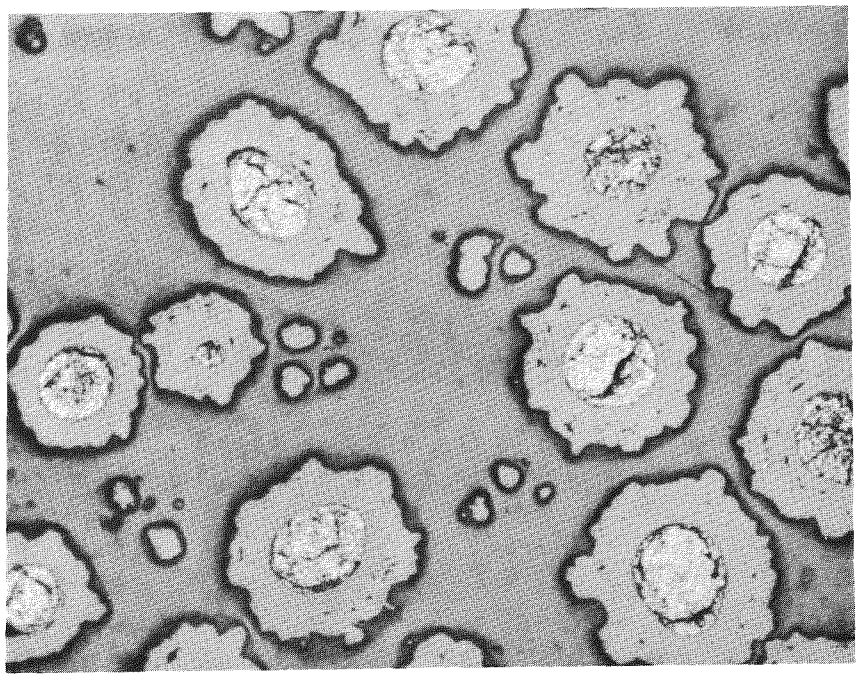

FIG. 4-6 Al_2O_3 Coating on UO_2, from batch 6F. 100x

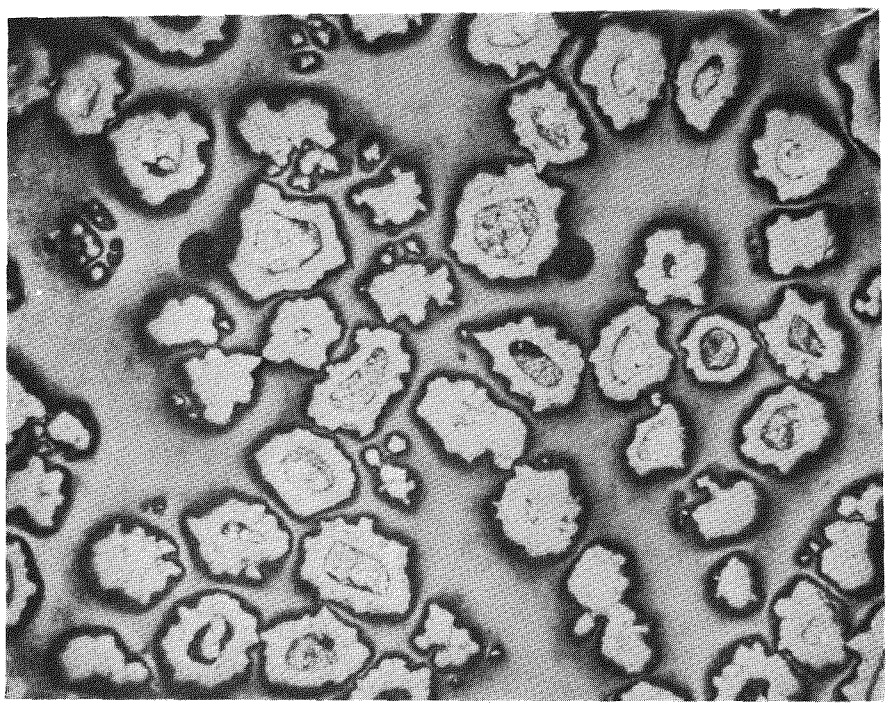

FIG. 4-7 Al_2O_3 Coating on ThO_2/UO_2 from batch 7H 50x

Batch 8G. This batch was prepared with two special features in mind: (1) a large UO_2 particle was used (297/350 micron) so that a thick coating could be applied and not exceed limitations on carbon moderator displacement when dispersed in a graphite sphere, and (2) a porous inner layer of alumina was used which would have the advantage of providing a reservoir for fission gases and a cushion to prevent thermal cycle fracture of the outermost impermeable alumina coating. A thin 2 micron coating was first deposited at 1830°F so that any uranium contamination arising from dusting of the bare UO_2 particles during the early stages of fluidization could be leached away. Next, a 20 micron layer of porous Al_2O_3 was deposited at 1380°F. Additional impermeable alumina was deposited at 1830°F until a total alumina thickness of 150 microns was reached. 5 gm. samples were removed from the batch at coating thicknesses of 30, 50, 77, 106, 122 and 150 microns in order to evaluate the effect of coating thickness on thermal cycle rupture. Fig. 4-8 shows a particle from batch 8A which has been coated with only the thin impermeable layer and the porous layer of alumina. Fig. 4-9 shows several particles from the final batch, 8G. The dark band near the UO_2 particle is the porous alumina. Some evidence of annular porosity in the UO_2 particles can be noted. Occasional growths of alumina can be seen to protrude from the outer surface of the coating. In several instances, a dust particle inclusion can be noted at the base of alumina growths. Similar growths have been noted in pyrolytically deposited carbon coatings which were also believed to arise from soot particles.

Batches 9 and 9A. These batches were prepared in order to explore the effect of faster deposition rate on coating integrity. All previous batches were prepared at a deposition rate of about 6 gms/hr which would not cause excessive plugging of the exhaust system by Al_2O_3 fines. This rate was increased to 12, 24, and 48 gms/hr as a result of improvements in operating procedure and equipment design. No difficulties were experienced at 12 gms/hr (Batch 9). At 24 gms/hr (Batch 9A), a plug formed at the top of the reaction vessel after several hours of operation. Further plugging was observed at 48 gms/hr.

Batch 11C. This batch was prepared with fully enriched UO_2 and was intended to be a duplicate of batch 8G, containing a porous inner layer of Al_2O_3. A supply of irregularly shaped enriched UO_2 was used because of the extended delivery time for large spherical shot. After 59 microns has been deposited, it was noted that portions of the coatings on many of the particles had chipped off. Efforts were made to weed out the faulty particles by leaching and thermal cycling but this did not help. This type of difficulty is believed due to the combinationof the porous inner layer on irregularly shaped particles. Further coating of this batch was abandoned.

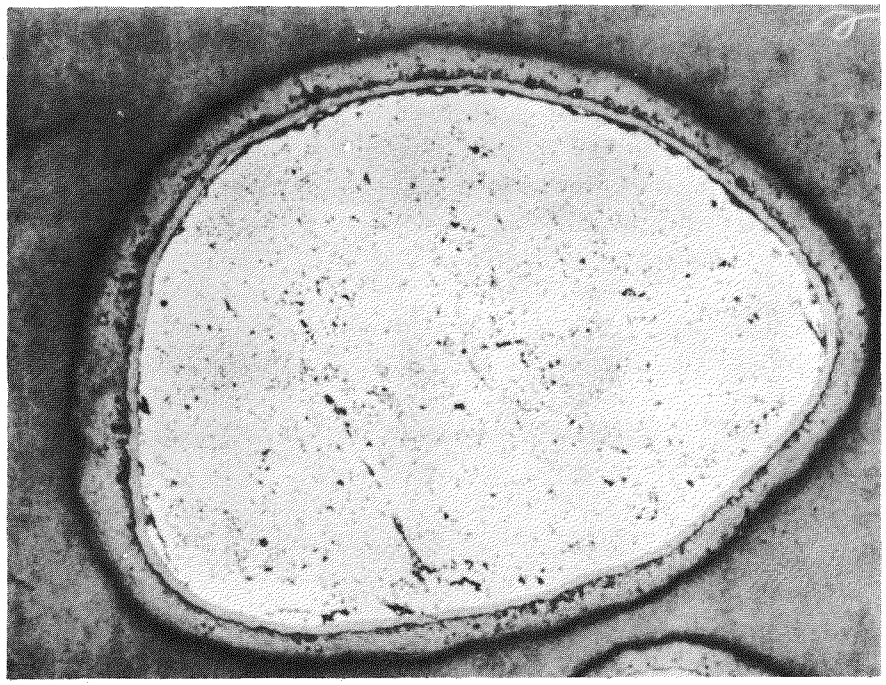

FIG. 4-8 Batch 8A showing thin impermeable layer of Al_2O_3 and porous layer of Al_2O_3 on UO_2 particle (500X).

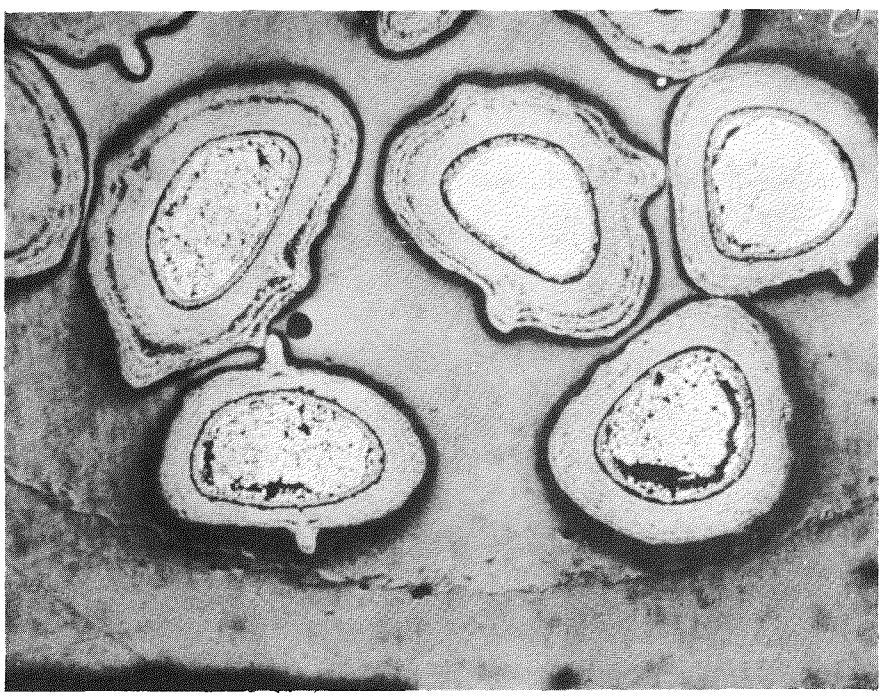

FIG. 4-9 Batch 8G showing Al_2O_3 coating with porous inner layer on UO_2 (50X).

Batch 12H. This batch was obtained from the Nuclear Materials & Equipment Corp. The same vapor deposition technique at 1830°F as previously described was used except that a rotating kiln was used in place of a fluidized bed. The 40 micron coating was deposited in eight steps. Figure 4-10 shows sections of the particles from batch 12H. The coatings appear dense and continuous with no evidence of gaps between successive layers of coatings.

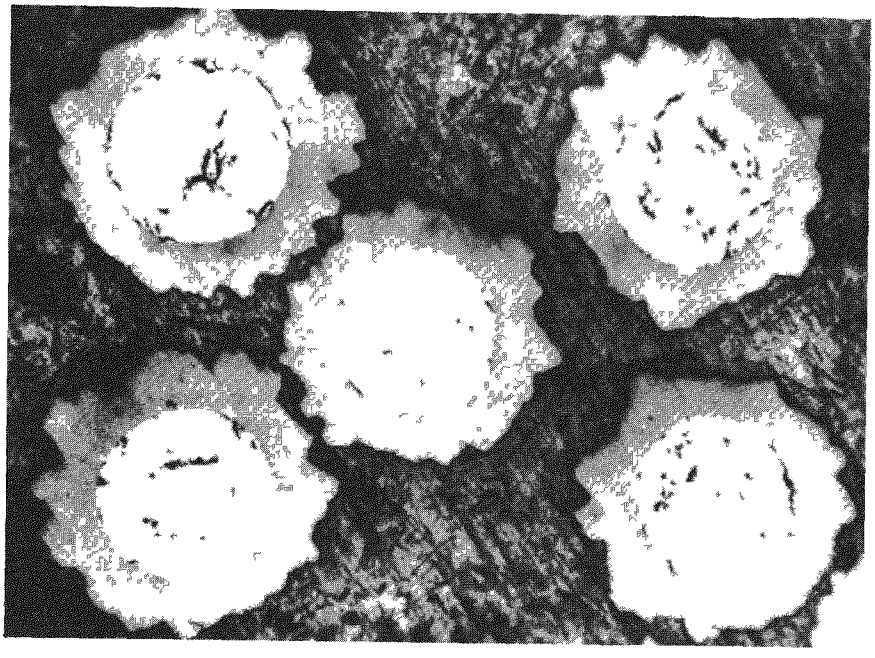

FIG. 4-10 Al_2O_3 Coating on UO_2 from Batch No. 12H. (100X)

4.2 Pre-Irradiation Evaluation of Coated Particles

A number of standard screening tests are used for alumina coated fuel particles. In general, each batch of particles which has been fabricated is subjected to the following tests:

1. Alpha Assay: Uranium contamination on the surface of the particles is detected by placing a thin layer of the coated particle in a 2π proportional gas flow counter and measuring the alpha emission rate.

2. Coating Integrity: Coated particles are exposed to air at 1200°F. Any faults in the coating cause the underlying UO_2 to be oxidized to U_3O_8 which further ruptures the coating due to expansion of the fuel particle. Thus, weight gain after this test is a measure of lack of coating integrity. An entire batch of particles can be subjected to this test so that exposed uranium can be subsequently removed from faulty particles by leaching.

3. Thermal Cycling: Particles are thermal cycled between room temperature and 2500°F in an inert atmosphere to determine whether the slightly higher expansion coefficient of UO_2 as compared with the alumina coating will cause the coating to fail when the particle is heated above its fabrication temperature.

4. Metallographic Examination: Routine metallography is done up to 500X. On occasion, electron microscopy is used for more detailed study.

Table 4-2 is a summary of pre-irradiation test results on Al_2O_3 coated particles. The most striking results are from the coating integrity tests where uniformly good coatings were found for every batch. Even in the later batches where the entire batch was subjected to the hot air oxidation test, extremely small weight changes were found. In earlier work with other types of particle coatings, weight gains as high as 10% to 50% were often found in similar tests. The weight loss reported for some batches is due to further devolatilization of adsorbed air and moisture.

Since the thermal expansion coefficient of UO_2 (10×10^{-6}/°C) is slightly higher than for Al_2O_3 (8.5×10^{-6}/°C), it was of interest to learn whether heating the coated particles above their fabrication temperature would rupture the Al_2O_3 coatings. A top temperature of 2500°F was selected for the thermal cycle tests because this appeared to be the upper limit due to reaction between Al_2O_3 and graphite. The first thermal cycle test was run on batch 2A and was done in air. The alpha count was found to increase

TABLE 4-2

Pre-irradiation Tests on Alumina Coated Fuel Particles

1. Batch No.	1B	2A	3C	4E	5D	6F	6H	7H	7J	8G	9	9A	12H
2. UO_2 Size, μ	105/149	105/149	105/149	105/149	250/420	105/149	105/149	105/149	105/149	297/350	105/149	105/149	105/149
3. Coating Thickness, μ	20	38	50	55	40	42	48	40	44	150(f)	14	26	40
4. UO_2 Content, w/o	71.0	48.9	32.6	36.0	66.1	27.3	26.6	35.4(e)	34.5(e)	42.8	-	-	43
5. As Fabricated													
(a) Alpha assay (a)	7.3 ± 1.3	1.4 ± 1.0	0.8 ± 0.8	20.7 ± 2.5	0.2 ± 0.8	0.4 ± 1.2	0.4 ± 1.2	2.0 ± 0.4	0.5 ± 1.0	1.0 ± 0.6	-	-	0.0 ± 1.3
(b) Exposed U(b)	1.5×10^{-5}	4.5×10^{-6}	4.0×10^{-6}	3.0×10^{-5}	4.5×10^{-7}	4.5×10^{-7}	4.5×10^{-7}	9.0×10^{-6}	2×10^{-7}	3.5×10^{-6}	-	-	0.0
6. Coating Integrity (c)													
(a) Sample Wt, gms	19.66	5.0	28.1	61.6122	2.81	109	125	89	132	162	-	-	5
(b) Weight Change, gms	-.0027	nil	+.10	-0.0343	-.001	+.0004	- 0410	-.0005	nil	+.0005	-	-	+.0024
(c) Alpha Assay (a)	-	76.1 ± 5.2	0.8 ± 0.8	-	-	-	-	-	-	0.6 ± 0.7	46.0 ± 3.1	1.8 ± 0.8	-
7. Thermal Cycle (d)													
(a) Weight Change, %	-	-0.25	-0.02	-	10.0	-	-	-	-	-	-	-	-
(b) Alpha Assay (a)	-	-	2.0 ± 1.0	-		-	-	5.9 ± 2.0	0.4 ± 0.8	3.4 ± 1.2	193 ± 6.0	32.6 ± 2.6	-

(a) Reported as cpm/gm of sample
(b) Reported as fraction of total uranium in sample
(c) Sample heated in 1200°F air for 5 hours
(d) Sample heated 3 times to 2500°F in inert atmosphere
(e) $ThO_2 + UO_2$ content
(f) Consists of 20 microns of porous Al_2O_3 and 130 microns of impermeable Al_2O_3

to 44.2 ± 2.0 cpm from the as-fabricated value of 1.4 ± 1.0 cpm. Metallographic examination revealed that some of the coatings were cracked. In order to determine whether oxygen diffusion into the particles at 2500°F might have been the cause, the thermal cycle test was repeated in a reducing atmosphere of N_2 + 10 v/o H_2 using material from batches 2A and 3C. Metallographic examination of both batches revealed no cracks in the coatings of either batch. An alpha assay of the batch 3C material showed an increase in exposed uranium of only a factor of 2. Alpha assays of batches 7H, 7J, and 8G after thermal cycling also showed no significant change. Thus, when the Al_2O_3 coating thickness is at least 30% of the UO_2 diameter, no damage occurs to the coating when the particles are heated up to 500°F above their fabrication temperature. However, significant coating failure was found when a thickness-to-diameter ratio of 10% was used (batch 5D) in a similar thermal cycle test as evidenced by weight gain in a subsequent hot air test.

ThO_2/UO_2 particles were used to prepare batches 7H and 7J and, as expected, no differences were found compared with an all-UO_2 fuel particle.

In the preparation of batch 8G, a number of smaller batches having intermediate coating thicknesses were withdrawn for examination. The results of tests on these intermediate batches are shown in Table 4-3.

TABLE 4-3

Evaluation of Batches 8A through 8G Which Incorporate a Porous Inner Layer of Alumina

Batch No.	Coating Thick, μ	Weight Gain, %[b]	Alpha Count Rate, cpm/gm sample		
			As-Fab.	Hot Air[b]	Thermal Cycle[c]
8A	22[a]	2.8	53.0 ± 3.3	—	—
8B	30	0.5	1.4 ± 0.7	—	—
8C	50	0.03	0.4 ± 0.5	106 ± 5	90.6 ± 4.3
8D	77	0.003	0.2 ± 0.4	51.8 ± 3.3	—
8E	106	0.04	0.8 ± 0.6	10.8 ± 1.6	6.4 ± 1.4
8F	122	0.04	0.4 ± 0.5	5.0 ± 1.2	—
8G	150	0.0003	1.0 ± 0.6	0.6 ± 0.7	3.4 ± 1.2

(a) Includes 2 micron flash coat (impermeable Al_2O_3) and 20 micron coat of porous Al_2O_3.
(b) After exposure in 1200°F air for 5 hrs.
(c) After nine cycles between 550°F and 2500°F in a reducing atmosphere.

A relatively high weight gain can be noted in batch 8A which contains a 2 micron impermeable alumina layer which probably was cracked, and a 20 micron porous layer. However, improvement can be seen in subsequent coating thicknesses. The alpha assay of the as-fabricated batches showed uniformly good quality once the first impermeable layer had been placed over the porous material (batch 8B through 8G). The hot air test showed uniformly good quality from batches 8C through 8G by the weight gain method. However, the somewhat more sensitive alpha assay technique showed a decreasing contamination with increasing coating thickness indicating that some surface uranium was covered by successive coating layers. In the thermal cycle test, there was some evidence of failure in batch 8C, but batches 8E and 8G showed no significant effect. In general, the batches with the thickest coatings passed all tests well.

Batches 9 and 9A were prepared in the course of studies to increase the Al_2O_3 deposition rate. The thicker coating on batch 9A resulted in lower uranium contamination after the coating integrity test. It is believed that the damage in thermal cycle testing was due to the lower coating thickness-to-UO_2 diameter ratio rather than effects of the increased Al_2O_3 deposition rate used in making these batches.

A sample from batch 12H was leached in hot nitric acid and an alpha assay was made before and after leaching. Before leaching, there was no measurable surface uranium contamination. After leaching, a count rate of 3.2 ± 1.2 cpm per gm of sample was found. This is equivalent to 0.0042 mg. U per gm of sample. The uranium found in the leach solution was equivalent to 0.0001 mg per gm of coated particles. These results suggested that there were probably some cracks in a few of the particles which would not have been indicated by the alpha assay but which would permit some uranium to be leached out and dispersed on other coating surfaces. The small amount of uranium found in the leach solution indicates that most of the exposed uranium was redistributed over the surfaces of the particles.

4.3 Graphite Matrix Fueled With Alumina Coated Particles

There are a number of conditions imposed upon alumina coated particles when they are considered for use in a graphite matrix. The volume occupied by the coated particles should be low enough so that the strength of the graphite matrix is not impaired. The size of the coated fuel particle should be small enough so that uniform mixtures of coated particles in graphite can be achieved. The coatings should be strong enough to prevent their damage during the mixing and molding steps. The temperature to which the fueled body is subjected during manufacture and operation should be low enough to prevent reaction between the Al_2O_3 and the graphite. The coated particles should be securely attached to or buried within the graphite matrix to prevent their loss during use.

As noted in Table 4-1, 13 graphite spheres fueled with Al_2O_3 coated UO_2 have been made to date. The primary function of these spheres was to provide specimens for irradiation testing, however some information relating to the conditions cited above was obtained.

4.3.1 Sphere Manufacture

Most of the spherical fuel element specimens made to date have been molded in dies which leave a rather prominent molding flash around the equator of the sphere. Since close tolerances were required for specimens used in high flux capsule irradiations, the standard practice for specimens fueled with uncoated fuel particles was to grind off the molding flash. In view of the potential damage to Al_2O_3 particle coatings, special alpha assays were made on three FA-22 specimens where the molding flash was removed by grinding. The results of this test are shown in Table 4-4 where positions E are on the equatorial molding flash and positions N and S are at opposite ends of the diameter perpendicular to the plane of the molding flash. The molding flash was removed by hand filing. As can be noted, a large increase in uranium contamination was found for specimens 436N (fueled with batch 1B material) and 448N (fueled with batch 2A material) indicating significant damage to the Al_2O_3 coatings. No significant damage to the particles in specimen 39-9N (fueled with batch 1B material) was noted. However, a subsequent radiograph of an equatorial slice from these specimens (see Fig. 4-11) showed an unexplained deficiency of fuel particles at the surface of specimen 39-9N. It was concluded that since the molding flash could not be safely removed, an allowance would be made in the design of the graphite blocks which hold the FA-22 specimen in place during capsule irradiation and no surface machining would be done on FA-22 specimens. Future designs of molds for PBR should minimize or eliminate the molding flash so that loss of fuel material by abrasion or impact will be avoided.

TABLE 4-4

Alpha Assays of FA-22 Specimens Where Molding Flash Has Been Removed

Specimen No.	Molding Flash Removal	Position	Net Alpha Count Rate, cpm (a)
FA-22(436N)	Before	N	12.6 ± 7.0
	"	S	2.8 ± 5.6
	"	E	1.4 ± 5.6
	After	E	636 ± 31
	"	E	318 ± 22
	"	N	22.4 ± 8.4
FA-22(448N)	Before	N	8.4 ± 6.3
	"	S	nil
	"	E	16.8 ± 6.3
	After	E	224 ± 19
	"	E	274 ± 21
	"	N	5.6 ± 6.3
FA-22(39-9N)	Before	N	16.8 ± 6.3
	"	S	4.2 ± 5.6
	"	E	7.0 ± 6.3
	After	E	2.8 ± 6.3
	"	E	2.8 ± 6.3
	"	E	14.0 ± 7.7

(a) Normalized to Whole Sphere Surface.

Uniform dispersions of Al_2O_3 coated UO_2 particles in graphite have been obtained, as seen in radiographs of slices from specimens FA-22(436N) and FA-22(448N) shown in Fig. 4-11. The apparent high particle density in 448N is due to the thicker Al_2O_3 coatings on these particles. It was concluded that there is no problem with achieving uniform particle dispersions up to the 250 micron size.

Several tests have been made to determine the extent of particle coating damage during the mixing and molding steps of sphere fabrication. Tests used to date have included alpha assays of the graphite mix, of the surface of the completed sphere, and of an unfueled graphite sphere. This last step was to determine whether equipment contamination was a possible source of uranium contamination. Since it is not possible to measure uranium

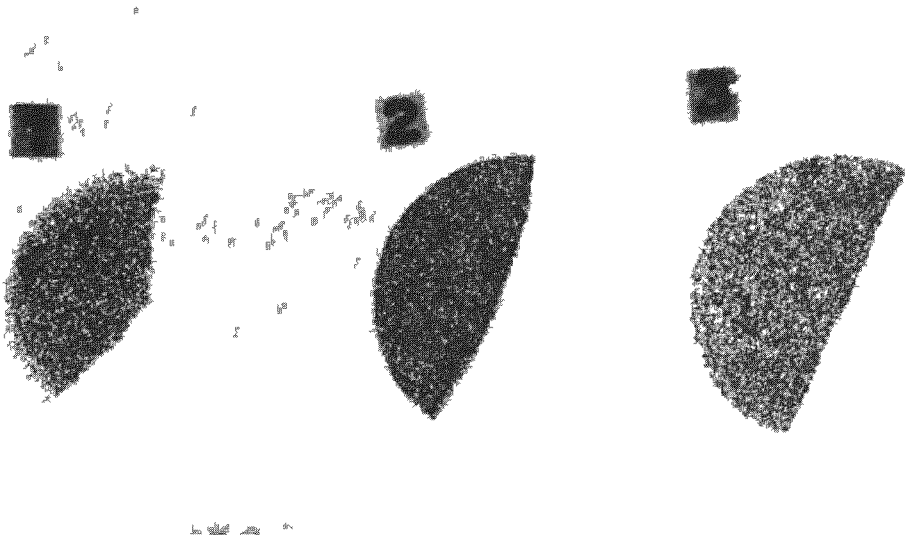

FIG. 4-11 Radiographs of slices cut from graphite spheres fueled with Al_2O_3 coated UO_2. #1 is from FA-22(39-9N), #2 is from FA-22(448N), #3 is from FA-22(436N).

contamination throughout the entire graphite matrix without destroying the finished sphere, a neutron activation test is considered the final test in determining whether coating fracture during manufacturing has been significant. A summary of alpha assays relating to particle damage are given in Table 4-5.

TABLE 4-5

Effect of Manufacturing Processes on Damage To Fuel Particle Coatings

	Net Alpha Count Rate, cpm, (a)	Uranium Contamination(b)	Fraction of Xe 133 Released (c)
A. Particles Only			
1. Sintered Al_2O_3/UO_2 (d)	0.5 ± 1.0	4.0×10^{-7}	9.3×10^{-5} (2450°F, 180 m)
2. Batch 1B	7.3 ± 1.3	1.5×10^{-5}	3.3×10^{-4} (2400°F, 210 m)
3. Batch 2A	1.4 ± 1.0	4.5×10^{-6}	1.3×10^{-6} (1500°F, 144 m)
4. Batch 4E	20.7 ± 2.5	3.0×10^{-5}	—
5. Batch 6H	0.4 ± 1.2	4.5×10^{-7}	—
6. Batch 12H	0.0 ± 1.3	0.0	2.6×10^{-5} (2500°F, 400 m)
B. Sphere Surface			
1. FA-22(437N)-(1B)	1.4 ± 5.6	4.0×10^{-7}	1.0×10^{-4} (2300°F, 140 m)
2. FA-22(449N)-(2A)	4.7 ± 5.8	1.3×10^{-6}	7.5×10^{-6} (1500°F, 270 m)
3. FA-22(471E)-(4E)	16.3 ± 6.1	9.2×10^{-7}	7.7×10^{-6} (1950°F, 240 m)
4. FA-22(548E)-(6H)	14.7 ± 5.9	8.4×10^{-7}	6.3×10^{-7} (2000°F, 240 m)
C. Graphite-Particle Mix (Using batch 6H)	114 ± 20	—	—
D. Unfueled Sphere (Made after Sphere 548E)	7.7 ± 2.1	—	—

(a) All values normalized to equivalent surface of 1 1/2" sphere except for particles which are reported as cpm/gm sample.
(d) Reported as ratio of uranium on surface to contained uranium in sample.
(c) See Neutron Activation Test results in Section 4.4.1.
(d) 400 micron sintered Al_2O_3 on 800 micron UO_2.

Uranium contamination on the surfaces of the spheres is seen to be about equal to or less than the contamination on the particles. This implies that there was no major damage to the particles even though the sphere assay only relates to the sphere surface and not to the contamination of the

interior portions of the graphite matrix. Comparison of the neutron activation data for batch 2A particles before and after incorporation into a sphere showed only a slight increase in Xe 133 release. The assay of the graphite-coated particle mixture did indicate that some slight damage occurred during the mixing process. The alpha assay of the unfueled sphere showed that contamination from equipment can be an additional source of uranium contamination. Thus, it can be concluded that there is no gross damage to Al_2O_3 coated UO_2 when incorporated into graphite spheres but that slight contamination can come from three sources: the coated particles as made, coated particle damage during ball fabrication, and from process equipment.

Figure 4-12 shows the surface of an FA-22 specimen which was made for capsule irradiation. The appearance of many fuel particles right at the surface can be noted. Future fuel element designs will incorporate features to prevent loss of these particles from the surface. These features will include surface coatings of either pyrolytic carbon or silicon carbide, carbonaceous layers added to the particles before mixing to permit better bonding to the graphite matrix, or an unfueled shell of graphite on the fueled sphere.

The presence of alumina in a graphite matrix imposes a temperature limitation in order to avoid reaction between the alumina and the graphite. There are indications in the literature (11) that this temperature may be as high as 3600°F. However, to avoid any possibility of damage to the particles during the manufacturing process, the short time graphite bake cycle was limited to a maximum temperature of 2500°F. A series of long time carburization tests was performed using several types of alumina and graphite. These results are reported in the Section 4.3.2 and ref. (24).

4.3.2 Carburization Studies

Two series of tests have been run to study the reaction between Al_2O_3 and graphite. The first series involved sintered Al_2O_3 coated UO_2 in graphite samples prepared by Battelle. Three types of graphite were used: (1) AGOT graphite flour with Barrett pitch binder, (2) AGOT graphite flour with BV1600 resin binder, and (3) Texas 55 coke flour with Barrett pitch binder. Samples with resin binder and with coke flour showed severe reaction between the Al_2O_3 and the graphite at 2500°F. The sample with graphite flour and pitch binder showed no reaction after 168 hrs at 2500°F as seen in Fig. 4-13. However, when this latter material was held at 3000°F for only a 6 hr. period, a severe reaction was noted, as seen in Fig. 4-14.

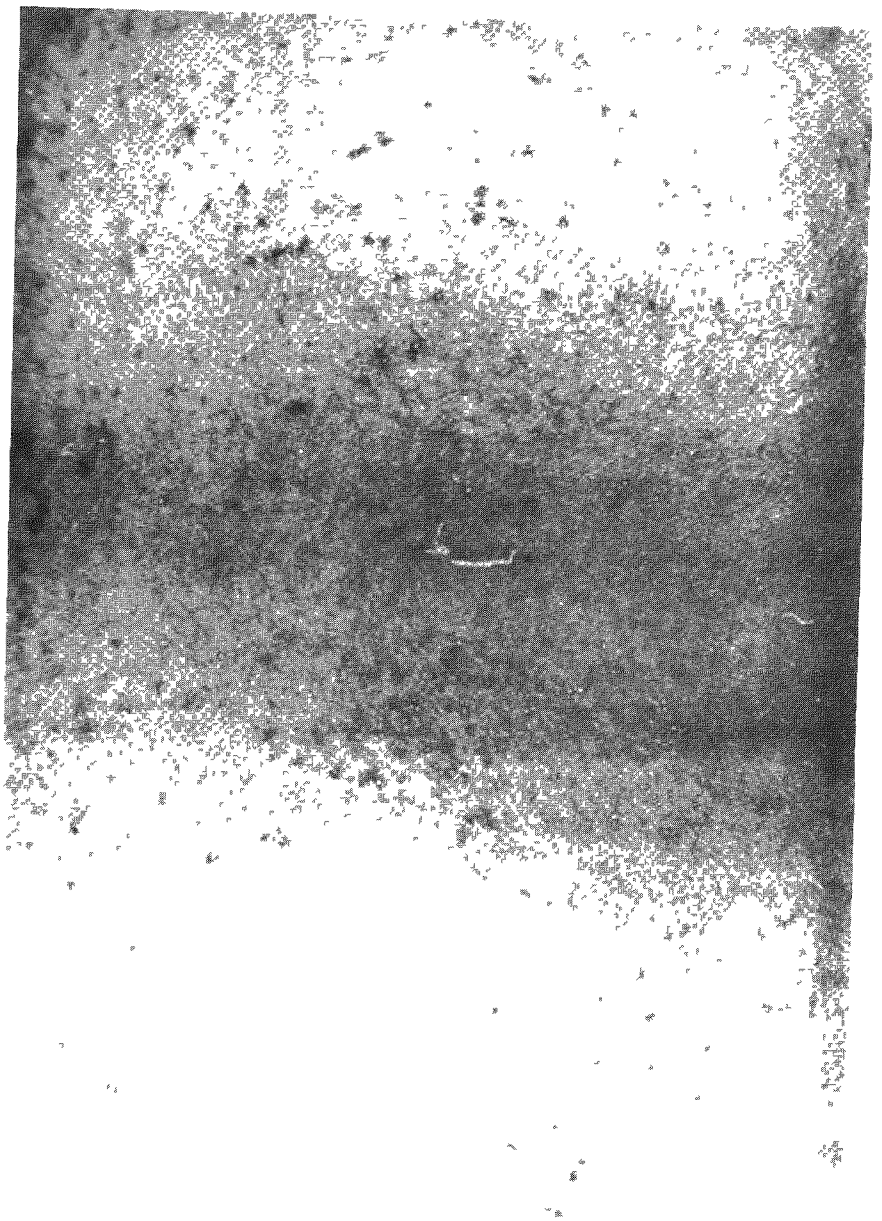

FIG. 4-12 External view of an FA-22 specimen showing Al_2O_3 coated UO_2 particles at the surface.

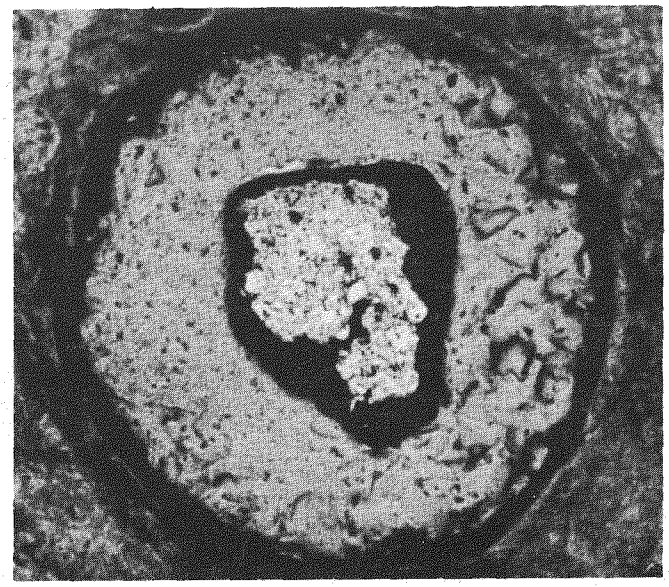

FIG. 4-13 Sintered Al_2O_3 on UO_2 heated in graphite at 2500°F for 168 hrs. (50x)

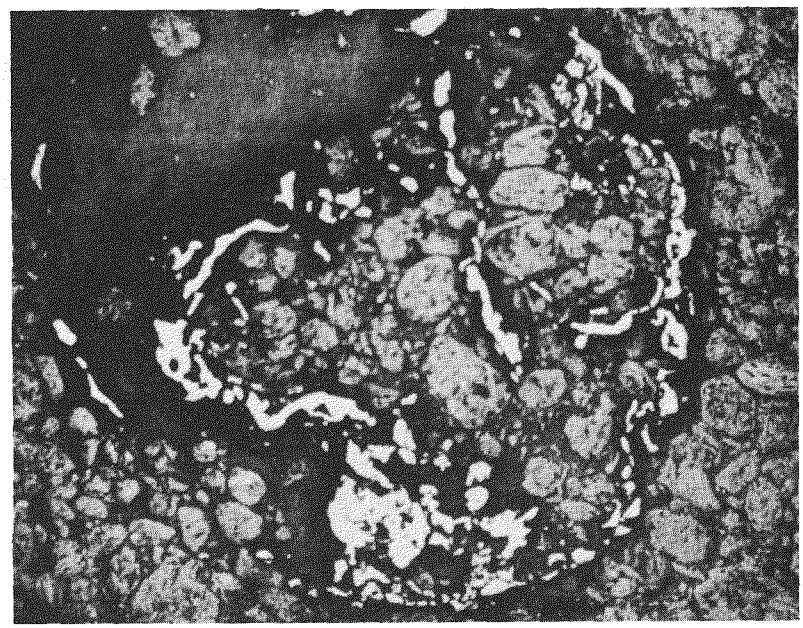

FIG. 4-14 Sintered Al_2O_3 coated UO_2 particle after reaction with graphite at 3000°F for 6 hrs. (50x)

The second series of tests involved vapor deposited alumina. Specimens were heated for periods of 168, 500 and 1000 hrs. at 2500°F based on results from the sintered alumina carburization test. The samples used in the second series are described in Table 4-6.

TABLE 4-6

Samples Used in Second Carburization Test

Sample Type No.	Particle Batch No.	Graphite Filler	Pitch Binder	Max. Bake Temp., °F
1	1B	AGOT	Barrett	1700
2(a)	1B	2301	Coal Tar	2300
3(a)	2A	2301	Coal Tar	2300

(a) Pieces from an FA-22 fuel element.

In all three heating runs, a deposit formed on the inside walls of the furnace tube. The deposits consisted of alumina, silicon carbide, aluminum nitride, and/or iron silicide in addition to an unidentified phase. It is believed that the silicon and the alumina came from the Mullite insulation tube, the iron from the graphite, and nitrogen from the furnace atmosphere. The unidentified phase was found on both the furnace walls and the specimen surfaces.

A typical view of the specimens before testing is seen in Fig. 4-15 which shows a section of a Type 2 specimen fueled with the thin coated particles. Some cracks were noted in the particle coatings of Type 1 specimens after fabrication.

Some degree of attack was noted in all three types of samples. However, more severe reaction was noted in coated particles located near the edge of the graphite specimen as compared with particles located near the center of the specimen. After 168 hrs, several particles in Type 1 were attacked and there was essentially no attack in Type 2 and Type 3. After 500 hrs the coatings in Type 1 were completely destroyed, some thinning of the coatings in Type 2 was noted; and some attack was beginning to occur to the Type 3 coatings. After 1000 hrs, the particles in Type 1 were almost completely converted to a metallic phase, and the coatings in Type 2 were almost entirely destroyed, with greater attack being noted at the edge of the sample. Coatings near the center of Type 3 samples were generally intact although there was some deterioration of the alumina as seen in Fig. 4-16.

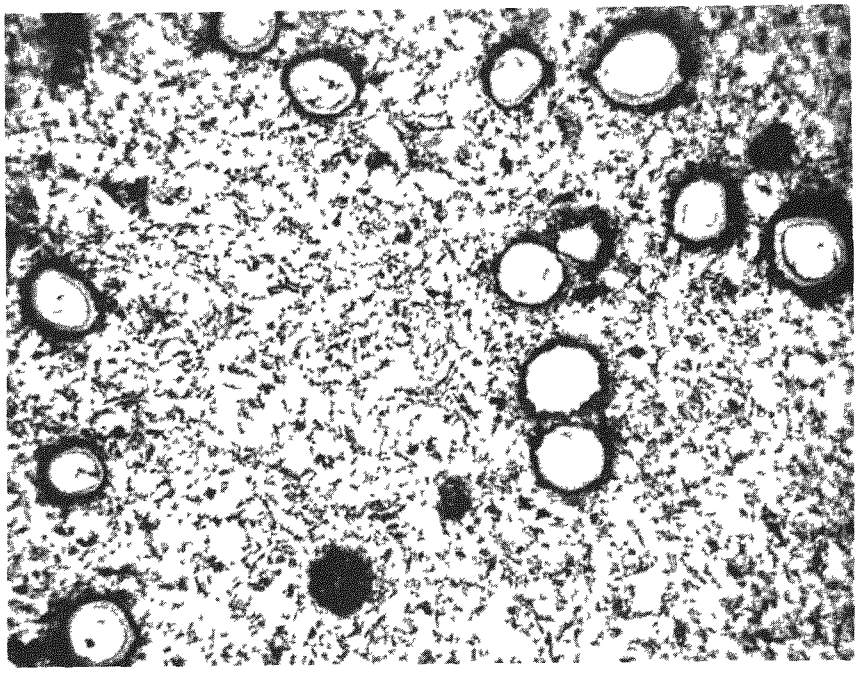

FIG. 4-15 Graphite-Al_2O_3 Specimen Type 2, as fabricated (50X).

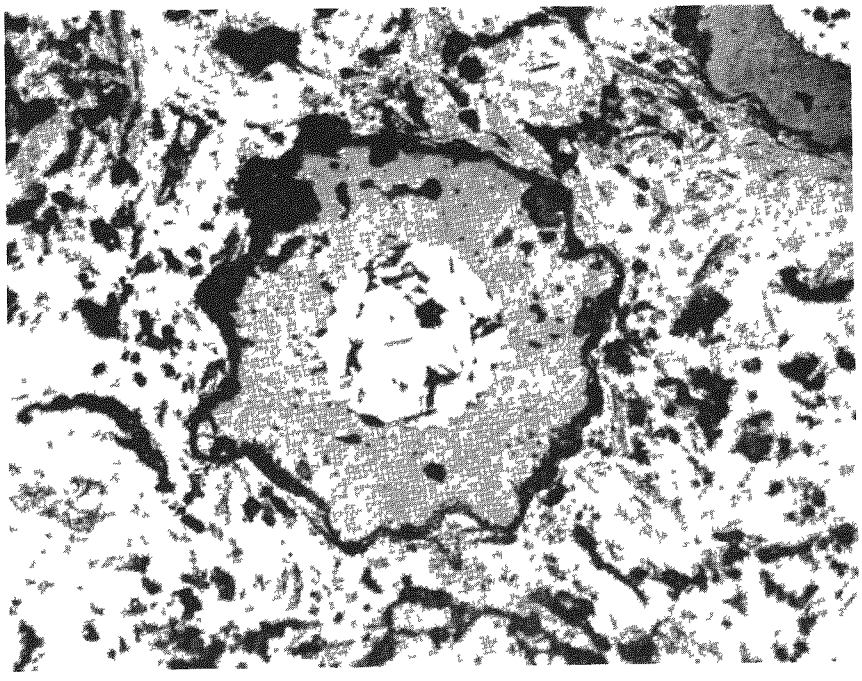

FIG. 4-16 Graphite-Al_2O_3 Specimen Type 3, after 1000 hrs at 2500°F. View at center of specimen (250X).

Near the surface of the sample, complete coating attack was again noted. It is possible that the spurious deposits noted in the furnace tube were responsible for accelerating the attack on particle coatings near the surfaces of the graphite samples.

It is believed that the initial cracks in the coatings of Type 1 and the thin coatings of Types 1 and 2 could have been factors in the more rapid deterioration of these coatings by the early exposure of the UO_2 particles. Since there was some evidence of attack even in the thickest alumina coating, the maximum safe temperature must be below 2500°F until a better understanding can be obtained of the factors which cause attack of the Al_2O_3.

4.3.3 Evaluation of Fueled Spheres

Due to the small number of graphite spheres fueled with Al_2O_3 coated UO_2 (Type FA-22) which were procured primarily for irradiation testing, there has only been a limited amount of test data on these spheres, exclusive of the data on fission product retention which is described in Section 4.4.

A complete summary of all alpha assays performed on the surfaces of FA-22 specimens is given in Table 4-7. Each data point represents a different portion of the sphere surface and the value shown has been normalized to the whole surface. Since each specimen is fueled with 4.75 gms of uranium, the fraction of exposed uranium on the surface of these specimens ranges from 3×10^{-7} to 1.3×10^{-5} as predicted by these alpha assays. A rather uniform pattern of uranium contamination can be seen over the surfaces of the specimens. The locally high reading obtained in a few cases was probably due to a collection of slightly damaged particles right at the surface.

Several impact and compression tests have been run on FA-22 specimens. The graphite used in the FA-22 specimens is similar to that used in the FA-1 specimens. A fully graphitized filler material is used in both specimens but the pitch binder is not graphitized due to the low bake temperature in order to avoid graphite reactions with the Al_2O_3 or the UO_2. The bake temperatures were 2560°F for the FA-1 type and 2300°F for the FA-22 type. Impact and compression data for these two types are summarized in Table 4-8.

TABLE 4-7

Surface Uranium Contamination of Graphite Spheres Fueled with Al_2O_3 Coated UO_2.

Specimen No.	Coated Particle Batch No.	Net ∝ Count Rate, cpm	Equivalent Surface Uranium, mg.
FA-22(436N)	1B	12.6 ± 7.0	0.017
		2.8 ± 5.6	0.0037
		1.4 ± 5.6	0.0019
FA-22(437N)	1B	2.8 ± 5.6	0.0037
		nil	nil
		1.4 ± 5.6	0.0019
FA-22(448N)	2A	8.4 ± 6.3	0.011
		nil	nil
		16.8 ± 6.3	0.022
FA-22(449N)	2A	2.8 ± 5.6	0.0037
		7.0 ± 6.3	0.0092
		4.2 ± 5.6	0.0055
FA-22(39-9N)	1B	16.8 ± 6.3	0.022
		4.2 ± 5.6	0.0055
		7.0 ± 6.3	0.0092
FA-22(470E)	4E	16.8 ± 6.3	0.0046
		28.0 ± 7.7.	0.0076
		221 ± 18.2	0.060
FA-22(471E)	4E	23.8 ± 7.0	0.0065
		12.6 ± 5.6	0.0034
		12.6 ± 5.6	0.0034
FA-22(472E)	4E	44.8 ± 9.8	0.012
		18.2 ± 7.0	0.0050
		16.8 ± 7.0	0.0046
FA-22(546E)	6H	49.0 ± 9.1	0.013
		11.2 ± 5.6	0.0030
		39.2 ± 7.0	0.011
		70.0 ± 10.5	0.019
FA-22(547E)	6H	112 ± 13	0.030
		64.4 ± 9.8	0.017
		70.0 ± 10.5	0.019
		30.8 ± 17.7	0.0084
FA-22(548E)	6H	22.4 ± 7.0	0.0061
		7.0 ± 4.9	0.0019
		5.6 ± 4.9	0.0015
		23.8 ± 7.0	0.0065
FA-22(549E)	6H	33.6 ± 8.4	0.0091
		25.2 ± 7.0	0.0068
		75.6 ± 10.5	0.021
		199 ± 17	0.054
FA-22(550E)	6H	12.6 ± 5.6	0.0034
		22.4 ± 7.0	0.0061
		12.6 ± 5.6	0.0034
		14.0 ± 6.3	0.0038

TABLE 4-8

Impact and Compression Tests on FA-22 and FA-1 Specimens

Specimen Type	Compression Failure			Impact Failure
	Load, lbs.	Deflection, in	Modulus, lbs/in	Load, ft-lbs
FA-22	4465	0.079	68,000	7.0
	4435	0.078	71,000	
FA-1	2410	0.0433	55,900	11.5
	2865	0.0508	56,400	11.5
				7.3

Both of these specimen types in Table 4-8 are fueled with the same volume fraction of UO_2 but the FA-22 type has the added volume fraction of the Al_2O_3 coatings. From the test data, the presence of the Al_2O_3 is seen to have no deleterious effect on the strength of the graphite sphere. The significantly higher compressive strength and load modulus of the FA-22 specimens is thought to be associated with its slightly lower bake temperature.

In order to determine the extent of damage to the Al_2O_3 coatings when the graphite spheres were broken, portions of several of the specimens were alpha assayed on their fractured surfaces. In addition, one specimen was subjected to repeated low level impact loads on one spot. The results are summarized in Table 4-9. The specimen fueled with the massive sintered Al_2O_3 coatings showed no significant increase in uranium contamination while there was evidence of some damage to the thinner vapor-deposited Al_2O_3 coatings.

TABLE 4-9

Alpha Assays of Fractured FA-22 Specimens

Sphere Condition	Al_2O_3 Coating Thickness,	Net Alpha Count Rate on Fractured Surface, cpm[a]
1. After Compressive Failure	250	4.2 ± 3.5
		1.4 ± 2.8
		8.4 ± 4.9
2. 100 impacts of 3 in-lbs	48[b]	11.2 ± 2.8 (before)
		166 ± 6 (after)
3. After Impact Failure	48[b]	202 ± 18
		411 ± 25
		488 ± 27

(a) Normalized to surface area of 1 1/2" sphere.
(b) On enriched UO_2 particles.

4.4 Fission Product Retention

Al_2O_3 coated UO_2 particles have been subjected to all three of the standard fission product retention tests, namely neutron activation, furnace capsule irradiation, and sweep capsule irradiation. Test specimens have included both coated particles and 1-1/2" graphite spheres fueled with coated particles.

4.4.1 Neutron Activation Tests

Table 4-10 summarizes the results of neutron activation tests on Al_2O_3 coated UO_2. Although the specimens have some variation in coating thickness, very low amounts of Xe 133 were released during the test periods. It is interesting to note that the thinner vapor deposited Al_2O_3 coatings showed as good fission product retention as did the thick sintered Al_2O_3 coatings. A comparison of these release fractions with surface uranium contamination estimated from alpha assays in Table 4-5 indicates that the Xe 133 was most likely released from this external contamination. A thermal cycle test on sphere FA-22(449N) between 1900°F and 600°F caused no noticeable increase in Xe 133 release. On batch 12 H, an increase in temperature from 2200°F to 2500°F caused a significant increase in Xe 133 release. It is not clear whether this indicates a sudden increase in fission product diffusion through Al_2O_3 at this temperature since the amount of Xe 133 released was approximately equal to the exposed uranium fraction of 10^{-5} found for batch 12 H in acid leach tests. (See Section 4.2)

4.4.2 Furnace Capsule Tests

Furnace Capsule SPF-3 contained specimen FA-22(449N) fueled with Al_2O_3 coated UO_2 from batch 2A. One of the objectives of this experiment was to determine whether there was any significant increase in fission product leakage through the Al_2O_3 coatings as the specimen temperature was raised to 1900°F, the maximum capability of this type of capsule.

The leakage factors obtained from this specimen during the course of the experiment are listed in Table 4-11. The capsule was operated during March 1960 at 1000°F and 1500°F using the gas train which is normally used for Sweep Capsule experiments. However, with the startup of Sweep Capsule SP-5, operation of Furnace Capsule SPF-3 was suspended until August while a separate gas train was constructed. Data was taken over the range of 280°F to 1900°F, with repeat samples being taken at several temperatures. These repeat samples, at a given temperature,

TABLE 4-10

Neutron Activation Tests on Al_2O_3 Coated UO_2

Specimen	Test Temp., °F	Time, Min.	Fractional Release of Xe 133
1. Sintered Al_2O_3 (a) Coated UO_2	1500	30	(b)
	1800	30	2.4×10^{-5}
	2000	60	1.4×10^{-5}
	2200	30	(b)
	2450	30	5.5×10^{-5}
2. Batch 1B	1850	100	$<1.7 \times 10^{-4}$
	2250	75	1.7×10^{-4}
	2400	135	1.6×10^{-4}
3. FA-22(437N) fueled with Batch 1B	1650	80	$<8.1 \times 10^{-6}$
	1800	50	1.6×10^{-5}
	2200	60	4.9×10^{-5}
	2350	30	2.6×10^{-4}
4. Batch 2A	1500	144	1.3×10^{-6}
	1500	60	$<3.7 \times 10^{-5}$
	2000	50	$<3.7 \times 10^{-5}$
5. FA-22(449N) fueled with Batch 2A	1500	270	7.5×10^{-6}
	1900	60	$<9.4 \times 10^{-6}$
	1900 (c)	60	$<9.4 \times 10^{-6}$
	1900 (c)	135	$<9.4 \times 10^{-6}$
6. Batch 12H	1600	60	5.1×10^{-6}
	1800	70	5.1×10^{-6}
	2000	80	1.3×10^{-6}
	2200	65	1.3×10^{-6}
	2500	130	1.3×10^{-5}
7. FA-22(471E) fueled with Batch 4E	1950	240	7.7×10^{-6}
8. FA-22(548E) fueled with Batch 6H	2000	240	6.3×10^{-7}

(a) 400 micron thick sintered Al_2O_3 coatings on 800 micron UO_2.
(b) Activity level included as part of subsequent reading
(c) Prior to these runs, the specimen was cooled to 600°F in 7 min and reheated to 1900°F in 10 min.

TABLE 4-11.

Summary of Fission Product Release Data from Specimen FA-22 (449N) in Furnace Capsule SPF-3

Sample No.	Date	Temp. °F	R/B (Release Rate/Production Rate) Kr 85	Kr 87	Kr 88	Xe 133	Xe 135
1	3/17	1000	5.6(-7)[a]	4.2(-7)	2.6(-7)	1.2(-6)	1.7(-7)
2	3/18	1500	2.0(-6)	1.0(-6)	3.2(-7)	5.8(-6)	1.7(-6)
3	8/3	290	1.1(-6)	<2.0(-7)	2.0(-7)	7.8(-6)	3.8(-7)
4	8/8	280	<8.0(-7)	<2.0(-7)	<2.0(-7)	<4.8(-6)	1.9(-7)
5	8/12	460	3.6(-6)	8.2(-7)	1.8(-6)	2.0(-5)	1.5(-6)
6	8/18	560	1.9(-6)	1.3(-6)	6.8(-7)	6.4(-6)	1.9(-6)
7	8/26	1020	6.2(-6)	1.7(-6)	2.1(-6)	1.8(-5)	4.5(-6)
8	8/31	1120	5.2(-6)	1.7(-6)	2.2(-6)	1.4(-5)	3.6(-6)
9	9/14	1100	2.3(-6)	4.7(-7)	9.2(-7)	4.2(-6)	1.1(-6)
10	9/23	1480	1.6(-5)	3.5(-6)	6.8(-6)	3.7(-5)	6.2(-6)
11	9/27	1510	1.4(-5)	3.4(-6)	5.3(-6)	3.8(-5)	9.5(-6)
12	9/30	1500	1.4(-5)	2.9(-6)	6.2(-6)	3.7(-5)	1.0(-5)
13	10/6	1895	4.6(-6)	9.2(-7)	1.7(-6)	9.0(-6)	2.7(-6)
14	10/12	1035	1.7(-7)	<2.0(-7)	<2.0(-7)	1.4(-6)	2.6(-7)
15	10/27	1800	5.2(-5)	1.6(-5)	2.2(-5)	2.8(-4)	5.6(-5)
16	10/28	1790	1.8(-5)	3.6(-6)	1.1(-5)	9.5(-5)	1.1(-5)

(a) Numbers in parentheses denote power of 10.

taken within a two-week period, showed excellent reproducibility. However, it is not known why the earliest samples taken at 1000°F and 1500°F (samples 1 and 2) are approximately one order of magnitude lower than the later samples. Shortly after the 1900°F sample (No. 13), a failure in the inner container caused a loss of vacuum in the outer jacket. This caused a drop in specimen temperature to about 1000°F at the same heat output. With maximum heat input, a specimen temperature of 1800°F was achieved for the last two samples.

The leakage factors for two of the five fission products measured in this experiment (Kr 87 & Xe 133) are plotted in Figure 4-17 as a function of specimen temperature. The leakage factors for the other three fission products (Kr 85m, Kr 88 and Xe 135) follow the same trend with temperature and have been omitted from Figure 4-17 for clarity. Also, data from samples #1, 2, 13 and 14 have been omitted. As can be noted, increasing the specimen temperature from about 300°F up to about 1100°F causes essentially no increase in fission product leakage. An increase in specimen temperature from 1100°F to about 1800°F then causes about a one order of magnitude increase in leakage. It is most probable that the greatest contribution to the fission product release from this specimen is due to exposed uranium contamination and that increasing the specimen temperature has merely affected the fission products escaping from this exposed uranium through the graphite matrix. Although the total irradiation time for this specimen was of the order of 100 days, radiation damage effects are insignificant due to the use of normal enrichment uranium and a thermal flux of only 3×10^{11}nv.

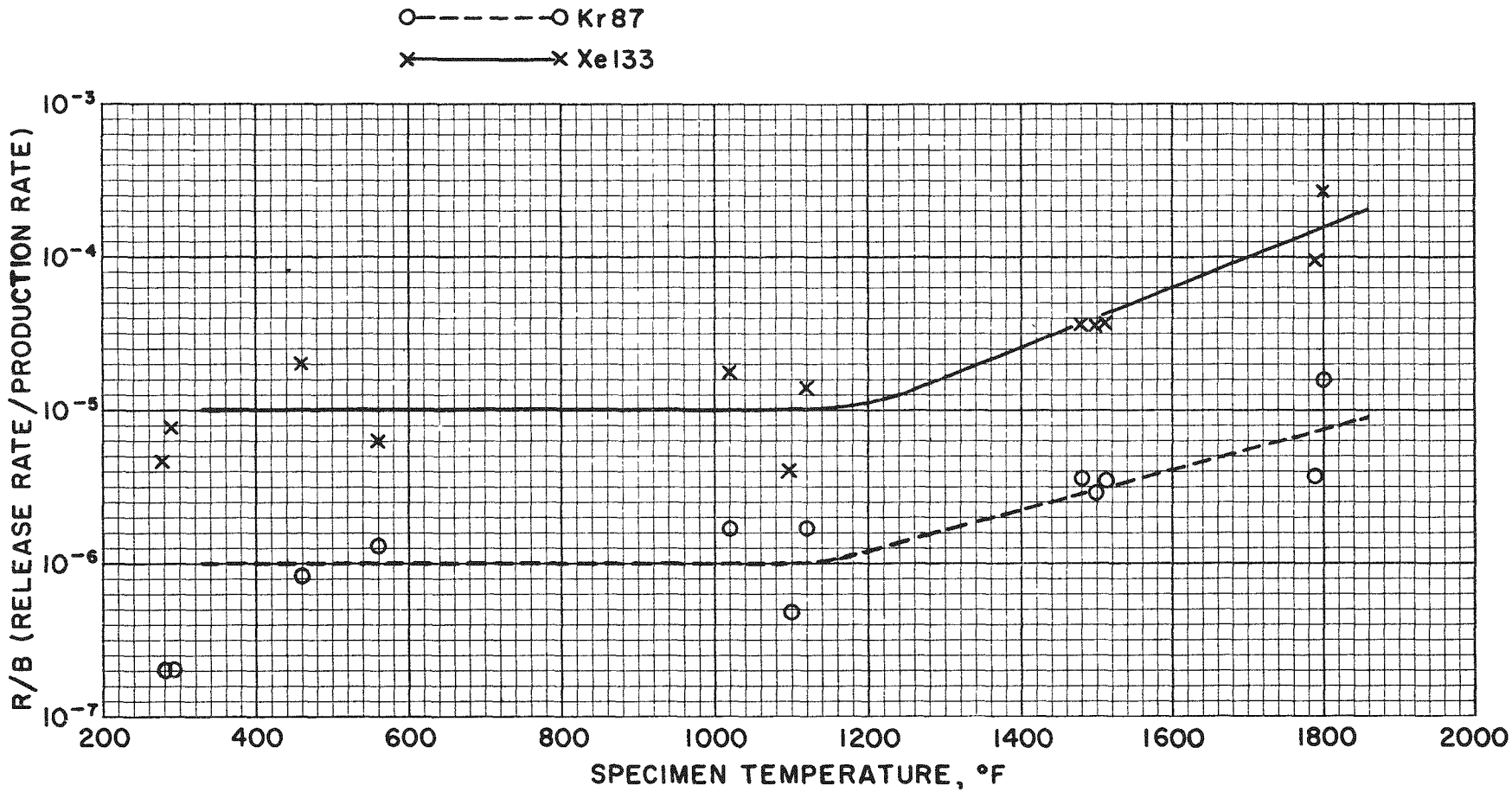

TYPICAL FISSION PRODUCT RELEASE DATA
FOR SPECIMEN FA-22(449N)
IN FURNACE CAPSULE SPF-3

FIG. 4-17

4.4.3 Sweep Capsule Tests

Specimen FA-22(471E) fueled with Al_2O_3 coated UO_2 from batch 4E was encapsulated in the sweep compartment of Sweep Capsule SP-5 in order to determine the effect of irradiation on fission product retention by the Al_2O_3 coatings. An additional FA-22 specimen was included in the static compartment of Capsule SP-5. The design and operating conditions of Capsule SP-5 are described in Section 8.5. Briefly, specimen FA-22(471E) operated at nominal conditions of 1.5 KW, a surface temperature of 1350°F and a central temperature of 1550°F. Capsule SP-5 was under irradiation from April 6 to November 14, 1960. On October 15, further responsibility for Capsule SP-5 was transferred to Battelle's Coated Particle Program under Contract W-7405-eng-92. The estimated burnup in both of the FA-22 specimens at the end of the irradiation was 6 a/o U235.

During the course of the irradiation, 27 samples of the off-gas stream were analyzed for long-lived gaseous fission products and 3 samples were taken using a special non-volatiles trap to measure the leakage factors for short-lived gaseous fission products and other isotopes such as iodine and cesium. Data for the last 5 gaseous fission product samples and the 3rd non-volatile trap are taken from ref. (20).

All of the leakage factors for the long-lived fission product gases are listed in Table 4-12. The data for the first 22 samples are plotted in Fig. 4-18. A plot of specimen temperature is also included. Temperatures are estimated beyond the 130th day due to failure of the last thermocouple in Capsule SP-5. The estimated drop in temperature to 950°F, which occurred on the 146th day, held for the remainder of the irradiation.

No data was taken during the period between samples 9 and 10 while certain revisions were made to the gas train. Although there was no helium flow over the specimen during this period, it remained under full power irradiation. Samples 11 and 12 were taken on the same day to check reproducibility of the sampling and analysis procedure. Good agreement was found between these two samples. Although there were several perturbations in the trends of the leakage factors, some of which appear to be associated with specimen temperature variations, some special tests were made to determine whether the 2 order of magnitude dip in sample 15 (i.e. at 111 days) was in any way attributable to the sampling procedure. The sample trap used for #15 was used again for sample #16 but with the addition of a backup trap. For sample #16, less than 1% of the total activity

TABLE 4-12

Summary of Long-Lived Gaseous Fission Product Release from Specimen FA-22(471E) in Capsule SP-5

Sample No.	Days of Irradiation	R/B (Rate of Release/Rate of Production)				
		Kr 85m	Kr 87	Kr 88	Xe 133	Xe 135
1	5	1.6(-8)(c)	(a)	2.2(-9)	1.8(-7)	1.9(-8)
2	9	5.9(-8)	1.8(-8)	2.7(-8)	1.0(-7)	4.0(-8)
3	19	4.7(-7)	1.8(-7)	2.9(-7)	1.9(-6)	4.9(-7)
4	23	7.3(-6)	(b)	(b)	5.8(-6)	2.1(-6)
5	24	2.6(-8)	(a)	1.6(-8)	1.3(-7)	8.2(-9)
6	27	7.0(-9)	(a)	7.1(-9)	4.8(-8)	4.2(-9)
7	28	3.1(-9)	(a)	4.7(-9)	4.0(-8)	1.6(-9)
8	32	1.8(-8)	(a)	7.7(-9)	9.1(-7)	1.2(-8)
9	38	7.6(-9)	(a)	1.9(-9)	5.0(-8)	4.0(-9)
10	72	4.0(-6)	1.6(-7)	(a)	2.8(-4)	7.8(-7)
11	83	5.9(-6)	1.3(-7)	(a)	8.0(-4)	7.9(-7)
12	83	2.1(-6)	2.0(-7)	6.2(-7)	2.1(-4)	5.3(-7)
13	91	6.1(-6)	2.9(-7)	1.0(-6)	1.2(-3)	1.5(-6)
14	102	1.2(-5)	1.1(-6)	3.2(-6)	1.1(-3)	4.2(-6)
15	111	1.2(-7)	3.7(-8)	(a)	2.6(-5)	2.0(-7)
16	122	4.7(-4)	(a)	(a)	4.1(-3)	1.4(-4)
17	132	2.5(-4)	7.6(-6)	4.8(-5)	4.7(-3)	1.4(-4)
18	134	4.8(-4)	3.3(-5)	1.4(-4)	8.1(-3)	2.4(-4)
19	137	2.5(-4)	1.9(-5)	7.4(-5)	1.7(-2)	1.9(-4)
20	143	4.6(-4)	2.7(-5)	1.1(-4)	9.7(-3)	2.3(-4)
21	148	3.0(-5)	5.9(-6)	1.2(-5)	6.9(-4)	2.2(-5)
22	149	3.7(-5)	6.3(-6)	1.6(-5)	1.5(-4)	1.8(-5)
23	154	5.2(-5)	1.1(-5)	1.9(-5)	1.9(-4)	3.0(-5)
24	156	4.4(-5)	3.4(-6)	2.0(-5)	2.0(-4)	1.9(-5)
25	160	5.9(-5)	1.8(-5)	1.8(-5)	3.2(-4)	3.5(-5)
26	168	9.5(-5)	1.9(-5)	3.5(-5)	3.5(-4)	3.0(-5)
27	170	6.8(-5)	1.2(-5)	3.0(-5)	2.4(-4)	3.9(-5)

(a) Below sensitivity
(b) Decayed out prior to analysis
(c) Numbers in parentheses denote power of 10

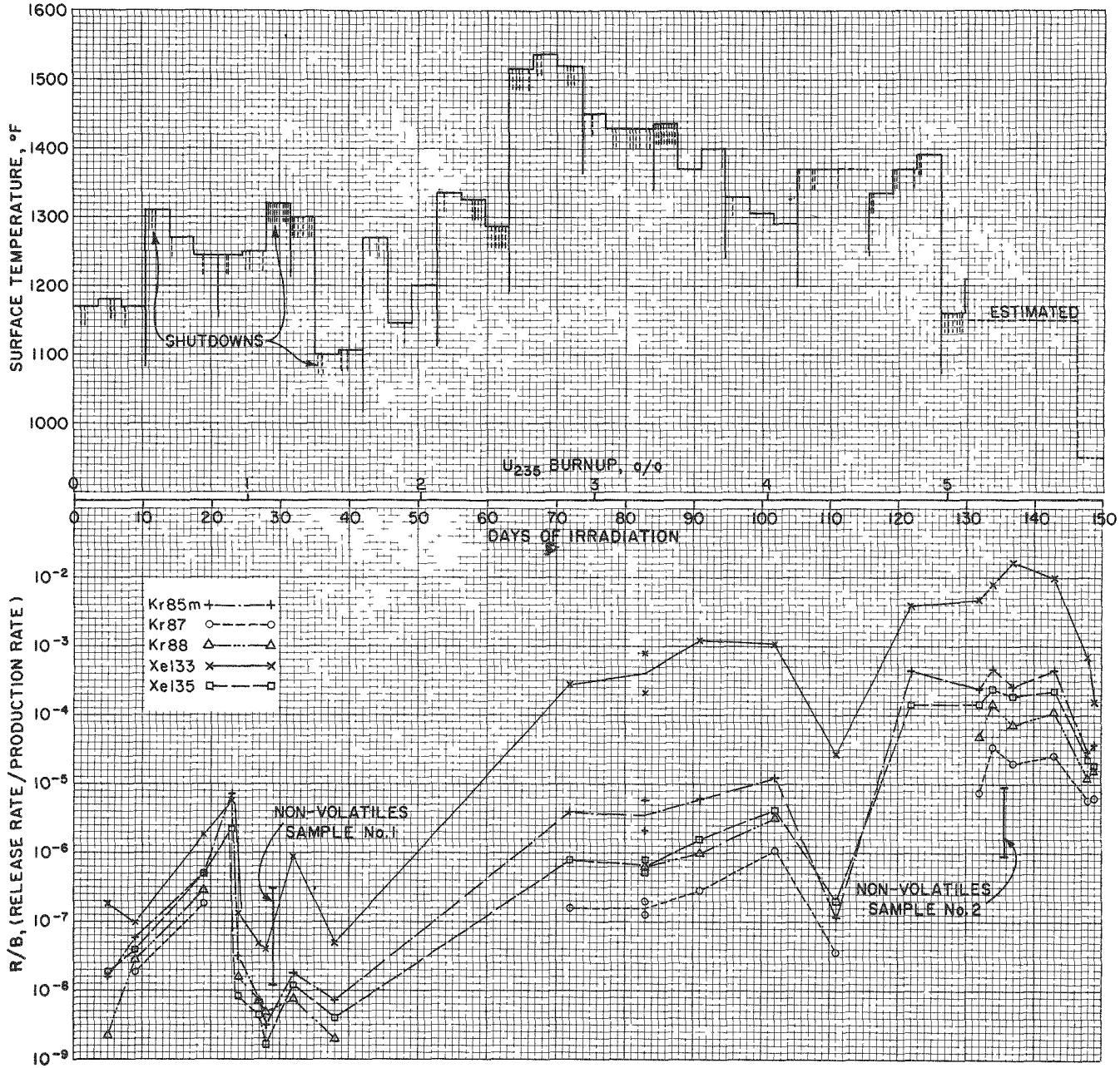

PERFORMANCE OF SPECIMEN FA-22(471E) IN SWEEP CAPSULE SP-5

FIG. 4-18

was found in the backup trap indicating that the first sampling trap was in good condition. Thus, it was concluded that the charcoal may have been contaminated with air or moisture when sample 15 was taken resulting in little or no fission product adsorption. It was estimated that if the activity present in sample 15 was present only in the gas spaces in the charcoal bed, the calculated leakage factors would have been of the same order as those reported for sample 16.

The three non-volatile trap samples were taken at approximately 1 a/o, 5 a/o and 6 a/o burnup. These traps are located in the BRR pool near Capsule SP-5 so that the transit time from the capsule to the trap is only 2 sec. A description of the non-volatiles trap is given in Section 8.5. In normal capsule operation, the helium stream bypasses the non-volatiles trap. When a sample is taken, the helium stream is diverted through the trap for a 48 hr period with a residence time of 90 sec. During this time isotopes which are non-volatile at the pool water temperature are deposited in the trap. Species of interest include strontium, barium, and cerium which are daughter products of certain short lived gaseous products, and iodine, tellurium, and cesium which could themselves diffuse out of the fuel element. See ref. (12) for further details.

Since the trap consists of a number of stainless steel mesh pads in series, the pattern of fission product deposition as a function of residence time (i.e. trap length) can be measured. Conventional radiochemical techniques are used to separate, identify, and assay the individual isotopes. A check of the trap walls showed that more than 98% of the Sr 89, Ba 140 and Ce 141 activity was in the stainless steel mesh pads so that wall effects were neglected in reporting the data.

Typical results obtained from this type of experiment are shown in Fig. 4-19 (Sr 89, Ba 140, Ce 141) and Fig. 4-20 (I 131, I 133) which are the data from non-volatiles trap sample #1. If it is assumed that non-volatile daughter products deposit on the stainless steel mesh immediately upon the decay of its volatile parent isotope, then the concentration of the non-volatile daughter product through the trap should be a function of the half-life of the gaseous precursor. These predicted deposition curves are also shown in Figure 4-19. As can be noted, there is excellent agreement between the theoretical curves and the actual data points. Essentially all of the Ba 140 and Ce 141 was deposited in the trap. Only about 30% of the Sr 89 was deposited in the trap with the remainder passing out of the trap as undecayed Kr 89. There is practically no decay of the I 131 and I 133 during their passage through the trap. The assumption

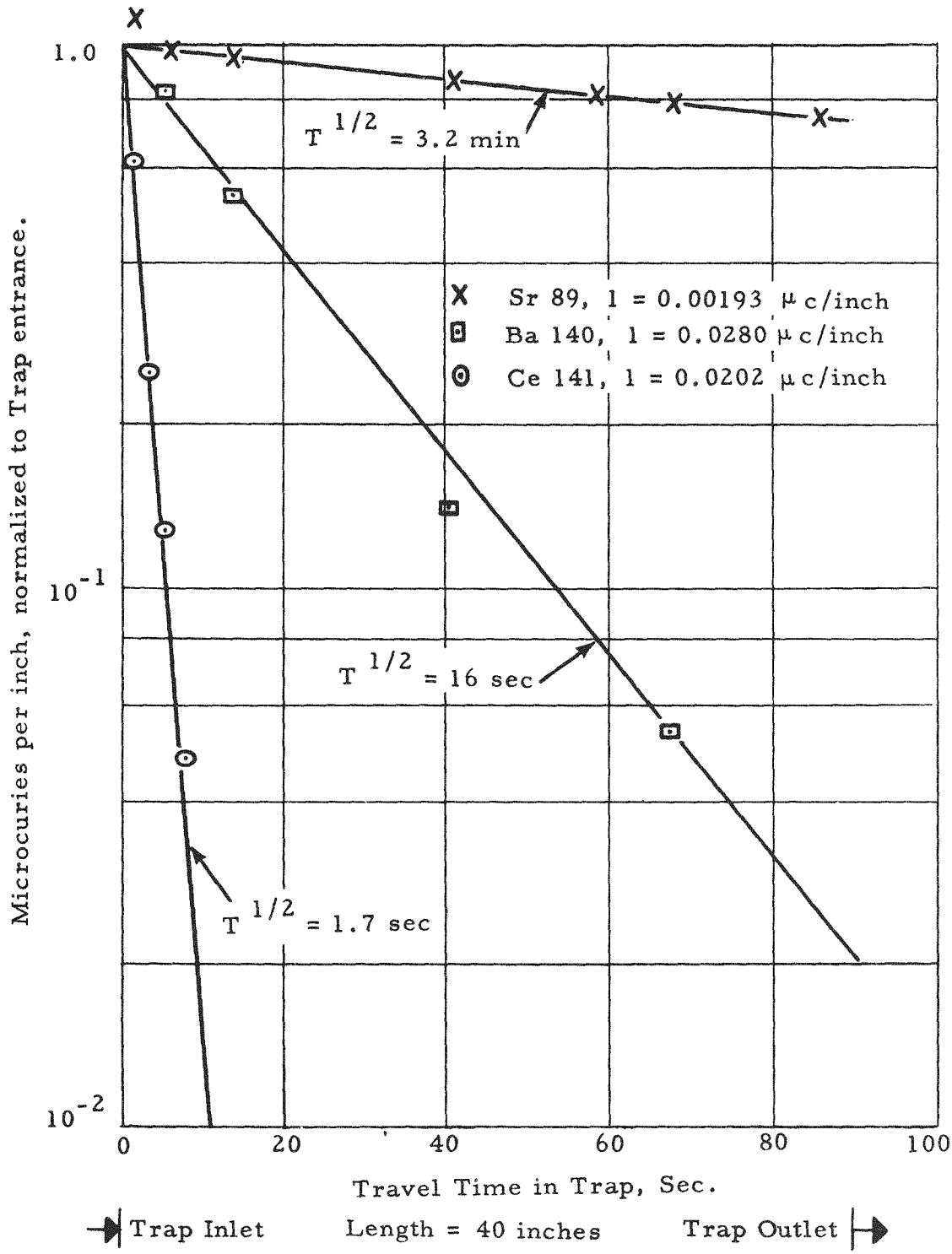

FIG. 4-19 Distribution of Sr 89, Ba 140, and Ce 141 in Non-Volatiles Trap for Specimen FA-22(471E).

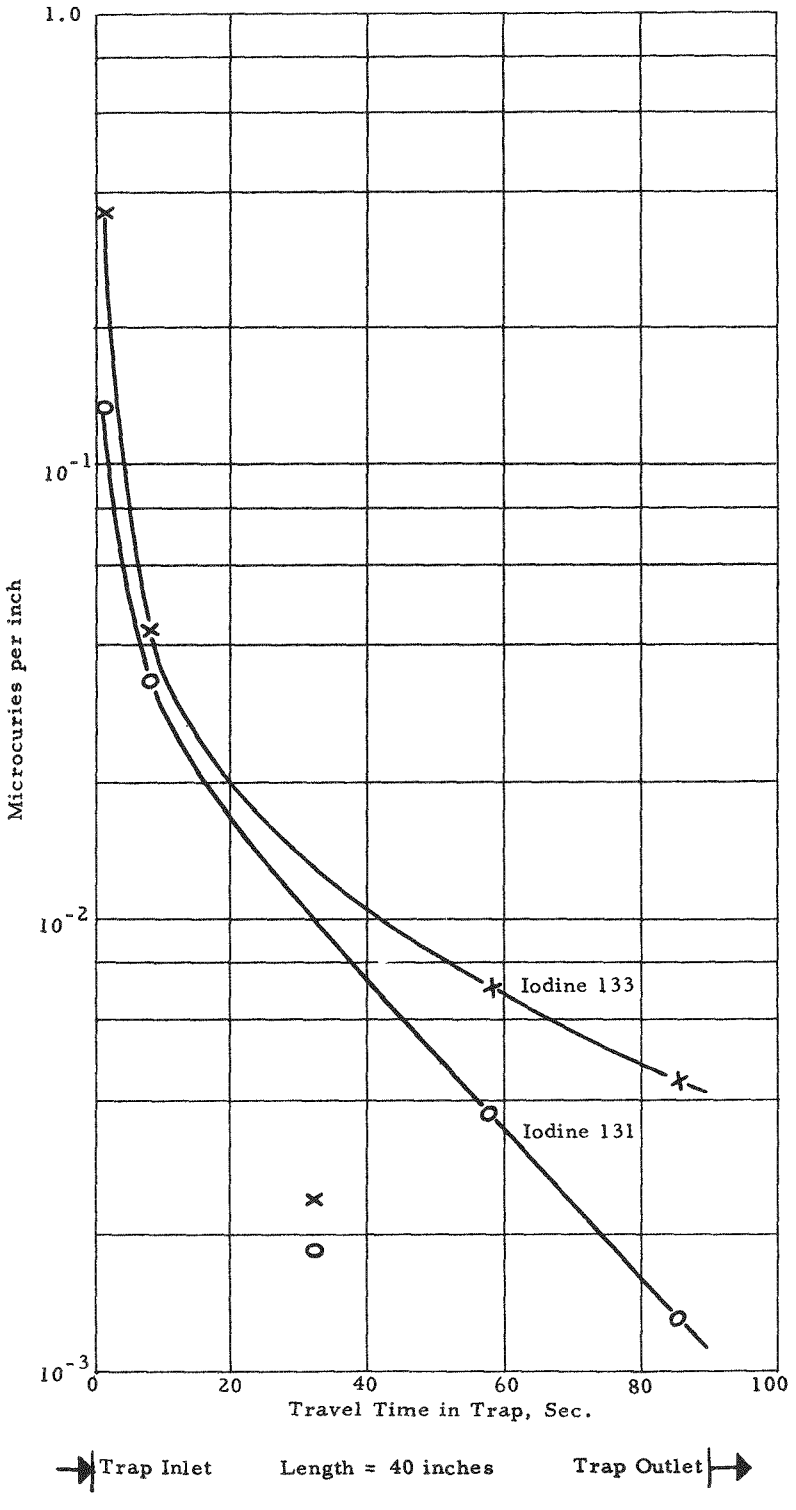

FIG. 4-20 **Distribution of I 131 and I 133 in Non-Volatiles Trap for Specimen FA-22(471E)**

of a constant removal efficiency per inch of trap would explain the exponential nature of the iodine curves seen in Figure 4-20. Essentially all of the iodines are removed by the trap.

Somewhat similar results were obtained for non-volatiles trap sample #2. During a portion of the sampling period for Trap #2, the flow rate was inadvertently lowered (i.e. gas transit time increased) so that the data for Sr 89, Ba 140, and Ce 141 would consequently be expected to fall on curved lines rather than straight lines as in Fig. 4-19. This was found to be the case. However, the activity distributions for I 131 and I 133 were both found to be maximum at the trap inlet and outlet and minimum in the center of the trap. The cause for this type of distribution is not known.

The leakage factors for these various isotopes are based on the non-volatiles trap data and are summarized in Table 4-13 and also superimposed on Fig. 4-18. In addition to the isotopes plotted in Figs. 4-19 and 4-20. Cs 137, Te 132, and Y 91 were also found. Cs 137 was detected in Trap #1 in such a small amount that leakage factors could not be calculated. However, the Cs 137 activity was sufficiently high in Trap #2 that its distribution plot was found to coincide with the predicted distribution based on Xe 137 diffusion from the specimen. This implies that cesium isotopes which have a boiling point of 1240°F probably did not diffuse from the fuel element and that the Cs 137 found in the trap came from Xe 137 which diffused from the fuel element and decayed in the trap. The slight traces of Te 132 found in each trap indicate that there may have been some diffusion of tellurium which is molten at the specimen operating temperature.

TABLE 4-13

Summary of Non-Volatile Trap Data for Specimen FA-22(471E) in Capsule SP-5

Trapped Species		Principal Gaseous Precursor Isotope		Leakage Factors (a) Trap #1	Trap #2	Trap #3 (f)
54d	Sr 89	3.2m	Kr 89	3.0×10^{-7}	8.9×10^{-6}	1.1×10^{-5}
64.4h	Y 91	9.8s	Kr 91	(e)	4.0×10^{-6}	5.9×10^{-6}
12.8d	Ba 140	16s	Xe 140	1.0×10^{-7}	9.2×10^{-7}	5.4×10^{-6}
32d	Ce 141	1.7s	Xe 141	1.3×10^{-7}	1.4×10^{-6}	6.3×10^{-6}
25.6y	Cs 137	3.9m	Xe 137	(b)	7.1×10^{-6}	1.0×10^{-5}
8.05d	I 131			1.2×10^{-8}(c)	(d)	(e)
20.8d	I 133			1.4×10^{-8}(c)	(d)	(e)
77h	Te 132			(b)	(b)	(e)

(a) Release rate/production rate; Trap #1 at 1 a/o burnup, Trap #2 at 5 a/o burnup, Trap #3 at 6 a/o burnup.
(b) Activity level only high enough to permit qualitative identification
(c) Leakage factor for the trapped iodine isotope.
(d) Due to peculiar distribution within the trap, the release rate for this isotope could not be calculated.
(e) Chemical analysis for this isotope was not performed.
(f) Data from ref. (20).

4.4.4 Post-Irradiation Examination

The Hot Cell examination of the specimens in Capsule SP-5 was conducted under Battelle's Coated Particle Program. The information in this section was taken from refs (21, 22). The two Al_2O_3 coated UO_2 fueled specimens from SP-5 were examined in the Hot Cell. Specimen FA-22(471E) had been irradiated in a sweep compartment of SP-5 and the fission product release from this specimen was shown in Fig. 4-18. Specimen FA-22(470E) was irradiated in the static compartment of SP-5. Both specimens were estimated to have received a burnup of 6 a/o U235.

Visual Examination. Upon their removal from the capsule, both specimens appeared clean and shiny with no visible cracks or flaws in the graphite matrix. There were two exceptions. One area on specimen 471E, about 1" diameter, appeared dull and pitted. This dull area was located in a region which was believed to have been adjacent to the sweep helium inlet position in the Capsule indicating that the sweep gas may have caused some erosion or corrosion of the fuel element surface. During the capsule opening, specimen 471E was inadvertently nicked by the cut-off wheel, leaving a 1/2" diameter flat on the specimen. Close examination of this region showed that some of the coated particles had been wholly removed and that there was no apparent damage to the remaining coated particles.

Weight and Dimension Measurements. Weight and dimension changes for the FA-22 specimens are shown in Table 4-14. The large difference between the polar and equatorial shrinkage in specimen 470E was surprising. In all previous tests on molded graphite spheres, there was no significant difference between the shrinkages in these two directions (i.e. see Table 7-7). The FA-22 specimens had a slightly lower net graphite density and bake temperature than the other molded graphite specimens but it is not known whether either of these factors could be responsible for the large polar shrinkage noted in specimen 470E. There was no significant difference between the equatorial shrinkage of the FA-22 specimens and other molded specimens in previous capsule tests. The weight loss for specimen 470E was about twice as high as for previous specimens. One reason may have been loss of coated particles from the surface of the specimen although the loss of about 1000 particles would have been required in order to account for the difference.

TABLE 4-14

Weight and Dimension Changes for FA-22 Specimens in Capsule SP-5

Specimen	Weight Change, %	Diameter Change, %
FA-22(470E)	-0.22	-0.5 (a) -2.5 (b)
FA-22(471E)	(c)	-0.2 (a) —— (c)

(a) Average change excluding diameter parallel to direction of molding plane.
(b) Change in direction of molding force.
(c) Measurement not obtained due to inadvertent damage to specimen while opening capsule.

Compression Test. Specimen 470E was subjected to a compression test. The specimen was found to fracture at a load of 4520 lbs and a deflection of .0725 in. The load modulus was 69,000 lbs/in. These values are about equal to the pre-irradiation values shown in Table 4-8. However, post-irradiation increases in both the compressive load at failure and the load modulus had been noted for graphite spheres fueled with uncoated fuel particles. One of two conclusions could be drawn from the lack of increase in the load modulus of the irradiated FA-22 specimen. One is that fission fragment damage to a graphite matrix fueled with uncoated particles is the significant factor in increasing post-irradiation graphite hardness since the fuel particles were coated in the FA-22 specimen, preventing recoil damage to its matrix. The other is that neutron irradiation caused no further hardening of the FA-22 graphite matrix due to its low degree of graphitization.

Metallographic Examination. Specimen 471E was sectioned to permit metallographic examination of the coated particles inside the specimen. Two spherical wedge-shaped sections were mounted and examined. Numerous photomicrographs were made at various locations in the sections. Typical post-irradiation views are shown in Figs. 4-21 and 4-22. The Al_2O_3 coated UO_2 particles in specimen 471E were from batch 4E. No change in the general appearance of the Al_2O_3 coatings can be noted when compared with the pre-irradiation view in Fig. 4-5. The dark bands of porous Al_2O_3 can still be noted between the first impermeable layer of Al_2O_3 and the remainder

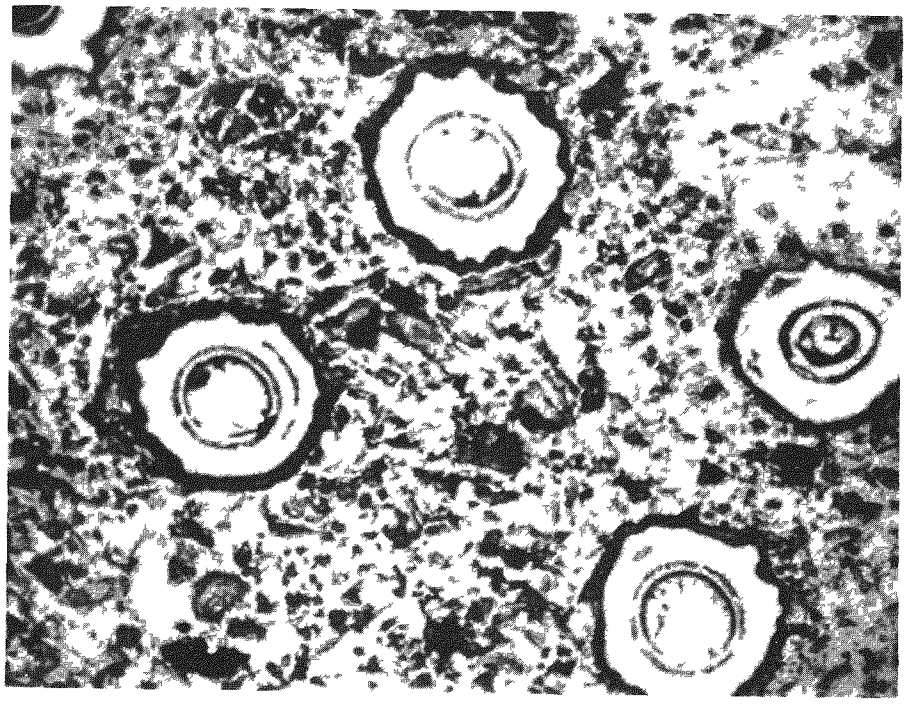

FIG. 4-21 Al_2O_3 Coated UO_2 Particles Near the Center of Specimen FA-22(471E) After Irradiation in Capsule SP-5. (100X)

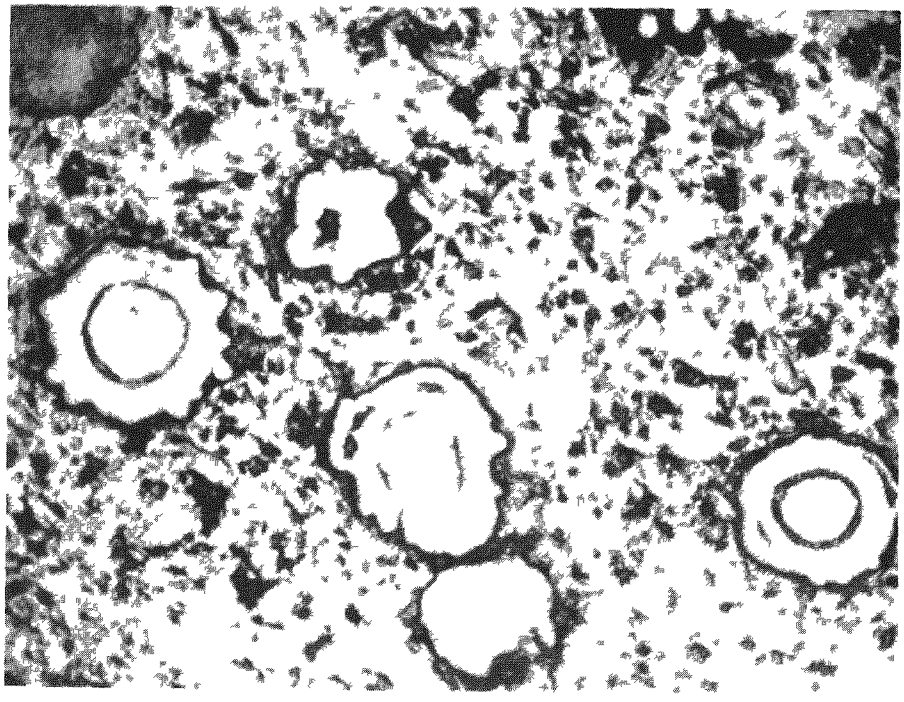

FIG. 4-22 Al_2O_3 Coated UO_2 Particles Near the Edge of Specimen FA-22(471E) After Irradiation in Capsule SP-5. Note Cracks in Al_2O_3 Coatings. (100X)

of the impermeable Al_2O_3 coating. Some cracks were noted in the coatings on some of the particles as can be seen in Fig. 4-22. The cracks generally ran radially through the coating and there were usually 2 or more cracks in a particle. When there were only 2 cracks, they were 180° apart. In several cases, the cracks originated at the depressed region between two protrusions on the outer surface of the coating. A statistical count of the incidence of cracked coatings was made from the numerous post-irradiation photomicrographs. It was found that 8 to 11% of the particles had cracks in their coatings. Most of these cracked particles were located between the midradius and the surface of the graphite sphere.

4.4.5 Analysis of the Data

The term R/B (i.e. the ratio of release rate to the production rate) is used because it is a convenient way of expressing the fission product leakage data. The experimentally determined release rates are simply divided by an equilibrium production rate which is based on the estimated flux, uranium loading in the specimen, and the fission yield. Also, the R/B term can be used directly to compute the reduction in equilibrium primary loop activity when comparing coated fuel element performance with that for uncoated fuel. However, if fission products are released by a diffusion mechanism, the actual isotope concentration (rather than production rate) at the time of sampling determines the release rate. Fortunately, most of the isotopes of interest reach an equilibrium concentration level within 24 hours after startup which is the minimum time period before samples are taken. The one exception is Xe 133 which requires nearly 30 days to reach equilibrium concentration.

A mathematical model has been devised by S. D. Beck of BMI to approximate fission product diffusion from a coated fuel particle. This model is based on the assumption that equilibrium conditions have been achieved, that fission products are generated uniformly in fuel particles only, and that the diffusion coefficients are equal for both the fuel particle material and the coating material. The relationship is:

$$\frac{R}{B} = \frac{3(a/b)^3}{a\sqrt{\lambda/D}\,\sinh a\sqrt{\lambda/D}} \left[b\sqrt{\lambda/D}\,\cosh b\sqrt{\lambda/D} - \sinh b\sqrt{\lambda/D} \right]$$

where:

R = rate of release, atoms/sec
B = rate of production, atoms/sec
a = outer radius of coating, cm
b = inner radius of coating, cm
λ = decay constant, sec^{-1}
D = diffusion coefficient, cm^2/sec

This relationship has been used to construct a graph of R/B as a function of half-life with D as a parameter for use in analyzing the fission product release data from FA-22(471E) in Capsule SP-5 as shown in Fig. 4-23. Although the assumptions used to derive this relationship are oversimplified, the diffusion model does show the very strong effect of isotope decay constant on fission product leakage. When a volatile isotope is

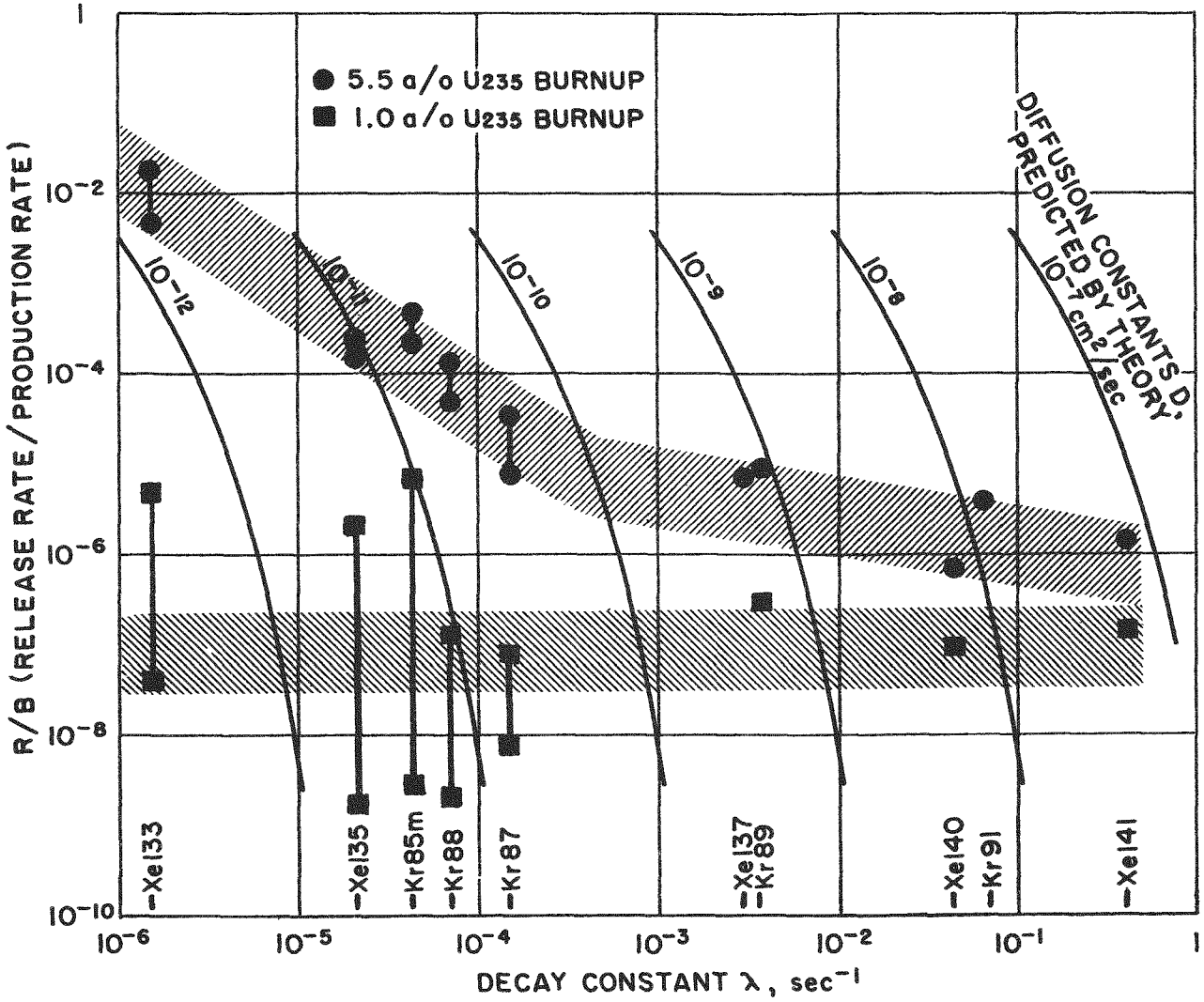

COMPARISON OF DATA FOR SPECIMEN FA-22(471E)
IN SWEEP CAPSULE SP-5
WITH THEORETICAL PREDICTIONS

FIG. 4-23

diffusing through the coating and it decays into a non-volatile isotope, it is assumed that no further diffusion occurs. Thus, very low leakage rates would be expected for short-lived isotopes.

The leakage data at 1 a/o and 5 a/o burnup are plotted in Fig. 4-23. The leakage data at 6 a/o is only slightly higher than the 5 a/o data and follows the same trend. At 1 a/o burnup, the leakage factors for all isotopes are approximately equal in the range of 10^{-6} to 10^{-8} and there is no tendency for the data to fall along lines of constant diffusion coefficients. This indicates that the "leakage" from the specimen most probably arises from uranium contamination external to the fuel particle coatings. There was no significant leakage through the coatings. The leakage factors are of the same order as found in the low-level irradiation test of another FA-22 specimen in Capsule SPF-3 (see Fig. 4-17). However, at 5 a/o, the leakage factors for the longer-lived isotopes do tend to approximate the lines of constant diffusion coefficient implying a measurable fission product release from the UO_2 particles. The leakage factors for the short-lived isotopes at 5 a/o burnup show only a slight half-life dependency and are about an order of magnitude higher than the corresponding 1 a/o data.

As can be noted in Fig. 4-18, certain of the perturbations in the R/B curve can be associated with temperature variations in the specimen, most noticeably the 1 to 2 order of magnitude decrease of leakage factor for the last two samples corresponding to a temperature drop of about 1150°F to 950°F. This indicates a strong temperature dependency for the highly irradiated coatings in distinction to the small temperature dependency at low burnups noted in Capsule SPF-3. The perturbations during the early part of the irradiation do not entirely correspond to temperature changes and it is not clear whether other factors in the test procedure were responsible for these variations.

The Hot Cell examination of FA-22(471E) had revealed that 8 to 11% of the coated particles in this specimen had cracks in their coatings and that most of these cracked particles occurred in the outer half of the graphite sphere. These cracks are responsible for the increased leakage of the short-lived gaseous fission products at 5 and 6 a/o burnup. It is interesting to note that the short-lived isotope leakage factors for the FA-22 specimen are two orders of magnitude lower than the leakage factors for the FA-23 specimen (see Table 3-9) rather than only one order of magnitude lower as might be expected from the number of cracked fuel particle coatings in the FA-22 specimen. The nature of the cracks in these coatings as seen in Fig. 4-22 was such that they were still able to cause some delay in the release of the short-lived gaseous isotopes.

There is no direct evidence to date that radiation damage caused a change in the physical properties of the vapor deposited Al_2O_3 coatings, other than the cracks which were noted. There was no change in the appearance of the Al_2O_3. X-ray diffraction studies of these irradiated particles which are planned at Battelle may show some changes. The greater incidence of cracked particle coatings near the surface of the sphere suggests that the cracks are associated with an irradiation effect since the estimated neutron flux in the center of the fueled sphere during capsule irradiation was about 70% of the flux at the surface of the sphere. Estimates of the pressure buildup within a coated particle due to fission product gases indicate that the resulting tensile stress in the Al_2O_3 coating would be about 3000 psi at 6 a/o burnup. This is well below rupture stresses of 30,000 psi reported for unirradiated Al_2O_3 (11). This suggests that an irradiation induced embrittlement may have seriously weakened the Al_2O_3 to the point where fission gas pressure caused the coatings to crack. Further irradiations of numerous batches of Al_2O_3 coated UO_2 of the type planned for the Battelle Coated Particle Program are needed to resolve this matter.

5.0 Pyrolytic Carbon Coated Fuel Particles

Interest in pyrolytic carbon coated fuel particles stems from previous experience with pyrolytic carbon coatings on the surface of fuel elements. Advantages of pyrolytic carbon as a particle coating material are that it removes the temperature limitation imposed by the chemical reaction between metal oxide particle coatings and the graphite matrix and that the pyrolytic carbon coating material does not effectively displace moderating material when dispersed in graphite.

An exploratory program on pyrolytic carbon coated UC_2 particles was conducted at the Battelle Memorial Institute. Also, several types of these particles, as well as coated particle fueled graphite spheres, were procured from commercial sources for evaluation.

5.1 Coated Particle Fabrication

Pyrolytic carbon is formed by the pyrolysis of a hydrocarbon gas which causes a layer of carbon to build up on the surface to be coated. A fluid bed process was used at Battelle to coat UC_2 particles. The basic apparatus consisted of a 1" diameter by 24" long reaction tube, located inside an electrical resistance furnace. A helium stream containing either acetylene or methane was used to fluidize the bed. An enlarged disentrainment section was located above the reaction tube. For the 1800°F runs, a quartz reaction tube was used and a thermocouple well was located inside the reaction tube. For the 2400°F runs, a Mullite reaction tube was used with an external thermocouple.

A summary of the process conditions for the particles fabricated at Battelle is given in Table 5-1. UC_2 particles for batches PyC-1 and PyC-2 were obtained from the Carborundum Co. and were crushed and sieved from UC_2 pellets. The spherical UC_2 shot used in batches PyC-5 and PyC-6 was obtained from the Minnesota Mining & Mfg. Co.

TABLE 5-1

Pyrolytic Carbon Coated Fuel Particles Prepared At Battelle

Batch No.	UC_2 Shape	UC_2 Size, μ	Gas	Temp, °F	Coating Thickness, μ	w/o U
PyC-1	Irreg.	177/250	CH_4	2060	7	
			C_2H_2	1870	21	
			C_2H_2	1990	12[a]	70.6
PyC-2	Irreg.	177/250	C_2H_2	1860	17	84.4
PyC-5	Spher.	150/250	C_2H_2	2450	160	22.9
PyC-6	Spher.	150/250	C_2H_2	2450	80	53.8

(a) Final coating thickness was 40μ .

Photomicrographs of particles from batches PyC-1 and PyC-2 are shown in Figs. 5-1 and 5-2. As seen in both figures, all particles have been rather uniformly coated with a continuous carbon phase in spite of the irregular shapes of the UC_2. One particle from batch PyC-1 in Fig. 5-1 has a crack at one end through the inner two coating layers but the outer layer is continuous over the crack. The interface between the second and third coating layers can be readily detected which indicates that successive layers of pyrolytic carbon are not as well bonded as in the case of Al_2O_3.

The thickness of pyrolytic carbon applied in a single run at about 1900°F (Batches PyC-1 and PyC-2) was limited by carbon soot formation which tended to plug the discharge lines from the reaction vessel. Several attempts were made to eliminate this problem by introducing CO_2 to react with the excess carbon but no significant effect was found.

Batch PyC-5 was prepared with the objectives of determining whether the higher deposition temperature would resolve both the soot problem and the thermal cycle fracture problem, and also to utilize spherically-shaped UC_2 particles. The UC_2 shot used in batches PyC-5 and PyC-6 was procured from the Minnesota Mining and Manufacturing Co.

When batch PyC-5 was fabricated, the coating process was found to proceed at a very rapid rate. The entire 160 micron coating was deposited in only two hours. The absence of soot formation at the higher deposition temperature of 2450°F permitted this thick coating to be deposited in one step. A photomicrograph of particles from batch PyC-5 is shown in Figure 5-3.

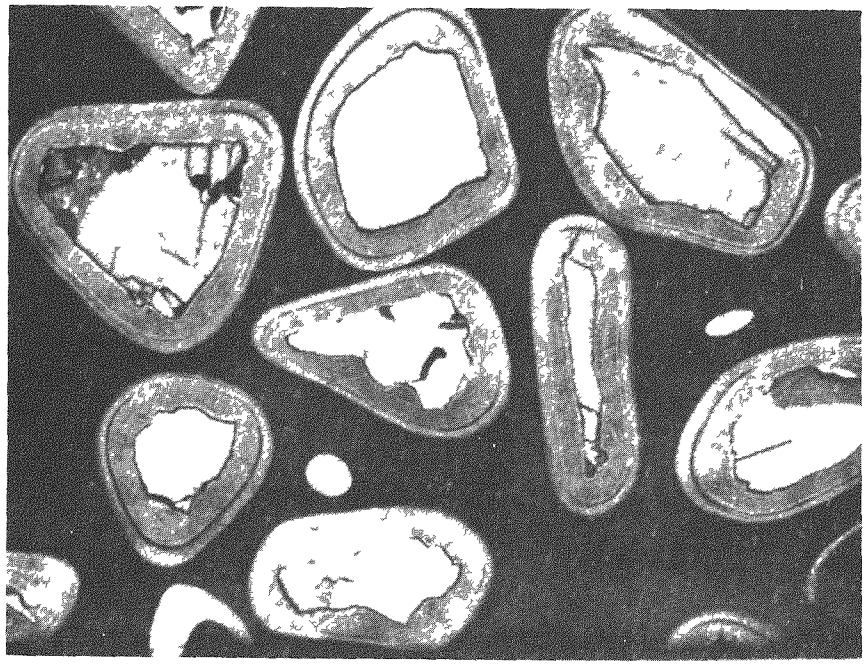

FIG. 5-1 Batch PyC-1 showing pyrolytically deposited carbon coatings on UC_2 particles (100X)

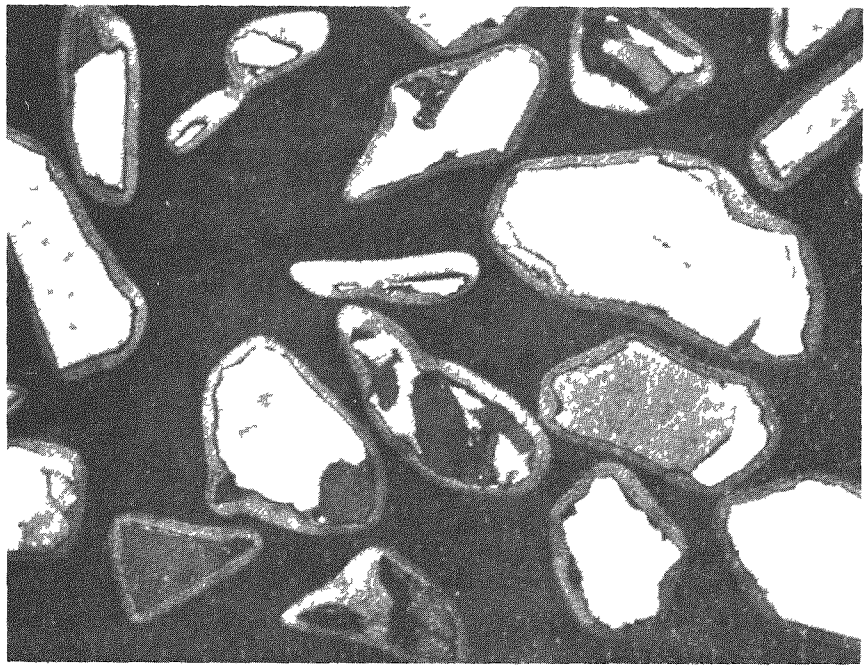

FIG. 5-2 Batch PyC-2 showing pyrolytically deposited carbon coatings on UC_2 particles (100X)

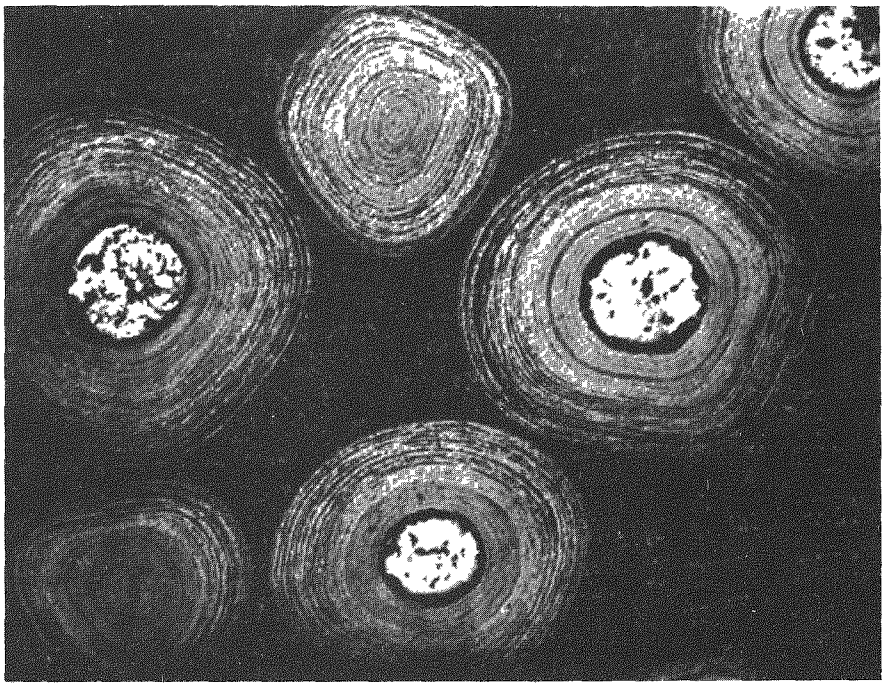

FIG. 5-3 Batch PyC-5 showing pyrolytically deposited carbon coatings on UC_2 (80X)

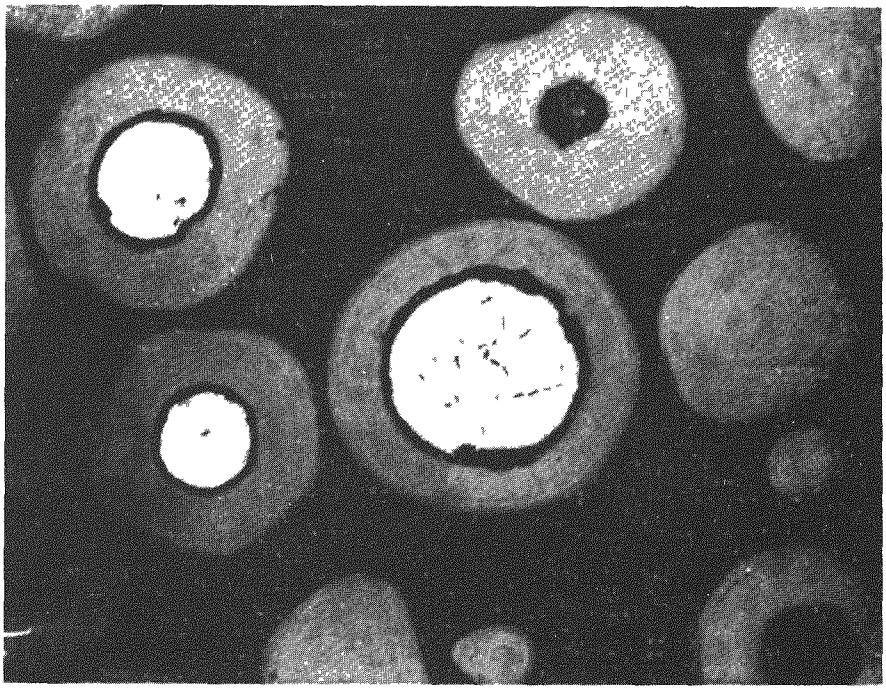

FIG. 5-4 Batch PyC-6 showing pyrolytically deposited carbon coatings on UC_2 (100X)

The spherical UC_2 particles are seen to be uniformly coated. However, an increasing amount of annular porosity can be noted with increasing radius producing an "onion-skin" effect. The individual layers of pyrolytic carbon appear to be continuous. The layer formation is believed to be due to either recycle of particles between hot and cold zones in the reaction vessel or the differences in thermal contraction rates in the normal and tangential directions in the pyrolytic carbon.

The next run was made with the same materials at the same conditions but the run was stopped when only half of the previous coating thickness (i.e. 80 microns) was deposited. A photomicrograph of particles from batch PyC-6 is seen in Figure 5-4. As can be noted there is no gross porosity in the coatings on this batch. The coatings are somewhat similar to the inner half of the coatings on batch PyC-5 in Figure 5-3. The dark band between the coating and UC_2 particles is a void region formed by the greater contraction of the UC_2 particle in cooling down from the deposition temperature. In general, the uniformly dense and impermeable appearance of these coatings was most encouraging.

Four batches of pyrolytic carbon coated UC_2 particles were obtained from commercial sources for evaluation. All of these batches utilized 177/250 micron spherical UC_2 shot and were coated with 80 microns of pyrolytic carbon at deposition temperatures ranging up to 3600°F. Table 5-2 lists the batches which were procured from commercial sources for evaluation. All of these particles were subjected to a 3600°F thermal cycle test and an acid rinse by the manufacturer.

TABLE 5-2

Commercially Obtained Pyrolytic Carbon Coated UC_2 Particles

	Manufacturer	
Batch No.	Coating	UC_2 Shot
PyC-7	Minn. Mining & Mfg.	Minn. Mining & Mfg.
PyC-8	High Temp. Materials	Minn. Mining & Mfg.
PyC-9	National Carbon	National Carbon
PyC-10	Am. Metal Products	Am. Metal Products

Fig. 5-5 shows sections of several coated particles from batch PyC-8 under normal light. Fig. 5-6 shows one of these particles under polarized light where the conical growth patterns can be seen which is typical of pyrolytic

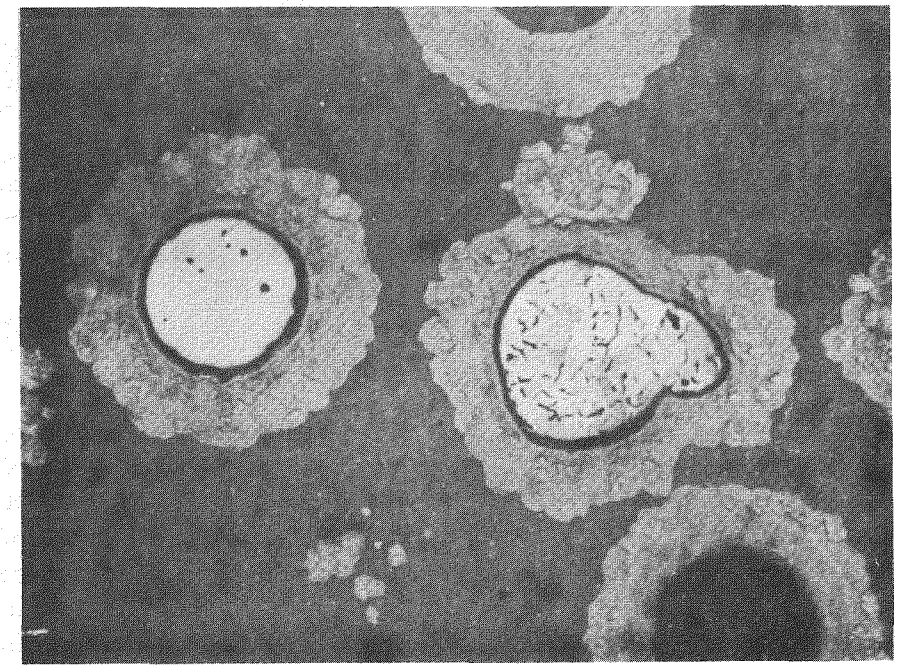

FIG. 5-5 Pyrolytic Carbon Coated UC_2 from Batch PyC-8. Bright field at 100X.

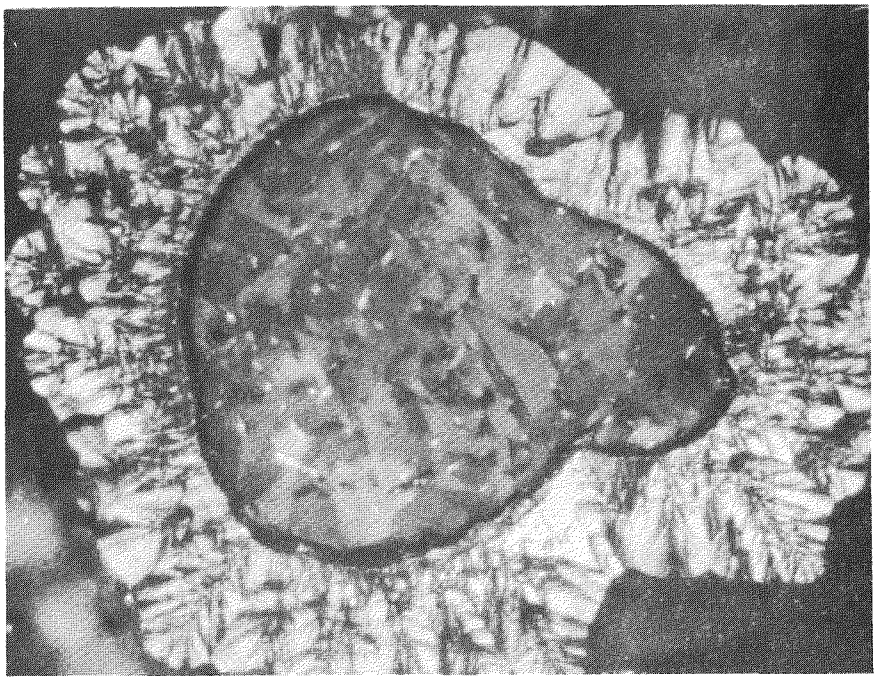

FIG. 5-6 Pyrolytic Carbon Coated UC_2 from Batch PyC-8. Polarized light at 250X.

carbon deposited near 3600°F. The outer surface of the coating is irregular due to the protrusions of the carbon growths.

Fig. 5-7 shows sections of several coated particles from batch PyC-7 under normal light and Fig. 5-8 shows one of these particles under polarized light. The coatings are smooth and continuous. The layered structure is similar to the structure noted in the PyC-6 particles in Fig. 5-4. The absence of the conical growth patterns under polarized light indicated that these coatings were deposited at less than 2900°F.

Fig. 5-9 shows sections of several coated particles from batch PyC-9 under normal light and Fig. 5-10 shows one of these particles under polarized light. Again, the coatings are smooth and continuous and have a layered structure similar to the PyC-7 particles. Occasionally, batches of UC_2 shot have been received in which a number of the UC_2 particles were stuck together. This condition can be noted in Fig. 5-9 where a continuous coating was applied to a pair of joined UC_2 particles. As on all the pyrolytic carbon coated UC_2 particles, a dark region can be noted between the coating and the UC_2 particle. This dark region is created by the relatively greater shrinkage of the UC_2 as the particle is cooled from the coating deposition temperature. Most often, a third phase material can be noted in this region which probably consists of carbon and/or uranium. The structure of the coating on the PyC-9 particles indicates that most of the coating was probably deposited at an actual temperature below 2900°F. In Fig. 5-10, portions of the innermost coating layer contain what could be particulate fuel material caused by fuel particle abrasion in the early stages of coating.

Fig. 5-11 shows sections of several coated particles from batch PyC-10 under normal light and Fig. 5-12 shows one of these particles under polarized light. All the coatings appear continuous but they have a coarse structure. Some evidence of a very fine but scattered conical growth structure can be noted in Fig. 5-12 which indicates that these coatings were deposited at an actual temperature of about 3000°F to 3200°F. The bright spots in the coating could indicate the possible presence of particulate fuel contamination.

Macrophotographs at 33 1/3X of two types of pyrolytic carbon coated particles can be seen in Figs. 5-13 (Batch PyC-8) and 5-14 (Batch PyC-7). The irregular surfaces due to the conical carbon growths in batch PyC-8 and the smoother surfaces of batch PyC-7 can be noted.

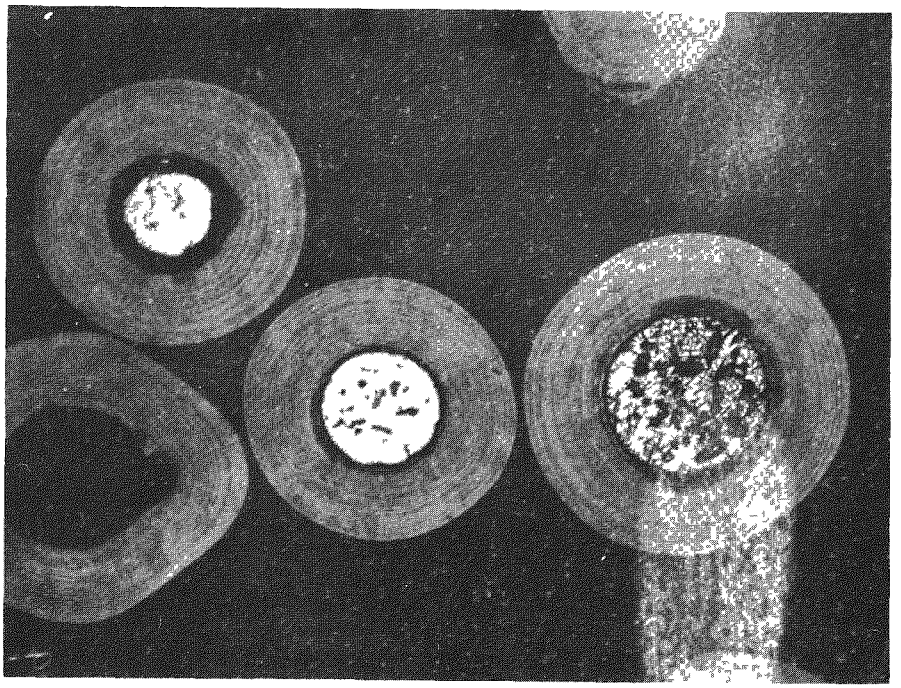

FIG. 5-7 Pyrolytic Carbon Coated UC_2 from Batch PyC-7. Bright field at 100X.

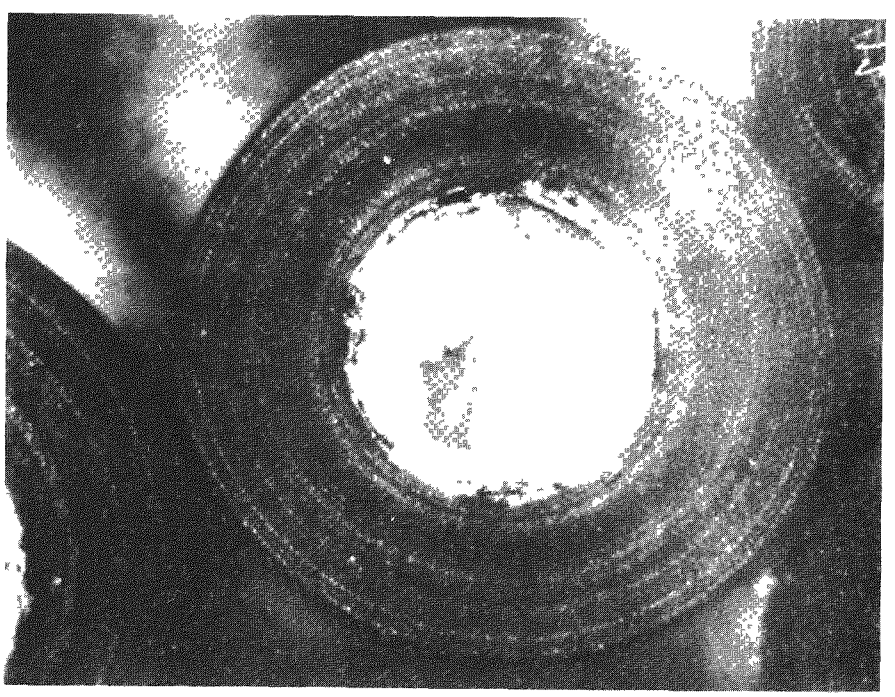

FIG. 5-8 Pyrolytic Carbon Coated UC_2 from Batch PyC-7. Polarized light at 250X.

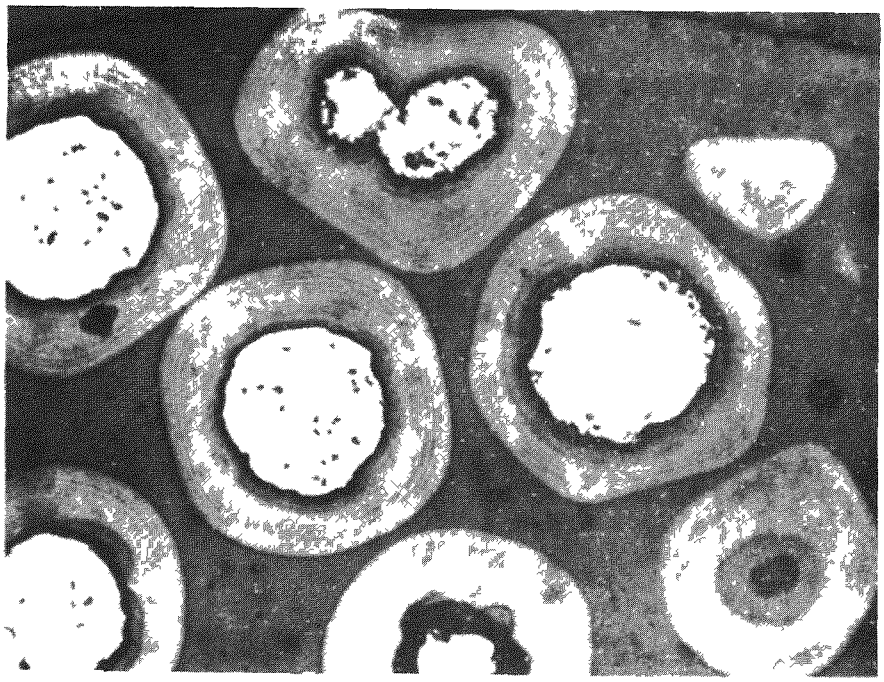

FIG. 5-9 Pyrolytic Carbon Coated UC_2 from Batch PyC-9. Bright Field at 100X.

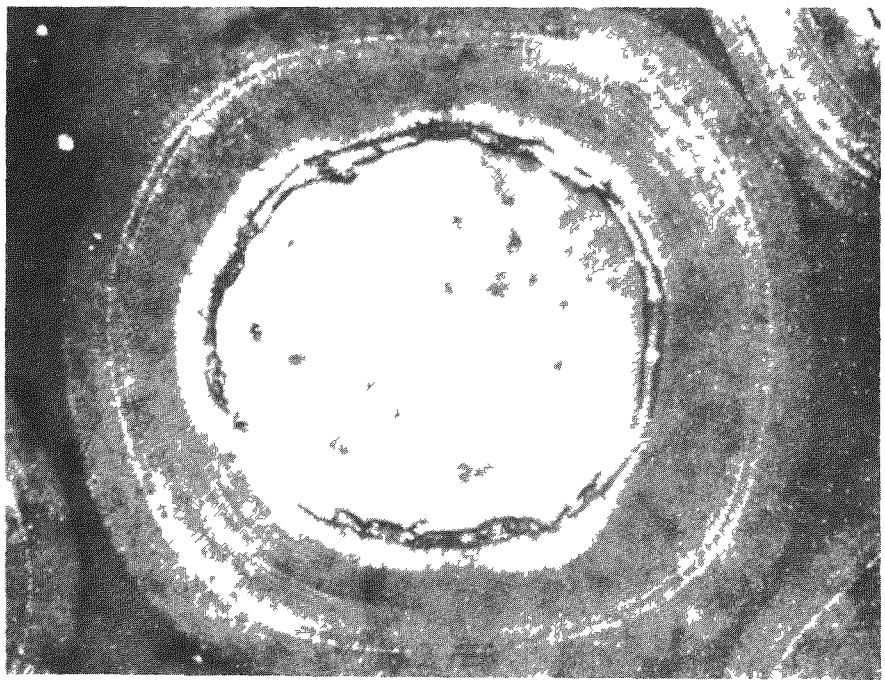

FIG. 5-10 Pyrolytic Carbon Coated UC_2 from Batch PyC-9. Polarized Light at 250X.

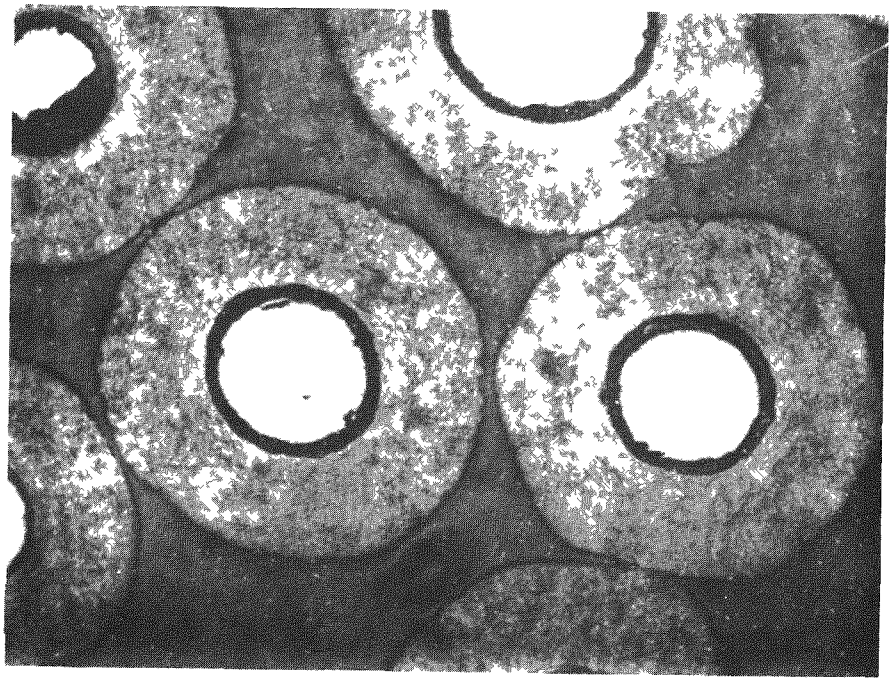

FIG. 5-11 Pyrolytic Carbon Coated UC_2 from Batch PyC-10. Bright Field at 100X.

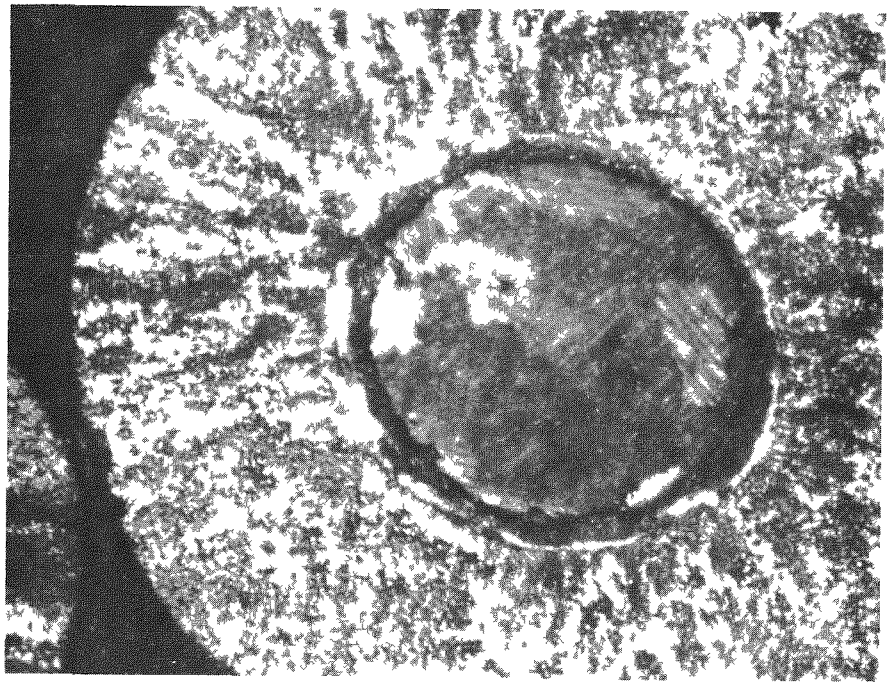

FIG. 5-12 Pyrolytic Carbon Coated UC_2 from Batch PyC-10. Polarized Light at 250X.

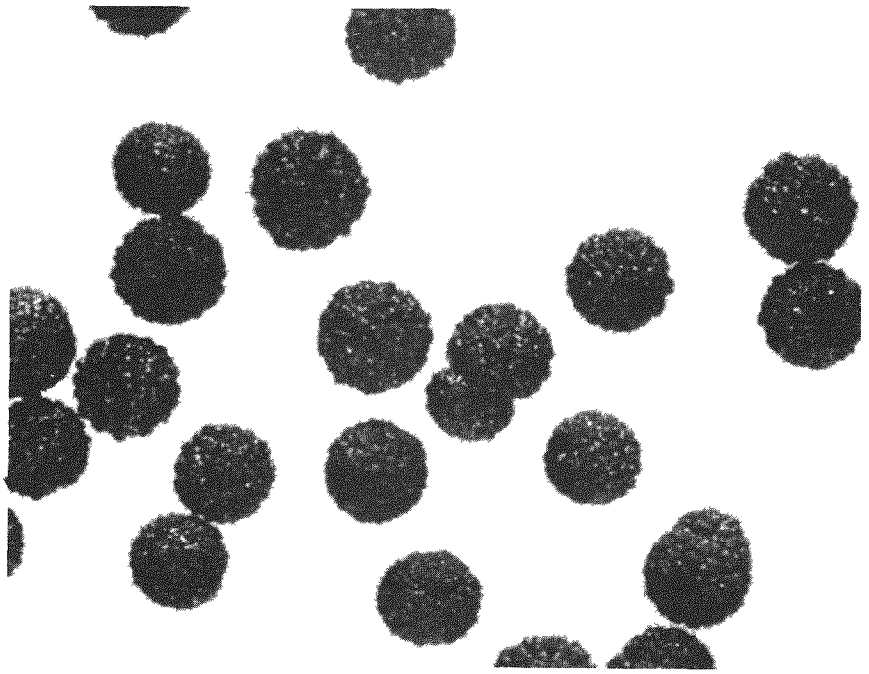

FIG. 5-13 Particles from Batch PyC-8, at 33 1/3X.

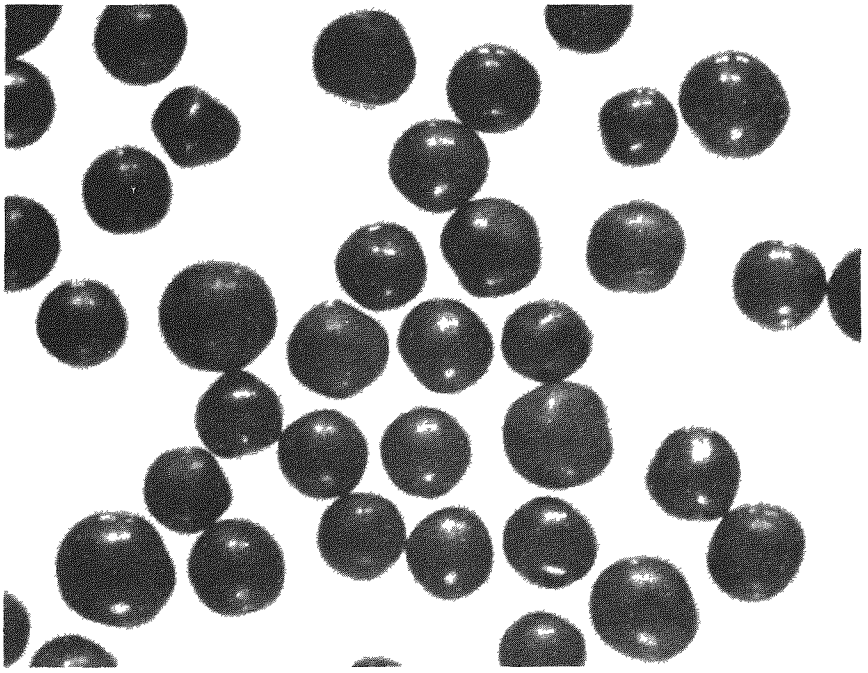

FIG. 5-14 Particles from Batch PyC-7, at 33 1/3X.

5.2 Evaluation of Coated Particles

The standard screening tests performed on pyrolytic carbon coated UC_2 particles are generally similar to those used on alumina coated particles except that a nitric acid leach is used for the coating integrity test rather than the hot air oxidation test. Test results on the pyrolytic carbon coated particles are summarized in Table 5-3.

Batches PyC-1, -2, -5 and -6 were tested in the as-facbricated condition. Uniformly good quality was found for the coatings in all these batches based on the results of the nitric acid leach test. The uranium contamination in these four batches was found by alpha assay to be very low except for batch PyC-2. In this case, it is believed that direct alpha recoils from the UC_2 particles through the thin coatings were responsible for the higher alpha count. The thermal cycle test temperature of 3600°F was selected because of an interest in using the pyrolytic carbon particle coating to prevent chemical reaction between silicon and uranium in an Si-SiC coated fuel element. At this temperature, very severe damage to the coatings in batches PyC-1 and PyC-2 was noted by alpha assays after thermal cycling. Figure 5-15 is a photomicrograph of batch PyC-1 after the thermal cycle test where many of the coating cracks can be seen at the sharper corners of the UC_2 particles. This cracking was due to the higher thermal expansion coefficient of the UC_2 and the rather large difference between the coating fabrication temperature (1950°F) and the test temperature (3600°F). There was much less evidence of thermal cycle cracking in the 2450°F coatings on batches PyC-5 and PyC-6 as noted by alpha assays after thermal cycling. However, a leach test on batch PyC-5 after thermal cycle indicated that a rather large fraction (0.6%) of the particles must have been cracked by this test.

Batches PyC-7, -8, -9 and -10 had all been subjected to a 3600°F thermal cycle test and an acid rinse by the manufacturers prior to the tests noted in Table 5-3. A rather high surface uranium contamination was noted on the as-received particles, about the same as noted on the PyC-5 and -6 batches after thermal cycle. In most cases, further acid leaching removed very little additional uranium and had little effect on the alpha assay. This could mean that uranium contamination measured by the alpha assays was within the coating surfaces or that the initial acid rinsing distributed uranium over the surfaces of whole or cracked particles in such a manner that it could could not be removed by subsequent leach tests. It is not clear from these tests whether this uranium contamination was due to the presence of a few faulty particles in the as-fabricated material

TABLE 5-3

Pre-Irradiation Tests on Pyrolytic Carbon Coated UC_2 Particles

Sample No.	Condition[a]	Net Alpha Count Rate, cpm/gm sample	Exposed Uranium Fraction[b]	Uranium in Leach Solution[b]
PyC-1	As-fab.	0.7 ± 1.1	1.3×10^{-6}	
	Leached	-	-	4×10^{-5}
	T. cycle	2610 ± 31	5×10^{-3}	
PyC-2	As-fab.	244 ± 7	4×10^{-4}	
	Leached	-	-	4×10^{-5}
	T. Cycle	3680 ± 30	6×10^{-3}	
PyC-5	As-fab.	1.9 ± 1.3	9×10^{-6}	
	Leached	-	-	1×10^{-5}
	T. Cycle	21.4 ± 3.7	1×10^{-4}	6×10^{-3}
PyC-6	As-fab.	1.9 ± 1.3	5×10^{-6}	
	Leached	-	-	1×10^{-4}
	T. Cycle	65.6 ± 5.2	1.6×10^{-4}	
PyC-7(1)	As Rec'd	94.7 ± 5.0	1.6×10^{-4}	
	Leached	90.0 ± 4.6	1.5×10^{-4}	2.4×10^{-5}
PyC-7(3)	As Rec'd	65.1 ± 3.8	1.1×10^{-4}	
	Leached	66.0 ± 4.0	1.1×10^{-4}	2.0×10^{-5}
PyC-7(5)	As Rec'd	94.2 ± 5.4	1.6×10^{-4}	
	Leached	85.0 ± 5.2	1.3×10^{-4}	3.2×10^{-3}
PyC-8	As Rec'd	9.7 ± 2.4	2.2×10^{-5}	
	Leached	37.6 ± 3.3	8.6×10^{-5}	2.8×10^{-3}
PyC-9	As Rec'd	38.2 ± 5.2	8.4×10^{-5}	
	Leached	45.4 ± 8.4	1.0×10^{-4}	3.0×10^{-6}
PyC-10(1)	As Rec'd	19.5 ± 3.8	4.1×10^{-5}	
	Leached	20.5 ± 6.5	4.2×10^{-5}	1.0×10^{-5}
PyC-10(2)	As Rec'd	43.0 ± 4.8	8.9×10^{-5}	
	Leached	76.8 ± 9.9	1.6×10^{-4}	$1.0 \text{ c } 10^{-5}$

(a) As-fab. = As fabricated; Leached = After leaching in 1: 1 nitric acid solution at 95°C; T. Cycle = After thermal cycle to 3600°F in an argon atmosphere; As Rec'd = Aas received from manufacturer who had subjected particles to thermal cycle and acid leach.

(b) Expressed as fraction of uranium contained in particles.

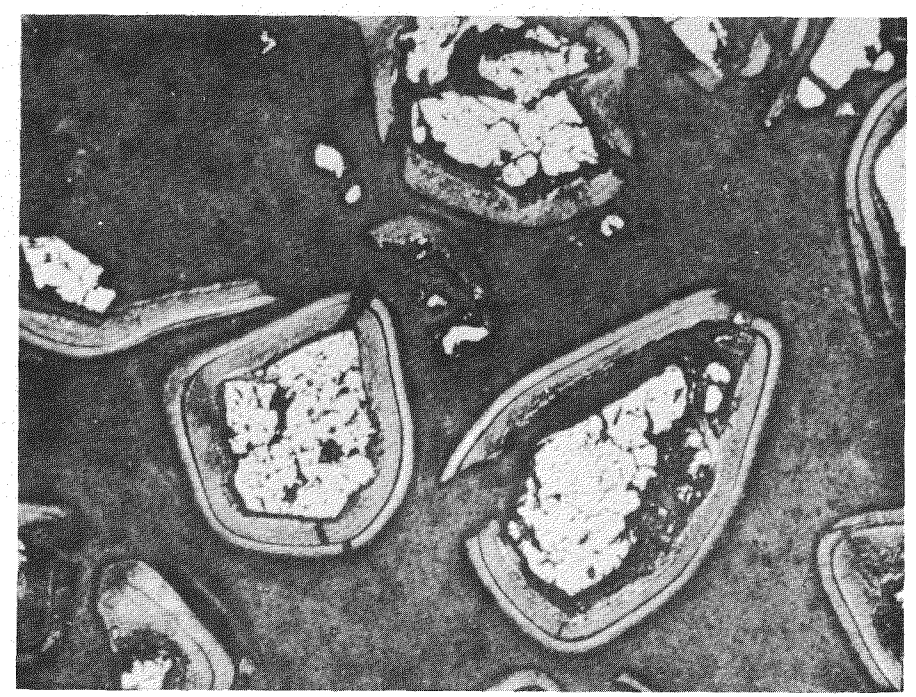

(a) View at 100x.

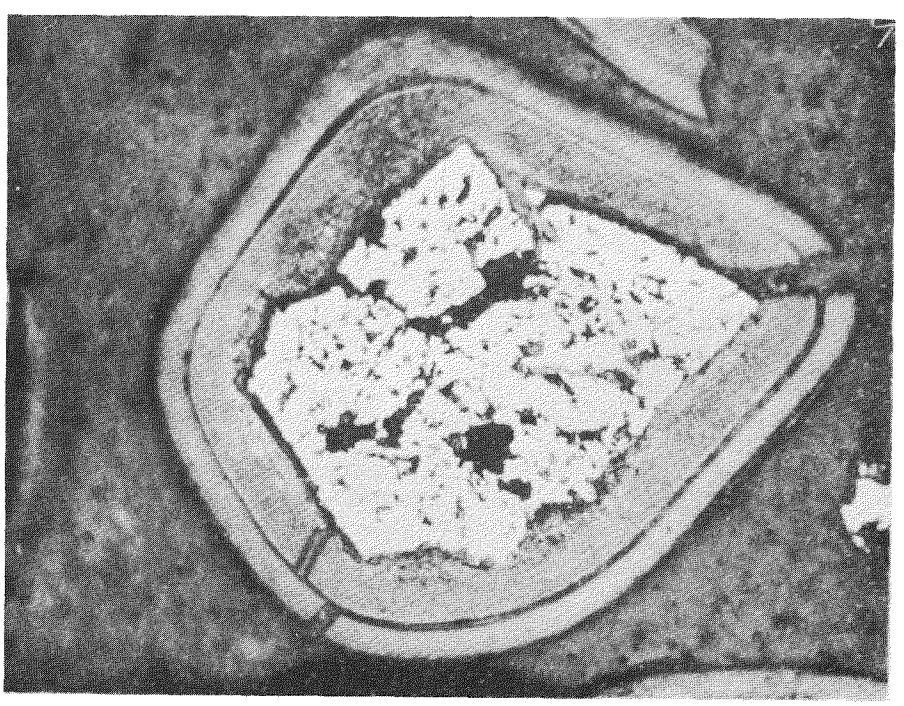

(b) View at 250x.

FIG. 5-15 Particles from batch PyC-1 after thermal cycling to 3600°F

or whether the thermal cycle tests caused some additional coating failures. It should be noted, however, that metallographic inspection of the as-received particles (i.e. after thermal cycling),as typified by Figures 5-5 through 5-12, did not reveal the presence of cracked particles in these batches.

Three batches of pyrolytic carbon coated UC_2 particles were subjected to the neutron activation test for fission product retention. Additional neutron activation tests were run on pyrolytic carbon coated particles after incorporation into a graphite matrix as described in Section 5.3. The results of the tests on the particles only are summarized in Table 5-4.

TABLE 5-4

Neutron Activation Tests on Pyrolytic Carbon Coated Particles

Specimen	Test Temp., °F	Time Min.	Fractional Release of Xe 133
1. Batch PyC-1	1600	160	$<4.5 \times 10^{-6}$
	2000	93	$<4.5 \times 10^{-6}$
	2400	65	4.7×10^{-4}
2. Batch PyC-5	1500	60	(a)
	2000	60	(a)
	2500	65	(a)
	600/2500 (b)		$<6.5 \times 10^{-6}$
	2500	210	2.5×10^{-5}
3. Batch PyC-6	1500	55	(a)
	2000	58	(a)
	2500	55	$<5.2 \times 10^{-5}$
	600/2500 (b)		$<1.0 \times 10^{-4}$
	2500	240	4.2×10^{-4} (c)

(a) Activity level below sensitivity and included in subsequent reading.
(b) Temperature cycled six times.
(c) This Xe 133 release occurred during the last hour of heating.

The neutron activation results on batch PyC-1 showed that up to 2000°F (i.e. the coating deposition temperature), this pyrolytic carbon coating had good fission product retention. At 2400°F, the increased Xe 133 leakage indicates that some of the coatings have cracked which confirms the previous thermal cycle results. In spite of the annular porosity in batch PyC-5, these coatings exhibited good fission product retention. Thermal cycling to 2500°F did not appear to damage the coatings. Batch PyC-6 showed good fission product retention up to its coating deposition temperature of 2500°F. After thermal cycling, the release remained low during the first three hours at 2500°F. During the fourth hour, a rise in Xe 133 release was noted. A subsequent microscopic examination revealed a crusty, glazed white deposit on some of the particles. Peeling of the coating was noted on some of the particles. It is believed that a reaction between the coating and the Alundum crucible used to hold the particles caused this type of damage to the coatings.

5.3 Evaluation of Fueled Spheres

Four types of graphite spheres fueled with pyrolytic carbon coated UC_2 particles were evaluated during the Program. The fuel element type numbers and the coated particle batch used to fuel each type are as follows:

Type FA-24 with batch PyC-1
Type FA-25 with batch PyC-7
Type FA-26 with batch PyC-6
Type FA-27 with batch PyC-9

The 1-1/2" graphite spheres of each type were fueled with a uniform dispersion of the coated particles except for Type FA-26 which consisted of a fueled 1-1/4" graphite core surrounded by a 1/8" graphite shell. Two groups of FA-25 specimens were received, FA-25(N1) through (N8) and a later improved group FA-25(N9) through (N12). A further coating of either Si-SiC of pyrolytic carbon could be applied to any of these fueled spheres but the surface coatings were purposely omitted in order to permit evaluation of the fueled graphite matrix. A further description of these fuel element types is given in Table 2-1.

One problem in the design of a graphite sphere containing a uniform dispersion of coated fuel particles is the molding flash at the equator of the sphere which results from the use of two hemispherical dies in molding the sphere. Abrasion during normal operation could result in the undesirable damage or loss of the graphite molding flash which would contain some coated fuel particles. Attempts to grind off the prominent molding flash on Al_2O_3 coated UO_2 fueled FA-22 specimens resulted in a significant increase in exposed uranium as noted in Table 4-4. Consequently, efforts were made to eliminate or minimize the molding flash in the FA-25 and FA-27 specimens. The successful results can be seen in Fig. 5-16. This photograph shows an FA-25 and an FA-27 fuel element specimen as received from the manufacturer. The presence of coated fuel particles can be noted at the surface of each specimen. Both of these specimens would be an acceptable PBR fuel element provided that a further surface coating were applied to prevent loss of fuel particles.

The surface uranium contamination found on the four types of fueled graphite spheres by the alpha assay method is given in Table 5-5. The high amount of surface contamination found in the FA-24 specimens indicates that there was damage to some of the particle coatings which exposed more uranium. The data for the FA-26 specimen, which has an unfueled graphite

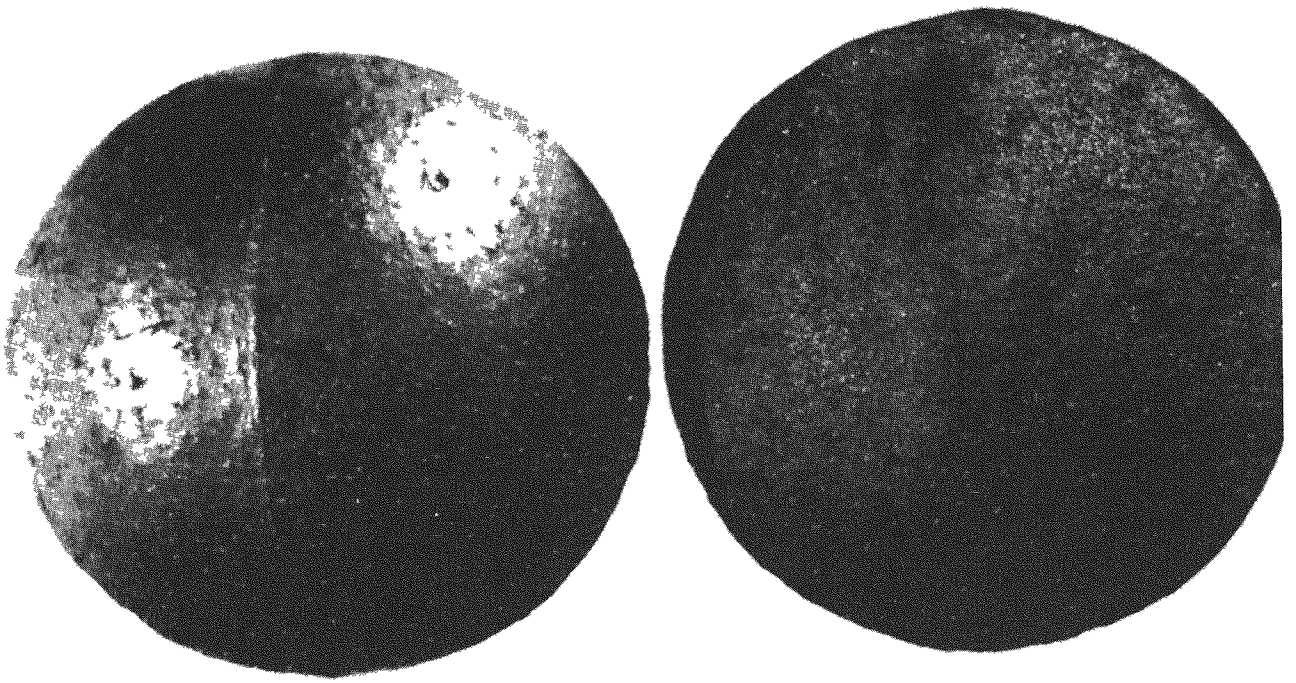

Fuel Element Type FA-27 Fuel Element Type FA-25

FIG. 5-16 1 1/2 inch diameter graphite spheres fueled with Pyrolytic Carbon Coated UC_2 Particles showing minimum molding flash.

TABLE 5-5

Surface Uranium Contamination of Graphite Spheres Fueled with Pyrolytic Carbon Coated UC_2 Particles.[a]

Specimen No.	Position[b]	Net Alpha Count Rate, cpm	Equivalent Surface Uranium, mg[c]
FA-24 (N1)	1	106 ± 13	0.140
	2	82.6 ± 11.2	0.110
FA-24 (N2)	1	61.5 ± 9.1	0.082
	2	84.0 ± 11.2	0.110
FA-24 (N3)	1	77.0 ± 10.5	0.100
	2	64.4 ± 9.8	0.086
FA-25 (N1)	P	16.4 ± 4.9	0.022
	E	15.4 ± 4.0	0.020
FA-25 (N2)	P	44.1 ± 7.7	0.058
	E	14.0 ± 4.5	0.018
FA-25 (N3)	P	35.0 ± 7.4	0.046
	E	35.0 ± 7.4	0.046
FA-25 (N4)	P	9.8 ± 4.9	0.013
	E	9.8 ± 4.9	0.013
FA-25 (N5)	P	14.7 ± 4.5	0.019
	E	11.9 ± 4.2	0.016
FA-25 (N6)	P	14.0 ± 4.4	0.018
	E	10.5 ± 3.8	0.014
FA-25 (N7)	P	11.2 ± 5.2	0.015
	E	9.1 ± 5.1	0.012
FA-25 (N8)	P	18.9 ± 6.3	0.025
	E	8.4 ± 4.5	0.011
FA-25 (N9)	P	9.1 ± 4.2	0.012
	E	18.2 ± 4.2	0.024
FA-25 (N10)	P	6.3 ± 4.2	0.008
	E	4.9 ± 3.5	0.006
FA-25 (N11)	P	2.8 ± 4.2	0.004
	E	11.2 ± 4.9	0.015
FA-25 (N12)	P	8.4 ± 4.2	0.011
	E	13.3 ± 4.9	0.017
FA-26 (N1)	P	2.8 ± 3.5	0.004
	P	11.2 ± 4.2	0.015
	E	7.7 ± 4.2	0.010
	E	0.0 ± 2.8	0.000
FA-27 (N1)	P	15.4 ± 6.3	0.020
	E	18.2 ± 6.3	0.024
FA-27 (N2)	P	35.7 ± 6.3	0.047
	E	29.4 ± 6.3	0.039

(a) Normalized to whole sphere surface
(b) P = polar region; E = equatorial region
(c) 0.001 mg = 2.1×10^{-7} of total uranium in specimen

shell, indicates that trace amounts of uranium from either the fuel particles or the manufacturing equipment were either mixed with or migrated into the unfueled shell. There is no significant difference in the alpha assays at the polar and equatorial regions of the FA-25 and FA-27 specimens indicating that this type of fuel element can be successfully made with a minimum molding flash.

Since a surface alpha assay does not give a quantitative evaluation of the condition of the coated particles below the surface of a fueled graphite sphere, a series of neutron activation tests were performed on the four types of fuel element specimens. The results of these tests are given in Table 5-6. The data is also shown in Fig. 5-17 where the fraction of Xe 133 released is plotted as a function of time. The specimen temperatures associated with each increase in Xe 133 release are also shown on the curves. Temperature equilibrium is achieved with a 5 minute period.

TABLE 5-6

Neutron Activation Tests on Graphite Spheres Fueled with Pyrolytic Carbon Coated UC_2

Specimen No.	Test Temp., °F	Time at Temp., min	Fraction of Xe 133 Released
FA-24(N1)	1000	30	1.7×10^{-3}
	1700	25	3.4×10^{-4}
	2100	60	6.8×10^{-4}
	2500	30	1.5×10^{-3}
	2700	10	4.9×10^{-4}
FA-25(N1)	1650	60	3.3×10^{-4}
	2100	70	4.2×10^{-4}
	2400	50	3.9×10^{-4}
FA-25(N10)	1500	90	5.7×10^{-5}
	2000	90	1.8×10^{-5}
	2400	100	3.4×10^{-5}
FA-26(N1)	100	388	4.4×10^{-4}
	1600	2	5.4×10^{-4}
FA-27(N1)	1500	60	2.4×10^{-4}
	2000	40	5.9×10^{-5}
	2400	55	1.7×10^{-4}

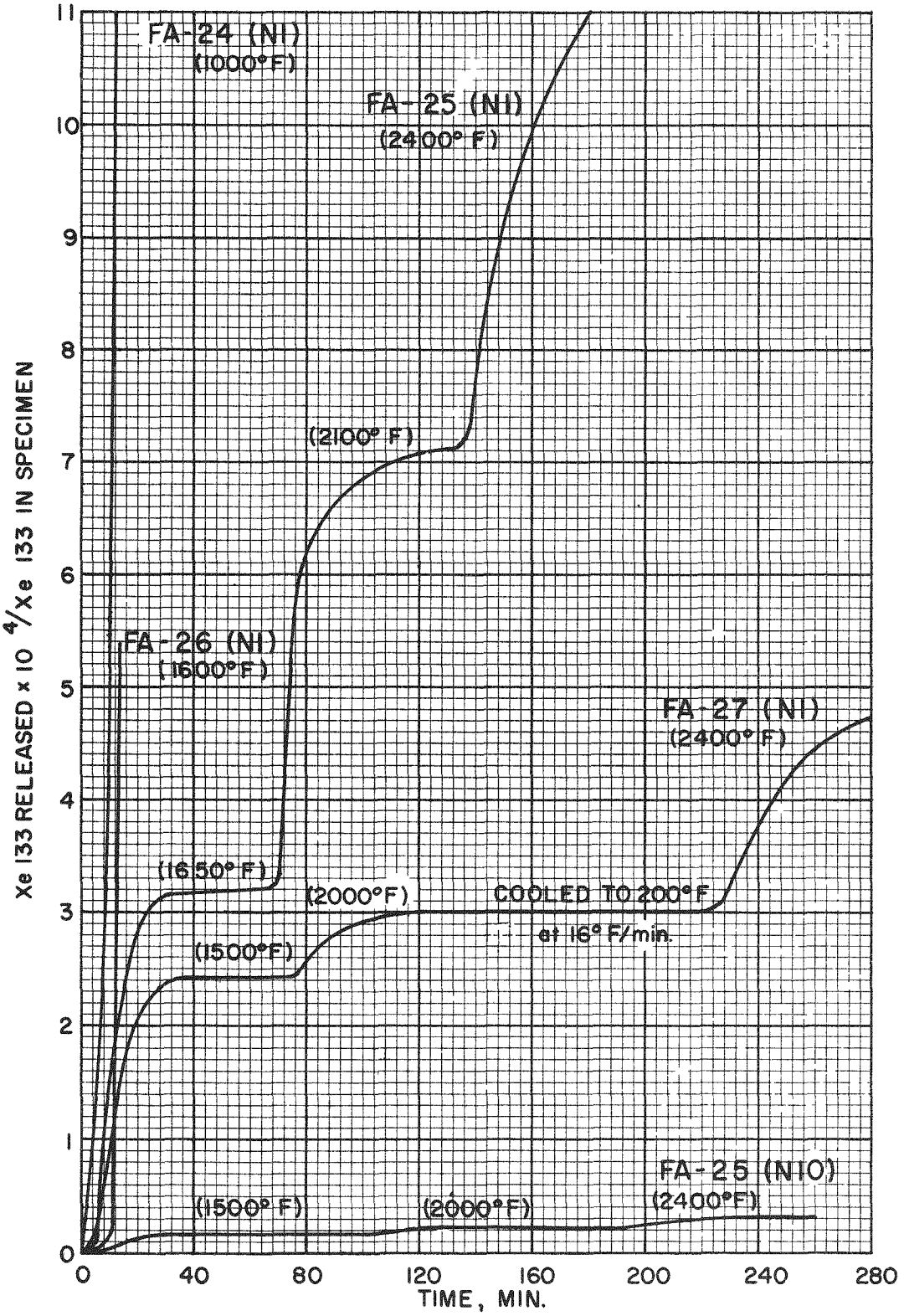

FIG. 5 - 17 NEUTRON ACTIVATION TESTS OF PYROLYTIC CARBON COATED UC_2 FUELED GRAPHITE SPHERES

The very rapid Xe 133 release for the FA-24 and FA-26 specimens indicated that the fuel particle coatings in these specimens were most likely damaged during sphere fabrication, causing UC_2 particles to be exposed. The tendency to reach a plateau in the release-time curve can be noted for the other three specimens. A plateau indicates no further Xe 133 release at the given temperature and implies that Xe 133 release prior to the plateau came from relatively small amounts of exposed uranium. Specimens FA-25(N1) and FA-27(N1) showed no evidence of plateau formation at the higher temperatures which could be attributed to Xe 133 release from uranium contamination just within the pyrolytic carbon coating surface or a small number of cracked fuel particle coatings. The best Xe 133 retention was found for specimen FA-27(N10). Although not apparent in Fig. 5-17, a very slight slope was noted for the FA-27(N10) specimen at the 2000°F and 2400°F test temperatures, of the order of 10^{-8} per min.

In order to determine whether significant amounts of exposed uranium could be removed from this type of fuel element, specimen FA-25(N6) was selected for an acid leach test. This sphere was leached in 1:1 nitric acid at 200°F. The leach solution was analyzed for uranium content and the surface alpha assay was repeated after leaching. Analysis of the acid solution showed that 0.6 mg of uranium was removed from the sphere. The alpha assay results are shown in Table 5-7. From these results, it appears that there was a significant amount of exposed uranium in this specimen, the increase in sphere surface contamination being due to deposition of uranium from the acid solution on large amount of graphite surface area in the sphere.

TABLE 5-7

Acid Leach Test on Specimen FA-25(N6)

	Before Leaching		After Leaching	
Position[(a)]	Total Surface Count Rate, cpm	Surface Uranium, mg	Total Surface Count Rate, cpm	Surface Uranium, mg.
Area 1 (P)	15.4 ± 4.9	0.020	147 ± 15	0.194
Area 2 (P)	12.6 ± 4.2	0.017	371 ± 23	0.490
Area 3 (E)	4.2 ± 2.8	0.0056	155 ± 15	0.205
Area 4 (E)	16.8 ± 4.9	0.022	464 ± 26	0.612

(a) P denotes polar region, E denotes equatorial region.

Table 5-8 compares the amounts of exposed uranium in batch PyC-7 particles and two FA-25 specimens fueled with these particles as found by alpha assay, acid leaching, and neutron activation.

TABLE 5-8

Amounts of Exposed Uranium in PyC/UC_2 Materials [a]

Specimen	Condition	Apparent Surface Contamination (by Alpha Assay)	U Removed by Leaching	Total
Batch PyC-7(5)	As-Rec'd	1.6×10^{-4}	—	—
"	Leached	1.4×10^{-4}	3.2×10^{-3}	3.3×10^{-3}
Sphere FA-25(N6)	As-Rec'd	2.9×10^{-6}	—	—
"	Leached	7.9×10^{-5}	1.3×10^{-4}	2.1×10^{-4}
Sphere FA-25(N1)	As-Rec'd	4.5×10^{-6}	—	—
"	Neut. Act.	—	—	1.1×10^{-3} [b]

(a) Expressed as fraction of contained uranium, except where noted.
(b) Amount of Xe 133 released in 3 hours, expressed as fraction of contained Xe 133, taken from Table 5-6.

In all cases where the samples were leached, the amount of uranium which was removed by leaching far exceeded the apparent amounts of surface uranium found by the alpha assays. This indicates the presence of cracks through the coatings of a type which expose very little uranium surface area in the alpha counter. The total exposed uranium fraction (i.e. leached uranium plus residual surface uranium) for sphere FA-25(N6) is an order of magnitude lower than either the coated particle sample or the neutron activated sphere FA-25(N1). Obviously, a surface alpha assay on the sphere surface does not account for exposed uranium in the center of the sphere. However, it is also apparent that the acid leach did not bring all of the exposed uranium out in solution, leaving most of it behind on the internal surfaces of the graphite.

The neutron activation test cannot be considered a quantitative test because the time period during which the released Xe 133 accumulates in the trap is arbitrarily selected and because Xe 133 diffusion through the coating can be a contributing factor. However, it is interesting to note the

rather close agreement in Table 5-8 between the total exposed uranium fraction in the coated particle sample and Xe 133 release fraction from the fuel sphere. This suggests that no further damage occurred to the coated particles during sphere fabrication and that the relatively high Xe 133 release found in the neutron activation test was due to the initial condition of the coated particles.

Two fuel element specimens were sectioned in order to examine the condition of the coated particles in these specimens. The typical condition of the particles can be seen in Fig. 5-18 showing specimen FA-27(N2) and Fig. 5-19 showing specimen FA-25(N9). No particles with cracked or broken coatings could be found after a thorough examination of both sections. The presence of particulate UC_2 can be more clearly noted in the coatings of specimen FA-27(N2) than in the as-fabricated particles seen in Figs. 5-9 and 5-10. The remaining UC_2 particles appear badly fractured and one is missing completely. It appears that this condition was caused by the sectioning and polishing steps since there is no damage to the coatings. The coated particles in specimen FA-25(N9) appear in excellent condition.

An evaluation of pyrolytic carbon coated particles and graphite spheres fueled with this material has shown somewhat more problems than were experienced in the earlier evaluation of Al_2O_3 coated UO_2 particles. Many of the pyrolytic carbon coated particles had higher uranium contamination in their coatings as shown by both alpha assay and the negligible reduction in contamination by acid rinsing. Better control of uranium dusting during the initial coating stages can alleviate this problem. In some cases where exposed uranium was measured, it was not possible to discern whether it might have instead been due to the presence of a number of poorly coated UC_2 particles. Metallographic examination of several fueled graphite spheres (FA-25 and FA-27) showed that it was possible to incorporate pyrolytic carbon coated particles into a graphite matrix without damage to the coatings. However, there was definite evidence of particle coating damage in other cases (FA-24 and FA-26), as shown by neutron activation tests. This type of damage could have been due to irregular shaped UC_2 particles, the type of coating, or an excessively vigorous mixing step prior to molding. The fission product release from the other fueled graphite spheres appeared to be related to the condition of the coated particles prior to incorporation into the graphite matrix (i.e. uranium contamination and/or the presence of a few poorly coated particles). One factor, which could not be evaluated in the present program, was the influence of the density and permeability of the pyrolytic carbon coating on fission product retention. Also, the effects of irradiation damage remain to be assessed.

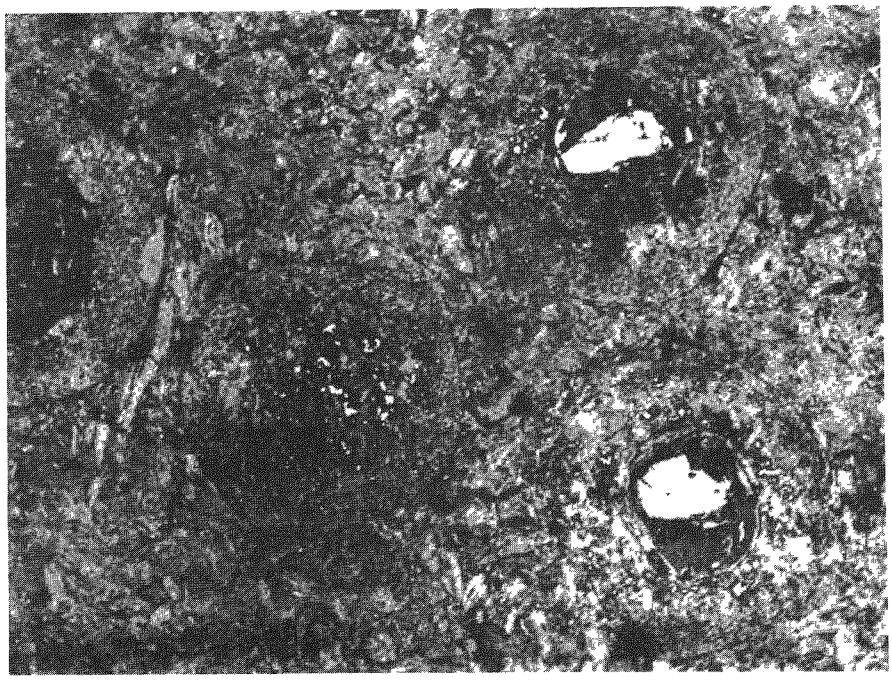

FIG. 5-18 Section of an FA-27 specimen fueled with Pyrolytic Carbon Coated UC_2 from Batch PyC-9. (100X).

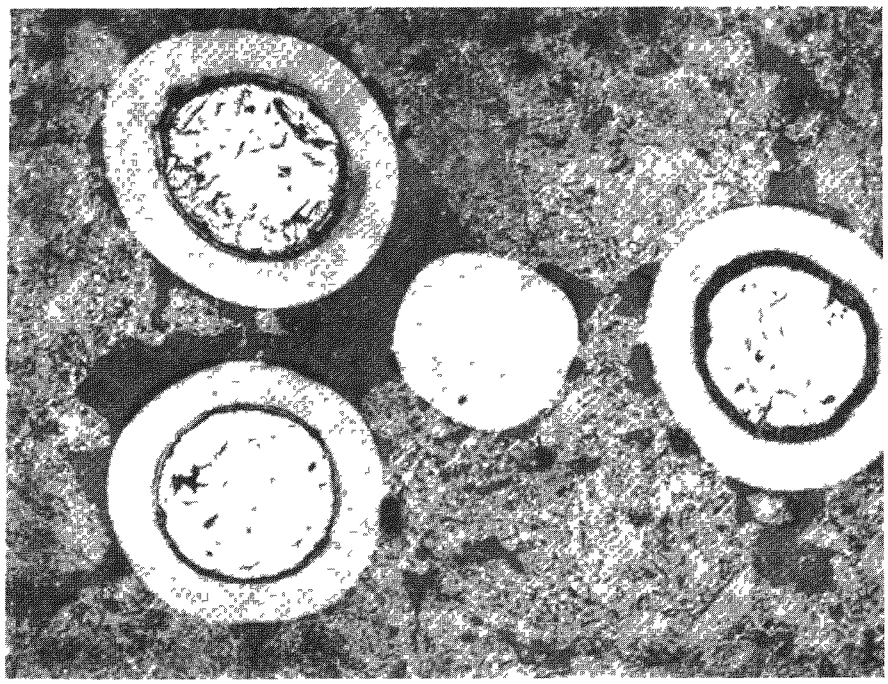

FIG. 5-19 Section of an FA-25 specimen fueled with Pyrolytic Carbon Coated UC_2 from Batch PyC-7. (100X).

6.0 Miscellaneous Coated Specimens

Several other types of fuel element coatings were developed and/or evaluated for the PBR Fuel Element Development Program in addition to the materials discussed in Sections 3.0, 4.0, and 5.0. These included the development of a variety of subsurface coatings for graphite spheres; metal carbide surface coatings such as SiC, TiC, and ZrC; and metal coatings for UO_2 particles, such as Ni, Cr, and Nb.

6.1 Subsurface Coatings

The two primary methods of fission product retention which were explored in the PBR Fuel Element Development Program were coatings on the surface of the spherical fuel element and coatings on individual fuel particles. Another method, conceived by R. F. Benenati of Sanderson & Porter (13), was to locate the coatings beneath the graphite surface. The coating would surround a pellet of either fissile material or fissile material dispersed in graphite. An unfueled graphite shell would in turn surround the coating. The primary advantage of locating the coating beneath the graphite surface is to protect it from the external loads imposed on PBR fuel elements, such as impact or compressive loads which normally would fracture most types of coating located directly on the fuel element surface. Another advantage of a subsurface coating is that, through suitable choice of materials, a coating operating in the plastic or molten range would tend to seal pores and fissures in the lower temperature zone of the unfueled graphite shell.

The exploratory program on subsurface coatings was performed at the Battelle Memorial Institute and consisted of (a) compatibility studies in which the compatibility of various potential coating materials with graphite in a simple shape were investigated; and (b) fabrication studies with fueled graphite spheres.

6.1.1 Materials

Two varieties of the subsurface coatings were studied. In one, materials having melting points in the range of peak PBR operating temperatures were used. In the other, materials with a higher melting point were used so that the coating could be "set" in a baking furnace prior to use. The pertinent properties of materials tested are given in Table 6-1.

TABLE 6-1

Materials Used in Subsurface Coating Studies

Material	Melting Point, °F	Absorption Cross-Section, barns
Cu	1980	3.6
4 glasses	1800 - 2500	(See Table 6-2)
Si	2600	0.13
Ni	2640	4.5
Cr	2940	2.9
Zr	3090	0.18
Ti	3270	5.6
$MoSi_2$	3690	2.7

A number of special glasses were prepared to have softening points in the range of 1800°F to 2500°F. The composition of these glasses are shown in Table 6-2.

In selecting these materials the glasses were included for the reason that they represent a ceramic that can be tailored in melting point and wettability by adjusting composition. $MoSi_2$ which was known to be compatible with graphite, was included to provide a common material in the compatibility and fabrication studies. Copper, nickel and silicon were selected as metals for possible subsurface application because of their range of melting temperatures, their reactions with graphite, and compatibility characteristics with graphite. Ti, Cr and Zr were included as high melting materials which readily formed metal carbides.

TABLE 6-2

Composition of Glasses Used in Subsurface Coating Studies

Material	Glass #1	Glass #2	Glass #3	Glass #4
$CaSiO_3$	27.4	19.2	19.2	35.6
Al_2O_3	8.6	6.0	6.0	18.0
SiO_2	21.2	14.8	14.8	-
BaO	42.8	60.0	55.0	-
MoO_3	-	-	5.0	-
KNO_3	-	-	-	19.6
MnO	-	-	-	9.0
TiO_2	-	-	-	4.4
CaF_2	-	-	-	13.4
σ_a, barns	0.65	0.98	0.78	3.3

6.1.2 Compatibility Tests

Materials' compatibility was studied using graphite crucibles filled with coating materials of interest. Also, a number of graphite-metal diffusion couples were tested.

The crucible studies were primarily to test wettability of potential coating materials. The materials were placed in small graphite crucibles and held at controlled temperatures for short periods of time after which they were cooled, sectioned and examined metallographically. The temperatures used were 1800°F, 2200°F and 2600°F and the time at temperature was 5 min.

The results of these tests are summarized in Table 6-3. It can be seen by examination of this table that at 1800°F there was no penetration of the graphite by any of the materials tested. There was some wetting of the surface by copper as well as silicon, as determined by metallographic examination of the interface between the crucible and the melt. At 2200°F, there was definite wetting of the graphite by copper, silicon and #3 glass and there may have been some penetration by the metals but not by the glass. At 2600°F the copper, silicon, nickel and #1 and #3 glasses all wet the surface. The copper, nickel and #1 glass all showed slight penetration while the silicon showed a greater penetration probably in the form of cilicon carbide. The #2 glass showed some adherence to the graphite surface with slight penetration. The #4 glass neither wet nor penetrated the graphite, however there was some slight erosion of the crucible. The #1 glass penetrated slightly but seriously eroded the crucible. The molybdenum disilicide showed selective adhesion to the graphite.

The diffusion couples were prepared by compressing thin layers of potential coating materials between 1/4 inch thick plates of graphite and heating in argon at 2600°F for 8 hours. This test was thought to be more similar to actual conditions that would exist in a subsurface element. The materials tested were Cu, Ni, Zr, Si, $MoSi_2$ and #3 glass. The results are shown in Figure 6-1 through 6-6.

In Figure 6-1, the copper is seen to be distributed as spherical particles with no penetration of the graphite. In Figure 6-2, the nickel is seen to be well adhered to the graphite and to penetrate into the graphite pores. The dark flakes in the nickel are carbon which dissolved in the nickel and precipitated on cooling. In Figure 6-3, the zirconium was found as loose flakes of ZrC with no evident penetration of the Zr into the graphite. In

TABLE 6-3

Compatibility Tests of Subsurface Coating Materials In Graphite Crucibles

Type of Material	Wet Graphite at Crucible Interface	Degree of Penetration into Graphite Crucible	Observations
		Heated at 1800°F for 5 minutes	
Copper	Yes	Slight	Some particles adhered to wall.
Silicon	Slight	None	
No. 1 glass	None	None	
No. 2 glass	None	None	
No. 3 glass	None	None	
No. 4 glass	None	None	
Nickel	None	None	
$MoSi_2$	None	Slight	Some particles adhered to crucible wall.
		Heated at 2200°F for 5 minutes	
Copper	Yes	Slight	Particles adhered to crucible wall
Silicon	Yes	Very slight	
No. 1 glass	None	None	
No. 2 glass	None	None	
No. 3 glass	Slightly	None	Some adherence
No. 4 glass	None	None	Slight erosion of crucible
Nickel	None	None	
$MoSi_2$	None	Slight	
		Heated at 2600°F for 5 minutes	
Copper	Yes	Slight	Adhered to graphite
Silicon	Slightly	1/8 in. or greater	
No. 1 glass	Yes	Slight	Crucible badly eroded
No. 2 glass	None	Slight	Adhered to graphite
No. 3 glass	Yes	None	
No. 4 glass	None	None	Slight adherence
Nickel	Yes	Slight	
$MoSi_2$	None	None	

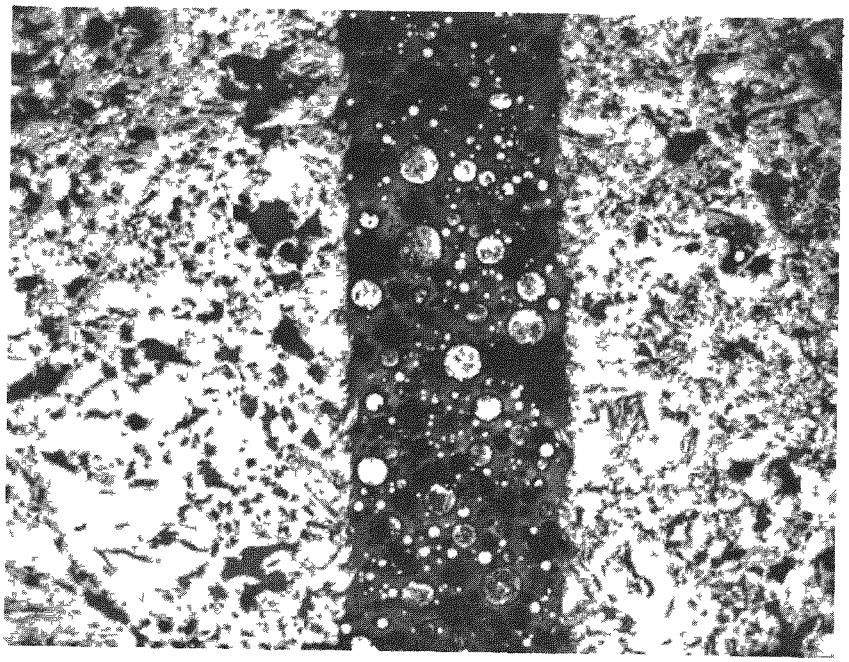

FIG. 6-1 Copper-Graphite. Copper appears as spherical particles. (50X)

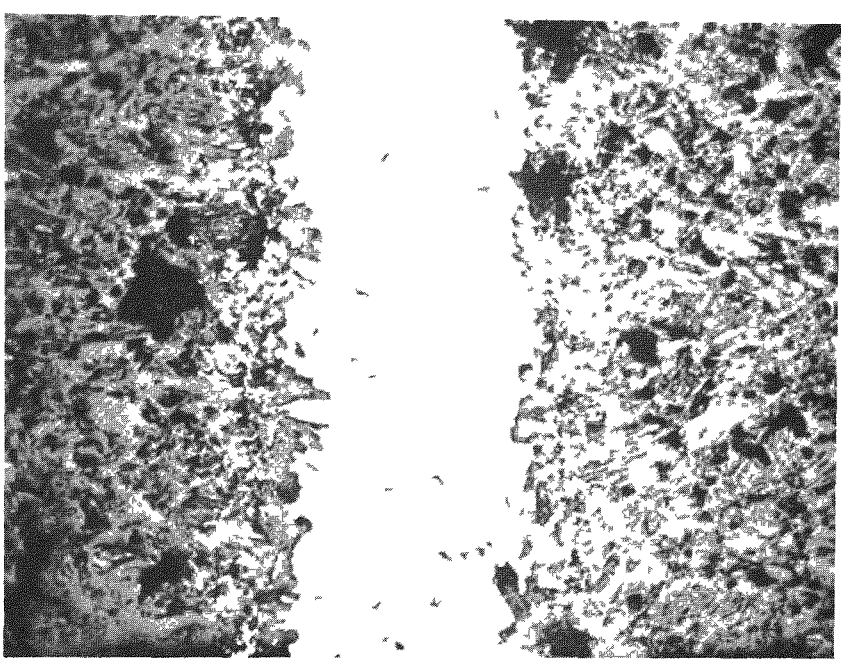

FIG. 6-2 Nickel-Graphite. Dark flakes in nickel are graphite. (50X)

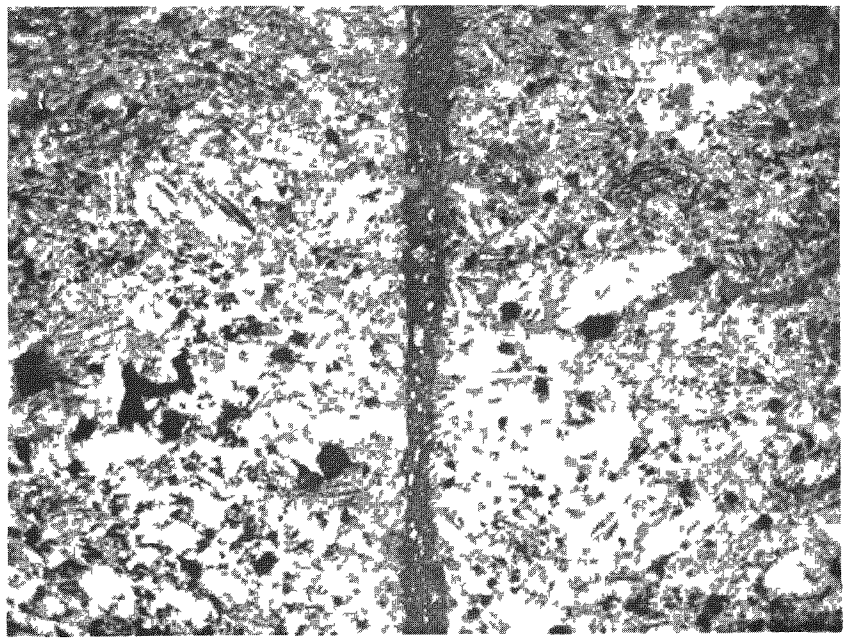

FIG. 6-3 Zirconium-Graphite. Small flakes in zirconoum phase are probably ZrC. (50X)

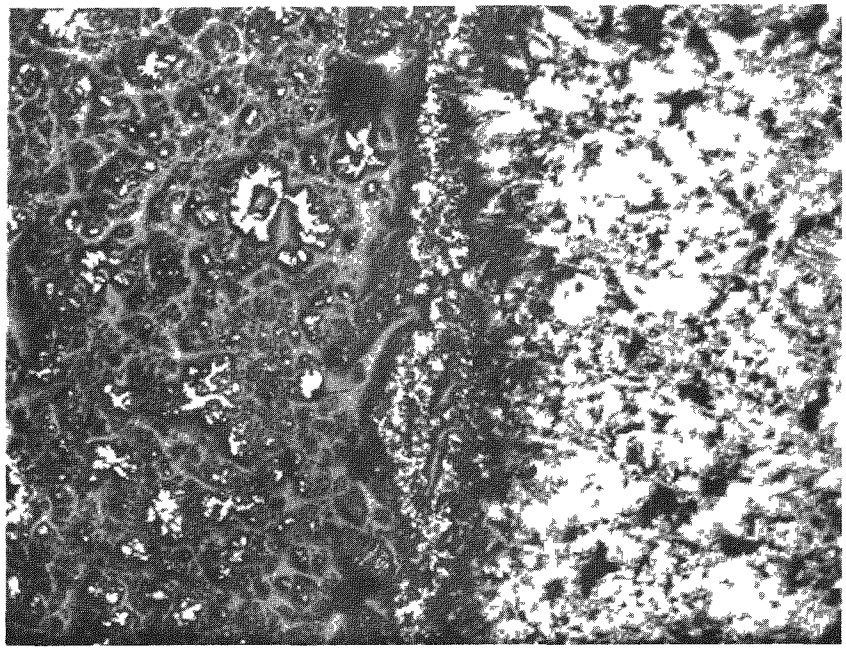

Fig. 6-4 Silicon-Graphite. Small grey particles are SiC. (50X)

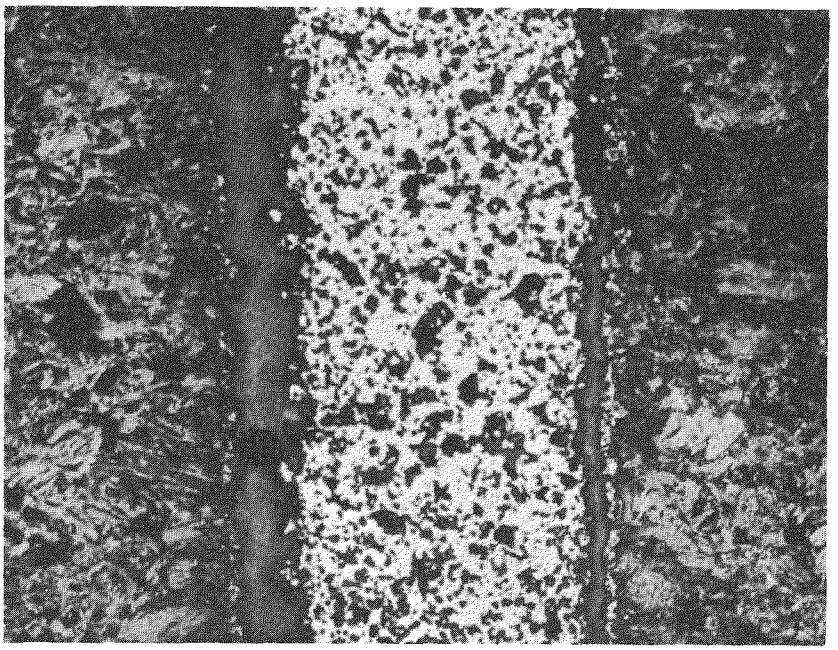

FIG. 6-5 **Molybdenum Disilicide-Graphite. Gaps at interfaces are filled with mounting resin. (50X)**

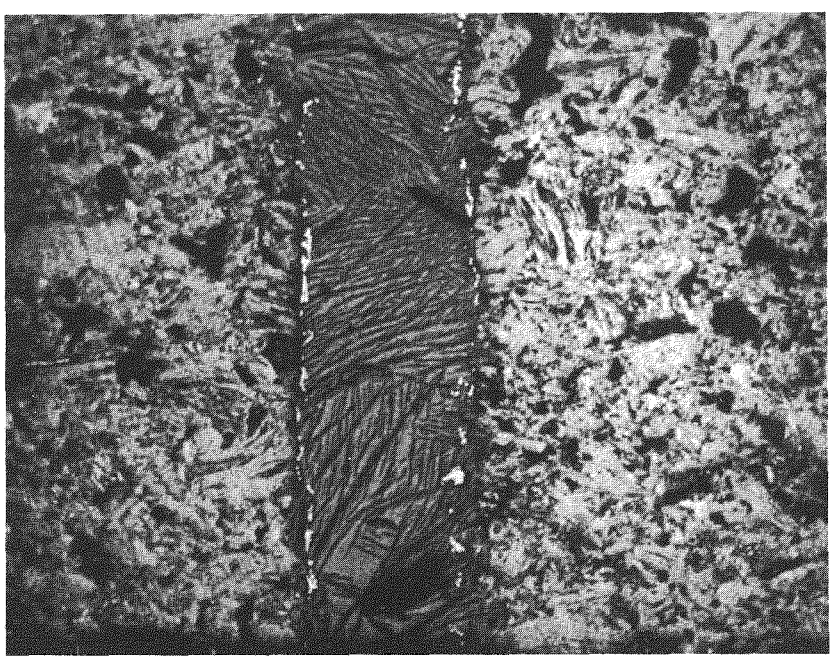

FIG. 6-6 **No. 3 Glass-Graphite. Metallic-like phase at the interface is** unidentified. (50X)

Figure 6-4, the silicon was converted to small particles of SiC with penetration of the graphite. In Figure 6-5, the molybdenum disilicide is seen to have separated from the graphite except for a thin adherent layer. In Figure 6-6, the #3 glass is seen to bond well to the graphite and remain as a continuous layer. An unidentified metal phase can be noted at the graphite-glass interface.

6.1.3 Sphere Fabrication

A number of 1-1/2 inch diameter spheres were fabricated with various types of subsurface coatings surrounding fueled graphite core. The first group of spheres was made by cold pressing. The fueled core was first molded, then the coating material was molded onto the fueled core, and finally, the outer graphite shell was molded on. The spheres were first cured at 350°F to set the binder and then given a slow bake treatment at 200°F for 8 days. Degassing of all three regions occurred at the same time.

The first group of spheres contained coatings of copper, nickel and #3 glass (low-melting materials) and titanium, chromium and molybdenum disilicide (high-melting materials). These materials were generally applied to the fuel cores in a powder form mixed with carbonaceous binder. All of the spheres looked satisfactory after the 350°F cure. After the 8-day bakeout however, most of the spheres had severely cracked outer shells and some of the metal coatings had cracked as well. A high degree of metal (or metal carbide) penetration into the fueled shell was noted in most cases. The glasses did not penetrate but there was evidence of chemical reaction with the graphite. There was only slight penetration with copper but this material tended to ball up and leave gaps near the top of the sphere due to gravitational effects.

Several attempts were made to seal two thin copper hemispheres around a fueled graphite core, but outgassing and chemical reactions prevented the making of a satisfactory brazed joint.

In order to determine whether the high temperature coatings could be made to fuse into a leaktight coating, the defective graphite shells were completely removed from the Cr, Ti, and $MoSi_2$ specimens of the first group. New graphite shells were cold-pressed onto the clad fueled cores and they were all heated at 4660°F in order to melt the metal coatings. During this process, molten chromium ran out a crack which developed in the graphite shell. The titanium layer failed to penetrate the graphite shell probably due to a titanium carbide layer which had formed during the

8-day bakeout at 1500°F. The $MoSi_2$ coating, which had several cracks prior to the application of the new graphite shell, was fused together. After manually removing the shell, a hot oil test of the coated fueled core piece showed only one pinhole leak in the coating.

The next variable investigated was hot pressing. It was hoped the application of pressure while the coating layer was in its molten state would minimize coating penetration and produce a dense tight coating. A second group of spheres was prepared using this hot-pressing technique. The spheres, consisting of a fueled core, a coating and an unfueled graphite shell, were initially formed by cold pressing. The spheres were baked at 1500°F to remove volatiles in the binder and then were hot-pressed in a graphite die under 10,000 psi pressure. Spheres containing Ni, Si, Cu and No. 3 glass were hot-pressed at the melting point of the coating material. Spheres containing $MoSi_2$, Cr and Ti were hot-pressed at only 2000°F because of limitations of the hot-pressing equipment. This latter group of spheres was subsequently heat-treated to the melting point of the seal material in a carbon resistor furnace.

Visual inspection of sectioned spheres indicated that each coating material formed a continuous layer except copper, which appeared to bead and become discontinuous. Cracking was observed in the shells of spheres containing Cr, $MoSi_2$ and Ti coatings. These spheres were not under pressure when the coating melted and the coating appeared to flow into the cracks. No cracks appeared in the specimens that were under pressure during the period when the coating was molten. Radiography indicated that the coating materials penetrated into the pores of the unfueled graphite shell.

In order to assess the coating integrity of these specimens without destroying them, the spheres were subjected to the hot oil leakage test by immersing them in silicone oil at 400°F. Bubbling by gas entrapped during fabrication was then observed. Spheres without a coating which were subjected to similar fabricating conditions exhibited bubbling for 20 to 40 min. In the coated elements, gas release would be expected to come from only the unfueled graphite shell outside the coating. Therefore, if a good seal were obtained, the bubbling could cease in a much shorter time. Results of the hot oil testing of the second group of spheres is given in Table 6-4.

As noted in Table 6-4, the best result were obtained with the high temperature coatings (i.e. $MoSi_2$, Cr and Ti) even though there were cracks in the outer shells of these specimens. The exploratory program was concluded with the hot oil testing of these hot-pressed spheres.

TABLE 6-4

Leakage Test on Hot-Pressed Spheres with Subsurface Coatings

Coating Type	Hot Press. Temp. °F	Further Heat Treatment, °F	Time Required for Bubbling to Stop, Min. (1)
#3 glass	2500	-	7
Copper	2100	-	>7
Copper	2500	-	>7
Nickel	2550	-	6
Silicon	2540	-	>7
Silicon	2540	-	6
Chromium	2000	3272	6
Chromium	2000	3272	2-1/2
Chromium	2180	3272	>7
Titanium	2000	3272	4
$MoSi_2$	2000	3600	2-1/2

(1) Testing time was 7 minutes in silicone oil (400°F).

6.1.4 Conclusions

This exploratory program on subsurface coatings has shown that several types of subsurface coatings are possible. The use of materials such as nickel or #3 glass which melt in the range of PBR operating temperatures should cause these materials to penetrate into the pores of the outermost unfueled graphite shell and also into cracks which may be present in the unfueled shell. Both of these phenomena have been observed in the uniform heating of fuel element specimens in out-of-pile furnaces. The extent of penetration must of course be limited by the amount of coating material initially added so that a continuous coating will remain around the fueled core piece.

It was found that the best specimens could be made when pressure was applied to the sphere while the coating was in a molten phase during fabrication. Limitations to the experimental equipment prevented the use of hot-pressing with the high-temperature coating materials (i.e. Cr, Ti, and $MoSi_2$) but in spite of shell cracking these latter materials appeared to form the best seals based on the limited evaluation work. It is probable that hot-pressing would have prevented shell cracking in these latter specimens.

6.2 Metal Carbide Surface Coatings

Several types of metal carbide surface coatings were obtained for evaluation on both fueled and unfueled spheres. American Metal Products furnished coatings on two types of fueled spheres. Types FI-5 (SiC coating) and FI-6 (ZrC coating) consisted of a uniform dispersion of UC_2 throughout the graphite matrix. Fuel particle size ranged from 1 to 5 microns and a high density matrix was achieved by carbonaceous reimpregnation. The .001" metal carbide coatings were applied directly to the fueled spheres. AMP also furnished some lumped specimens. In types FL-1 (uncoated), FL-2 (ZrC coating), and FL-3 (SiC coating), all of the fuel is lumped in the center of the sphere in the form of a uranium dicarbide pellet. The fuel pellet was first mounted in a graphite cylinder which was then threaded into the center of the sphere. The .001" metal carbide coating is applied after the sphere has been reimpregnated. Fig. 6-7 is a radiograph of an FL-2 specimen which clearly shows the centrally located 3/8" diameter cylindrical fuel pellet. Some undersirable gaps around the fuel pellet cylinder can be noted. Fig. 6-8 is a typical view of this type of metal carbide coating and is specifically a section of the ZrC coating on an FL-2 specimen. The very fine radial porosity along the grain boundarys in the coating can be seen.

Plasmakote Corporation have developed techniques for depositing metal or metal carbide coatings by a flame-spraying technique. In order to evaluate this type of coating process, several unfueled specimens with two types of coatings were obtained. Type FX-1 was titanium carbide and type FX-2 was zirconium carbide. Unfueled 1-1/2" diameter graphite spheres, machined from Speer Carbon Company Moderator Grade B stock, were supplied to the manufacturer. Coating thickness ranged from .005 to .010". The coatings were given a high temperature fusing treatment, after being flame-sprayed on the graphite, in an attempt to form a continuous impermeable coating. However, as shown in Figure 6-9, the coating appeared quite porous. As noted below, impact tests on both types showed poor adherence to the matrix, however, this could be partially attributable to the type of graphite surface.

The metal carbide surface coated specimens were subjected to evaluation tests consisting of hot-oil permeability, alpha assay, impact, compression, and neutron activation. A total of 15 specimens were subjected to the hot oil test and all were found to leak. In general, the FI-5, FI-6, FL-2, and FL-3 specimens exhibited fine bubble streams over much of their surfaces while the FX-1 and FX-2 specimens exhibited coarse bubble stream over their surfaces. In the case of the lumped specimens FL-2 and FL-3, several coarse bubbles were noted at the plug outlines.

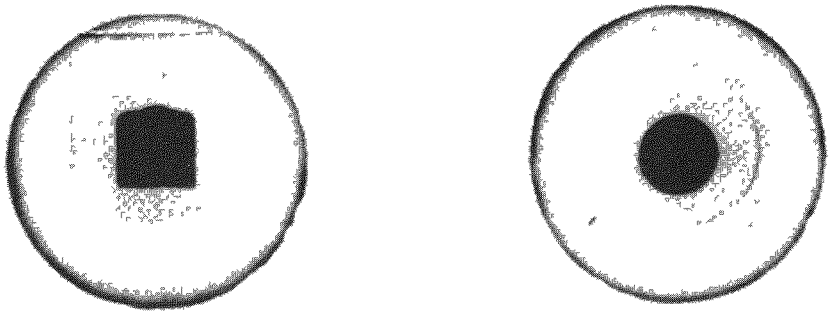

FIG. 6-7 Radiograph of FL-2 Specimen

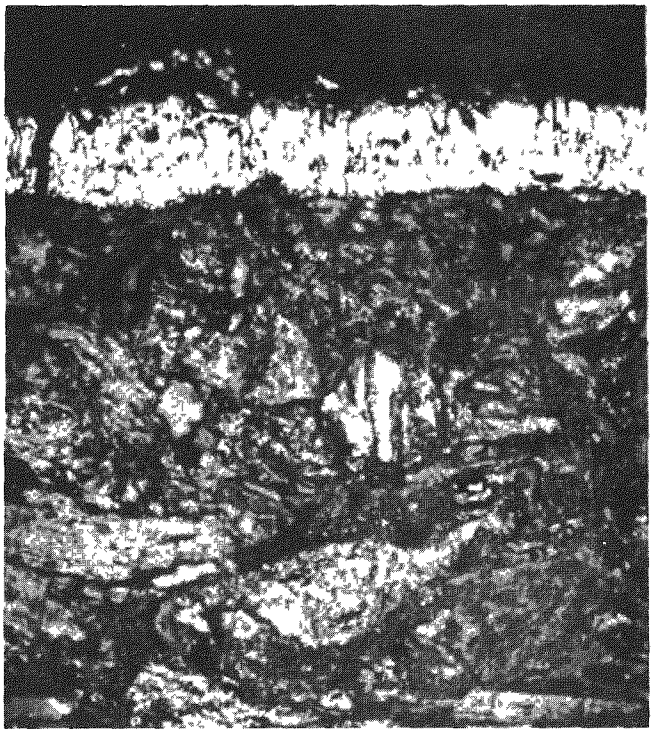

FIG. 6-8 ZrC Coating on an FL-2 Specimen. (500X)

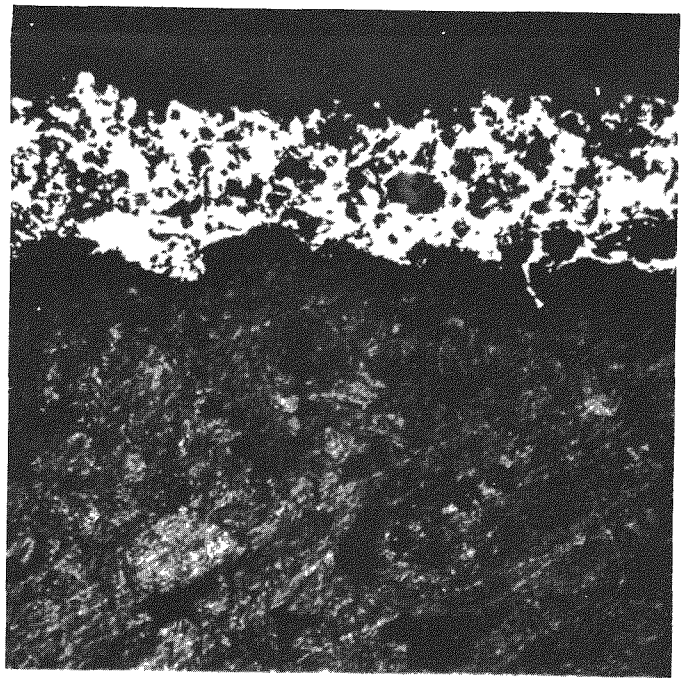

FIG. 6-9 Flame Sprayed and Fused Zirconium Carbide Coating on FX-2 Specimen (100X)

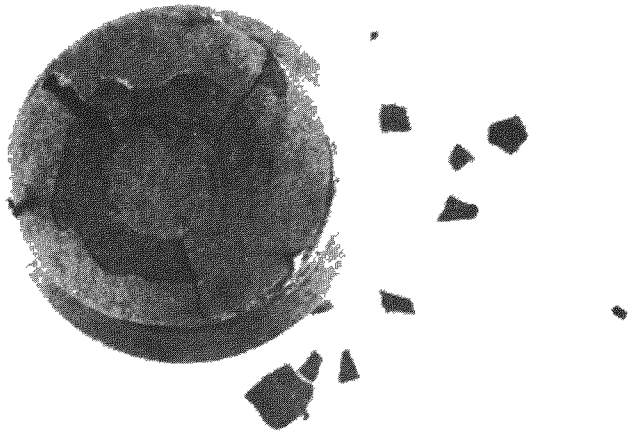

FIG. 6-10 FX-1 Specimen After Compression Test.

The results of impact and compression tests are given in Table 6-5. All of the coatings were fractured at less than the desired 2.0 ft-lb. impact load. Many of the coatings failed by chipping away from the underlying graphite surface. A typical view is seen in Fig. 6-10 where an FX-1 specimen is shown after failure under a compressive load.

TABLE 6-5

Impact and Compression Tests on Metal Carbide Surface Coated Specimens

Fuel Element Type	Impact Energy at Failure, ft-lbs		Compressive Failure	
	Coating	Matrix	Load, lbs.	Deflection, in.
FL-1	—	1.7	800	0.047
FL-2	0.9	1.7	915	0.031
FL-3	0.6	2.5		
FI-5	0.7	>7.0		
FI-6	1.1	>7.0		
FX-1	0.8	>7.0	3350	0.131
FX-2	0.8	>7.0	2995	0.127

An alpha assay was made of several of the fueled specimens to determine the extent of uranium contamination in the coatings. The typical amount of uranium contamination found in the coatings of the FL-2 and FL-3 specimens was about 5×10^{-6} of the total uranium in the specimen while a similar value for the FI-5 specimen was 1.5×10^{-4}. The higher contamination for the FI-5 specimen is caused by the dispersed uranium in the graphite sphere surface.

Only one neutron activation test was run on a metal carbide coated specimen. An FL-2 specimen was heated for 30 min at 1500°F after activation and 3×10^{-4} of the contained Xe 133 was released. This rather high release fraction reflects the porous nature of the coating and only slight retention by the unfueled graphite shell.

In view of the more promising results obtained with metal carbide coatings having a free metal phase (i.e. siliconized silicon carbide), further work on the types of metal carbide coatings described in this Section was abandoned.

6.3 Metal Coated UO_2 Particles

Metal coatings for UO_2 particles were being developed by the Nuclear Materials & Equipment Corporation for other applications under another AEC contract. A quantity of these coated fuel particles were obtained from NUMEC to determine whether they could be applied to Pebble Bed Reactor requirements. Although the available metals had a significant thermal neutron adsorption cross-section and were known to react with carbon to varying degrees, it was desired to see whether a metal or metal-carbide coating on the fuel particles would offer a significant degree of fission product retention. Three types of metal coatings were obtained: nickel, nickel-chromium, and niobium. 105/149 micron UO_2 shot was used as the fuel particle. The Ni and the Nb coatings were 10 microns thick. In the third type, a 2 micron Ni undercoat was followed with an 8 micron chromium layer. The metal coating techniques are described in (14).

Photomicrographs of the as-received particles are shown in Fig. 6-11 (nickel), Fig. 6-12 (nickel-chromium), and Fig. 6-13 (niobium). Rather uniform coating thicknesses can be seen in all cases. However, occasional breaks in the coating can be seen.

Evaluation of these coated particles consisted of hot air testing, alpha assay, and reaction with graphite. Weight gains of 12.7 w/o for the Ni coated particles and 26.9 for the Ni-Cr coated particles were found after heating in 1200°F air for 1 hr. This indicated some porosity in the particle coatings. Alpha assay results are shown in Table 6-6. After making the assay on the as-received particles they were leached in nitric acid and the assay was repeated. Since there was no significant change in data after leaching, it was concluded that the uranium contamination was distributed within the coating.

TABLE 6-6

Uranium Contamination of Metal Coated UO_2 Particles

	U Contamination, mg/gm of particles	
Coating	Before Leaching	After Leaching
Ni	7.4	6.6
Ni-Cr	2.4	3.0
Nb	18	18

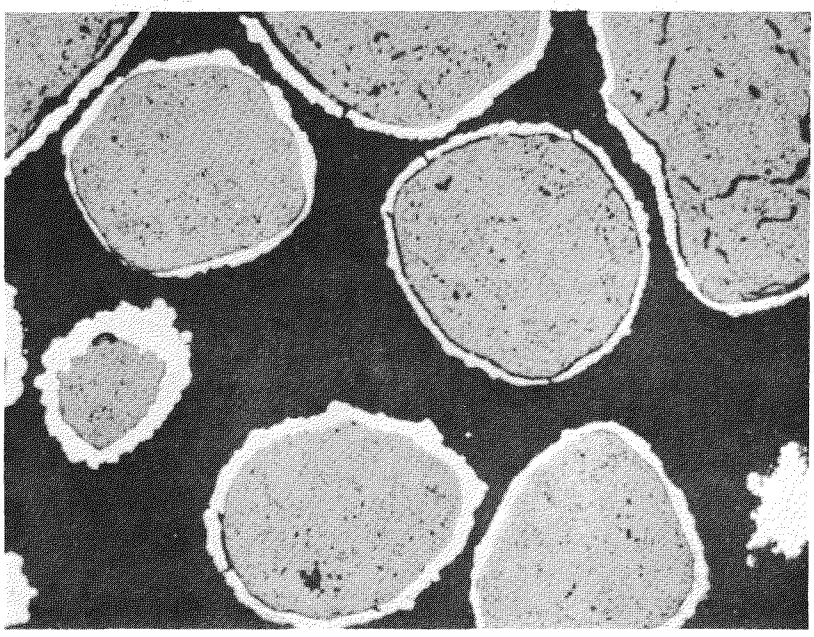

FIG. 6-11 Nickel Coated UO_2. (250X)

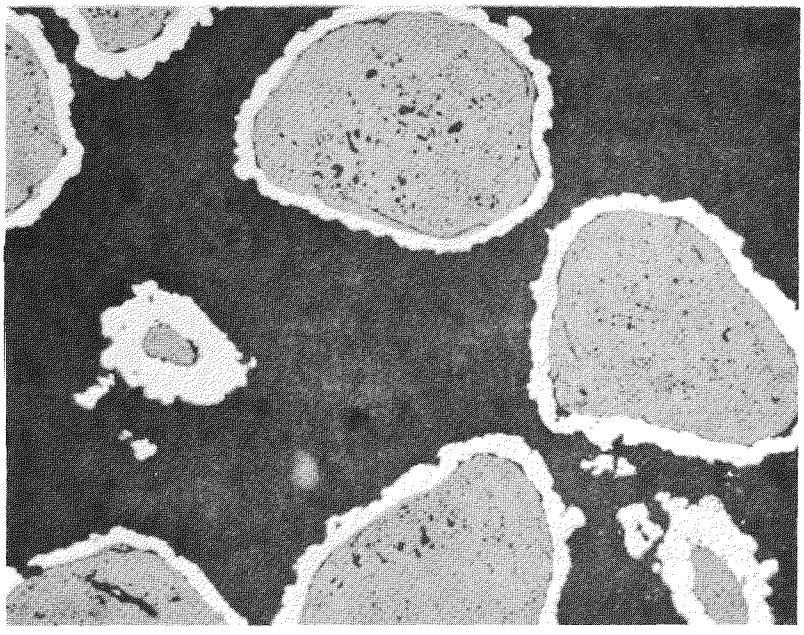

FIG. 6-12 Chromium-on-Nickel Coated UO_2. (250X)

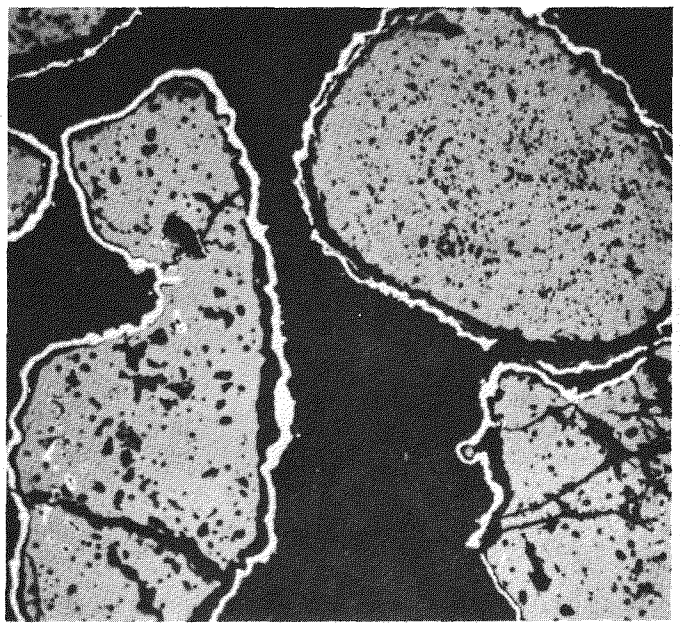

FIG. 6-13 Niobium Coated UO_2 . (250X)

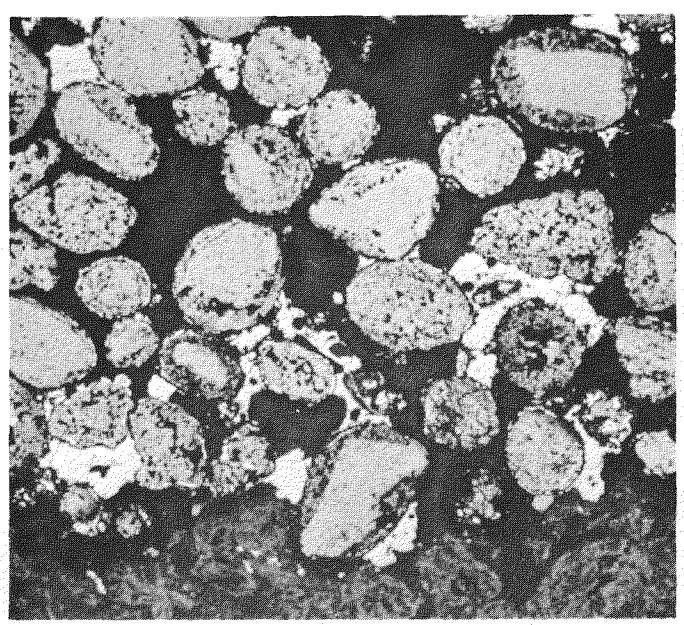

FIG. 6-14 Cr-Ni Coated UO_2 after reaction with graphite at 1700°F for 4 hrs. (100X)

A series of graphite reaction tests were performed by mounting each type of coated particle in two types of graphite. Both graphites were made with a coal tar pitch binder. One was made with a graphite powder (AGOT) filler and the other with a Texas 55 coke filler. After molding, the specimens were baked for 4 hrs at 1700°F. After fabrication, the specimens were heated in helium at 2500°F for 168 hrs and at 3000°F for 6 hrs. In all cases, the coatings were nearly completely destroyed. Agglomerations of metal or metal carbide phases were noted. A typical result is shown in Fig. 6-14 where Ni-Cr coated UO_2 particles in AGOT-filler graphite after the 4 hr. treatment at 1700°F can be seen.

In view of the limited application of metal coated UO_2 particles in the PBR program and the extensive development work which would have been required for this application, no further work was done on this type of coated fuel particle under the present contract.

7.0 Uncoated Fuel Element Specimens

Although the major emphasis in the PBR Fuel Element Development Program was on coatings for fission product retention, there were numerous portions of the work which did not involve coatings. These included a study of the use of natural graphite in preparing a high density matrix material, a study of the thorium oxide loadings which could be achieved in graphite by infiltration with thorium nitrate, the effects of irradiation on uncoated UO_2 fueled graphite, fission product release studies from uncoated UO_2 fueled graphite using the neutron activation method, and the strength characteristics of unfueled graphite spheres.

7.1 Natural Graphite

An inherent characteristic of the Pebble Bed Reactor concept is the fixed 39% voidage in the ball bed region. One method of increasing the amount of carbon moderator in a Pebble Bed core to account for this high voidage is to replace some of the spheres with solid graphite posts. This increases the amount of carbon in the core but at the same time decreases the amount of heat transfer surface in the core. Another method of increasing the amount of carbon moderator is to increase the graphite density of the fueled spheres. For example, in the reference design for the 125 eMW-PBR (2), a graphite density of 1.68 g/cc was used and it was found necessary to replace 25% of the core volume with solid graphite posts to achieve the optimum conditions for that plant. The same effective carbon loading could have been achieved if 2.1 g/cc graphite spheres were used with no fixed graphite posts, thus increasing the thermal capacity by about 33% for the same total core size.

The general method of achieving high density graphite is by successive carbonaceous reimpregnations and regraphitizations of the graphite body. Densities up to about 1.9 g/cc have been achieved by this technique. Another method is the use of suitable starting materials which can be molded and baked to directly form a high density graphite body in only one step. One such material is natural graphite powder.

An exploratory program on the fabrication of graphite bodies using natural graphite as the filler material was conducted at the Battelle Memorial Institute. Densities in excess of 2.0 g/cc had been achieved using natural graphite powder with no binder. However, these bodies had little

strength. One of the major objectives of this program was to determine whether suitable strength characteristics could be achieved by the addition of a binder without a serious decrease in density.

7.1.1 Pellet Fabrication

Three types of purified natural graphite powder were obtained from the Charles Pettinos Graphite Corp. as described in Table 7-1.

TABLE 7-1

Natural Graphite Materials

Grade No.	Description	Impurities	Particle Size
138	Mexican, amorphous	0.9%	99%, -325 mesh
6387	Madagascar, crystalline	0.1% (B $<$ 1 ppm)	100%, -200 mesh, avg. particle size, $\sim$10.6 μ
6405	Madagascar, crystalline	0.1%	0.03%, + 100 mesh 2.03%, -100, +200 mesh 17.98%, -200, +325 mesh 79.96%, -325 mesh.

A series of 1/2" x 1/2" cylindrical pellets were prepared using the three types of natural graphite shown in Table 7-1. Four types of binder were used, including two types of phenolic resin, a coal tar pitch, and furfural alcohol. Binder content ranged from 0 to 40 gms per 100 gms of natural graphite. After mixing, the pellets were cold pressed, cured at 400°F, prebaked in vacuum at 1500°F, and finally baked at 2500°F in argon. Density measurements were taken at each stage of fabrication and crushing strengths of the finished pellets were measured. A summary of the results is given in Table 7-2.

Several trends can be noted in Table 7-2. Lower densities result with a high binder content. Lowest densities resulted with coal tar pitch binder. The strengths of the resin bound pellets were generally higher than for the pitch bound pellets. For comparison purposes, two 1/2" x 1/2" cylinders were machined from AGOT graphite of 1.70 g/cc density. The compressive strengths for these pieces were found to be 3,139 psi and 3.445 psi.

TABLE 7-2

Density and Strength of Natural Graphite Pellets (1st Series)

Graphite Composition[a]	Gms. binder per 100 gms of filler	Green Density, g/cc[b]	Baked Density g/cc[c]	Compressive Strength psi[c]
6387-none	none	2.14	1.95[b]	1,000[d]
6387-BV1600	20	2.00	1.92	5,000
6387-BV1600	35	1.66	1.55	4,700
6387-BV1600	50	1.74	1.77	5,200
6387-pitch	30	1.87	1.60	3,900
6387-pitch	35	1.86	1.49	3,200
6387-pitch	40	1.81	1.45	2,700
6387-79L	20	1.91	1.85	3,800
6387-79L	30	1.78	1.67	2,500
6387-FA	40	1.72	1.68	2,600
6405-none	none	2.03[c]	2.06	1,900
6405-BV1600	20	2.02	2.02	2,900
6405-BV1600	35	1.93	1.93	3,400
6405-BV1600	50	1.89	1.88	3,400
6505-pitch	30	1.90	1.60	2,400
6405-pitch	35	1.89	1.63	3,300
6405-pitch	40	1.86	1.57	3,000
138-none	none	1.71[c]	1.72	2,400
138-BV1600	20	1.86	1.79	4,800
138-BV1600	35	1.81	1.77	5,200
138-BV1600	50	1.79	1.74	5,300
138-pitch	30	1.85	1.52	3,500
138-pitch	35	1.81	1.56	4,900
138-pitch	40	1.81	1.58	5,100
138-79L	20	1.79	1.62	1,600
138-79L	30	1.73	1.62	2,100
138-FA	40	1.65	1.55	600

(a) The first part designates the type of natural graphite described in Table 7-1. The second part designates the binder material as follows: BV1600: Bakelite phenolic resin; 79L: phenolic resin supplied by Old Ironsides Co; pitch: Barrett No. 2. medium hard pitch; FA: furfural alcohol.
(b) Average of 3 samples.
(c) Average of 2 samples.
(d) One sample tested.

The highest densities were achieved with the 6405 and 6387 graphities with the lower BV1600 binder contents. Consequently an additional series of pellets was prepared to explore this range in somewhat more detail. The use of thermax carbon black was also investigated using the same fabrication and test procedures used for the pellets in Table 7-2. The results are shown in Table 7-3.

TABLE 7-3

Density and Strength of Natural Graphite Pellets (2nd Series)

Graphite Compositions[a]	Gms. binder per 100 gms of filler	Green density g/cc[b]	Baked density g/cc[b]	Compressive strength, psi[c]
6387-none	0	2.14	1.95	1,000[d]
6387-BV1600	5	2.01	1.96	1,800
6387-BV1600	10	2.00	1.95	4,800
6387-BV1600	15	1.99	1.88	3,300
6405-none	0	2.03[c]	2.06	1,900
6405-BV1600	5	2.12	2.06	3,100
6405-BV1600	10	2.09	2.01	2,700
6405-BV1600	15	2.04	2.02	3,500
6405-BV1600-10T	20	1.89	1.86	2,200
6405-BV1600-20T	35	1.79	1.70	2,700
6405-pitch-10T	40	1.82	1.51	2,500
6405-pitch-20T	35	1.84	1.56	2,200

(a) Designations are same as used in Table 7-2 except that 10T and 20T designate 10% and 20% thermax carbon black added to filler.
(b) Average of 3 samples.
(c) Average of 2 samples.
(d) One specimen tested.

As can be noted in Table 7-3, there has been some decrease in strength below the values shown in Table 7-2 for the higher binder contents. Maximum strengths in the lower binder content range appear to be at 10 parts binder with the 6387 graphite and 5 parts binder with the 6405 graphite. Additions of the thermax carbon black had little effect on the strength but did decrease the final density.

7.1.2 Sphere Fabrication

The final step in the exploratory program was the fabrication and testing of spheres to determine whether they would meet PBR requirements. Madagascar Grade 6405 natural graphite filler was used in one set of spheres. For comparison, another set of spheres was prepared using a high density synthetic graphite powder (National Carbon Grade 195) which had approximately the same particle size distribution as the 6405 material. BV1600 resin was used as the binder material in both cases. The spheres were molded in a heated (300°F) steel die at 20,000 psi. Pressure and heat were maintained on the specimens for a period of 10 minutes to cure and partially set the resin binder. The spheres were then partially baked at 1500°F in vacuum. The final bake treatment was at 2500°F in an argon atmosphere.

The test program consisted of impact tests, compression tests and density measurements. The results are summarized in Table 7-4.

TABLE 7-4

Mechanical Strength of Natural and Synthetic Graphite Spheres

Filler	Binder Content pph of filler	Green Density g/cc[a]	Baked Density g/cc[a]	Load at Failure Compressive lbs.[b]	Load at Failure Impact ft. lbs[c]
Natural (6405)	5	2.11	2.04	570	1.0
"	10	2.08	1.99	430	1.0
"	15	2.09	2.00	430	1.2
"	20	2.07	1.99	410	1.5
Synthetic (195)	20	1.91[b]	1.75[b]	580	1.9
"	40	1.84	1.68	670	3.0

(a) Average of five specimens
(b) Average of two specimens
(c) One specimen tested

As noted in Table 7-4, densities of about 2.0 g/cc were obtained with the natural graphite filler while the synthetic graphite filler definitely produced lower densities. The compressive strengths of 410 to 570 lbs. for the natural graphite spheres are close to the desired 500 lbs. while the

impact strengths of 1.0 to 1.5 ft-lbs are below the desired 2.0 ft-lbs. Although the synthetic graphite spheres listed in Table 7-4 barely met the strength requirements, it should be recalled that commercially prepared synthetic graphite spheres such as the FA-1 and FA-22 types consistently showed compressive strengths over 2000 lbs. and impact strengths over 7 ft-lbs. This discrepancy with commercial specimens tends to cloud the present results obtained with natural graphite.

Although there were a limited number of specimens used to obtain the data in Table 7-4, there is some evidence that higher strengths but lower densities are obtained with higher binder content. During the course of testing, it was noted that the natural graphite specimens began to flake as impact loading was increased. This was not observed on the synthetic graphite specimens. A typical mode of failure for the natural graphite spheres was the separation of spherical shell segments from the outer surface of the spheres indicating poor radial bonding.

7.1.3 Conclusions

This exploratory program has shown that crystalline natural graphite, when used as the filler component, can produce bulk graphite densities in excess of 2.0 gm/cc. The coarse-grained crystalline graphite is slightly superior to the fine-grained crystalline graphite and both crystalline grades are superior to the amorphous natural graphite. It is necessary to use the resin type binders rather than conventional pitch binders in order to achieve the high densities.

However, rather poor strengths were found for the natural graphite spheres even though the compressive strengths of natural graphite pellets compared favorably with synthetic graphite pellets. The mode of failure of the natural graphite spheres indicated that poor radial bonding caused the sphere failure. In order to utilize the higher densities obtainable with natural graphite, it will be necessary to find methods of improving the strength of these spheres and preventing spalling or flaking of the sphere surface.

7.2 Thorium Nitrate Infiltration of Graphite

One method of fueling a graphite body is to infiltrate the pores of the graphite body with fuel-bearing solution, dehydrate the body, and bake it to convert the fuel to a stable solid form, deposited in the pores of the graphite. This infiltration procedure has been of interest to the PBR Fuel Element Development Program because of its potential as an economic method of fueling large batches of spheres, particularly when partially decontaminated fuel is used. A number of spheres fueled with approximately 5.4 gms of fully enriched UO_2 (Specimen type FI-1) had previously been prepared for evaluation as core fuel elements, as described in Appendix B of ref. (2).

In order to fully utilize the infiltration process in a Pebble Bed Reactor, the process should also be suitable for preparing blanket elements loaded with ThO_2. However, the available pore volume of a graphite sphere limits the amount of fuel which can be added to the sphere by the infiltration process. Previous studies of a blanketed PBR core (1) showed that 30 to 45 gms. of ThO_2 per 1-1/2" diameter graphite sphere would be required in blanket elements. Consequently, the Speer Carbon Co. undertook a study to establish process conditions for graphite spheres loaded with ThO_2 by infiltration with thorium nitrate and also to determine the amount of ThO_2 which can be added to graphite as a function of graphite density. Reference (16) includes complete details of this work.

7.2.1 The Infiltration Process

Six sets of 1-1/2" graphite spheres having nominal densities of 1.25, 1.35, 1.45, 1.55, 1,65 and 1.75 g/cc were machined from extruded blocks of Moderator Grade B graphite (Speer Carbon Co.) for use in the program. A summary of the mercury porosimetry data on these spheres is given in Table 7-5.

TABLE 7-5

Densities and Porosities of Graphite Spheres

Nominal Density, g/cc	Avg. Apparent Density, g/cc	Avg. Pore Volumes, cc/g			
		Total	D > 100μ	100μ < D > .06μ	D < .06μ
1.25	1.240	0.364	0.009	0.305	0.050
1.35	1.339	0.305	0.007	0.250	0.048
1.45	1.421	0.263	0.015	0.200	0.048
1.55	1.579	0.192	0.014	0.118	0.060
1.65	1.666	0.159	0.013	0.110	0.036
1.75	1.732	0.136	0.009	0.074	0.052

After experimenting with several variables, the following standard procedure was adopted for loading the spheres.

1. 3 to 4 spheres of a particular group were outgassed for 15 hrs. to a pressure of 5-15 microns of mercury.

2. A water solution containing 76 w/o $Th(NO_3)_4 \cdot 4 H_2O$ was prepared. This solution was nearly saturated at the infiltration temperature of 25°C.

3. The outgassed spheres were then flooded under vacuum for 30 minutes with the thorium nitrate solution.

4. Atmospheric pressure was applied to flooded spheres for an additional 15 min.

5. The spheres were removed from the solution, wiped clean of solution, and stored at ambient temperature for 16 hours.

6. The spheres were placed in a Vycor tube and heated in a flowing argon stream in accordance with the following schedule:

   a. Temperature raised to 160°C in 30 min. and held for 3 hours to remove water.

   b. Temperature raised to 700°C in 1 hour and held for 3 hours to decompose thorium nitrate to thorium oxide.

7. Where additional ThO_2 loading was required, the above procedure was repeated.

A number of variations in this process were tried. When a 100°C solution containing 85 w/o $Th(NO_3)_4 \cdot 4H_2O$ was tried, a slight increase in ThO_2 loading per infiltration was found but was not felt sufficient to warrant the complications of providing heated production apparatus. When the vacuum pretreatment was omitted, there was a significant decrease in ThO_2 loading. When longer infiltration times were used, there was no increase in ThO_2 loading. Other variables which were not found to increase the ThO_2 loading were the use of 10 psig pressure during infiltration, a slower heating rate to 700°C, and the use of 12 psig pressure during firing. Shorter heating times at the final temperature and a higher final temperature (950°C) were also investigated. It was found that the standard heating cycle

produced complete denitration although some further slight weight losses occurred at the higher temperature due to mechanical losses of ThO_2 and graphite in the further handling.

7.2.2 Results of Infiltration Tests

The primary experimental task was to determine the limits of ThO_2 loading in graphite spheres of various densities. Initial experiments showed that the use of successive infiltrations was the best method of raising the ThO_2 loading. It was found that after eight infiltrations, the spheres still did not appear to be near their saturation points. However, a systematic series of runs were made using just eight infiltrations at each of the six graphite densities. The results of these runs are summarized in Figure 7-1 where the cumulative ThO_2 loading is plotted vs. the number of infiltrations for each of the six density groups. Each data point is the average of three spheres. This data is also shown in Figure 7-2 where the atom density of thorium is plotted vs. the atom density of carbon. As can be noted in Figure 7-1, loadings of 30 gms. of ThO_2 can be achieved only in the lower density graphite and that a minimum of 5 infiltrations would be required.

The uniformity of the ThO_2 dispersion in the graphite spheres was checked by sectioning several spheres and analyzing segments from the center region and the edge region. This was done on a number of spheres which had been infiltrated from 1 to 8 times. The ThO_2 distribution was quite uniform. Loadings in the outer region were 4% to 6% higher than the loadings in the center region, the higher values being associated with the greater number of infiltrations.

From this work it is concluded that graphite bodies can be loaded with ThO_2 by the thorium nitrate infiltration process but that relatively large loadings will require use of lower density graphite and many infiltration steps.

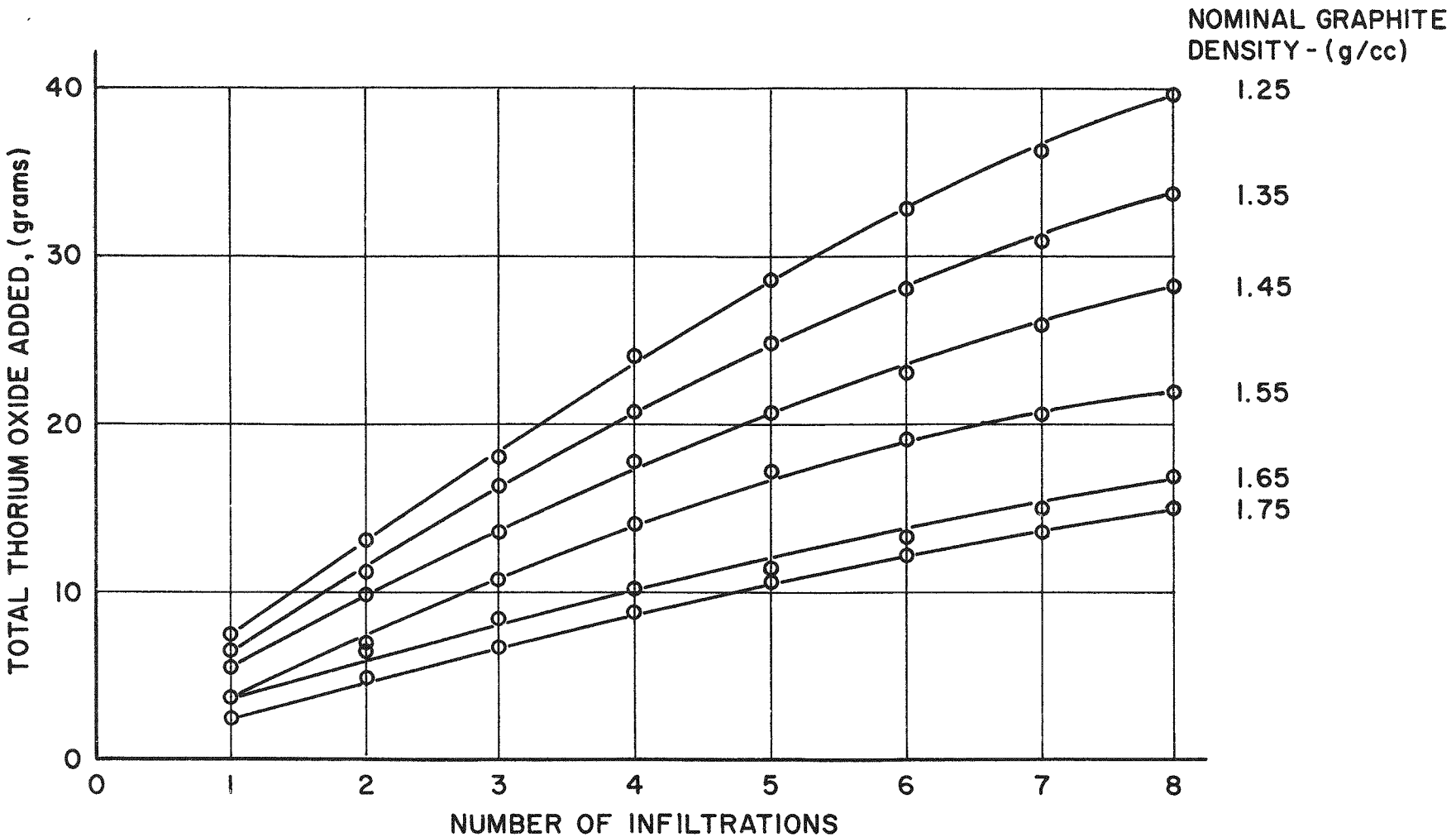

THORIUM OXIDE LOADING vs INFILTRATION FREQUENCY

FIG. 7-1

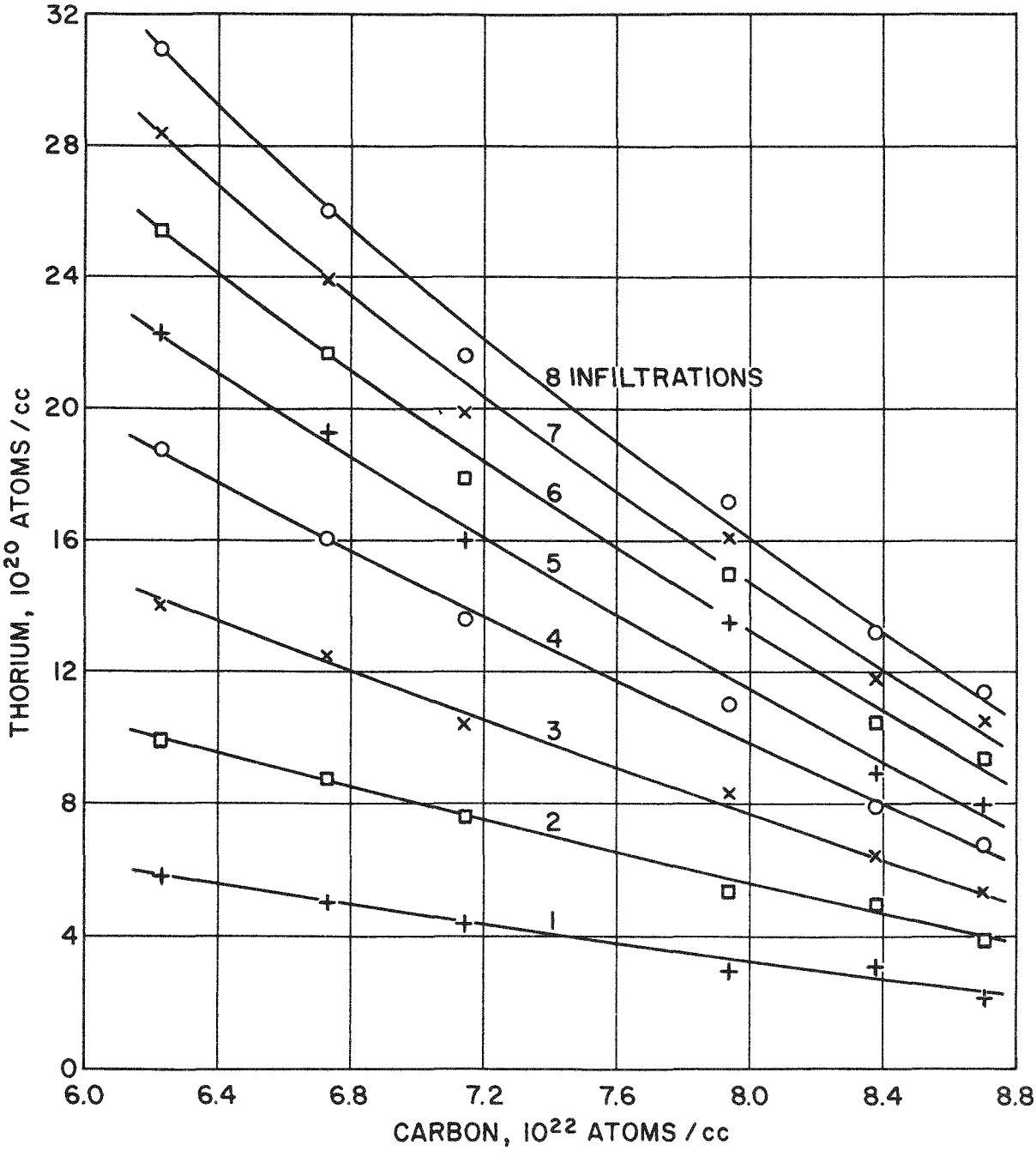

THORIUM AND CARBON DENSITIES
IN INFILTRATED GRAPHITE SPHERES

FIG. 7-2

7.3 Irradiation Tests of Uncoated UO_2 Fueled Specimens

In selecting the fissile material compound in a uranium-graphite fuel element, the oxide form has a number of advantages over the carbide form, such as ease in handling during fabrication and ease of reprocessing. The greated limitation on UO_2 is its reaction with the graphite matrix at high temperatures. Evidence of reaction at temperatures as low as 2400°F have been reported (15), however during the short baking time at 2560°F during fabrication stability is excellent. By dispersing fissile material throughout the graphite moderator, the Pebble Bed Reactor offers the best opportunity of producing high coolant outlet temperatures (1200 to 1400°F) while keeping fuel temperatures below 2100°F. Thus, UO_2 can be considered for PBR applications.

A capsule irradiation experiment was performed in an attempt to determine whether radiation would affect the reaction between UO_2 and graphite at temperatures approaching 2100°F. Another objective of this experiment was to assess the effect of high temperature irradiation on the strength and dimensional changes of fueled graphite. Four types of uncoated graphite spheres each fueled with a different type of UO_2 were tested. The specimen designations and the UO_2 particle sizes were: FI-1 ($1\mu UO_2$), FA-2 ($67\mu UO_2$), FA-1 (100μ) and FA-10 (400μ). A further description of these types is included in Table 2-1. The specimens were irradiated in Static Capsule SP-4. The design and operation of this capsule is described in Section 8.4. The exposure conditions for the specimens are summarized in Table 7-6, where the burnup has been calculated from the thermal data and the irradiation time.

During the course of the SP-4 irradiations, there were the usual variations in the specimen operating conditions due to shifts in flux patterns, scrams, etc. The values listed in Table 7-6 are typical average values for the irradiation period. The maximum and minimum recorded temperatures in the center of the FA-1 specimen were 2070°F and 1510°F respectively. The fluctuations in the temperature difference between the measured central temperature and the measured block temperature of the FA-1 specimen were too great to permit a statement that this temperature difference increased with irradiation because of deterioration of thermal conductivity of the graphite.

TABLE 7-6

Exposure Conditions for UO_2 Fueled Specimens
In Capsule SP-4

Specimen Type	Measured Graphite Block Temp. °F	Ht. Gen. Rate, KW	Calculated Surface Temp. °F	Central Temp, °F	Burnup,(b) KWH/Ball
FI-1 (E8)	1400	2.3	1750	1850	7700
FA-2 (E8)	1400	2.2	1750	1900	7400
FA-1(E82)	1300	1.9	1600	1750(a)	6400
FA-10(E5)	1300	1.7	1600	1700	5700

(a) Measured temperature. One thermocouple was imbedded in the center of this specimen. All other central temperatures were calculated.

(b) For PBR specimens, 1 KWH is equivalent to 8.8 MWD/metric ton of U, 4.4×10^{15} fissions/cc of specimen, or .0011% of the U 235 atoms fission.

In parallel with the irradiation of Capsule SP-4, four specimens identical with those in the capsule were heated in an out-of-pile furnace duplicating the time-temperature pattern of the irradiated specimens. This step was taken in order to distinguish between radiation and temperature effects.

Special flats, approximately 1/2" in diameter, were machined and polished on all specimens so that "before and after" photomicrographs could be taken of specific fuel particles. The photomicrographs for all specimens in both the out-of-pile and in-pile tests have been shown in ref. (8) In all tests, there was no discernable evidence of uranium carbide formation. The most interesting effect was noted for the FA-1 specimen. Figure 7-3 shows three UO_2 particles in specimen FA-1 (E82) before irradiation and Figure 7-4 shows the same particles after irradiation in Capsule SP-4. No evidence of carbide formation can be noted. However, there is a noticeable increase in the void region around the UO_2 particles in Figure 7-4. The increase in radius of the graphite void is approximately 20 microns. Since fission fragment recoil range in graphite is also about 20 microns, this strongly suggests that the local graphite region directly affected by fission fragment recoil has become hardened and brittle and most probably came out during polishing of the specimen. Deterioration of the fuel particle itself is also noted, the decrease in radius being about 10 microns.

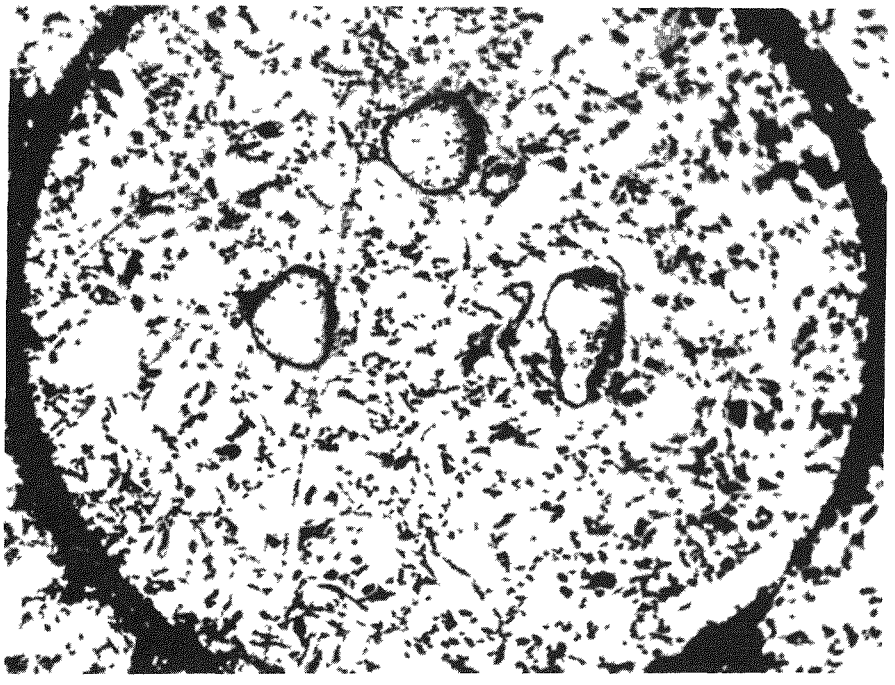

FIG. 7-3 UO_2 Particles in FA-1 Specimen Before Irradiation. (100X)

FIG. 7-4 Same UO_2 Particles Shown in Fig. 7-3 After Irradiation in Capsule SP-4. (100X)

Other measurements made on the in-pile and out-of-pile specimens were macroscopic examination, weight change, dimensional change, and impact strength. The weights and dimensions of all specimens prior to testing are given in Table 7-7.

These specimens had additional flats machined on their surfaces to permit accurate measurement of their diameters. The dimensional shrinkages noted in Table 7-7 are predominantly due to irradiation effects since insignificant shrinkages were found for the out-of-pile specimens except in the case of the FI-1 type. The irradiation-induced shrinkages do not decrease with increasing UO_2 particle size (i.e. decreasing recoil fission fragment exposure to the matrix) as might be expected which implies that properties of the graphite matrix and/or neutron damage are the significant factors rather than damage by fission fragment recoil. The FI-1 specimen has a fully graphitized matrix (Type AGOT). The low shrinkage of the FA-2 specimen could be related to the low degree of graphitization and low density (1.50 g/cc) of this specimen which was made with a coke filler and baked at only 2000°F. Both the FA-1 specimen and the FA-10 specimen have a graphite filler but the pitch binders were not graphitized, again due to the relatively low bake temperature. The FA-10 specimen was reimpregnated several times to raise its density to 1.80 gm/cc. The graphite density for the FA-1 specimen was 1.62 gm/cc. It would appear that the high shrinkage of the FA-10 specimen, in spite of the minimum fission fragment exposure due to its large 400μ fuel particles, is associated with its large number of reimpregnations.

Identical specimens from the same production batches as the FA-1 and FI-1 type had also been irradiated in a previous capsule, SP-1. This irradiation was described in ref (2). The dimensional changes from Capsule SP-1 are compared with those observed in Capsule SP-4 in Table 7-8. The infiltrated specimen (FI-1) showed a smaller shrinkage at the longer exposure which indicates that the lower temperature of the SP-1 irradiation may have been the dominant factor. This effect is not borne out in the case of the admixture specimen (FA-1), although the shrinkage increase with the higher temperature irradiation is only 50% of the exposure increase. Due to the lower fission fragment recoil exposure (i.e. larger fuel particle size) in the admixture specimen, the effect of fast neutron damage could be relatively more significant in the admixture element than in the infiltrated element.

TABLE 7-7

WEIGHTS AND DIMENSIONS OF UNCOATED UO_2 FUEL SPECIMENS IN OUT-OF-PILE AND IN-PILE TESTS

Specimen Type and No.	Test	Weight Change		Dimensional Change			
				Polar (a)		Equatorial (b)	
		Initial, gms.	Change, %	Initial, in.	Change, %	Initial, in.	Change, %
FI-1(E8)	In-Pile	52.3128	-0.40	1.477	-0.76	1.476	-0.67
FA-2(E8)	"	45.1378	-0.55	1.447	-0.03	1.452	-0.08
FA-1(E82)	"	51.8004	-0.11	1.478	-0.47	1.490	-0.52
FA-10(E5)	"	56.0927	-0.06	1.469	-0.69	1.469	-0.81
FI-1(E2)	Out-of-Pile	52.621	-0.77	1.487	-0.07	1.479	-0.10
FA-2(E7)	"	45.351	-2.55	1.447	0.0	1.449	-0.07
FA-1(E76)	"	51.892	-0.45	1.476	0.0	1.476	0.0
FA-10(E6)	"	55.727	-0.09	1.474	0.0	1.471	0.0

(a) Molding or extrusion axis

(b) Perpendicular to molding or extrusion axis

TABLE 7-8

Comparison of Dimensional Changes Observed in Capsule SP-1 and SP-4 for FA-1 and FI-1 Specimens

	Type FI-1			Type FA-1		
Capsule	Temp. °F	Exposure KWH/Ball	Dimensional Change, %	Temp. °F	Exposure KWH/Ball	Dimensional Change, %
SP-1	1350	1500	-0.93	1350	1400	-0.22
SP-4	1800	7700	-0.71	1700	6400	-0.50

The weight loss data shown in Table 7-7 clearly indicates that temperature effects are most significant since the weight losses are all larger for the out-of-pile specimens. It is interesting to note that the relative order of weight losses are the same for both the out-of-pile and the in-pile specimens. The major factor in these weight losses is probably further devolatilization of adsorbed gases.

Impact tests were performed on these specimens by dropping a steel weight onto the specimen from successively increasing heights to the point of failure. Since previous tests ref. (2) had shown that PBR specimens actually increase in compressive strength with irradiation, this test was not selected for the SP-4 specimens. The impact test results for the out-of-pile and the in-pile specimens are summarized in Table 7-9. For purposes of comparison, the impact data on as-received specimens, and the admixtured and infiltrated specimens after irradiation in Capsule SP-1 are also included.

TABLE 7-9

Impact Data on Uncoated Spheres

	As-Received		After Out-of-Pile Heating		After SP-1 Irradiation		After SP-4 Irradiation	
Specimen Type	Failure, Ft-lbs.	No. Impacts	Failure, Ft-lbs.	No. Impacts	Failure, Ft-lbs.	No. Impacts	Failure Ft-lbs.	No. Impacts
FI-1	12.5	12	9.4	22	10.4	12	11.7	35
"	11.5	11						
"	13.6	11						
FA-1	11.5	11	6.8	16	8.4	10	9.4	28
"	11.5	11						
"	7.3	5						
FA-2	7.5	15	6.8	16			3	9
FA-10	10.4	10	10.6	23			12.5	37

Although there is random scatter in this impact data, all values are significantly above the design objective of 2.0 ft. lbs. for PBR specimens except the FA-2 type. No significant effect of irradiation on impact strength can be noted, although there is a slight drop in impact strength for several of the specimens.

The effect of irradiation on the impact and compressive strengths of fueled graphite spheres is illustrated in Figures 7-5 and 7-6. A slight decrease in impact strength of uncoated graphite spheres can be noted in Figure 7-5 while the impact strength of the one Si-SiC specimen (Type FA-8) which was tested is seen to increase. Both of these effects are due to the increased hardness of the graphite matrix after irradiation. The same effect is also noted in Figure 7-6 where the incresed compressive strength of both coated and uncoated specimens can be noted.

The Capsule SP-4 irradiation has demonstrated that more than one type of uranium-graphite material has adequate structural properties to meet the reference design conditions of a large Pebble Bed Reactor. Some further work will be required to establish the cause and nature of the weight losses observed, but nonetheless, our initial selection of graphite as a high temperature ceramic structural material for use in PBR fuel elements appears fully justified.

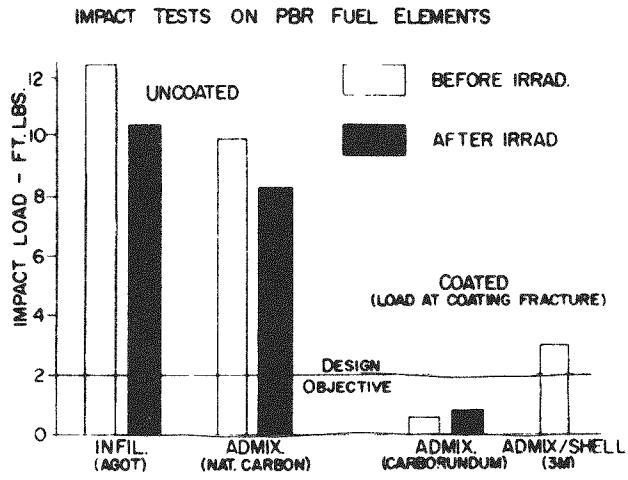

FIG. 7-5 Results of Impact Tests on PBR Fuel Element Specimens.

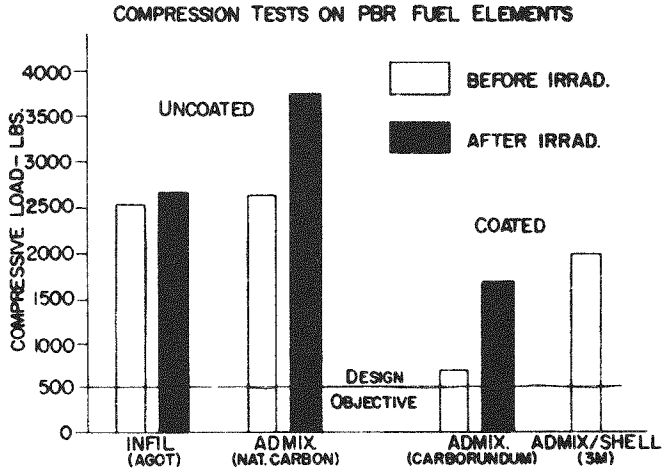

FIG. 7-6 Results of Compression Tests on PBR Fuel Element Specimens.

7.4 Fission Product Release from Uncoated Specimens

Although most of the work in the PBR Fuel Element Development Program involved fission product retention by coated fuel elements, several tests were performed on uncoated specimens to provide a frame of reference for assessing the worth of coatings in retaining fission products. Uncoated specimens were tested only by neutron activation. A description of the neutron activation test apparatus is given in Section 8.1. The test specimens included the FA-1 type (fueled with uncoated UO_2 shot), the FA-14 type (fueled with uncoated ThO_2/UO_2 shot) and a sample of UO_2 particles not incorporated in graphite. The UO_2 particles were in the 600 to 900 micron size range and were made by a sintering process as part of the work on sintered Al_2O_3 coated UO_2 discussed in Section 4.0.0. The results of the neutron activation tests on these specimens are given in Table 7-10.

A typical plot of the data is shown in Figure 7-7 for specimen FA-1(283N). Temperature and percentage of Xe 133 released are plotted vs. time. The curves are similar to previous results on neutron activation tests of uncoated specimens (2) in that a rapid release rate is noted at first, followed by a small or negligible release rate. The initial rapid release rate is presumably due to Xe 133 loosely held on the surfaces of the graphite matrix although the rapid release during successive runs at the same and higher temperatures indicated that it is associated with heating up of the specimen (i.e. the thermal expansion of the matrix and its pore structure). Although the count rate at the trap held constant after reaching an apparent maximum (i.e. postulating no further Xe 133 release) it is most probable that a longer test time would have shown a small but definite release rate.

As seen in Table 7-10, reproducibility between similar specimens is only within one order of magnitude. However, for FA-1(282N), three runs at 1500°F show quite good agreement. No significant trend with temperature can be noted. The presence of thoria in the fuel particles of the FA-14 specimen caused a small reduction in leakage which is not considered significant. The large release of Xe 133 from the UO_2 particles can be contrasted with the low release found for coated particles of the order of 10^{-4} to 10^{-6} in several hours as reported in Section 4.4.1.

Prior to the present Contract, several additional neutron activation tests were reported on uncoated specimens. These tests on specimen types FI-1, FA-1, FA-5 and FA-7 are reported in ref. (2). Also a sweep capsule irradiation (Capsule SP-2) of specimen types FA-1 and FI-1 were reported in ref. (2). No data was obtained on the infiltrated specimen FI-1 in Capsule

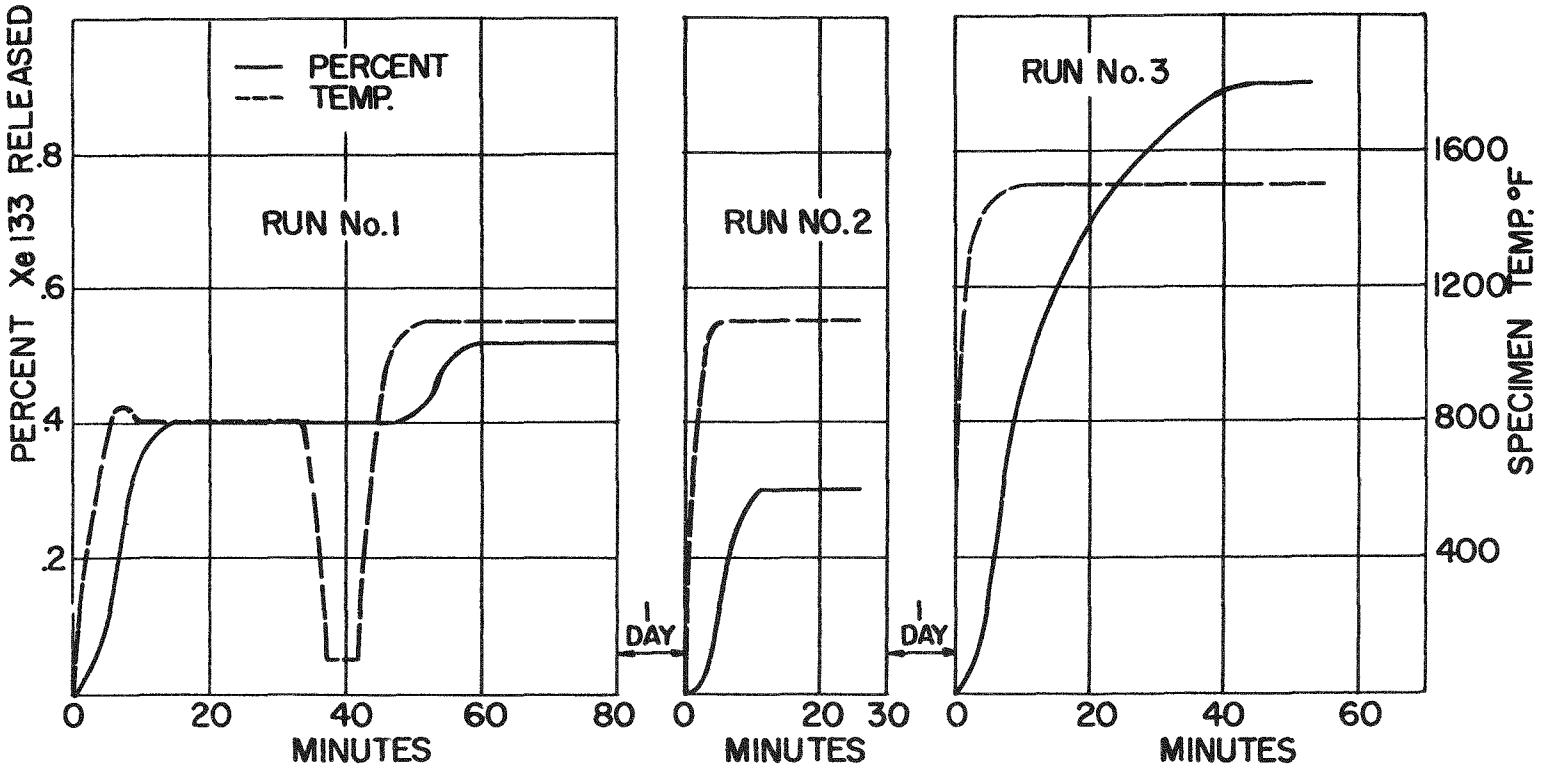

FIG. 7-7 Neutron Activation Data for Specimen FA-1(283N)

SP-2 because of excessive radiation levels in the off-gas train. Two gas samples were analyzed for the FA-1 specimen. The leakage factors (i.e. R/B, the release rate/production rate) were found to be 5.2×10^{-2} and 6.4×10^{-2} for Kr 85m and 6.3×10^{-3} and 1.7×10^{-2} for Xe 135 at a specimen temperature of about 1200°F. A similar FA-1 specimen was irradiated in the In-Pile Loop at the BNL reactor and results of this irradiation are discussed in Section 9.0.

TABLE 7-10

Neutron Activation Tests on Uncoated Specimens

Specimen No.	Test Temp., °F	Time at Temp., min.	Fraction of Xe 133 Released
FA-1 (278N)	1000	10	4×10^{-3}
	1500	20	9×10^{-3}
	1900	20	6×10^{-3}
FA-1 (282N)	1000	20	1×10^{-3}
	1500	60	6×10^{-3}
	1500	60	7×10^{-3}
	1500	90	7×10^{-3}
FA-1 (283N)	800	30	4×10^{-3}
	1100	40	1×10^{-3}
	1100	25	3×10^{-3}
	1500	55	9×10^{-3}
FA-14 (373N)	800	15	1×10^{-3}
	1500	40	2×10^{-3}
UO_2 Particles	1600	15	3×10^{-3}
	2500	45	20×10^{-3}

7.5 Strength Characteristics of Unfueled Graphite Spheres

Due to the relatively small number of fueled graphite spheres of a particular type which were received for evaluation, it was not possible to conduct numerous destructive tests on a given type of fuel element. Usually only one impact and one compression test were made on a single type although occasionally two or three such tests were made. In order to explore the statistical variations in these types of tests, 50 unfueled graphite spheres were procured. The spheres were 1-1/2" in diameter and were machined from Speer Carbon Co. Moderator Grade B stock having a density of 1.64 gm/cc. Half of the spheres were subjected to the compression test and the other half to the impact test.

The compression test results are listed in Table 7-11. The minimum and maximum loads at failure were 2270 lbs. and 3360 lbs respectively. The mean value was found to be 2932 $\pm$ 113 lbs based on a 95% confidence range.

The impact test results are listed in Table 7-12. The mean value of the impact load at failure was 16.4 $\pm$ 0.4 ft-lbs based on a 95% confidence range. The impact tests were performed by dropping a steel weight on the graphite sphere and increasing the impact energy in 0.5 ft-lb increments until failure was noted. Three additional spheres were used to evaluate the effect of the starting impact energy on the load at failure. These results, together with one of the data points from Table 7-12, are given in Table 7-13. A slight increase in the load at failure can be noted.

TABLE 7-13

Effect of Starting Impact Energy on Load at Failure

Starting Impact Energy, ft-lbs.	Load at Failure, ft-lbs
2.0	13.5
11.5	16.4
16.5	19.5
16.5	18.0

Typical load-deflection curves obtained from compression tests on uncoated graphite spheres are shown in Fig. 7-8. In these tests, the

TABLE 7-11

Statistical Compression Tests on Unfueled Graphite Spheres

Load at Failure, lbs.	Deflection at Failure, Lbs.	Load Modulus, lbs/in[a]
3235	0.136	26,500
2795	0.125	24,500
2900	0.129	25,000
2910	0.122	26,500
2940	0.138	24,500
2980	0.139	23,500
2570	0.122	23,000
2765	0.127	24,000
2645	0.125	23,500
3090	0.137	25,000
3110	0.141	24,000
3125	0.135	25,500
3140	0.137	26,000
3020	0.130	26,500
3245	0.136	26,500
3360	0.119	31,500
3200	0.133	27,000
2415	0.126	21,000
3255	0.143	25,000
2925	0.119	26,500
2270	0.117	21,500
2825	0.123	24,500
2980	0.129	25,000
2580	0.114	26,000
3015	0.137	24,500
Mean values 2932 ± 113[b]	0.130 ± 0.003[b]	25,000

(a) Based on best straight-line portion of the load deflection curve.
(b) Based on a 95% confidence range.

TABLE 7-12

Statistical Impact Tests on Unfueled Graphite Spheres

Starting Impact Energy, ft-lbs.[a]	Impact Energy at Failure, ft-lbs.
10.5	16.0
11.5	14.5
11.0	15.5
11.5	17.0
"	16.5
"	15.0
"	17.5
"	17.0
"	17.5
"	16.5
"	16.0
"	15.0
"	16.5
"	18.0
"	16.5
"	16.5
"	17.5
"	17.0
"	17.5
"	16.5
"	14.5
"	16.5
Mean value	16.4 ± 0.4[b]

(a) Impact energy was increased in 0.5 ft-lb increments.
(b) Based on a 95% confidence range.

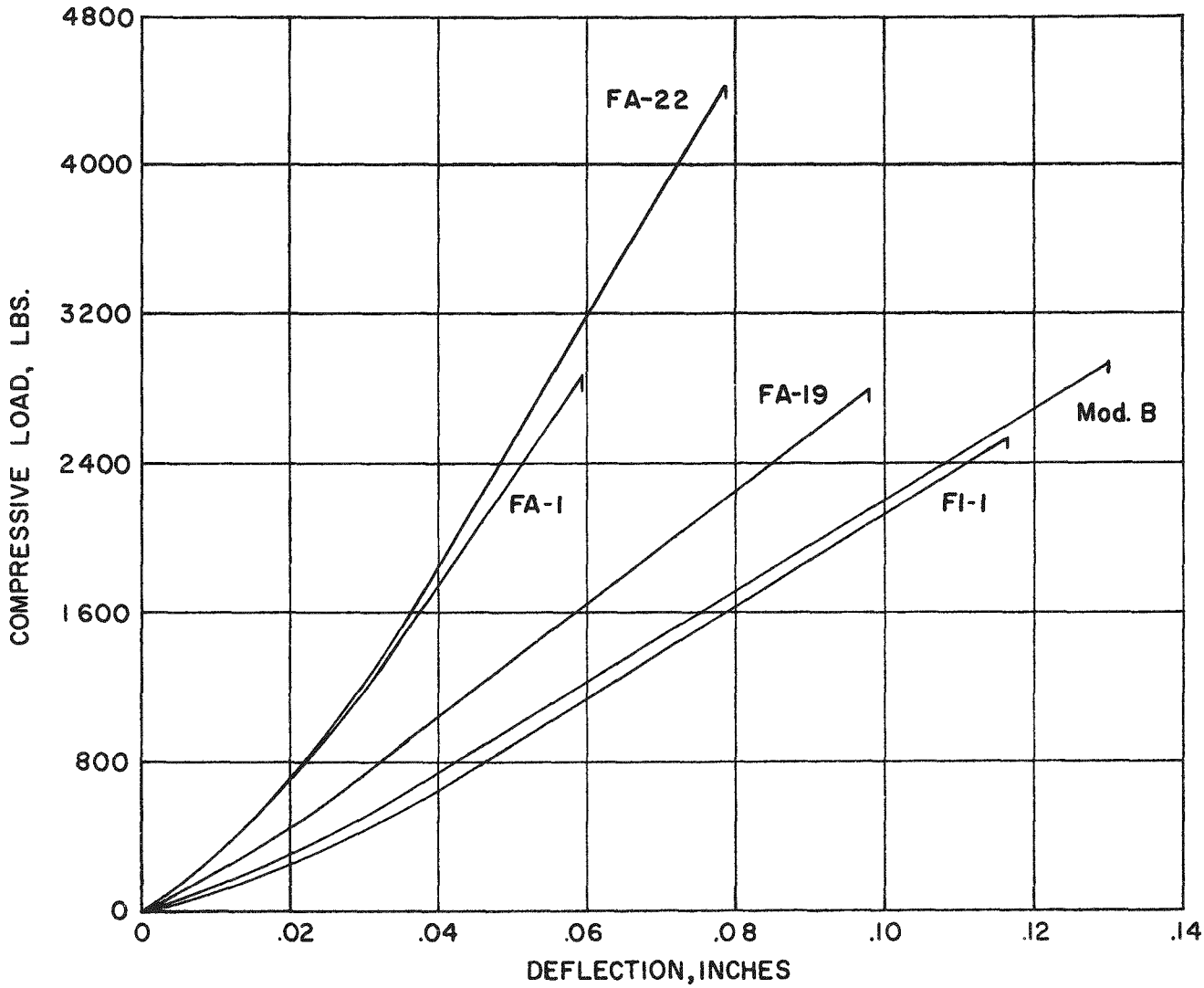

LOAD DEFLECTION CURVE
FOR GRAPHITE SPHERES UNDER COMPRESSION

FIG. 7-8

graphite spheres were loaded between two flat steel surfaces. A more rapid deflection rate can be noted as the compressive load is first applied. This is followed by a linear relationship between load and deflection up to the point of sphere failure. The slope of this linear portion of the curve was found to be dependent on the type of graphite which was used. This slope has been arbitrarily defined as the "load modulus" and has units of lbs/in. The values of load modulus for the specimen types shown in Figure 7-8, are given in Table 7-14.

TABLE 7-14

Load Modulus of Uncoated Graphite Spheres in Compression Tests

Sphere Type	Final Bake Temperature, °F	Compressive Load Modulus, lbs/in.
FI-1	>4800	25,000
Mod. B(a)	>4800	25,000
FA-19	4400	30,000
FA-1	2560	60,000
FA-22	2300	70,000

(a) Unfueled spheres machined from Speer Carbon Co. Moderator Grade B stock.

The lowest load moduli were found for the FI-1 specimens and the unfueled Speer Carbon Co. Moderator Grade B spheres both of which are fully graphitized materials. The FI-1 specimens were made by uranyl nitrate infiltration of spheres machined from National Carbon Co. Grade AGOT graphite stock. The highest load moduli were found for the partially graphitized FA-1 and FA-22 specimens. These specimens were made with a graphite powder filler but their pitch binder constituent was not fully graphitized in order to avoid carburization of their UO_2 and Al_2O_3 loadings. The FA-19 specimens consisted of FA-1 specimens which had been baked at about 4400°F thus converting the UO_2 to UC_2 and more completely graphitizing the binder constituent. This resulted in a corresponding decrease in load modulus.

A higher load modulus is due to the increased hardness and lower resiliency of the partially graphitized matrix material. This same effect was also found in post-irradiation compression test of fueled graphite spheres.

8.0 Equipment for Fission Product Release Experiment.

Three types of experiments have been used to measure fission product release rates from PBR fuel element specimens. In Neutron Activation tests, the quantity of released Xe 133 is measured after subjecting the specimen to a low level neutron activation. In Furnace Capsule tests, the rate of fission product release is measured while the specimen is under low level irradiation at a selected temperature. In Sweep Capsule tests, the rate of fission product release is measured while the specimen is under high level irradiation at a set temperature. The equipment design for each of these tests is described in the following sections.

One incidental advantage of the PBR fuel element concept is the ease of testing full scale fuel elements under conditions closely approaching those of a large power reactor with the use of relatively simple capsule irradiations. By replacing the thorium in the reference fuel element with additional enriched uranium, a relatively low powered research reactor such as the 2 MW Battelle Research Reactor can produce power densities in test specimens up to 75% of the desired maximum power density. Thus, irradiation damage effects are included in the results of Sweep Capsule Tests. Occasionally, separate static compartments and/or static capsules, having no sweep gas connections, were used. The design of Static Capsules and the operating history of all Static and Sweep Capsules operated under the present Contract are included in the following sections. Two capsules were operated prior to this Contract. These were Static Capsule SP-1 and Sweep Capsule SP-2. The design and operation of these capsules were described in ref. (2) and pertinent results are included in the present report.

Table 8-1 has been prepared to show the various specimens which were subjected to the three types of fission product release experiments.

8.1 Neutron Activation

Neutron activation tests have been used as an inexpensive and rapid method for determining the relative fission product retention ability of numerous types of specimens. The specimen is first irradiated at ambient temperature to a thermal neutron exposure of up to 10^{15} nvt. This activation is sufficient to produce a measurable amount of fission products yet permit convenient handling in laboratory facilities. The activated specimen is

TABLE 8-1

Specimens Irradiated in the PBR Fuel Element Development Program

Specimens	Neutron Activation	Furnace Capsules	Static & Sweep Capsules SP-1	SP-2	SP-3	SP-4	SP-5
A. Fueled Spheres							
FI-1	2		2	2		1	
FA-1	4		2	2		1	
FA-2						1	
FA-4			2				
FA-5	1						
FA-6	1				2		
FA-7	1						
FA-8	3				2	1	
FA-10						1	
FA-11	1						
FA-14	1						
FA-16	3						
FA-20	3	1				1	2
FA-21	1						
FA-22	4	1					2
FA-23	1	1					2
FA-24	1						
FA-25	2						
FA-26	1						
FA-27	1						
FL-2	1						

B. Coated Particles

The following batches of coated fuel particles were subjected to the neutron activation test.

Bare UO_2: 1 batch

Sintered Al_2O_3 coated UO_2: 1 batch

Vapor Deposited Al_2O_3: Batches 1B, 2A, 12H

Pyrolytic Carbon Coated UC_2: Batches PyC-1, 5, -6.

allowed to decay for 3 to 7 days to permit better resolution of the 5.27d Xe 133 isotope which is the only isotope measured in this type of experiment.

A schematic diagram of the laboratory apparatus used to measure the Xe 133 release is shown in Fig. 8-1. After the decay period, the specimen is installed in the vycor furnace tube. An induction heating coil is used which is capable of heating the specimen to 2500°F in 10 minutes. Atmospheric pressure helium is passed over the specimen which is heated at various selected temperatures, carrying the escaping Xe 133 to the collection train.

A dry ice cold trap first removes condensibles such as moisture and non-gaseous fission products which may come off the specimen. The Xe 133 is adsorbed in a quartz wall charcoal trap. This trap and a well-type scintillation crystal are mounted in dry ice. A continuous recorder is provided so that a record of activity released as a function of time can be obtained. A backup trap and exhaust system are also provided.

The detection limit on the fraction of Xe 133 released is a function of the activation level, decay time, and background count. Fractional Xe 133 releases as low as 10^{-7} have been detected with this apparatus. Further details of the apparatus can be found in reference (17).

8.2 Furnace Capsules

The first measurements of fission product release rates (i.e. rather than the release fraction measured in neutron activation tests) were in the high level Sweep Capsule SP-2 which contained uncoated specimens. Experience with this capsule indicated that a simpler, less expensive technique of getting fission product release rates would be desirable. Consequently, the Furnace Capsule experiments were conceived which would involve low radioactivity levels, permit startup and shutdown independant of the BRR cycles, and permit operation at a variety of selected temperatures, although irradiation damage effects would not be significant.

Fig. 8-2 is a drawing of a typical furnace capsule. A 1 1/2" PBR fuel element specimen is supported in the center of an inner container. Helium inlet and outlet lines are provided to carry escaping fission product gases to an external trapping system. An electrical heater is located in the annulus between the internal and external containers which permits the specimen to operate at any selected temperature up to 2000°F. The capsule operates in the pool adjacent to the BRR core. The location of the

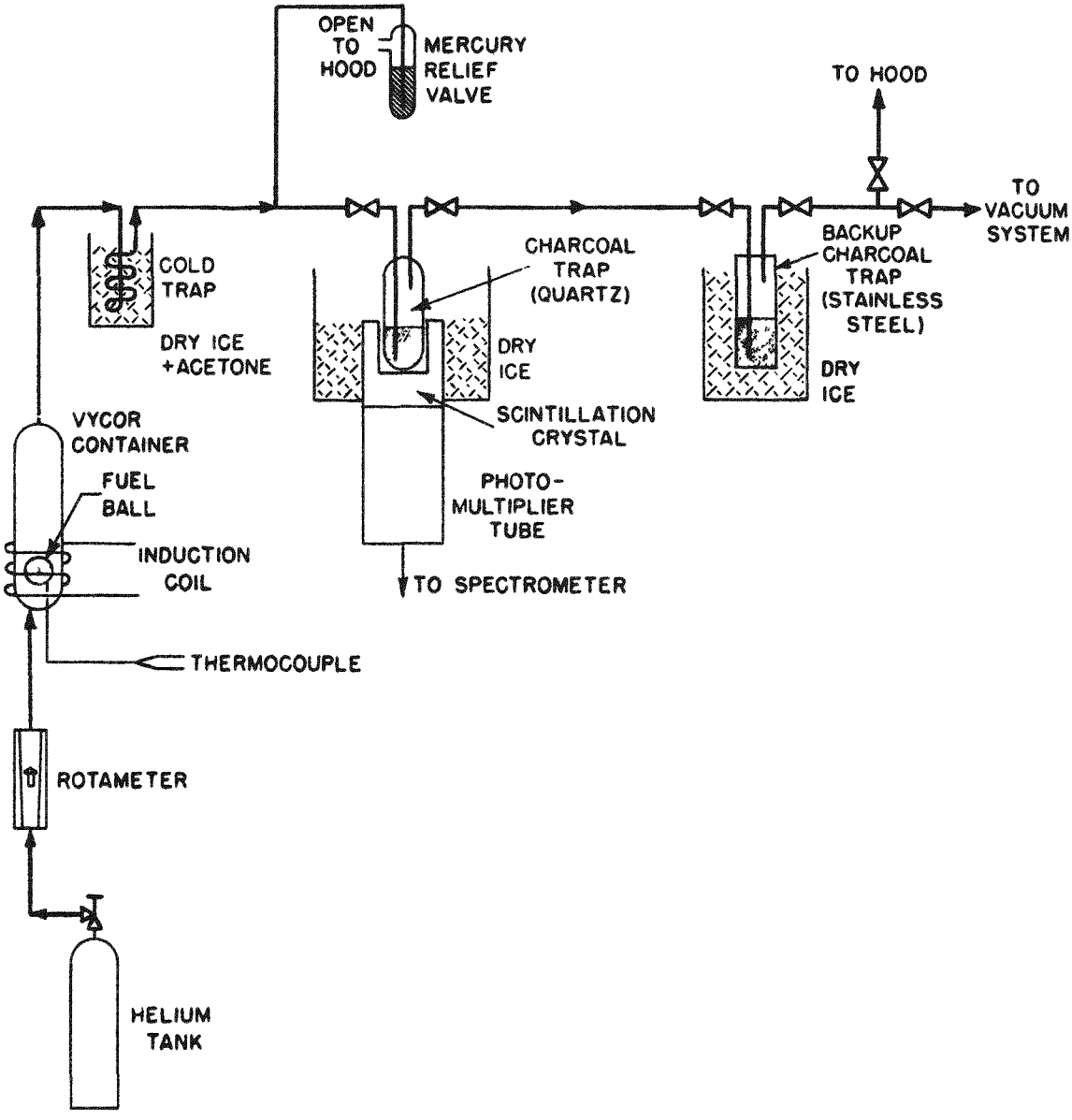

FIG. 8-1 Schematic Diagram of Gas Train for Neutron Activation Experiments.

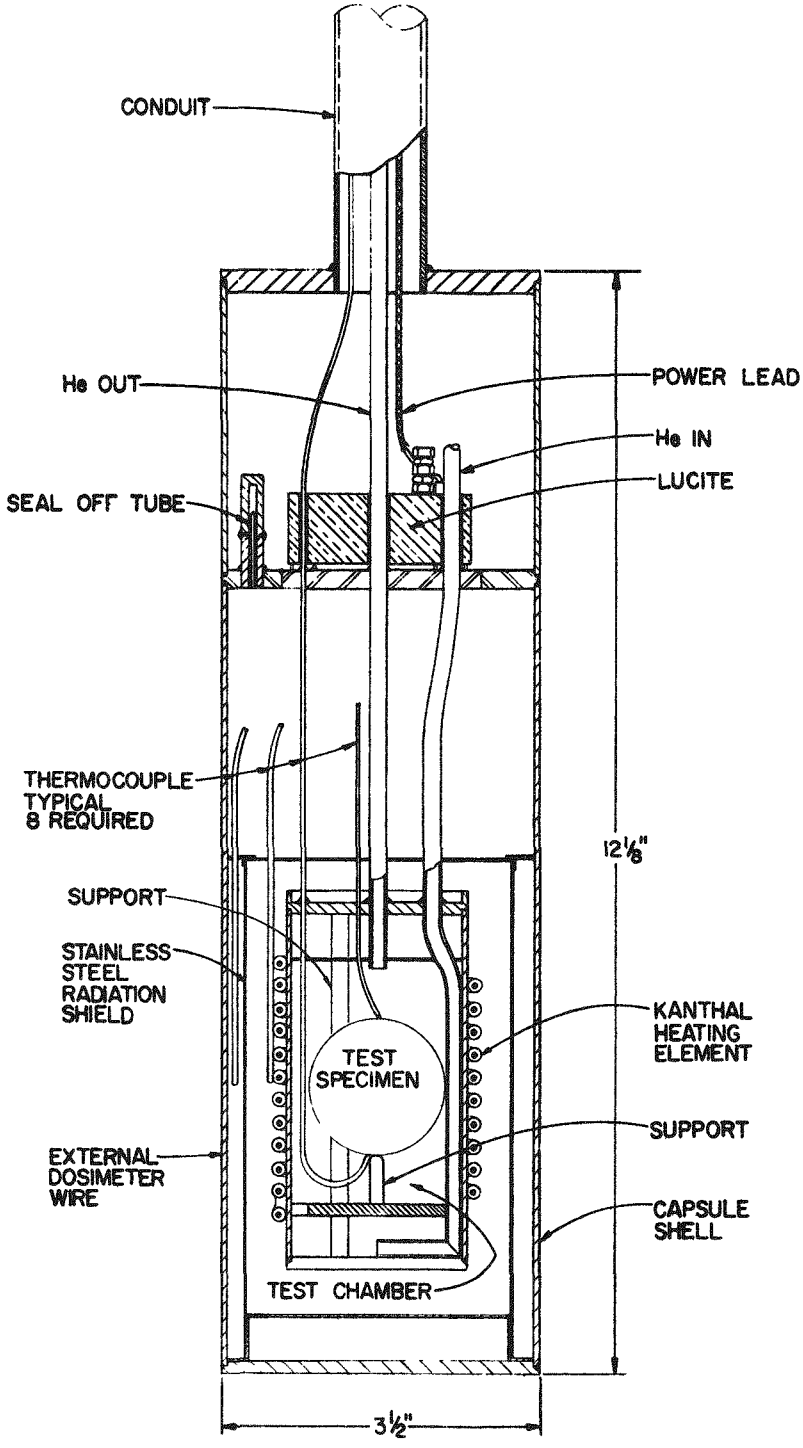

FIG. 8-2 Typical Furnace Capsule Design

capsule can be varied to permit irradiation in any desired thermal neutron flux up to a maximum of $3x10^{12}$ nv. The leakage rates of Xe 133, Xe 135, Kr 85m, Kr 87, and Kr 88 are normally measured in Furnace Capsule Tests. The gas train which was built for use with Sweep Capsules was used with Furnace Capsules SPF-1 and SPF-2. A description of this gas train is given in Section 8.3. A separate gas train was built for use with Furnace Capsule SPF-3. Further design and operating details can be found in reference (18).

Test results can be found for Capsule SPF-1 (containing a pyrolytic carbon coated FA-20 specimen) in Section 3.2.3, for Capsule SPF-2 (containing an Si-SiC coated specimen) in Section 3.1.3, and for Capsule SPF-3 (containing an Al_2O_3 coated UO_2 fueled specimen) in Section 4.4.2.

8.3 Sweep Capsule SP-3

The primary purpose of this irradiation was to investigate the fission product retention characteristics of two types of Si-SiC coated specimens. These were types FA-6 and FA-8.

The design features of Capsule SP-3 are shown in Fig. 8-3. The capsule was designed without auxiliary electric heaters, depending solely on nuclear heat generation and thermal resistances in the capsule to achieve the desired specimen temperature. Each specimen is mounted in a split graphite cylinder. A 30 mil annulus is provided around each specimen. This annulus is filled with a free-flowing graphite powder which minimizes the thermal resistance of the gap while permitting the specimen to expand or contract without restraint. A finned inner capsule is fitted over the graphite cylinders. Two inner capsules are provided, one containing two FA-6 specimens and the other containing two FA-8 specimens. A single outer capsule is fitted over the finned inner capsules and heat is rejected from this outer capsule wall directly to the BRR pool water. Thermocouples are located in the graphite cylinders adjacent to each specimen.

Separate sweep helium inlets and outlet lines are connected to each of the inner capsules. The gas flow is directed through the powder annulus surrounding each specimen. Escaping fission products are carried to an off-gas train located on the main floor above the BRR pool.

A schematic diagram of the off-gas train used to measure fission product leakage rates is shown in Fig. 8-4. Two independent gas trains are included. Sweep helium flow is maintained continuously throughout the irradiation. The flow is normally through a doubly-contained bypass

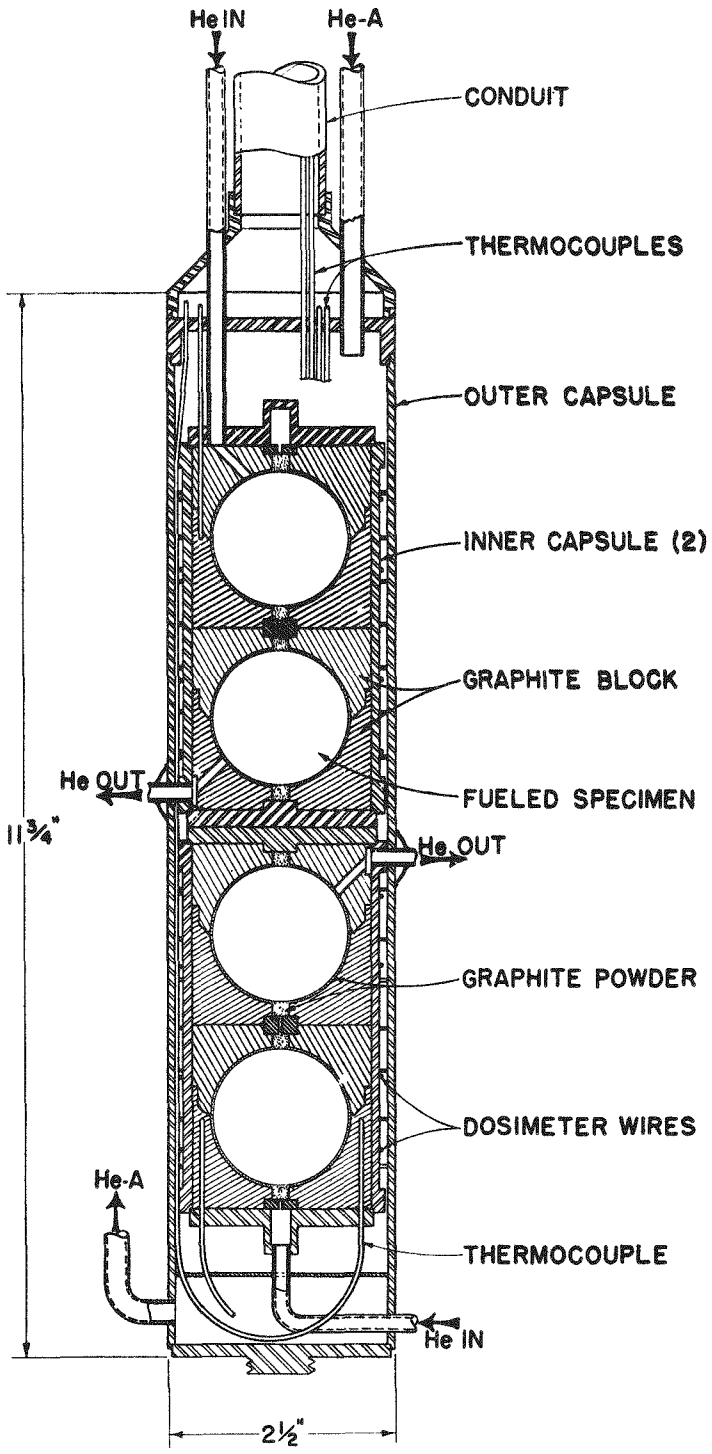

FIG. 8-3 Sweep Capsule SP-3

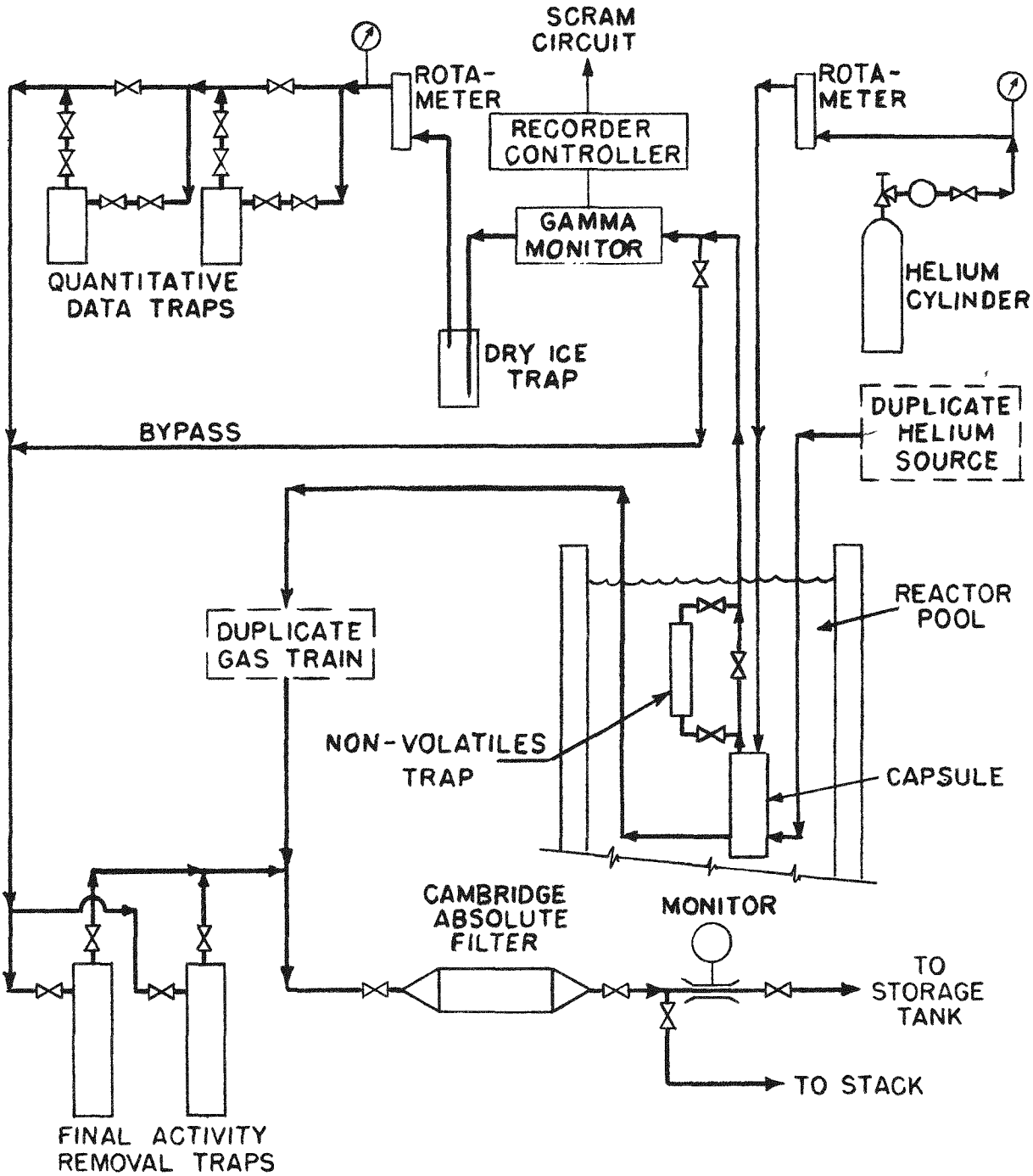

Fig. 8-4 Gas Train for Measuring Volatile Fission Product Release From Sweep Capsule Specimens.

line directly to the final activity removal traps. Fission product concentrations in this helium stream are measured by diverting a portion of the flow through the analytical train for a period of about 2 hours.

Capsule SP-3 was inserted in the BRR core on May 6, 1959 and was removed on August 3, 1959. During this period, several intentional low power runs were made to permit fission product release data to be obtained because higher than anticipated release rates were found as described in Section 3.1.3. Much of the time, Capsule SP-3 was operated as a static capsule with both the helium inlet and outlet valves shut off. The capsule was irradiated at the full BRR power level of 2 MW for 61 days of the total elapsed calendar time of 83 days. During one 31 hr. period (June 17-18), the BRR operated at a power level of 2.5 MW when the estimated specimen surface temperatures rose to 1850°F for FA-6 and 2300°F for FA-8. The average operating conditions during the irradiation are summarized in Table 8-2.

TABLE 8-2

Summary of Capsule SP-3 Operating Conditions

Specimen	Measured Block Temp. °F	Calc. Spec. Surface Temp. °F	Calc. Spec. Center Temp. °F	Calc. Ht. Gen. Rate KW/Ball	Total Exposure Calc.	Total Exposure Dosim.
FA-6 (18E)	1000	1300	1450	1.7	2500	2400
FA-6 (20E)	1000	1300	1450	1.7	2500	1950
FA-8 (E4)	1200	1600	1700	2.2	3200	2400
FA-8 (E5)	1200	1600	1700	2.2	3200	2600

The fission product release data for these specimens are given in Section 3.1.3 and the results of the post-irradiation hot cell examination are given in Section 3.1.2.

8.4 Static Capsule SP-4

The primary purpose of this irradiation was to investigate the stability of UO_2 fueled graphite spheres under high temperature irradiation. Four 1 1/2" diameter uncoated graphite spheres fueled with different types of UO_2 were included. These specimens and the experimental results on them are described in Section 7.3. Two additional coated specimens were included. These were coated with Si-SiC and pyrolytic carbon and are described in Sections 3.1.2 and 3.2.2 respectively.

The design features of Capsule SP-4 are shown in Fig. 8-5. Since this experiment was concerned solely with the effects of irradiation on physical properties of the specimens, no helium lines were included for detecting fission product leakage. The method of mounting each specimen in a split graphite cylinder is the same as described for Capsule SP-3. A finned inconel inner capsule was fitted over the six graphite cylinders. The number of fins and fin thickness were selected to achieve a specimen surface temperature of 1900°F which would result in specimen central temperatures of 2000 to 2100°F. A stainless steel outer capsule was fitted over the fins. A total of 13 thermocouples were installed in the capsule. Two thermocouples are located in the graphite cylinder just outside the equator of each specimen. In addition, a hole was drilled to the center of the uppermost specimen (Type FA-1) and a thermocouple installed therein. The specimen power level actually obtained can be calculated from the measured temperatures in the graphite cylinder, the pool water temperature, and the effective thermal conductivity of the capsule parts. Using this power level, the specimen temperatures can then be calculated, again starting from the measured graphite cylinder temperature.

Capsule SP-4 was inserted into the BRR on August 25, 1959. Typical operating conditions are summarized in Table 8-3.

TABLE 8-3

Operating Conditions for Capsule SP-4

Specimen	Measured Graphite Block Temp. °F	Ht. Gen. Rate, KW	Calculated Surface Temp.	Central Temp., °F
FA-1(E82)	1300	1.9	1600	1750[a]
FA-8(E6)	1400	2.2	1750	1850
FI-1(E8)	1400	2.3	1750	1850
FA-2(E8)	1400	2.2	1750	1900
FA-20(336E)	1250	2.0	1550	1750
FA-10(E5)	1300	1.7	1600	1700

(a) Measured temperature. One thermocouple is imbedded in the center of this specimen only. All other central temperatures are calculated.

As can be noted, the target temperature of 1900°F surface temperature was not achieved. Several factors were investigated in an attempt to explain

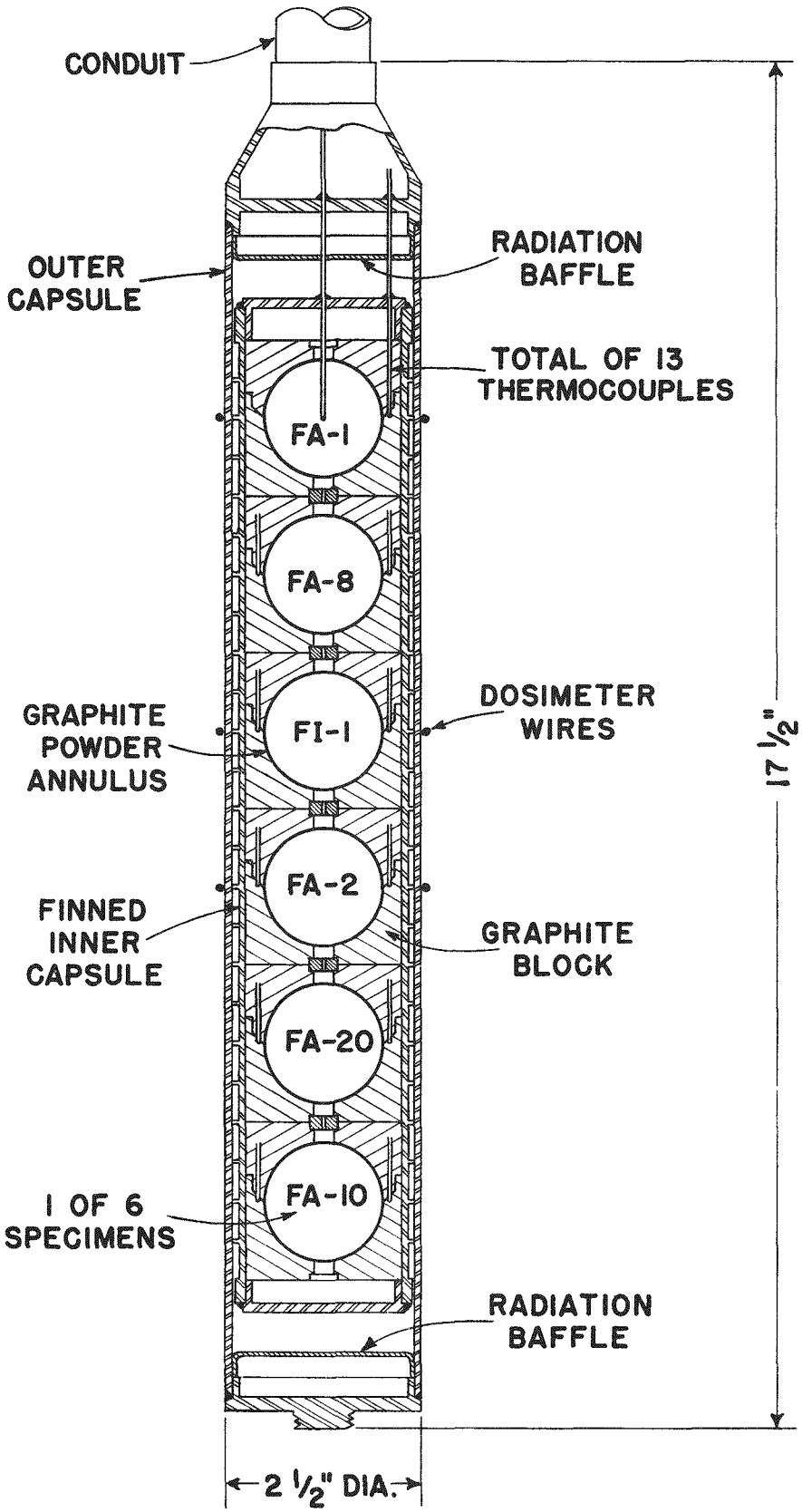

FIG. 8-5 Static Capsule SP-4

or improve the situation. Since no auxiliary electrical heaters were included, the target temperature was to have been achieved by proper selection of the thickness and material of the various thermal barriers with respect to the anticipated flux levels. One factor was uncovered when laboratory measurements of the thermal conductivity of the Inconel-X used for the inner capsule showed that the literature value used in design was 20% low. An attempt was made to increase the neutron flux by rearranging fuel elements in the BRR core. However, there was no significant increase. Several plans were studied to apply an external thermal barrier to the capsule to increase the temperature. However, the close tolerance required at the capsule-barrier interface appeared impractical to achieve with remote handling devices under 23 ft. of pool water.

The irradiation of Capsule SP-4 was terminated on March 7, 1960. The accumulated full power operating time was 139.5 days. During the course of the irradiation, 6 thermocouples failed, 2 each for the FA-10 and FA-20 specimens, and 1 each for the FA-2 and FI-1 specimens. However, there was sufficient operating time with all thermocouples working so that temperatures where thermocouples had failed could be estimated with confidence based on thermocouple readings at other locations.

The estimated irradiation exposures for the specimens given in Sections 7.3, 3.1.2, and 3.2.2 were based on the calculated power levels listed in Table 8-3 and the equivalent full power operating time of 139.5 days. Analysis of the cobalt-nickel dosimeter wires for several of the specimens gave somewhat lower values. A comparison of these values is given in Table 8-4.

TABLE 8-4

Comparison of Estimated Exposures to Specimens In Capsule SP-4 By Two Methods

Specimen	Estimated Exposure, KWH/sphere	
	From Thermal Data	From Dosimetry
FA-1	6400	3700
FI-1	7700	4400
FA-2	7400	4400

Based on previous experience, burnups calculated from thermal data are usually within ± 30% of the dosimetry data. As noted in Fig. 8-5, the dosimeter wires are located on the outside wall of Capsule SP-4. The unperturbed thermal neutron flux in the experimental hole was about 3.5×10^{13} and a perturbed flux at the capsule wall should have been about 2×10^{13}. The flux level corresponding to the dosimetry data was only 1×10^{13}. Thus, it is felt that the dosimetry data is probably low but the source of the discrepancy is unexplained.

8.5 Sweep Capsule SP-5

The primary purpose of this irradiation was to investigate the fission product retention characteristics of promising fuel element specimens under high level irradiation. The two most promising specimens selected for Capsule SP-5 were the Si-SiC coated specimen (FA-23) and a specimen fueled with vapor deposited Al_2O_3 coated UO_2 (FA-22).

The design features of Capsule SP-5 are shown in Fig. 8-6. The general method of mounting each specimen in a graphite cylinder and using a doubly contained capsule with fins on the inner capsule is the same as for Capsule SP-3. However, the outer capsule of SP-5 is divided into two independant compartments. The upper compartment, called the sweep compartment, contained two separate inner capsules. Separate helium inlet and outlet lines were brought to each inner capsule. Gas flow, which was upwards through the graphite powder annulus surrounding each specimen, scavenged any fission products which leak from the specimens and carried them to trapping apparatus outside the capsule. An FA-22 and an FA-23 specimen were located in the two inner capsules of the sweep compartment.

A separate static compartment was located below the sweep compartment. No helium lines were connected to the static compartment. An additional FA-22 specimen, an additional FA-23 specimen, and two FA-20 specimens were included in the static compartment. A simple threaded connection joined the sweep compartment and the static compartment so that if it became desirable to examine the sweep compartment specimens (i.e. if large increases in fission product release rates indicate failure of both specimens), the upper compartment can be disengaged and the lower compartment left in the reactor for further irradiation. No thermocouples were included in the static compartment because of this disconnect feature. Temperatures and power levels for these specimens were estimated from temperature data in the sweep compartment and the axial flux profile in the experimental hole.

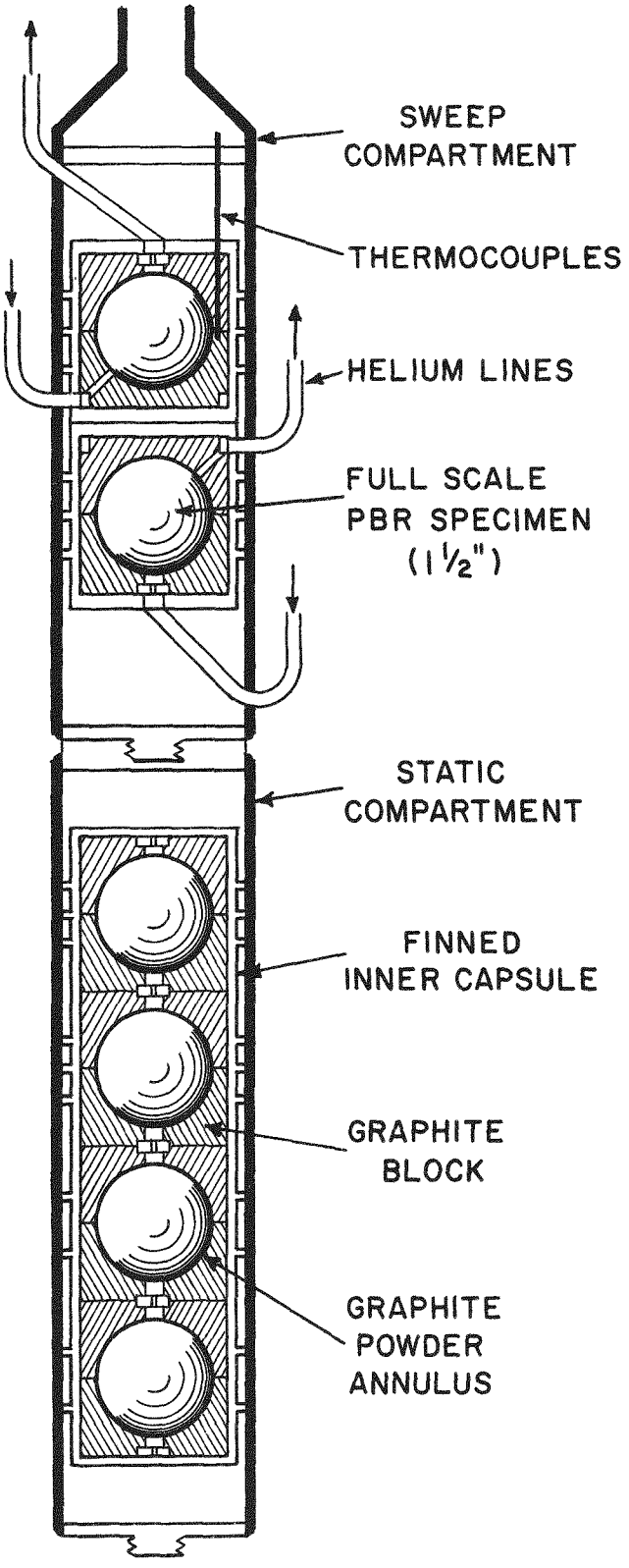

FIG. 8-6 Sweep Capsule SP-5

Irradiation of Capsule SP-5 was started on April 6, 1960 and terminated on November 14, 1960. On October 15, further responsibility for Capsule SP-5 was transferred to Battelle's Coated Particle Program under Contract W-7405-eng-92. Typical operating conditions during the irradiation are listed in Table 8-5.

TABLE 8-5

Typical Operating Conditions for Specimens in Capsule SP-5

Specimen No.	Measured Block Temp, °F	Ht.Gen Rate KW	Calc. Surface Temp, °F	Calc. Central Temp, °F	Burnup, KWH
Sweep:					
FA-22(471E)	1090	1.5	1360	1540	5400
FA-23(E8-7)	1010	1.6	1300	1440	5900
Static:					
FA-22(470E)	-	1.4	1360	1540	5400
FA-20(338E)	-	1.3	1360	1460	4500
FA-23(E8-12)	-	1.0	1300	1390	3600
FA-20(345E)	-	0.8	1360	1420	2700

Special underwater traps for the non-volatile daughter products of the short-lived noble fission product gases were installed as shown in Fig. 8-4. These traps consist of a stainless steel container 2 1/2 in. OD by 36 in. long filled with layers of stainless steel mesh. The sweep helium flow normally bypasses these traps. A sample is taken by actuating the underwater valves and diverting the full flow through the trap. Segments of the stainless steel mesh can be removed from the trap and radiochemically analyzed for such isotopes as Sr 89, Ba 140, Ce 141, and I 131.

Data obtained for the long-lived volatile fission product release and from the non-volatile trap is given in Section 3.1.3 for the FA-23 specimen and in Section 4.4.3 for the FA-22 specimen. Further details on the design operation of Capsule SP-5 will be found in ref. (23).

9.0 In-Pile Loop

An in-pile loop program to study the behaviour of fission products escaping from a PBR fuel element was conducted under a subcontract to the Nuclear Science and Engineering Corp. The objectives of the Loop Program were to study the fission product radioactivity levels in a recycled helium stream; methods of lowering gas stream activity levels; the amount, location, and nature of deposited fission products; and methods of decontaminating equipment surfaces. In addition to testing low release PBR fuel element specimens, it was planned to irradiate an uncoated uranium-graphite specimen to simulate problems of a "dirty" primary loop.

A complete summary of the design, operation and results from the In-Pile Loop program can be found in a Topical Report prepared by NSEC (26). The highlights of this work are described in the following sections.

9.1 Loop Design

The In-Pile Loop was designed for use at the Brookhaven Graphite Reactor. The in-pile section was inserted in experimental hole W-11 while the blowers, heat exchangers, sampling stations, etc. were located on the adjacent floor space. Design characteristics of the Loop were as follows:

Circulating Fluid	Helium
Operating Pressure	14 psia
Flow Rate	8 scfm
Max. Helium Temp.	1250°F
Min. Helium Temp.	250°F
Max. Specimen Temp.	1800°F
Max. Specimen Power	0.25 KW

Two major variables, the system pressure and the specimen power, were selected with a view to minimizing the cost of the loop. The use of sub-atmospheric pressure eliminated the need for double containment and the modest power level in the specimen provided measurable activity while minimizing the gas flow requirements and shielding costs.

Figure 9-1 is a schematic diagram of the in-pile loop. Gas leaves the in-pile section at 1250°F and enters the shell side of a coiled tube heat exchanger where it is cooled to 550°F. The exchanger was designed for easy replacement of the tube coil so that deposition on the tube surface

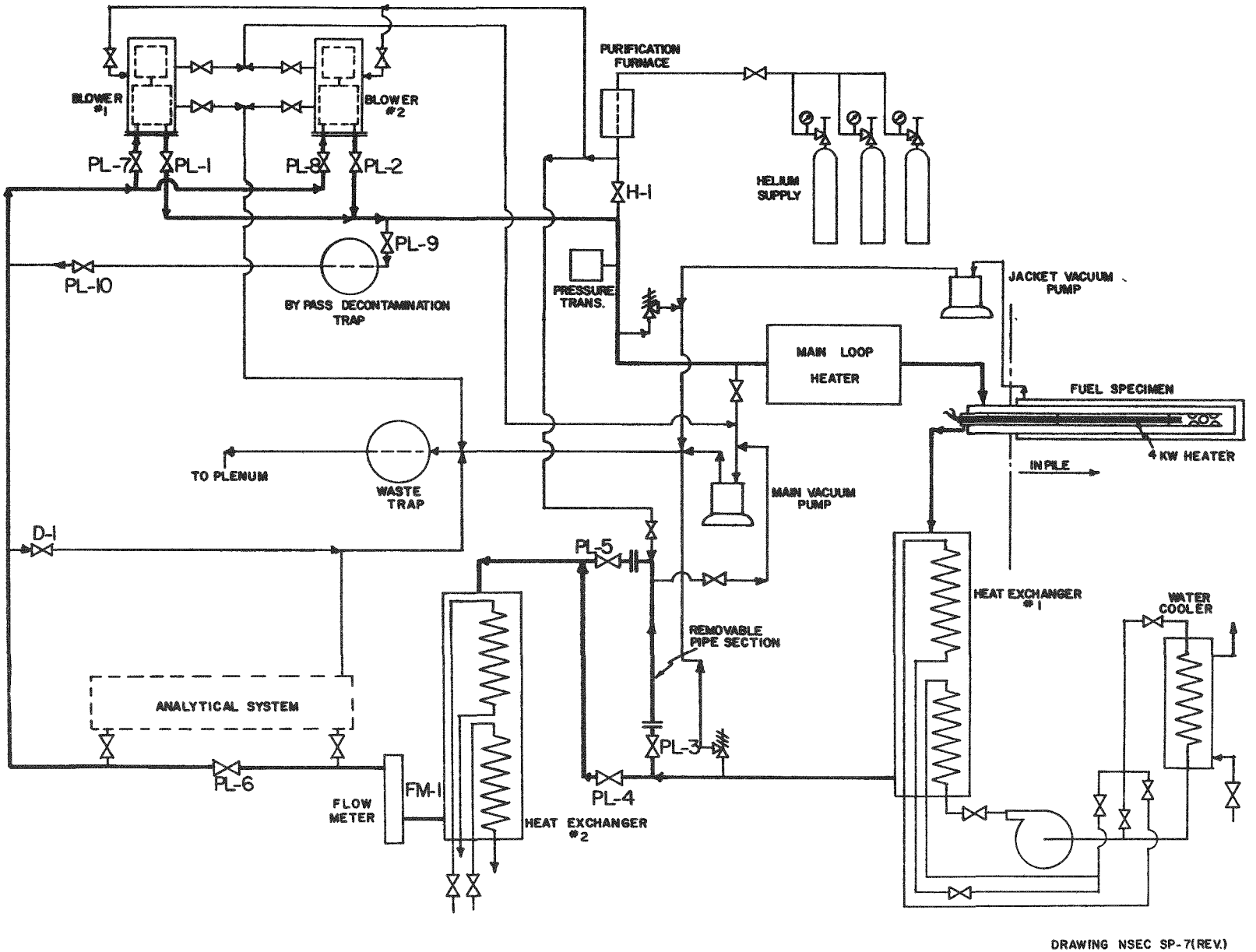

FIG. 9-1 Schematic Diagram of In-Pile Loop

as a function of temperature could be studied. An intermediate Dowtherm loop, which transports heat from this exchanger to a water-cooled sink, was included to permit adequate control of the helium outlet temperature. The helium next passes through a removable 550°F test section containing deposition coupons and a precooler to lower the temperature to 250°F which enables the use of an economical low temperature blower. Before entering the blower, provision was made for in-line or bypass operation of an analytical train in order to obtain data on fission product release rate and activity levels in the gas stream.

Two Dexter-Conde positive displacement blowers were provided, although only one was required for normal operation. Each blower and its drive motor were mounted in a canned enclosure so that leaktightness would not depend on a rotating seal. Flow variation was achieved by powering the drive motors from a variable frequency motor generator set. A bypass charcoal trap was provided from the blower discharge back to the blower inlet so that the effect of continuous gas decontamination could be studied. After leaving the blower, the helium temperature is raised to 1200°F by an electrical resistance heater and then enters the in-pile section.

A drawing of the in-pile section is shown in Figure 9-2. Inlet helium flows through the annulus of the co-axial pipe section, through the test specimen holder located at the innermost end of the center pipe, and returns through the center pipe. Separate offset inlet and outlet lines were used through the fixed shield plug. The specimen holder and hot leg coupons were replaceable through a flanged connection on the front end of the center pipe and a removable shield plug. A 3/4" OD x 15 ft long stainless steel sheathed tubular electric heater was located in the center pipe to make up for heat losses from the in-pile section. Fig. 9-2 reflects the design changes which were made prior to the fabrication of a second in-pile section which was necessary due to the development of a leak in the vacuum insulation annulus of the first in-pile section as discussed in Section 9.2. The principal change involved the addition of 0.4" of flexible "Min-K" blanket (Johns-Manville) in the vacuum annulus to replace the stainless steel foil radiation shields. The primary purpose of this insulation annulus was to prevent overheating of the moderator blocks in the Brookhaven Graphite Reactor.

A mockup of the test specimen holder is shown in Figure 9-3. Portions of unfueled graphite spheres were mounted in each half of a split graphite cylinder and all graphite surfaces were coated with siliconized silicon carbide. The fueled specimen was mounted between the unfueled graphite spheres to simulate a packed bed arrangement. Two thermocouples were imbedded in the

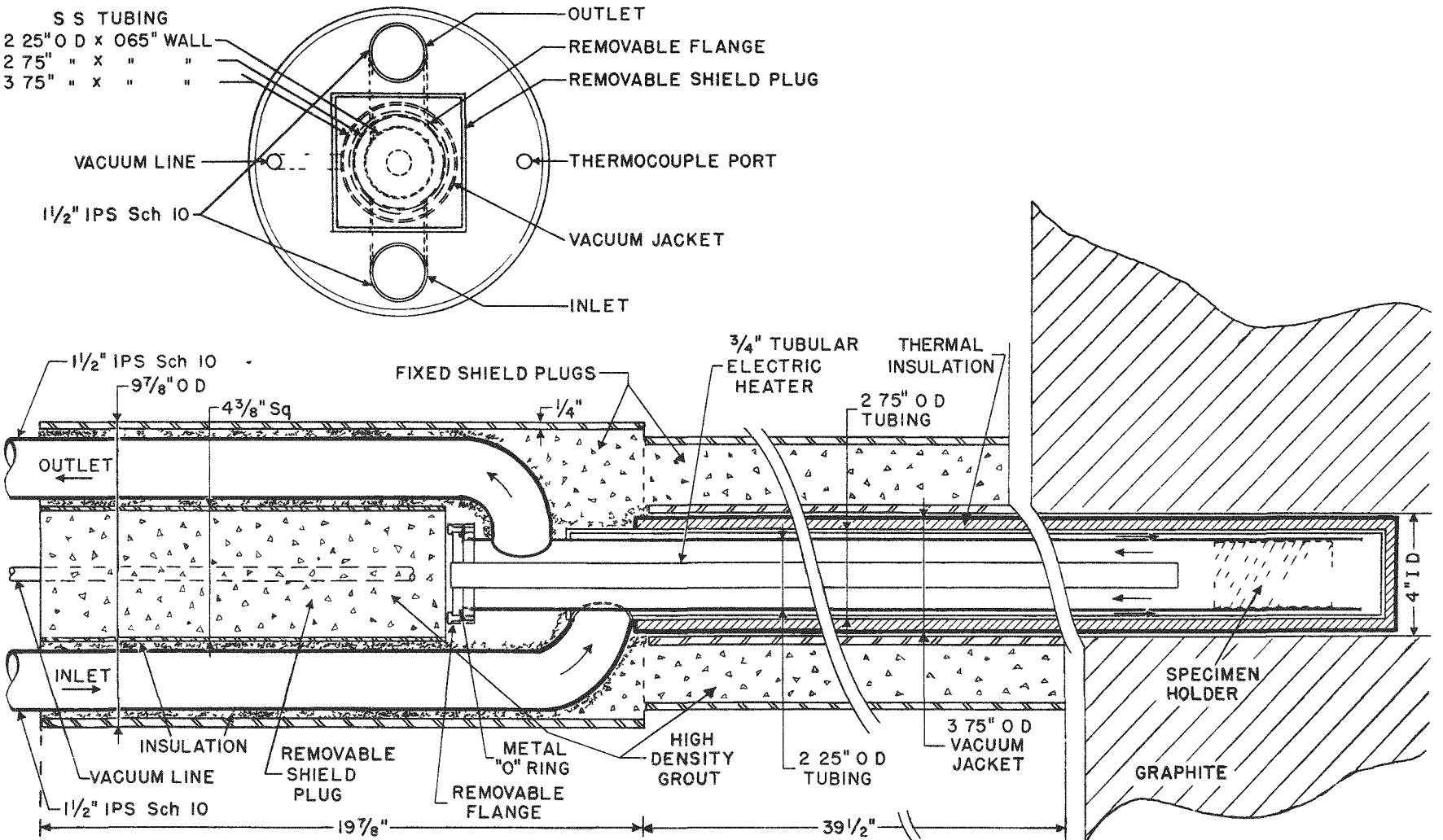

IN-PILE SECTION

FIG 9-2

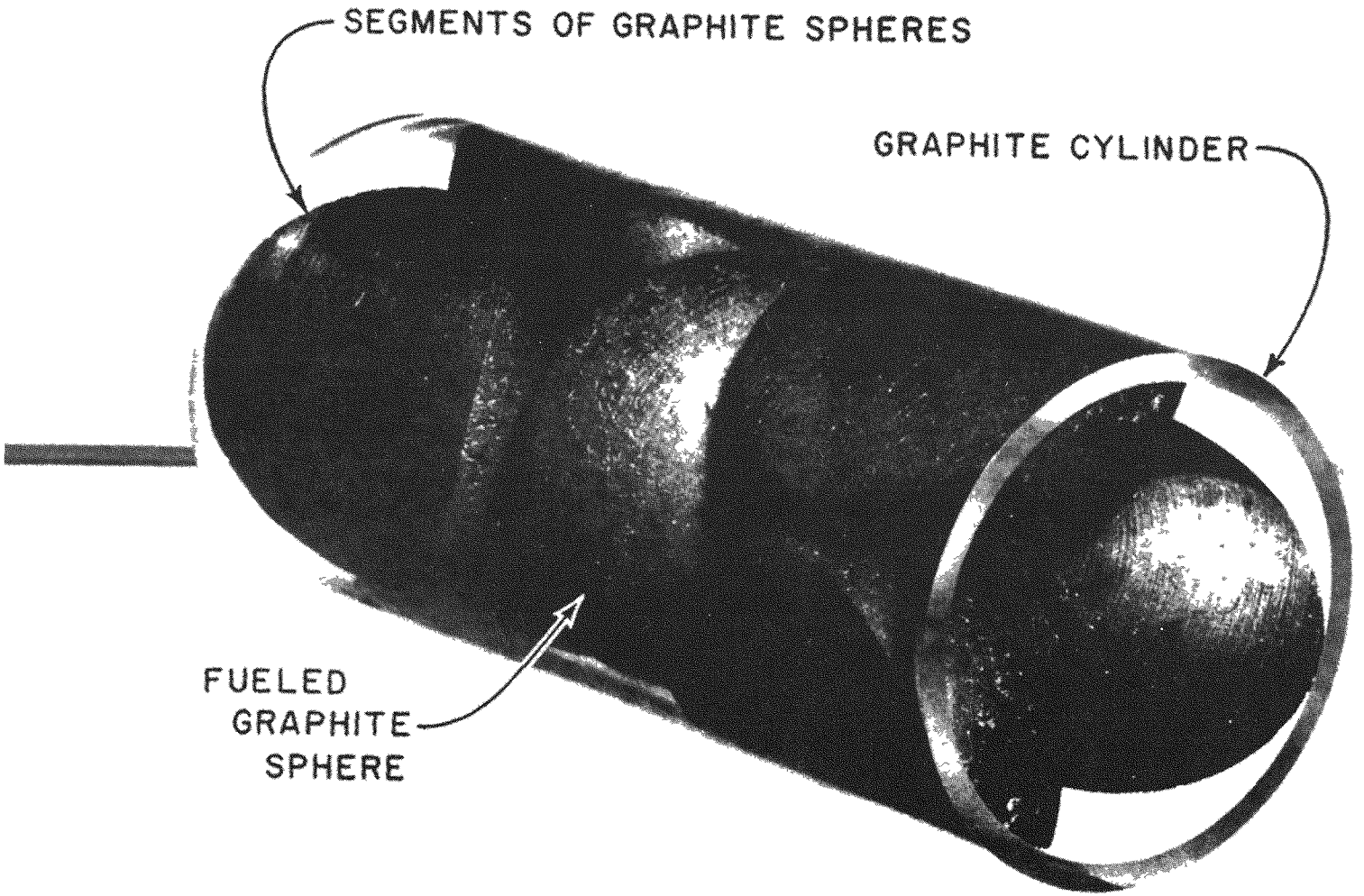

FIG. 9-3 Mockup of Test Specimen Holder For In-Pile Loop

surface of the fueled specimen to permit accurate temperature measurement.

Subassemblies of the loop components were prepared and tested for leaktightness prior to shipment to BNL on Aug. 1, 1960. The final assembly including the auxiliary water, air and Dowtherm systems was completed at BNL. A photograph of the assembled loop on the floor adjacent to hole W-11 at the Brookhaven Graphite Reactor is shown in Figure 9-4. The in-pile section is seen facing away from the pile face in order that shakedown tests could be performed prior to irradiation. During these out-of-pile tests, an unfueled graphite sphere containing a miniature 0.25 KW electrical heating element was used in place of the fueled specimen in order to simulate nuclear heating.

During the course of the shakedown tests, several problems arose. Excessive float bounce in the primary helium flow meter was corrected by the addition of a damping orifice at the meter outlet. An accumulation of a greasy substance in the blower casings caused the graphite vanes in the blower to seize and break during the startup of one of the blowers. The grease was found to have leaked in through a shaft seal because of either a faulty initial seal installation or a period of extended blower operation against its maximum rated head. After replacing the vanes and a thorough degreasing, the blower performance improved noticeably and smooth operation was achieved over the range of 2 to 24 scfm at 14 psia discharge pressure. One series of tests was run to measure the temperature difference between the specimen and the helium stream as a function of helium flow rate. At 0.2 KW input to the dummy specimen, temperature difference ranged from 140°F at 23 scfm to 330°F at 6.1 scfm. A temperature difference of 550°F had been estimated at 8 scfm and 0.25 KW using heat transfer correlations from packed bed data. The lower temperature differences actually obtained were attributed to additional conduction losses to the adjacent unheated support spheres. It was planned to achieve the design temperature difference by operating the specimen at 0.3 KW and using reduced helium flow rates of 5 scfm or lower.

A serious deficiency in the thermal capacity of the system was also uncovered during the shakedown tests. At low helium flowrates, the heat capacity of the circulating helium was insufficient to maintain gas temperatures throughout the hot leg piping and the in-pile section. This required the addition of auxiliary heaters to make up heat losses from the system. Flexible heating cable consisting of nichrome wire insulated with fiberglass, asbestos and stainless steel braid was wrapped on high temperature sections of the out-of-pile piping. Temporary heating coils were wrapped on the in-pile section so that its vacuum insulation annulus could be degassed at 1100°F.

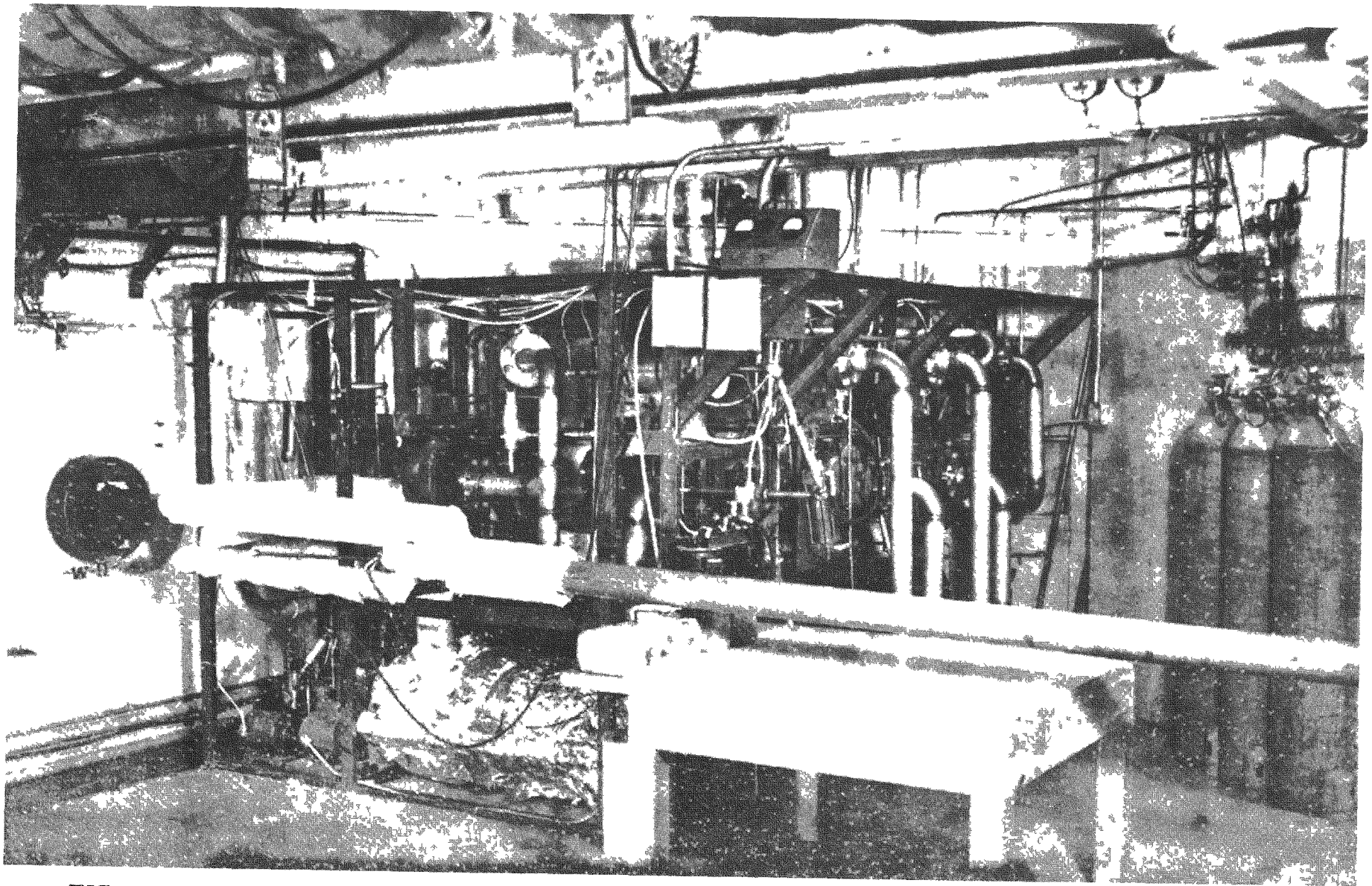

FIG. 9-4 In-Pile Loop Assembly Shown at the BNL Reactor with In-Pile Section Arranged for Pre-Irradiation Shakedown Tests

A 3/4" diameter stainless steel sheathed electrical heater was installed in the in-pile section. With these modifications, uniform pipe temperatures were achieved in the out-of-pile section and helium temperatures of 1100°F to 1125°F were achieved at the specimen holder in the in-pile section which was slightly below the design helium temperature of 1200°F. The surface temperature of the in-pile section was about 320°F which was well below the limit of 482°F imposed by BNL.

With the completion of these tests, approval was received to start in-pile operations with the provision that the unfueled electrically heated specimen be used for one cycle to permit a final test of the loop in the absence of fission product activity.

9.2 In-Pile Operation

The In-Pile Loop program was conceived at a time when the reference Pebble Bed Reactor fuel element was a fueled graphite sphere having a surface coating for fission product retention. Three types of fuel element irradiations in the Loop were planned: a whole coated specimen (low fission product release), a specimen with a cracked coating (intermediate fission product release), and a specimen broken completely in half (maximum fission product release). With the advent of the coated fuel particle, this plan was changed to two types of fueled specimens, as listed below.

1. Minimum release: Specimen FA-22(550E) fueled with 105/149 micron UO_2 particles coated with 48 microns of vapor deposited Al_2O_3 (i.e. Batch 6H, described in Section 4.0).

2. Maximum release: Specimen FA-1(90E) fueled with 105/149 micron UO_2 shot.

These two fueled specimens together with the unfueled electrically heated specimen were operated in the Brookhaven Graphite Reactor over a period of five cycles. A diagram schedule of the operating cycles and shutdown periods is shown below.

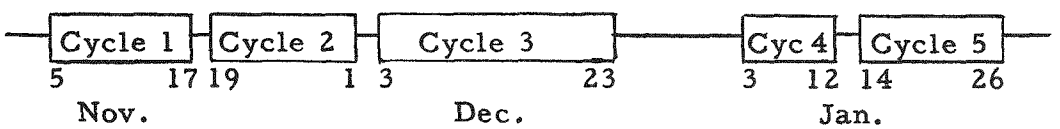

The in-pile section containing the unfueled electrically heated specimen was installed in Hole W-11 during the shutdown prior to Cycle 1. Exceptional difficulty was encountered in fitting the in-pile section into the experimental hole. A previous trial insertion and withdrawal during the shakedown period had been successfully completed. During the November 4th installation, the in-pile section was found to be slightly warped, probably due to the relief of strains in the tubing by annealing during the high temperature degassing runs. Numerous attempts were made to straighten and insert the in-pile section and the installation was finally made just before Reactor startup.

Due to insertion difficulties, only a cursory check of the vacuum annulus integrity was made before startup. After startup, it was found to be impossible to obtain a vacuum in the insulation annulus. No leaks were found in accessible portions of the vacuum system and conclusive evidence was found that no leak existed between the primary helium system and the vacuum annulus. During the remainder of Cycle 1, it was found that the in-pile section could not operate at design temperatures without exceeding the 482°F limit on skin temperature imposed by BNL to protect the Reactor graphite. It was experimentally determined that the safe gas temperature in the in-pile section could be about 500°F and the safe fuel temperature could be about 800°F in order not to exceed the skin temperature limitation.

During Cycle 1, a procedure was devised to locate the leak and provision was made to repair the leak if it were found in an accessible location. The leak detection procedure consisted of a long tube of calibrated length to pass helium over discrete portions of the outside of the in-pile section. This procedure was carried out on November 18th during the Reactor shutdown and the leak was found to be within 2" of the innermost end of the in-pile section. It was concluded that the leak was a result of the difficulties associated with insertion of the in-pile section. Due to the extensive neutron activation of this region, repair was not feasible at BNL.

The defective in-pile section and the unfueled specimen were left in place during Cycle 2. On November 22nd, it was decided that the best course of action would be to fabricate a new in-pile section and in the meantime operate the Loop with a "low release" FA-22 specimen during Cycle 3. Approval was received on November 30th and immediate steps were taken to procure and fabricate the necessary parts so that the new in-pile section could be installed during the extended Reactor shutdown at the end of Cycle 3. Several minor design changes were incorporated in the new in-pile section as described in Section 9.1.

Meanwhile, the unfueled specimen was discharged from the Reactor during the Dec. 1 shutdown and specimen FA-1(550E) was inserted in its place. During the first two days of full power reactor operation, tests were performed to determine the extent of temperature transients in the fuel element and on the surface of the in-pile section due to a loss of flow incident and to establish the minimum emergency helium purge flow required to maintain safe operating temperatures. These tests were requested by BNL as a result of the partial loss of thermal insulation in the in-pile section. The tests showed that the fuel temperature rose to a

value in excess of 1100°F. At this temperature, the skin temperature approached the limiting value of 482°F at which the loop emergency shutdown system will scram the reactor. The tests established that a purge flow of 1 - 2 scfm helium was required to limit the skin temperature to a value that would insure no unnecessary reactor scram incident. After these tests were concluded, continuous flow operations were initiated at a helium flow rate of 5.1 scfm. The temperature of the in-pile section and the hot leg and intermediate leg of the out-of-pile section were raised to between 500°F and 550°F, the maximum temperature permissible without danger of inducing a reactor scram. Sampling procedures for fission product gases were initiated after steady state temperatures were achieved.

Reactor operations were interrupted on December 12, due to highly inclement weather. No interruption in helium flow in the Loop occurred, but the temperatures of the fuel were seriously decreased. After full-power reactor operation and steady state loop operation were again achieved, the gas sampling procedures were again initiated. Several samples were taken throughout the remainder of the reactor cycle. The fuel temperature reached a maximum value of 900°F at a reactor power of 19 MW. This temperature then dropped to about 800°F at the same power level on December 20. It is believed that this reduction was due to a series of reactor control rod pattern shifts which occurred during this period.

A total of five gas samples were taken during Cycle 3 for the purpose of measuring the concentration of Xe 133, Xe 135, Kr 85m, Kr 87 and Kr 88 in the helium stream. The results of these samples are given in Section 9.3.

As scheduled, the defective in-pile section was replaced with the new in-pile section during the extended shutdown period after Cycle 3 and "high release" specimen FA-1(90E) was inserted. Initial operation during Cycle 4 was with 8 scfm helium flow and no external heat applied to the system.

Installation of the side concrete shielding blocks was completed by January 5. External heat was applied on January 6, raising the hot-leg and intermediate-leg portions of the system to 500°F. Over the weekend of January 7-8, experiments located on the concrete balcony above the Loop reported a significant rise in their background count. A review of this situation resulted in the conclusion that delayed neutron emitters, arising from such isotopes as 55s Br 87 and 22s I 137, were present in the out-of-pile portion of the Loop since the high count appeared only when helium was

being circulated through the Loop. Steps were immediately taken to add a paraffin-cadmium-lead shield on top of the loop. These modifications were made with no helium flow through the Loop since it had been found that under static conditions with no auxiliary heat, the maximum temperatures were 1100°F in the fueled specimen and 340°F on the surface of the in-pile section.

By the end of Cycle 4, sufficient shielding had been added to meet radiological safety requirements but the neutron background was still unsatisfactory. Consequently, BNL requested that specimen FA-1(90E) be removed at the end of Cycle 5 unless further shielding efforts during the first week of Cycle 5 were successful. Only a slight but insufficient improvement could be made. The reductions in gamma and neutron levels by the top shielding can be seen in Table 9-1. Since neutron counts were still high enough to interfere with experiments on the balcony, specimen removal was scheduled for Jan. 27. However, permission for operation (i.e. with helium flow) during the second week of Cycle 5 was obtained.

TABLE 9-1

Radiation Survey Data on Balcony Above Loop During Cycles 4 & 5

Date	Helium Flow	Top Shielding	Gamma Radiation, mr/hr	Fast Neutrons, cpm	Thermal Neutrons, cpm
1/10/61	no	no	1	12	43
1/10/61	yes	no	19	84	292
1/17/61	no	yes	1	9	60
1/17/61	yes	yes	2	34	105
Radiological tolerance			7	90	17,000

It had been planned to install the bypass cleanup trap during the shutdown after Cycle 4. In view of the shielding efforts, this could not be done. However, gas samples were taken to measure the activity levels arising from both long-lived and short-lived volatile fission products and a large number of coupons and loop sections were to be made available for deposition and decontamination studies. Also, two remote reading ionization chambers were installed to measure the gamma radiation field in the vicinity of the flowmeter and of the outlet from the in-pile section.

No further experimental operations were scheduled after Jan. 26. The loop was dismantled for disposal. Deposition coupons and certain pipe sections were retrieved for laboratory examination as discussed in Section 9.3.

9.3 Experimental Results

The "low release" specimen FA-22(550E) was irradiated during Cycle 3. Due to the loss of vacuum in the insulation annulus of the in-pile section, this specimen could not be operated at temperatures above 1000°F. Four gas samples were taken during Cycle 3. The results of the analyses of these samples are given in Table 9-2. The release rates are calculated from the measured isotope concentrations on the assumption that equilibrium has been achieved (i.e. that the escape rate of the isotope into the recirculating helium stream is equal to the decay rate of the isotope in the helium stream).

TABLE 9-2

Fission Product Release Data from Specimen FA-22(550E) During Cycle 3

Sample No.	Date	Fuel Temp, °F	Isotope	Conc, Atoms/ft^3	R[(a)]	R/B[(a)]
1	12/9	955	Xe 133	2.7×10^{9}	2.2×10^{6}	6.0×10^{-8}
2	12/16	850	Xe 133	$<9.0\times10^{8}$	$<5.0\times10^{5}$	$<2.0\times10^{-8}$
3	12/19	880	Xe 133	3.1×10^{10}	1.8×10^{7}	4.9×10^{-7}
			Xe 135	9.9×10^{9}	5.8×10^{7}	1.7×10^{-6}
4	12/20	880	Xe 133	5.0×10^{10}	2.6×10^{7}	7.0×10^{-7}
			Xe 135	9.5×10^{9}	5.5×10^{7}	1.6×10^{-6}
			Kr 85m	4.7×10^{8}	5.7×10^{6}	1.0×10^{-6}
			Kr 87	1.4×10^{8}	5.9×10^{6}	4.2×10^{-7}
			Kr 88	5.2×10^{8}	9.9×10^{6}	5.0×10^{-7}

(a) R = Release Rate, atoms/min; B= Production Rate, atoms/min.

The data in Table 9-2 are consistant with data for specimen FA-22(449E) obtained in Furnace Capsule SPF-3 and given on page 4-30. An alpha assay of the Al_2O_3 coated UO_2 in batch 6H indicated a surface uranium contamination of 4.5×10^{-7} of the contained uranium and an alpha assay of the surface of specimen FA-22(550E) indicated a surface uranium contamination of 9×10^{-7} of the uranium contained in the specimen. As also noted in previous tests, the fission product "leakage" measured for this type of specimen is actually due to the slight amount of uranium contamination external to the particle coatings rather than fission product diffusion through the particle coatings.

The "high release" specimen FA-1(90E), fueled with uncoated UO_2 shot, was irradiated during Cycles 4 and 5. Nine gas samples were analyzed for medium and long-lived fission gases and three gas samples were acquired for subsequent radiochemical analysis to determine the concentrations of the short-lived fission gases.

Eight of the gas samples were analyzed for Xe 133 and Xe 135. The concentrations of Kr 85m, Kr 87, Kr 88, and Xe 138 in the gas stream were also determined in several of these samples. One special sample was analyzed directly for Kr 89. The results of these analyses for the medium- and long-lived fission gases are given in Table 9-3.

The three short-lived isotope samples were radiochemically analyzed. Assays were performed for the non-volatile daughters of the following gaseous isotopes:

Gaseous Precursor	Non-Volatile Daughter
3.2m Kr 89	54d Sr 89
9.8s Kr 91	58d Y 91
3.9m Xe 137	26.6y Cs 137
16s Xe 140	12.8d Ba 140

The results of these analyses for the concentration of short-lived gaseous fission products resulting from the irradiation of specimen FA-1(90E) are given in Table 9-4.

The leakage factors for the short lived gaseous fission products Kr 89 and Xe 137 were about an order of magnitude lower than the leakage factors for the longer lived gaseous fission products. The upper limits for the other two short-lived gaseous fission products (Kr 91 and Xe 140) were substantially higher due to the detection limits for their non-volatile daughters. The data obtained by direct analysis of the gas stream for Kr 89 and by analysis for its decay product, Sr 89, were in fair agreement.

The average leakage factors for both the long-lived and the short-lived gaseous fission products from specimen FA-1(90E) are summarized in Table 9-5, and are compared with similar data from three other capsule-irradiated specimens which were either uncoated or had defective coatings. These other specimens were FA-1(81E) containing uncoated UO_2 shot just as in FA-1(90E), specimen FA-23(E8-7) fueled with uncoated UC_2 and having a cracked Si-SiC surface coating, and specimen FA-22(471E) after nearly 10% of its Al_2O_3 particle coatings were cracked.

TABLE 9-3

Medium-and Long-Lived Gaseous Fission Product
Release from Specimen FA-1(90E) during Cycle 4 and 5.

Sample No.	Date	Fuel Temp, °F	Isotopes	Conc., Atoms/ft^3	R[(a)]	R/B[(a)]
1	1/6	850	Xe 133	2.1×10^{14}	2.3×10^{11}	6.2×10^{-3}
			Xe 135	2.9×10^{13}	1.6×10^{11}	4.6×10^{-3}
2	1/9	850	Xe 133	3.0×10^{14}	$2,3\times10^{11}$	6.2×10^{-3}
			Xe 135	3.4×10^{13}	1.9×10^{11}	5.4×10^{-3}
3	1/12	850	Xe 133	3.1×10^{14}	1.9×10^{11}	5.2×10^{-3}
			Xe 135	2.4×10^{13}	1.5×10^{11}	4.2×10^{-3}
			Xe 138	7.9×10^{11}	1.5×10^{11}	4.7×10^{-3}
			Kr 85m	2.3×10^{12}	2.9×10^{10}	5.1×10^{-3}
			Kr 87	3.7×10^{11}	1.5×10^{10}	1.1×10^{-3}
4	1/12	850	Kr 89	$< 5\times10^{10}$	$< 5\times10^{10}$	$< 2\times10^{-3}$
5	1/23	980	Xe 133	1.9×10^{14}	1.4×10^{11}	3.7×10^{-3}
			Xe 135	3.1×10^{13}	1.7×10^{11}	4.9×10^{-3}
6	1/24	980	Xe 133	1.0×10^{14}	7.2×10^{10}	2.0×10^{-3}
			Xe 135	1.3×10^{13}	7.5×10^{10}	2.2×10^{-3}
			Kr 85m	8.4×10^{11}	1.0×10^{10}	1.8×10^{-3}
7	1/25	980	Xe 133	1.5×10^{14}	9.7×10^{10}	2.6×10^{-3}
			Xe 135	1.2×10^{13}	7.0×10^{10}	2.0×10^{-3}
			Kr 85m	3.1×10^{12}	3.9×10^{10}	7.0×10^{-3}
			Kr 87	1.6×10^{12}	6.5×10^{10}	4.6×10^{-3}
			Kr 88	1.7×10^{12}	3.5×10^{10}	1.7×10^{-3}
8	1/25	980	Xe 133	2.9×10^{14}	1.9×10^{11}	5.0×10^{-3}
			Xe 135	2.5×10^{13}	1.4×10^{11}	4.1×10^{-3}
			Kr 85m	4.7×10^{12}	5.7×10^{10}	1.0×10^{-2}
			Kr 87	1.2×10^{12}	4.9×10^{10}	3.4×10^{-3}
9	1/26	980	Xe 133	5.0×10^{14}	2.6×10^{11}	7.0×10^{-3}
			Xe 135	3.3×10^{13}	1.9×10^{11}	5.4×10^{-3}
			Kr 85m	3.7×10^{12}	4.6×10^{10}	8.2×10^{-3}
			Kr 87	5.2×10^{11}	2.2×10^{10}	1.6×10^{-3}

(a) R = Release Rate, atoms/min; B = Production Rate, atoms/min.

The leakage factors for the Loop specimen are in good agreement with the other uncoated UO_2 fueled specimen and the UC_2 fueled specimen. A very slight dependency of leakage factor on isotope decay constant can be noted which implies a relatively short diffusion time through the graphite matrix. Although about 10% of the Al_2O_3 coatings were cracked in the FA-22 specimen, relatively more holdup of the shorter-lived gas fission products can be noted implying that the condition of the cracks still caused a significant delay time in fission product diffusion.

TABLE 9-4

Short-Lived Gaseous Fission Product Release from Specimen FA-1(90E) During Cycle 5

Sample No.	Date	Fuel Temp, °F	Isotope	Conc. atoms/ft^3	R[(a)]	R/B[(a)]
1	1/24	980	Kr 89	1.1×10^{10}	1.1×10^{10}	4.4×10^{-4}
			Kr 91	$<3 \times 10^{11}$	$<3 \times 10^{12}$	$<8 \times 10^{-2}$
			Xe 137	8.3×10^{9}	6.8×10^{9}	2.0×10^{-4}
			Xe 140	$<1 \times 10^{10}$	$<7 \times 10^{10}$	$<2 \times 10^{-3}$
2	1/25	980	Kr 89	1.5×10^{10}	1.5×10^{10}	5.7×10^{-4}
			Kr 91	$<1 \times 10^{12}$	$<1 \times 10^{13}$	<0.3
			Xe 137	8.8×10^{9}	7.1×10^{9}	2.0×10^{-4}
			Xe 140	$<3 \times 10^{10}$	$<2 \times 10^{11}$	$<6 \times 10^{-3}$
3	1/26	980	Kr 89	1.3×10^{10}	1.3×10^{10}	5.2×10^{-4}
			Kr 91	$<6 \times 10^{11}$	$<6 \times 10^{12}$	<0.2
			Xe 137	2.1×10^{10}	1.7×10^{10}	5.0×10^{-4}
			Xe 140	$<2 \times 10^{10}$	$<1.5 \times 10^{11}$	$<5 \times 10^{-3}$

(a) R = Release Rate, atoms/min; B = Production Rate, atoms/min.

The significant amount of deposited radioactivity which would result from the release of short-lived fission product gases from an uncoated fuel specimen was measured in the Loop by two ionization chambers. One was located in the vicinity of the flowmeter and the other in the vicinity of the outlet pipe from the in-pile section. Radiation fields of 1.5 r/hr and 7.5 r/hr, respectively, were measured during steady state operation at the end of Cycle 5. These values dropped sharply just after helium flow was stopped and then decreased at a slower rate to values of 0.2 r/hr and 1.8 r/hr, respectively, eighteen hours after helium flow was stopped. There was no

TABLE 9-5

Comparison of Fission Product Leakage Factors for Several Uncoated Specimens

Specimen		FA-1(81E)	FA-23(E8-7)	FA-1(90E)	FA-22(471E)
Irradiated in		SP-2	SP-5	Loop	SP-5
Fuel Type		UO_2	UC_2 [b]	UO_2	Al_2O_3/UO_2 [c]
Burnup, a/o U235		0.1	6.5	0.1	5.3
Temperature, °F		1200	1100	900	1150
Leakage Factors [a]					
Isotope	Decay Const.				
Xe 133	1.52×10^{-6}	-	3.8×10^{-2}	4.6×10^{-3}	1.2×10^{-2}
Xe 135	2.11×10^{-5}	1.2×10^{-2}	6.0×10^{-3}	3.4×10^{-3}	2.1×10^{-4}
Kr 85m	4.41×10^{-5}	5.8×10^{-2}	1.2×10^{-2}	8.2×10^{-3}	3.6×10^{-4}
Kr 88	6.95×10^{-5}	-	4.6×10^{-3}	1.7×10^{-3}	1.1×10^{-4}
Kr 87	1.48×10^{-4}	-	2.7×10^{-3}	3.2×10^{-3}	2.6×10^{-5}
Xe 137	2.96×10^{-3}	-	-	3.0×10^{-4}	7.1×10^{-6}
Kr 89	3.63×10^{-3}	-	2.5×10^{-3}	5.1×10^{-4}	8.9×10^{-6}
Xe 140	4.33×10^{-2}	-	7.3×10^{-4}	-	9.2×10^{-7}
Kr 91	7.08×10^{-2}	-	9.8×10^{-4}	-	4.0×10^{-6}
Xe 141	4.08×10^{-1}	-	6.8×10^{-4}	-	1.4×10^{-6}

(a) R/B = Release Rate/Production Rate.

(b) Si-SiC surface coating on this specimen was cracked.

(c) Approximately 10% of the Al_2O_3 particle coatings were cracked.

noticeable change in the rate of activity decrease when the helium was evacuated from the system one hour after circulation had stopped. Actually, a sharp burst of activity was detected at the outlet pipe from the in-pile section as the gas was evacuated past this point.

A number of gamma scans were made at various locations on the out-of-pile portion of the Loop after shutdown. These data are summarized in Table 9-6. A trend of decreasing activity level in the direction of gas flow can be noted. The unusually high reading at the flowmeter was subsequently found to be caused by an accumulation of radioactivity on the flowmeter float. A somewhat higher activity was also found on the orifice, located just downstream from the flowmeter, compared with surrounding surfaces. During the following two week period, the activity level at the first heat exchanger was monitored and found to decay with an apparent half-life of about fourteen days.

The sharp drop in activity in the out-of-pile section of the loop when helium circulation was stopped implies that much of the activity was due to the presence of short-lived activity carried in the gas stream. This fact is further borne out by the decrease in residual activity with increasing distance from the fuel element. The contribution of noble fission product gases to the total activity about 1 hour after helium circulation stopped was insignificant since there was no noticeable change in the rate of decay when the helium was removed from the system.

TABLE 9-6

Radiation Fields Along Loop After Operation With Specimen FA-1(90E)[a]

Measurement Position	Scan No. 1[b] (1400 - 1/27/61)	Scan No. 2 (1400 - 1/28/61	Scan No. 3[d] (1430 - 1/31/61)
1. Upstream of first heat exchanger	700	600	1200[e]
2. First heat exchanger	1030	860	1060[e]
3. Downstream of first heat exchanger	320	183	170
4. Removable pipe section	132	124	--
5. Inlet to second heat exchanger	87	--	--
6. Flowmeter	2000	1500[c]	--
7. Blower No. 1, inlet pipe	40	28	25
8. Blower No. 1, exhaust pipe	62	40	28
9. Inlet to main heater	70	43	37

(a) All values have units of mr/hr.
(b) Helium and radioactive gases removed at ~1900, 1/26/61.
(c) Reading at ~1600, 1/28/61.
(d) Reactor operating during this scan.
(e) Increased readings due to radiation from unshielded reactor facility.

A number of coupons and pipe sections were retrieved from the Loop, as listed in Table 9-7. These components were retrieved in order to study fission product deposition as a function of surface material (i. e. stainless steel, carbon steel, Si-SiC), flow perturbations (i.e. pipe sections, stagnant regions at blind flanges, and orifices), and distance from the fuel element, and also to study methods of decontaminating these surfaces. Due to time and fund limitations, it was not possible to conduct these studies under the present Contract. However, the Oak Ridge National Laboratory agreed to examine these components as part of their program on gas-cooled loops and gas cooled reactors. The components were delivered to ORNL who will publish results when available.

TABLE 9-7

Sections Retrieved from In-Pile Loop

Description	Quantity	Material[b]	Location in Loop
1. Coupons[a]	6	SS	Hot Leg, In-Pile Section
2. Coupons[a]	5	Si-SiC	Hot Leg, In-Pile Section
3. Coupons[a]	3	SS	Intermediate Leg
4. Coupons[a]	4	CS	Intermediate Leg
5. Pipe Coil	1	CS	Heat Exch. #1
6. Pipe Coil	1	SS	Heat Exch. #2
7. Removable Pipe Section (incls. straight section, elbow, flanged joint).	1	CS	Intermediate Leg
8. Misc. Pipe Sections	6	SS	Various locations in out-of-pile section.
9. Blind Flanges	3	SS	Heat Exchs. #1 and #2; 2nd in-pile section.
10. Flowmeter	1	SS	Cold Leg
11. Damping Orifice	1	SS	Flowmeter Outlet.
12. Bellows	1	SS	Blower inlet
13. Solenoid Valves	7	SS	Helium supply and blower containment vessels
14. In-Pile Heater	2	SS	5" length at each end

(a) 1.9" OD x .08" wall x 2' long
(b) SS = stainless steel; CS = carbon steel; Si-SiC = Si-SiC coated graphite

LIST OF REFERENCES

Note: Asterisk denotes Progress Report or Topical Report issued under Contract AT(30-1)-2378.

1. NYO 8753; Vol. I; Design and Feasibility Study of a Pebble Bed Reactor-Steam Power Plant; Sanderson & Porter; May 1, 1958.
2. NYO 2373; Progress Report on the Pebble Bed Reactor Program; Sanderson & Porter; June 1, 1958 to May 31, 1959.
3.* S&P 1964-4; Quarterly Progress Report on the Fuel Element Development Program for the Pebble Bed Reactor; Sanderson & Porter; May 1, 1959 to July 31, 1959.
4.* NYO 2706; Phase I Progress Report on the Fuel Element Development Program for the Pebble Bed Reactor; Sanderson & Porter; May 1 to October 31, 1959.
5.* S&P 1964-14; Quarterly Progress Report on the Fuel Element Development Program for the Pebble Bed Reactor; Sanderson & Porter; November 1, 1959 to January 31, 1960.
6.* NYO 9058; Quarterly Progress Report on the Fuel Element Development Program for the Pebble Bed Reactor; Sanderson & Porter; February 1 to April 30, 1960.
7.* NYO 9061; Quarterly Progress Report on the Fuel Element Development Program for the Pebble Bed Reactor; Sanderson & Porter; May 1, 1960 to July 31, 1960.
8.* NYO 9062; Phase II Progress Report on the Fuel Element Development Program for the Pebble Bed Reactor; Sanderson & Porter; November 1, 1959 to October 31, 1960.
9.* NYO 9063; Quarterly Progress Report on the Fuel Element Development Program for the Pebble Bed Reactor; Sanderson & Porter; November 1, 1960 to January 31, 1961.
10.* BMI- 1471; Alumina Coating of UO_2 Shot by Hydrolysis of Aluminum Chloride Vapor; M. F. Browning, N. D. Veigel, T. E. Cook, W. S. Diethorn and J. M. Blocher, Jr; Battelle Memorial Institute; October 25, 1960.
11. AECU 4480; Symposium on High Temperature Technology; pp 108-133; W. D. Kingery.
12.* BMI 1466; Measuring the Release of Short-Lived Fission Gases During Capsule Irradiations; C. W. Townley, G. E. Raines, W. S. Diethorn, and D. N. Sunderman; Battelle Memorial Institute; September 12, 1960.
13. Internal Memorandum; R. F. Benenati; Sanderson & Porter; September 15, 1958.

List of References Continued

14. NYO 9187; Corrosion and Radiation Damage Resistant Fuel Material (Coated Fuel Particles); Nuclear Materials & Equipment Corp; April, 1961.
15. Summary Report on Phase I of AT(40-1)-2560; Graphite Matrix Nuclear Fuel Elements, Vol. I; National Carbon Company; December 22, 1959.
16.* NYO 9059; Thorium Oxide Infiltration of Graphite Spheres; W. E. Parker and F. Rusinko, Jr; Speer Carbon Co.; June 15, 1960.
17.* BMI 1444; Apparatus for the Study of Fission-Gas Release from Neutron-Activated Fueled Graphite; H. S. Rosenberg, R. Lieberman, D. N. Sunderman and W. S. Diethorn; Battelle Memorial Institute; June 7, 1960.
18.* Topical Report on the Design and Operation of Furnace Capsules; to be issued by Battelle Memorial Institute.
19. NYO 9069; Pebble Bed Friction Factor and Thermal Expansion Tests; C. A. Leeman; Babcock & Wilcox Co; August 31, 1960.
20. BMI 1480; Progress Relating to Civilian Applications During November, 1960; R. W. Dayton and C. R. Tipton, Jr; Battelle Memorial Institute; December 1, 1960.
21. BMI 1496; Progress Relating to Civilian Applications During January, 1961; R. W. Dayton and C. R. Tipton, Jr; Battelle Memorial Institute; February 1, 1961.
22. BMI 1504; Progress Relating to Civilian Applications During February, 1961; R. W. Dayton and C. R. Tipton, Jr; Battelle Memorial Institute; March 1, 1961.
23.* Topical Report on the Design and Operation of Sweep Capsule SP-5; to be issued by the Battelle Memorial Institute.
24.* BMI 1479; High-Temperature Compatibility of Al_2O_3-, BeO-, and Metal-Coated UO_2 Particles with Graphite and Coke; A. F. Gerds and A. K. Smalley; Battelle Memorial Institute; November 28, 1960.
25.* BMI 1483; The Effect of Irradiation on Selected Properties of Spherical Graphite Fuel Elements; A. K. Smalley, R. J. Burian, A. F. Gerds, G. E. Raines, and W. S. Diethorn; Battelle Memorial Institute; December 2, 1960.
26.* NSEC-47; In-Pile Loop Tests for the Pebble Bed Reactor Fuel Element Development Program; Nuclear Science and Engineering Corp; April 30, 1961.